ASSESSMENT OF SEPARATION EFFICIENCY IN MINERAL PROCESSING USING THE ULTIMATE UPGRADING CONCEPT - A HOLISTIC WINDOW TO INTEGRATE MINERAL LIBERATION DATA

Dissertation presented to Faculty of Engineering of University of Porto for the PhD degree in Mining and Geo-resources Engineering

by

Rui Jorge Coelho de Sousa

Supervisor
Professor Mário Rui Machado Leite

Co-supervisors:
Professor Aurora Magalhães Futuro da Silva
Professor António Manuel Antunes Fiúza

Department of Mining Engineering, Faculty of Engineering of University of Porto

September 2020

This thesis was financially supported by Fundação para a Ciência e Tecnologia (Portugal) through the PhD grant SFRH/BD/114764/2016.

"Tenho em mim todos os sonhos do mundo"
Fernando Pessoa

e este já o concretizei…

FEUP – Universidade do Porto

ACKNOWLEDGEMENTS

Mais um percurso termina, mas a caminhada é longa. Ninguém caminha feliz se caminhar sozinho, e este é o momento de agradecer a todos os que caminharam ao meu lado durante estes anos.

Aos que me deram suporte durante o percurso como aluno de PhD. O Prof. Machado Leite por ser bem mais que um orientador, por me ensinar algo novo todos os dias, por partilhar o seu conhecimento comigo e por me dar todas as condições para continuar a crescer. À Prof. Aurora, pela disponibilidade para ajudar, pelo apoio em todos os desafios que surgem e por todas as oportunidades que me deu durante este percurso. Ao Prof. António Fiúza, pelo exemplo de dedicação e partilha de conhecimento ao longo destes anos. A todos os Docentes e Colaboradores do DEM, pois todos foram fundamentais para a minha evolução e paixão pela Engenharia de Minas. Aos Colaboradores do LNEG que estiveram sempre disponíveis para me ajudar e que me fizeram sentir "parte da casa". Ao Prof. Noronha e à Violeta pelo apoio na interpretação mineralógica.

Aos amigos, que estiveram sempre lá quando foi preciso. Ao Diogo, Patricia, Joana, e Célia pela companhia no dia-a-dia, pelas pausas para café para desanuviar e pelos momentos que vou guardar na memória. Aos amigos de longa data, o Fernando, Tânia, Sabino, Vitor, Anastácio e João. Aos companheiros de treinos Renata, Jomy, Nuno e Tiago. À super família, Pedro, Carina e T's, pelo prazer de fazer parte das vossas vidas.

À minha irmã e às sobrinhas fantásticas que tanta alegria trazem à minha vida. À família que ganhei, João Luis, Maria José, João Pedro e Xana pelo carinho, disponibilidade e presença, e ao Kiko, que aí vem para nos trazer tão bons momentos. Ao meu avô, não podes estar aqui, mas vou trazer-te sempre comigo.

Aos meus Pais, não tenho como agradecer tudo o que fizeram e fazem por mim. Vocês são fantásticos, são um exemplo de determinação e dão-me a força que preciso todos os dias. Esta conquista também é vossa, e que seja apenas mais uma.

À melhor do Mundo, tu podias estar em qualquer parte deste texto. Porque partilhas o teu conhecimento e me dás apoio em todos os desafios que surgem. Estás nos bons e maus momentos, festejas as minhas conquistas como se fossem tuas e estás sempre lá para mim! Não te poderia pedir mais!

Muito obrigado a todos!

Thanks to all members of the FAME project team for the exchange of knowledge and great moments spent during the last 5 years. It was a great experience for me, both personally and professionally.

A special thanks to Chris Broadbent (WAI). He was the hearth of the FAME and an example of enthusiasm, dedication, talent and character.

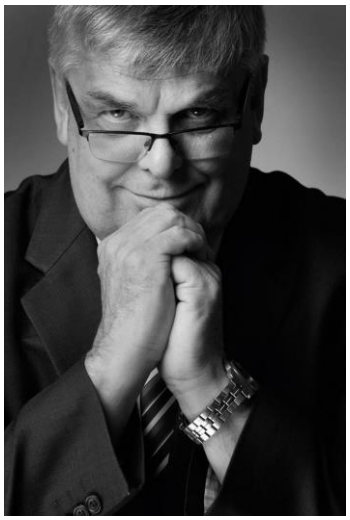

It is the author's willingness to dedicate this thesis to his memory, as a sign of recognition and gratitude!

ABSTRACT

The assessment of separation efficiency in mineral processing has been a constant concern for process engineers. In this work, a methodology to assess mineral separation efficiency was developed, having as main basis the creation of the Ultimate Upgrading concept, which, as the definition states, integrates mineral liberation data to define the technical limit of the separation process.

Once available, Ultimate Upgrading Curves can be compared with Experimental Upgrading Curves that are acquired using data from real separations, and Ideal Upgrading Curves that describe a perfect separation carried out with a full liberated ore. This comparison allowed for the assessment of the separation efficiency, distinguishing the effect of lack of technical efficiency from the effect of lack of liberation in the global separation efficiency. Furthermore, Ultimate Upgrading Curves can be applied to assess the feasibility of separation, using the technical limit of the separation as a plausible scenario for the separation performance. During the interpretation of this scenario, it is mandatory to have in mind that any experimental separation would result in a poor performance unless a perfect separator is applied.

The large set of experimental data generated during the FAME project, requiring proper analysis, was one of the most important reasons for the development of this methodology. According to this, in the framework of this PhD thesis, two reference ores from FAME project were studied: i) scheelite ore from São Pedro das Águias deposit (Tabuaço, Portugal); ii) lepidolite ore from Alvarrões deposit (Guarda, Portugal). Data collected during the experimental testwork on pre-concentration and concentration of both ores were assessed. Thus, samples of crushed material (pre-concentration size range) and ground material (concentration size range) were prepared for quantitative mineralogy analysis to collect data regarding the mineral liberation degree of the ores.

Mineral liberation analyses at concentration size ranges were carried out at Cambourne School of Mines (EXETER) using the QEMSCAN® system. In the case of the pre-concentration size range, a new methodology based on image analysis was developed by creating a straightforward algorithm that can read photos of lump or broken particles. Then, a quantitative analysis of the valuable mineral can be carried out by pixel counting. Both methods made it possible to acquire the grade histograms (wt%), which are

fundamental for the further steps of the work. During this task, the parameters P and Q of the statistical Euler Beta function were determined by fitting the predicted values to the generated histograms. P and Q parameters were then interpreted to better describe the mineral liberation degree. Furthermore, in the case of Pre-concentration, where a novel image analysis method was applied to collect quantitative mineralogical data, the Euler Beta function was crucial to validate the obtained data.

Then, using the experimental data, the acquired feed grade histograms (wt%) and an efficiency model based on the partition curve (Lynch model), it was possible to model the applied separator, and consequently to obtain a mored discretised representation of the Experimental Upgrading Curves. The model parameters m and AS can be interpreted, giving important information regarding the efficiency of the applied separator. The application of this efficiency model allowed for acquiring the concentrate grade histograms (wt%).

Finally, the comparison between Experimental Upgrading Curves, Ideal Upgrading Curves and Ultimate Upgrading Curves, represented by means of the Mayer Diagram, allowed for the assessment of separation efficiency of the experimental testwork carried out in the framework of FAME project: hand sorting and gravity separation in the case of São Pedro das Águias ore and optical sorting and flotation in the case of Alvarrões ore. Then, using the Henry (Washability) Curve, the feasibility of the pre-concentration of both studied ores was assessed. However, it should be highlighted that the purpose of this thesis was not to study the pre-concentration and concentration of São Pedro das Águias and Alvarrões ores but to demonstrate, using experimental cases, the application of the developed methodology.

RESUMO

Neste trabalho foi desenvolvida uma metodologia para avaliar a eficiência da separação, utilizando como base o conceito de *Ultimate Upgrading*. O objetivo principal é utilizar dados de libertação mineral para definir o limite técnico da separação – *Ultimate Upgrading,* que pode ser representado utilizando curvas de *upgrading*.

Uma vez disponíveis, as Curvas de *Ultimate Upgrading* podem ser comparadas com as Curvas de *Upgrading* Experimentais, obtidas utilizando resultados de separações reais, e Curvas de *Upgrading* Ideal que descrevem uma separação perfeita realizada com um minério totalmente liberto. Esta comparação permitiu a avaliação da eficiência da separação, distinguindo o efeito da falta de libertação do efeito da falta de eficiência técnica na eficiência total do processo de separação mineral. Além disso, as Curvas de *Ultimate Upgrading* foram aplicadas para avaliar a viabilidade da separação, utilizando o limite técnico da separação como um cenário plausível para a sua performance, o que deve ser interpretado com muito cuidado, tendo a noção que qualquer separação real apresentará uma performance inferior, a não ser que seja possível utilizar um separador perfeito.

A enorme quantidade de dados experimentais gerados durante o projeto FAME, que requerem uma análise cuidada, foi uma das principais razões para o desenvolvimento desta metodologia. Deste modo, no âmbito desta tese de doutoramento foram estudados dois dos minérios de referência do projeto FAME. Um deles trata-se de um minério de scheelite proveniente do jazigo de São Pedro das Águias (Tabuaço, Portugal) e outro de um minério de lepidolite preveniente do jazigo de Alvarrões (Guarda, Gonçalo). Os resultados das separações experimentais obtidos para ensaios de pré-concentração e concentração de ambos os minérios foram avaliados utilizando a metodologia desenvolvida. Para tal, amostras de material britado (calibre de pré-concentração) e moído (calibre de concentração) foram preparadas para realizar analises mineralógicas quantitativas com o objetivo de caracterizar o estado de libertação de cada minério, em ambos os estágios de cominuição.

As análises de libertação mineral a calibres de concentração foram realizadas pelo laboratório de *Cambourne School of Mines* (EXETER), recorrendo ao QEMSCAN®. No caso da pré-concentração, foi desenvolvida uma nova metodologia baseada em análise de

imagem, através da criação de um algoritmo que permite a leitura de fotos de amostras de mão e partículas fragmentadas. De seguida, a análise quantitativa do mineral útil é efetuada por contagem de pixéis. Ambos os métodos permitiram a obtenção dos histogramas de teor (%massa) fundamentais para as etapas seguintes do trabalho. Durante esta tarefa, os parâmetros P e Q da função estatística Beta de Euler foram determinados de forma a que os valores previstos se aproximassem dos valores reais obtidos durante a geração dos histogramas de teor. Estes parâmetros são interpretáveis, fornecendo informação fundamental sobre o grau de libertação mineral. Além disso, no caso da pré-concentração, onde foi aplicada uma nova metodologia de análise de imagem para obter dados mineralógicos quantitativos, a função Beta de Euler foi fundamental para validar os dados obtidos.

Após a obtenção dos histogramas de teores obtidos foi possível, utilizando os dados dos ensaios experimentais, aplicar um modelo de eficiência baseado na curva de partição (modelo de Lynch) que permitiu modelar os separadores utilizados e consequentemente simular representações contínuas das Curvas de *Upgrading* Experimentais. Os parâmetros m e AS do modelo de eficiência revelaram-se importantes, fornecendo informações relevantes quanto à eficiência do separador aplicado.

Finalmente, a comparação as Curvas de *Upgrading* Experimentias com as de *Upgrading* Ideal e as de *Ultimate Upgrading*, representadas através de Diagramas de Mayer, permitiram a avaliação da eficiência de separação dos ensaios realizados no âmbito do projeto FAME: separação manual com iluminação ultravioleta e separação gravítica no caso de São Pedro das Águias e separação ótica eletrónica e flutuação no caso de Alvarrões. De seguida, utilizando as curvas de Henry (lavabilidade), foi estudada a viabilidade da pré-concentração de ambos os minérios. No entanto, é importante destacar que o propósito principal desta tese não é o estudo da eficiência e potencial da pré-concentração e concentração dos minérios em análise, mas sim demonstrar a aplicabilidade da metodologia desenvolvida a casos reais.

TABLE OF CONTENTS

LIST OF FIGURES

LIST OF TABLES

1 INTRODUCTION

1.1 MOTIVATION AND RELEVANCE

The concept of mineral processing is quite simple to explain – the ore is extracted from the mine site, crushed and ground to achieve an adequate size, corresponding to an appraisable mineral liberation degree. Then, it moves forward to one or more separation steps to produce one or more final products that concentrated the mineral or the minerals of interest. In line with this, the main activities developed in a mineral processing plant consist of crushing and grinding, classifying and separating. However, when economics takes action in the process, there is a set of conditions that must be well considered. First, the energy required for the crushing and grinding stages is massive, which means that these stages must be well optimized to produce sufficient mineral liberation for the subsequent separation processes. Secondly, the separation must be well adjusted to guarantee the quality of the final products to meet demand needs and the maximum valuable minerals recovery to improve the income. Thus, there is a complex relationship between comminution, mineral liberation and separation efficiency that must be well balanced to ensure the success of any mineral processing plant, which represents one of the most important challenges of mineral processing design.

From the very beginning, several mineral processing researchers discussed the complex relationship between size and grade. Authors as Gaudin, King, Wiegel, Li, Andrews, Mika, Herbst, among others, discussed the correlated effect between size and grade[1-4]. In the late ’70s of XX century, Madureira launched a research team in the Mining Engineering Department of Faculty of Engineering of University of Porto (FEUP), focused in mineral liberation by size reduction as the most important concept of mineral processing.

Madureira supervised mineral processing research in the Mining Department of FEUP for many years. Particular emphasis must be given to works carried out by Machado Leite, Cavalheiro and Soeiro de Carvalho [5-8].

All these works addressed the study of comminution and mineral liberation models and the study of mineral liberation effect on the separation processes. The lack of reliable liberation data, representative of the mineral texture behaviour, when the ore is subjected to comminution, was the most significant and challenging bottleneck faced during those works. During that period, image analysis methodologies were in development, and the access to this type of data was challenging. In those times, modelling of mineral processing

operations was already on the trails [9-11]. The development of theoretical algorithms had been given important contributions for the knowledge and comprehension regarding comminution, liberation and separation. The lack of experimental mineralogical data of comminuted particles, that constitutes the complex object of mineral processing, was a critical point to go forward in the practical application of simulation models.

In fact, modelling of a certain phenomenon is fundamental for simulation purposes but also because, if it is successful, it gives relevant information about the phenomenon itself. All this foundation of knowledge built on Mining Engineering Department was one of the reasons behind the development of this thesis, creating the desire to join together all the scarce established knowledge and to apply them using some of the most recent advances in the mineral processing field, namely in what concerns quantitative mineralogy data.

During the preparation of the thesis, Project FAME (Flexible and Mobile Economic Processing Technologies) was ongoing, with a participation of a consortium of 16 partners (Fig. 1) from 7 European countries, including industry, academia and governmental institutions.

FAME project was focused in the study of six European reference ores, respectively tin-tungsten skarns (Tellerhäuser, Germany and Tabuaço, Portugal), lithium pegmatites (Länttä, Finland and Alvarrões, Portugal) and tin greisen ores (Cinovec, Czech Republic and Tellerhäuser, Germany), with the following main objectives:

- Increasing the competitiveness of the mining of European mineral resources;
- Enhancing mineral processing and mining skills within Europe;
- Reducing the reliance of European Industry and consumers on raw materials that currently must be imported from outside;

Fig. 1 – FAME project consortium.

Besides the great contribution of FAME project to the knowledge in the fields of mineral deposits geology and mineralogy and mineral processing, two great achievements were accomplished by pilot plant testing of two innovative process flow sheets:

- Alvarrões ore (pegmatite) to produce a Li-mica (Lepidolite) concentrate and recover by-products as cassiterite, feldspar and quartz concentrates;
- Tellerhäuser ore (skarn) to produce a commercial tin concentrate with the recovery of valuable by-products as zinc, copper sulfides and magnetite;

FAME provides an important contribution to the more efficient exploitation of European mineral resources by optimizing the production of critical raw materials from European ores.

The Portuguese National Laboratory for Energy and Geology (LNEG) and University of Porto (UP) played an important role in the FAME project, giving important contributions to mineralogy characterization and mineral processing. The study of mineral separation of the FAME reference ores generated a significant amount of data, ranging from quantitative mineralogical data to metallurgical balances of mineral processing operations (such as grade, yield and recovery). These data must be appropriately interpreted to fulfil one of the most important objectives of the project: improving mineral processing techniques.

FAME project was not intended to develop feasibility studies for specific mining projects, but mainly to analyze the achieved results to understand the causes of the experimental testwork performance (sometimes inefficiency) and to build up target scenarios. For this purpose, different performance indicators were calculated for the different mineral separation stages.

In summary, as may be observed in Fig. 2, the motivation for this work arose from the existent knowledge of the Mining Department of FEUP, together with the willingness to create and apply new concepts of mineral liberation analysis and the necessity for an adequate assessment of experimental separation results acquired during the FAME project. For this purpose, a new methodology to assess separation efficiency using the ultimate upgrading concept, based on the integration of mineral liberation data was developed. A holistic comprehension of the separation efficiency would be attained, allowing for an adequate interpretation of the mineral liberation analysis, for the

definition of the limit for the separation efficiency (separation target) and for the distinction between technical inefficient and lack of liberation in the overall efficiency of the separation.

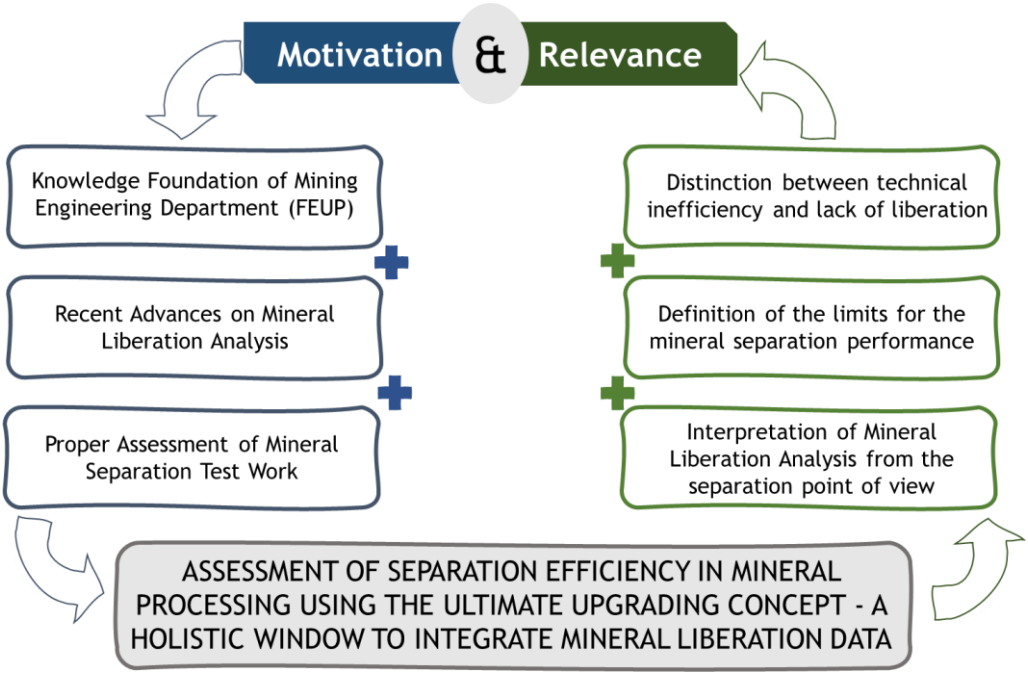

Fig. 2 – Summary of the motivation and relevance of the thesis.

1.2 OBJECTIVES AND MILESTONES

Over the years, the demand for efficient methods to assess mineral liberation produced by comminution and separation efficiency has been in the objective of many research programmes and studies, which have led to the development of technologies such as release analysis, liberation models and more recently accurate mineral liberation analysis (using technologies as QEMSCAN® and MLA®), along with the calculation of upgrading parameters allowing for the assessment of mineral separation efficiency [12-17]. As far as the access to accurate mineralogical data is facilitated by modern innovative technologies, it is imperative to develop new methodologies to use/integrate the acquired data adequately.

As mentioned, the aim of this work is to propose a methodology to assess separation efficiency based on the integration of mineral liberation data. According to this, it is possible to state two main challenges: i) acquisition and integration of mineral liberation

data to be applied in the assessment of separation efficiency; ii) use the acquired data to construct/develop useful separation efficiency indicators.

Experimental data acquired during the FAME project are used to demonstrate and validate the developed methodology. Results of two FAME reference ores (both Portuguese case studies) are presented: i) scheelite ore from São Pedro das Águias skarn deposit; ii) lepidolite ore from Alvarrões granite pegmatite deposit. Furthermore, in each case study, results from separations carried out at crushing (Pre-concentration) and at grinding sizes (Concentration) are considered.

In line with this, data from mineral liberation analysis at the corresponding sizes crushing (>6mm) and grinding (<2mm) are required. For the grinding sizes, the problem is well addressed by the existing technologies as QEMSCAN® and MLA. In the case of crushing sizes, a proper methodology is proposed due to the lesser availability of new technologies for that purpose at that time. The main objective of the data acquisition task was to build the grade histograms (wt%) of the material that feeds the separator, as the best descriptor of mineral liberation at the given size. These histograms were fitted accordingly to a liberation model based on the Beta Euler's law, aiming to validate the obtained histograms and searching for an adequate interpretation of the mineral liberation degree.

Then, using the grade histograms (wt%) that characterize the liberation degree at the given size (crushing or grinding), the maximum limit for the mineral separation efficiency is defined and named as Ultimate Upgrading Curve.

Finally, the Ultimate Upgrading Curve can be (i) used to compare with Experimental Upgrading Curves, allowing for the assessment of the separation efficiency, distinguishing lack of efficiency from lack of liberation, and (ii) used to assess the feasibility of the Pre-concentration stage, defining the technical limit of the separation. Within this process, an efficiency model, based on partition curves, is applied to experimental data to calculate continuous (along with the cut grade range) information regarding the separation efficiency.

In conclusion, this project intends to be a contribution to one of the challenges in mineral processing – the development of accurate separation efficiency indicators, which can be easily applied and that can provide useful information to support flowsheet design

and the fine-tuning of the separation process. The fundamental milestones of this work are the following:

- To emphasize the importance of knowing the adequate characterization of ore texture;
- To present a straightforward methodology to acquire quantitative mineralogical data of ore macro-textures that plays an important role in the Pre-concentration step;
- To convert mineral liberation analysis into grade histograms (wt%), furtherly validated by the application of the Beta Law model;
- To apply an efficiency model that allows for the representations of continuous experimental upgrading curves;
- To assess of separation efficiency and feasibility based on the definition of the unachievable separation performance, represented by the Ultimate Upgrading Curves;

1.3 THESIS OUTLINE

The thesis is structured in six chapters, including the introduction (Chapter 1) and conclusions. Supplementary data to the main text is presented in the appendix.

Chapter 2 - State of the art provides fundamental information regarding the main concepts required for the formulation of the presented work. Mineral liberation, separation processes and separation efficiency are the main subjects discussed in this stage.

The main steps and strategy applied to develop this work are introduced in Chapter 3 - Materials and Methodologies where the materials used in the thesis and preliminary activities are carefully described, including the results of experimental test work (presented as case studies). A scheelite ore from São Pedro das Águias skarn deposit (Tabuaço, Portugal) and a lepidolite ore from Alvarrões pegmatite deposit (Gonçalo, Portugal) were used in this work. In the case of scheelite ore, hand-sorting was applied to simulate the pre-concentration and gravity separation was used in the concentration stage. In the lepidolite case, optical sorting is tested as pre-concentration and flotation in the final concentration.

In Chapter 4 - Data Acquisition, the results of mineral liberation analysis applied to study the liberation degree at crushing and grinding sizes are presented. QEMSCAN® and

a proper image analysis procedure are applied to obtain mineral quantitative data. A model based on the statistical Beta law is applied to validate and collect important information regarding the liberation degree of the ore.

The following Chapter 5 – Separation Efficiency is dedicated to the assessment of separation efficiency by integrating mineral liberation analysis. The application of an efficiency model, based on partition curves is applied to obtain continuous representations of experimental upgrading curves, gathering important information regarding the separation process efficiency. Then, using mineral quantitative data collected in the previous chapter, Ultimate Upgrading Curves are computed and applied to assess the separation efficiency and feasibility.

Chapter 6 – Conclusions summarizes the main achievements and bottlenecks of this thesis and some suggestions for future work.

REFERENCES

1. Andrews, J.R.G. and T.S. Mika. *Comminution of a heterogeneous material: development of a model for liberation phenomena*. in *XI International Mineral Processing Congress*. 1975. Cagliari, Italy.
2. Gaudin, A.M., *Principles of Mineral Dressing*, ed. McGraw-Hill. 1939, New York, United States.
3. King, R.P., *A model for the quantitative estimation of mineral liberation by grinding.* International Journal of Mineral Processing, 1979. **6**(3): p. 207-220.
4. Wiegel, R.L. and K. Li, *A random model for mineral liberation by size reduction.* AIME Transactions, 1967. **238**: p. 179-189.
5. Cavalheiro, A., *Libertação de minério por cominuição - Modelo matemático*, 1984. *Departamento de Engenharia de Minas*,Universidade do Porto, PhD Thesis
6. Machado Leite, M.R., *Liberation by size reduction. Consequences and improvements on flotation kinetics*, in *Innovations in Advanced Flotation Technology*, N.A. SERIES, Editor. 1992, Kluwer Academic Publishers. p. 149-170.
7. Madureira, C.M.N., M.R. Machado Leite, A. Cavalheiro and J. Silva, *Size, Grade and Liberation: a stochastic approach to the fundamental problem of mineral processing*, in *XVI International Mineral Processing Congress*, E.S. Publisher, Editor. 1988: Stockholm.
8. Soeiro Carvalho, J., *Libertação dicriminatória de minérios: uma abordagem simulacional integrada*, 1995. *Departamento de Engenharia de Minas*,Faculdade de Engenharia da Universidade do Porto, PhD Thesis
9. Barbery, G., *Measurement, Simulation and Practical Use in Mineral Processing*. Les Editions GB. 1991, Canada.
10. Fuerstenau, D.W., *Coal surface control for advanced fine coal flotation*. 1988-1992, University of California, University of Columbia, University of Utah and Praxis Engineers Inc: California.
11. Lynch, A.J. and T.C. Rao. *Modelling and scale-up of hydrocyclone classifiers*. in *Proceedings of the 11th International Mineral Processing Conference*. 1975.
12. Dryzmala, J., *Atlas of upgrading curves used in separation and mineral science and technology (Part III).* Physocochemical Problems of Mineral Processing, 2008. **42**: p. 75-84.

13. Drzymala, J., *Mineral Processing - Foundations of theory and practice of minerallurgy*, ed. W.U.o. Technology. 2007.
14. Fandrich, R., Y. Gu, D. Burrows and K. Moeller, *Modern SEM-based mineral liberation analysis.* Internation Journal of Mineral Processing, 2007. **84**: p. 310-320.
15. Guimarães, C. and F. Durão, *Application of a cellular automata based simulation model of size reduction in mineral processing.* Minerals Engineering, 2007. **20**: p. 541-551.
16. Leibner, T., T. Mutze, K. Bachmann, S. Rode, J. Gutzmer and U.A. Peuker, *Evaluation of mineral processing by assessment of liberation and upgrading.* Minerals Engineering, 2013. **53**: p. 171-173.
17. Leißner, T., K. Bachmann, J. Gutzmer and U.A. Peuker, *MLA-based partition curves for magnetic separation.* Minerals Engineering, 2016. **94**: p. 94-103.

2 STATE OF THE ART

2.1 MINERAL LIBERATION

2.1.1 INTRODUCTION

A raw ore may be defined as a significant accumulation of a certain type of rock (in geological terms) in certain location in the upper crust that hosts one or more valuable minerals that can be economically extracted, whose occurrence is named a mineral deposit. Mining is the art of extracting the ore from the ore deposit, also known as mine exploitation. Mineral processing is the next step of the value chain and consists the treatment/valorisation of the raw ore, recovering the existing valuable minerals and producing one or more concentrates that can be considered end-products to feed the manufacturing industry in the case of non-metallic ores and coal, or intermediate products in the case of metallic ores, the metal extraction being carried out by pyrometallurgical smelting or hydrometallurgy [1, 2]. The general scheme of treatment is to liberate the valuable minerals from the interlocked textures by comminution, generating the physical characteristics of the comminuted particles in such a way that suitable forces can be used to separate valuable from gangue particles [3, 4]. Thus, mineral processing could be divided into two fundamental operations: i) liberation of valuable minerals from their waste gangue minerals; ii) separation of particles that contains the valuable minerals from the particles mainly composed by gangue minerals.

In the view of the above, mineral processing is applied to a particle population composed by a mass of comminuted particles that are in conditions to be separated [5]. In this sense, it is crucial to find the properties, called contrast properties, that can differentiate the valuable particles for those non-valuables. There are several properties such as colour, specific gravity, magnetic susceptibility and electric conductivity that must be considered [3]. However, there are two particle properties that are decisive for the success of any separation process: particles size and grade (percent content of the valuable mineral, or chemical element). One of the main objectives of the mineral processing plant is the production of a high-grade concentrate, which can be interpreted as an indicator that the concentration process is only grade-dependent. However, the grade of each particle is a function of its liberation degree, itself loosely dependent on the particle size. The relationship between particle size and grade is quite understandable, because large particles tend to have grades close to the average grade of the raw ore, while fine particles are expected to have particles with extreme grades, respectively, on the

gangue and on the concentrate ranges [5]. The liberation of the valuable minerals from the gangue is accomplished by comminution, which involves crushing and grinding until the adequate particle size is achieved so that the product is a mixture of relatively free particles of valuable mineral and gangue [1]. The understanding of the interaction between size, grade and degree of liberation is a contribution of the work presented in this project.

Mineral liberation is then considered the main key issue in mineral processing flowsheets, being achieved by breaking large pieces of the raw ore into smaller particles which are suitable for the subsequent separation process[6]. Its best definition is the capacity of freeing valuable minerals from the gangue, generating liberated particles composed only by the mineral of interest, allowing for the selective separation of both phases. The mass fraction of particles composed only by valuable mineral is called the degree of liberation, but its calculation is often difficult. If there are weak boundaries between valuable mineral and gangue, which is more frequent in some types of ores (such as sedimentary deposits and coarse textures resulting from some rock-forming processes), the degree of liberation would be higher. Unfortunately, in most cases, the intergrowth between gangue and valuable mineral is very strong, which leads to the production of a large number of locked particles, meaning a lower degree of liberation [7].

For a better understanding of the connection between mineral liberation and comminution, the scheme presented in Fig. 3 shall be analysed. A lump particle represented in a binary way – valuable mineral (dark grey) vs gangue mineral (light grey) was overlaid by a square grid to simulate the fractures generated by the comminution process. A set of smaller particles with different valuable mineral content is generated in which three grade classes of particles can be identified: some have grade above and others below the grade of the original lump and some of these have almost zero grade.

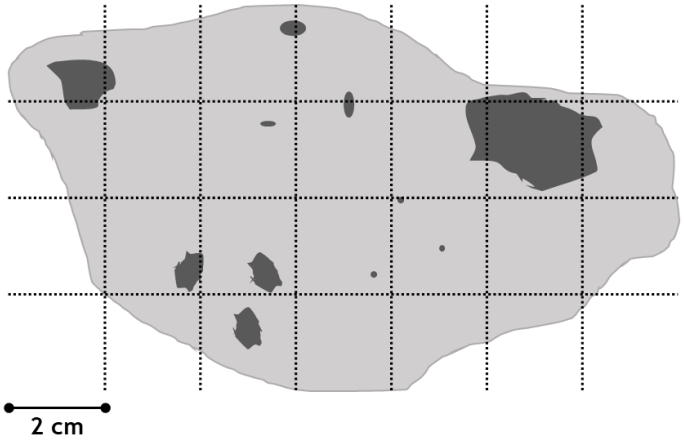

Fig. 3 – Simulation of the comminution of a lump particle binary represented – the valuable mineral is coloured dark grey, and gangue minerals are coloured light grey.

This is exactly the concept of liberation by comminution, in which, a former useless low-grade particle (lump) is replaced by a set of particles that can be classified as good to be recovered (high-grade particles). Others are too poor that are ready to be rejected and the third class of particles that have to continue in the beneficiation process. According to this, in Fig. 4, it is possible to classify all generated particles.

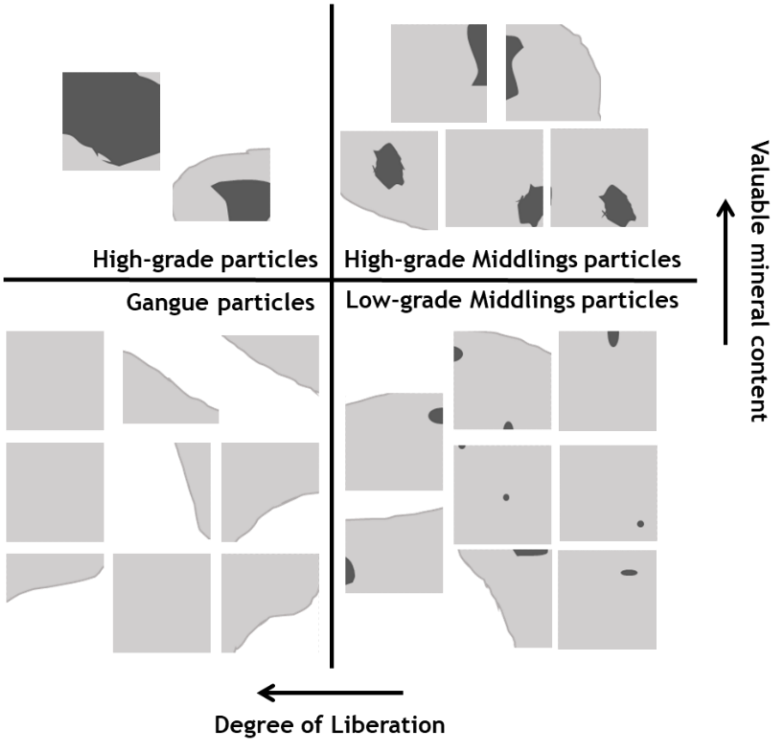

Fig. 4 – Classification of the particles generated by the comminution of a lump particle.

On the left side of the image, it is possible to observe the liberated or almost liberated particles generated by comminution. The recoverable particles are placed in the uppermost quadrant, while the rejectable gangue particles are placed in the lowermost one. On the right side of the image, middlings particles are presented. These particles are not yet liberated, which means that a decision must be taken. A new comminution stage could be applied to enhance its liberation. However, it would lead to higher energy costs and over-grinding. Thus, it is mandatory to carefully analyse what could be done with these particles to improve the process: if middlings are few they can be recirculated back, but when circulating loads tend to grow above a certain level, the comminution flowsheet has to be adjusted to guarantee a better liberation degree.

Considering the discussion presented in the previous paragraphs, the following conclusions could be drawn:

- Mineral liberation assumes a key role in the success of any mining project, due to its impact on comminution and separation stages;
- Comminution aims to generate mineral liberation;
- A good balance between mineral liberation, fine particles production and energy savings are mandatory for any mineral processing plant;

2.1.2 MINERAL PROCESSING EFFICIENCY BASED ON MINERAL LIBERATION

Once understood the concept of mineral liberation, it is important to describe how it affects the efficiency of the mineral processing plant.

Achieving full liberation of the valuable minerals is a very difficult task, and in most cases, it is not strictly necessary for a successful beneficiation process [8-10]. Optimal practical liberation size must be understood as the one that allows for an efficient separation in a technical and economic context. Two important issues for the assessment of the separation efficiency can be identified: i) the contrast property that allows for the differentiation between valuable and gangue particles; ii) the complexity and texture of the ore mineralization that drives the generation of the liberated (valuable and gangue) and locked particles by comminution and, consequently, the levels of property contrast in the particles subjected to separation. An effective balance between these variables is crucial to optimize mineral separation efficiency.

At this moment, two aspects associated with this concept of practical and optimal liberation have to be taken into account. First, it should be realized that the liberation of the most abundant mineral species in the ore is more likely to occur in the earlier comminution stages, while the release of the less abundant minerals will always occur after more intense fragmentation. In most metallic ores, where valuable minerals are clearly a minority, very often the liberation of gangue significantly occurs at crushing sizes and, if so, a Pre-Concentration separation will be technically feasible. However, as at this stage, valuable minerals are not yet liberated, for this purpose it is necessary that there would be sufficient property contrast for the separator to efficiently reject gangue particles, while recovering all particles that host valuable minerals above a given percentage of content. The production of a marketable final concentrate will require the fragmentation of the pre-concentrate until the practical release of the valuable minerals is carried out, which will be recovered in Concentration, as at those fine sizes both valuable and gangue species have reached considerable levels of liberation.

According to this, different processes would require different liberation degrees for a well succeed separation. The nature of the contrast property will define the most suitable separation techniques, the intensity of that contrast will determine the appropriate degree of liberation, and consequently, the optimal particle size.

It is clear that accurate mineralogical studies must be performed to identify the mineralogical assembly of the ore (paragenesis and texture), which is usually carried out by the examination of thin and polished ore sections to determine the *in situ* grain size, the dissemination (minerals distribution) and shape of the mineral aggregates.

An ore showing very fine dissemination will oblige longer grinding times, to achieve an adequate liberation degree, than another one in which valuable mineral occurs in a coarse texture. Mineralogical studies can also provide essential information about the intergrowth between valuable and gangue minerals, which is very important because a strong connection will result in higher production of middlings. Consequently, it would be harder to reach an adequate degree of liberation. Thus, mineralogical information is applied to predict grinding and concentration requirements, feasible concentrate grades and difficulties which may be encountered in the separation of valuable minerals from the host rock.

As a final remark, liberation is produced along with size reduction during the comminution process, according to the optimal liberation size defined by the study of the

contrast property and the ore mineralogy. These variables must be adequately tuned according to the objective of the separation process.

2.1.3 IMAGE ANALYSIS AS A FUNDAMENTAL TOOL TO ASSESS MINERAL LIBERATION

From the previous sections, it is clear that mineral liberation is fully characterized by the grade histogram (wt%). Now is the moment to discuss the available methodologies to acquire useful data for this purpose. Only apparently, it seems to be a simple task, because the experimental determination of the grade histogram (wt%) would imply a huge number of particles to be chemically assayed. The problem is that a great number of particles must be analysed to guarantee the representativeness of the process, which is prohibitively expensive without access to automated means. The development of automated image analysis gave the opportunity to obtain a fast, accurate and cheap characterization of mineral textures for liberation analysis [5, 11].

Since the appearance of the first image analysis methods, many researchers have been extensively studying the utilization of digital textural images to improve the reliability of mineral liberation assessment [12-17]. Peter King, in 1977, developed an automated methodology to acquire mineral liberation data from polished sections based on a system that measured the linear intercept lengths of the pyrite phase [18]. In 1993, King and Schneider, based on the principle of applying thresholding to a signal generated by the reflectance of a mineral to achieve phase discrimination, developed software that uses thresholds to the greyscale histograms from Backscattered Electrons (BSE) images of polished sections, allowing for the automated processing of high-resolution images, producing mineral liberation data [19]. A few years later, quantitative evaluation of materials by scanning electron microscopy (QEM-SEM) appeared, which was the first automated system to apply X-ray spectra to produce maps of digital images from particle sections[20]. In 1997, Mineral Liberation Analyser was presented as an innovative tool for scanning electron microscopy (SEM) based automated mineralogy. This method combines the BSE image analysis with X-ray mineral identification to provide accurate information about mineral liberation [21].

SEM-based automated mineralogy found an extensive application in the mineral processing industry, allowing for the acquisition of valuable information on the composition and mineralogy of the ore and for carrying mineral liberation studies [19,

22-24]. As stated before, this system combines BSE image analysis and X-ray analysis. In the first stage, BSE image analysis allows for the identification of distinct phases in each particle, defining the boundaries between different minerals, as can be seen in Fig. 5. After that, the identification of mineral species is performed by X-ray analysis [19].

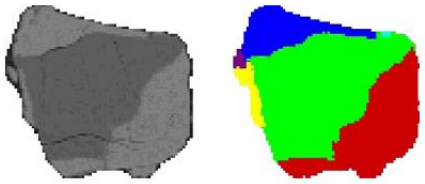

Fig. 5 - Phase identification by BSE image analysis (adapted from [19]).

The mineral liberation analysis using digital images is accomplished by attributing to each mineral a pre-defined colour [25]. There are two possibilities to generate mineral liberation data:

1. Analysis of fragmented particles, as shown in Fig. 5. In this case, image analysis of the particle surface allows for the computation of the particle grade, considering the ratio between the area of valuable mineral and the total area of the particle.
2. Analysis of a digital image that represents an unbroken texture, as shown in Fig. 6. In this case, the process is more complex, because it is necessary to apply an image analysis process that simulates the fragmentation of the ore texture, producing several particles. Notwithstanding the complexity of the process, this methodology allows for the acquirement of the liberation analysis for any desired particle size, which could be a great advantage in relation to the former option. Several methods to simulate fragmentation of digital textures have been developed. Cavalheiro (1984), Bonifazi and Massacci (1995), Soeiro de Carvalho (1995), Guimarães and Durão (2003,2007) and Wielen and Rollinson (2016) gave important contributions on this subject [12, 13, 17, 25, 26].

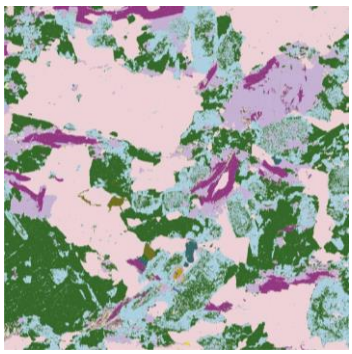

Fig. 6 - Digital image of an ore texture with mineralogical identification [25].

The above referred mineral liberation analysers have their field of application to sub-macroscopic sizes, being not used to characterize macro textures and single particles in the range of several centimetres, e.g. liberation analysis of pre-concentration at crushing sizes. As it will be observed in this work, due to the growing importance of pre-concentration, namely using electronic ore sorting, new analysing technologies have been developed to enhance the accuracy of automated mineralogy applied to coarse particle sizes and drill cores.

The recognition of mineral phases to obtain mineral maps is already possible due to recent technology in drill core scanning (e.g. HyLogger (Fig. 7)), taking advantage of hyperspectral techniques to quantify the textural information on the drill core surface [27-29].

Fig. 7 - GSWA's HyLogger-3 system [27].

Hyperspectral imaging is a non-destructive method, in which drill cores are illuminated and using distinct cameras, installed in the scanner, it is possible to measure light across different wavelength ranges is reflected from the surface of the drill core. A set of arrays of images of the same object/drill core is acquired, using a high number of sensor wavelengths, covering the visible light, near-infrared (NIR), middle-infrared (MIR), long-wavelength-infrared (LWIR) and thermal infrared areas. These data, combined with X-Ray Fluorescence (XRF) data, allow for the identification of the relationships between a sample's chemical stratigraphy and its physical properties like density, permeability, porosity or sonic. The hyperspectral scanners will be capable of

acquiring XRF, magnetic susceptibility, colour spectrophotometry, density and porosity, P-wave velocity, spectral and total natural gamma, and electrical resistivity, all integrated into one automated core logging system. Then, the data is processed and interpreted by a adequate software for automatic mineral identification and quantification [30, 31].

The mineral mapping scenario relies on the knowledge of the spectral features of the mineral classes for their identification. Such features are identified by the analysis of the spectra of clean minerals. Nowadays, hyperspectral analysis generates great sets of data, which must be carefully manipulated. Commonly, per-pixel manual analysis of spectral signatures and machine learning approaches are applied. Band ratios and minimum wavelength maps are useful to evaluate the relative abundance of chemical groups characteristic for specific minerals [29, 32-34]. Spectral angle mapper (SAM) can also be utilized for mineral identification, comparing unknown spectrum and reference spectra. The reference spectra can be acquired from spectral libraries [35]. Thus, hyperspectral technology can be applied to map the mineral distribution in drill cores, as can be seen in Fig. 8, but also in sawing cuts of lump particles, being the most promising methodology to assess mineral liberation data at coarse sizes.

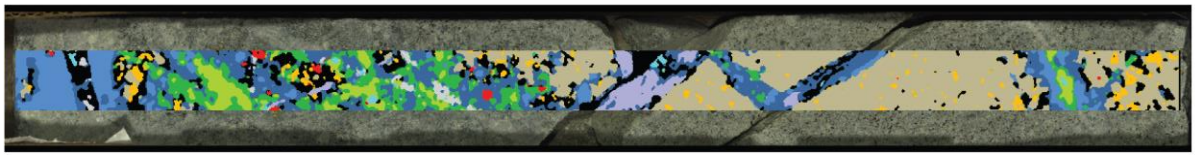

Fig. 8 - Hyperspectral core imaging data is used to identify and map mineralogy on drill cores.

In spite of the positive impact of hyperspectral techniques on the mining industry, innovative techniques are still required to process the hyperspectral data, and new programming skills need to be developed [36]. There are three main challenges to be faced: i) the high quantity of data generated by the hyperspectral sensors claims for highly sensitive detectors, larger data storage capacity and fast computing facilities and; ii) even in high-resolution images, each pixel contains information about a large area, giving a signal of the mineral mixture, mainly when analysing coarse mineral occurrences; additionally, surface properties such as purity, abundance, and grain sizes modify the resulting spectral shape; finally, scanning and noise bring distortions into the signal; to overtake these difficulties, standards of pure mineral spectra, available in databases are used for calibration; iii) another bottleneck is the output in the form of an image with a

continuous distribution, which requires additional efforts to define thresholds and separate different mineral mixtures [28, 34].

Image analysis based on 2D approaches inevitably result in stereological bias in the liberation distribution. For example, a 3-dimensional multi-phased particle, in which only one phase is observed in the 2D analysis can be considered as a liberated particle [8, 10]. Several methods have been proposed to correct the stereological bias based on the estimation of the degree of liberation in three dimensions (3D) by dividing the degree of liberation obtained via 2D measurements by an empirical coefficient called the "locking factor" [8] or based on the conversion of the liberation state obtained in 2D to 3D using a kernel function [11, 37]. It was stated that stereological bias of the degree of liberation depends on the particle texture, being evident that the stereological bias of particles with complex texture is low, that of particles with a simple texture is high. In fact, it has been reported that ores with complex texture exhibit negligible stereological bias [38]. Recently, T. Ueda, T. Oki and T. Koyanaka [39] proposed numerical simulation as an effective approach for establishing a versatile stereological correction model based only in measurable 2D parameters of the ore texture.

2.1.4 THE DESCRIPTOR OF MINERAL LIBERATION – EULER BETA LAW

The access to proper texture characterization and accurate mineral liberation data is the key to build a good prediction of the mineral processing operations. Methodologies based on image analysis make it possible, being a very useful tool for mineral processing engineers [40]. However, the huge amount of raw data obtained from the image analysis systems would be better worked if liberation models are applied for data integration.

Assuming that the grade histogram (wt%), representing the mass distribution by grade fraction, is an appropriate descriptor of the liberation degree of the ore at a given size, it is important to describe the four typical states that characterize liberation degree, as resumed in Table 1.

Table 1 - Description of the four typical liberation states.

Liberation State	Description	Implications
Low liberation	Higher abundance of particles in the intermediate grade classes, which means a high quantity of locked particles	Comminution is needed to promote liberation
Gangue liberation	Existence of significant liberated non-valuable particles, e.g. zero grade and very low-grade particles	Non-valuable and nearly non-valuable particles are rejected, whilst locked particles above a given threshold grade are accepted, which will continue in the next comminution stages to increase liberation
*This state occurs when ore grade is low, as it is in typical metallic ores		
Valuable mineral liberation	Existence of significant liberated valuable particles, e.g. totally free valuables, and high-grade particles	A high-grade concentrate is recovered, whilst locked particles below a given threshold are sent to next comminution steps to increase liberation
*This state occurs when ore valuables are more abundant than gangue		
High Liberation	Both valuables and non-valuables are in the form of free or nearly free particles, with a low number of locked particles	This is the most desired state and sometimes is achieved only after a long residence time comminution

Each liberation state corresponds to a typical histogram shape, which can be observed in Fig. 9.

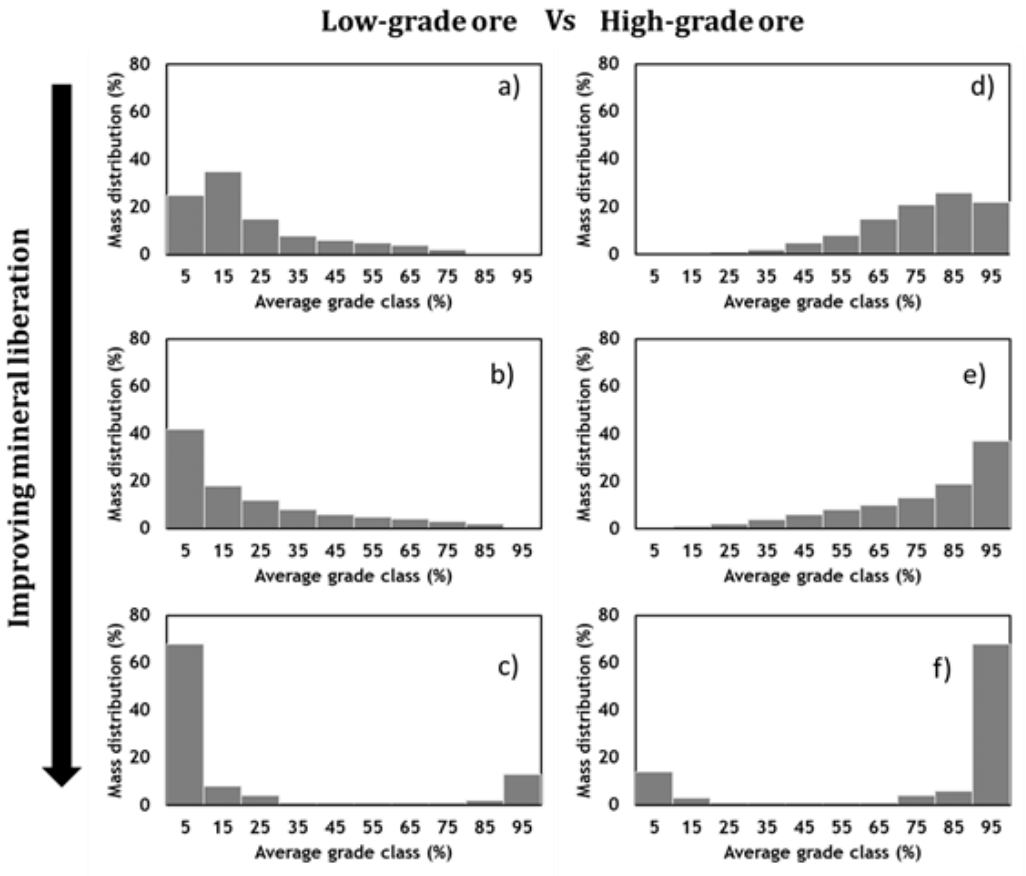

Fig. 9 - Typical histograms of mass distribution by grade class for low and high-grade ores: a) & d) Low degree of liberation; b) & e)Intermediate degree of liberation; c) & f) valuables and gangue liberated.

Each grade histogram (wt%) describes the liberation degree attained in an instantaneous moment of the size reduction process (i.e., it is only a static descriptor). Yet, it is obvious that the comminution process follows the histograms a), b) and c) or d), e) and f) depending on the ore grade, as shown in Fig. 9. From the coarsest to the finest size, it is difficult to make any acceptable prediction of the next stage without using a comminution/liberation model that would be able to integrate the available information. For example, a comminution circuit is producing particles in the size range 20/2mm, a sample of this fraction can be collected and analysed to compute its grade histogram (wt%), which allows assessing the liberation at that point of the comminution circuit. Similarly, if there is an interest in the study of the size fraction 5/2mm another sample must be collected and analyzed.

Liberation models have been the concern of several authors, as dully reported by Giles Barbery in his reference book about Mineral Liberation [41]. In the '70s, Madureira launched a research group in the Mining Department of the Faculty of Engineering of the University of Porto working in this field, which led to the development of a dynamic model allowing for the prediction of the degree of liberation of a mineral system based on the Euler Beta Law [5, 15, 42, 43]. This model, also referred by Giles Barbery, is briefly reported in the following paragraphs.

Euler's Beta function was considered to have adequate properties to fit well the grade histograms (wt%), being able to describe, with a reduced number of parameters, the information contained on the liberation histograms [5, 13]. Eq. 1 show the mathematical expression of Euler's Beta Function.

$$C_t(g|s, g_0) = \beta(g; p, q) = C_{pq}\, g^{p-1}\,(1 - g^{q-1}) \qquad \text{Eq. 1}$$

Where g is the grade of valuable, constrained to the range]0,1[and s is size, being $C_t(g|s,g_0)$ the grade distribution given the size s of an ore averaging g_o grade. C_{pq} is a constant and p and q are parameters that control the Beta function's shape. Thus, the grade histograms (wt%) can be obtained by integrating Eq. 1 and parameters p and q are adjusted to approach experimental data. There are three important characteristics of the Euler's Beta Function that must be highlighted, average (Eq. 2), mode (Eq. 3) and variance (Eq. 4).

$$\bar{g} = \frac{p}{p+q} \qquad \text{Eq. 2}$$

$$g_m = \frac{p-1}{p+q-2} \qquad \text{Eq. 3}$$

$$V_g = \frac{\frac{p \times q}{(p+q)^2}}{p+q+2} \qquad \text{Eq. 4}$$

The authors investigate the variation of the Beta function shape for different p and q parameters, defining the parameters that describe the most typical grade histograms (the same presented in Fig. 9). They found four regions of the P and Q diagram (Fig. 10), in which the Beta function assumes the most typical grade histograms (wt%) – p,q>1; p<1 and q>1; p>1 and q<1; p,q<1.

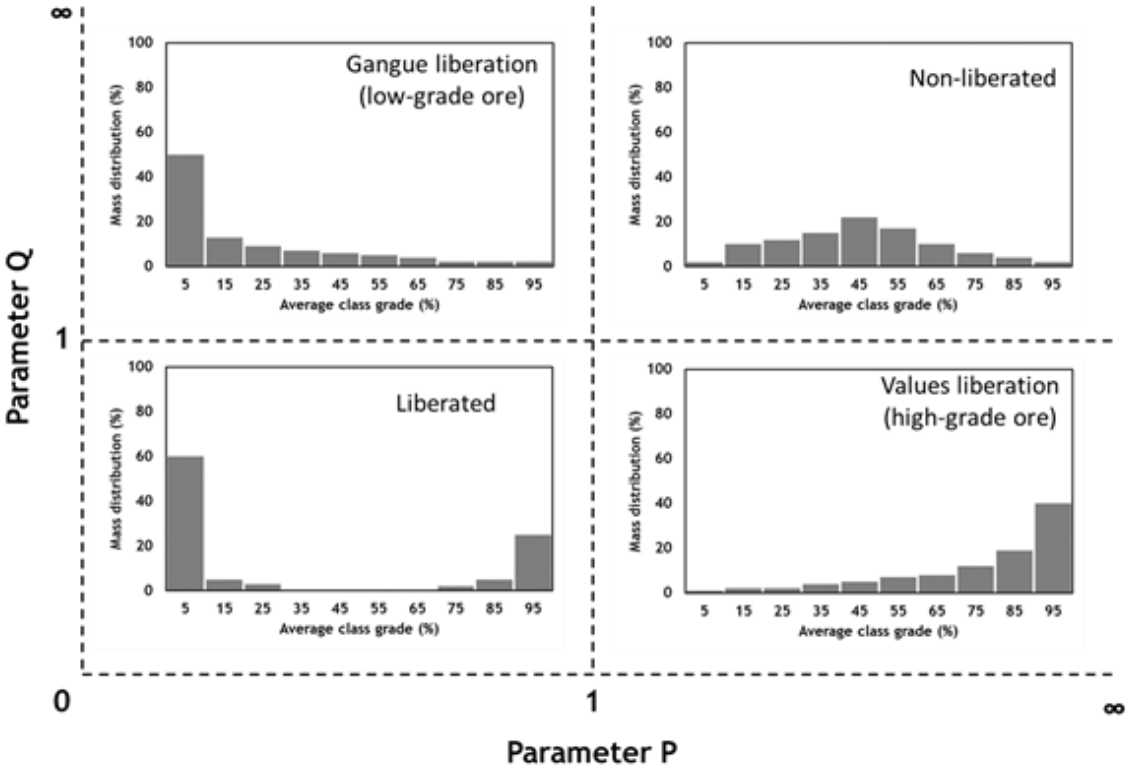

Fig. 10 - Correspondence between the Beta law parameters and the histogram shape.

During this investigation, they also observed that, considering random comminution, the average grade of a certain size fraction ($\bar{y}$) would be size-independent and equal to the average grade of the ore (y^*). Which means that invoking the Eq. 2 it is possible to state the following:

$$\bar{y} = \frac{p}{p+q} = y^* \qquad \text{Eq. 5}$$

Thus, in the case of random comminution, iso-grade lines can be drawn in the p and q diagram, according to Eq. 6.

$$q = p \times \frac{1-\bar{y}}{\bar{y}} \qquad \text{Eq. 6}$$

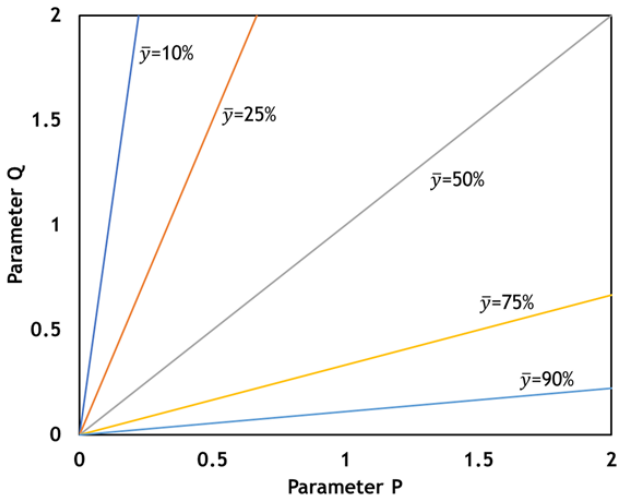

Fig. 11 – Iso-grade lines for different average ore grades.

Then, due to the assumption of random comminution, the variance of the grade y is dependent only on the particle size, which allowed to state that lines of equal-variance are lines of equal-size. Thus, there is a function $\phi(s)$ that can reflect the liberation degree of a certain size fraction, according to the Eq. 7.

$$\phi(s) = p + q \qquad \text{Eq. 7}$$

According to that, equal-size lines can be described as $q = \phi(s) - p$, being representable in the p and q diagram. At this point, it was necessary to calibrate the iso-size lines, as can be observed in Fig. 12, searching for an adequate function that can be fitted to $\phi(s)$. Then, topological law (Eq. 8), which describes the mineral texture of the ore, allowing for the definition of the variance of parameters p and q with the size s was proposed.

$$\phi(s) = K \times s \times e^{K \times s} \qquad \text{Eq. 8}$$

Where K is the so called topological constant that depends on the ore mineral texture and the occurrence size of the valuable mineral, according to this, the authors preferred to discretize the constant K as the ratio between the constant C (depends on the ore texture) and z (the in situ occurrence average size of the grain).

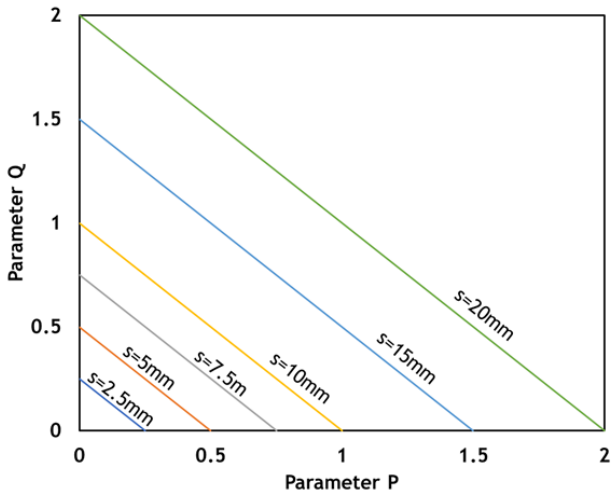

Fig. 12 – Iso-size lines.

The procedure to apply the Euler Beta Function to fit grade histograms (wt%) is summarized in Fig. 13.

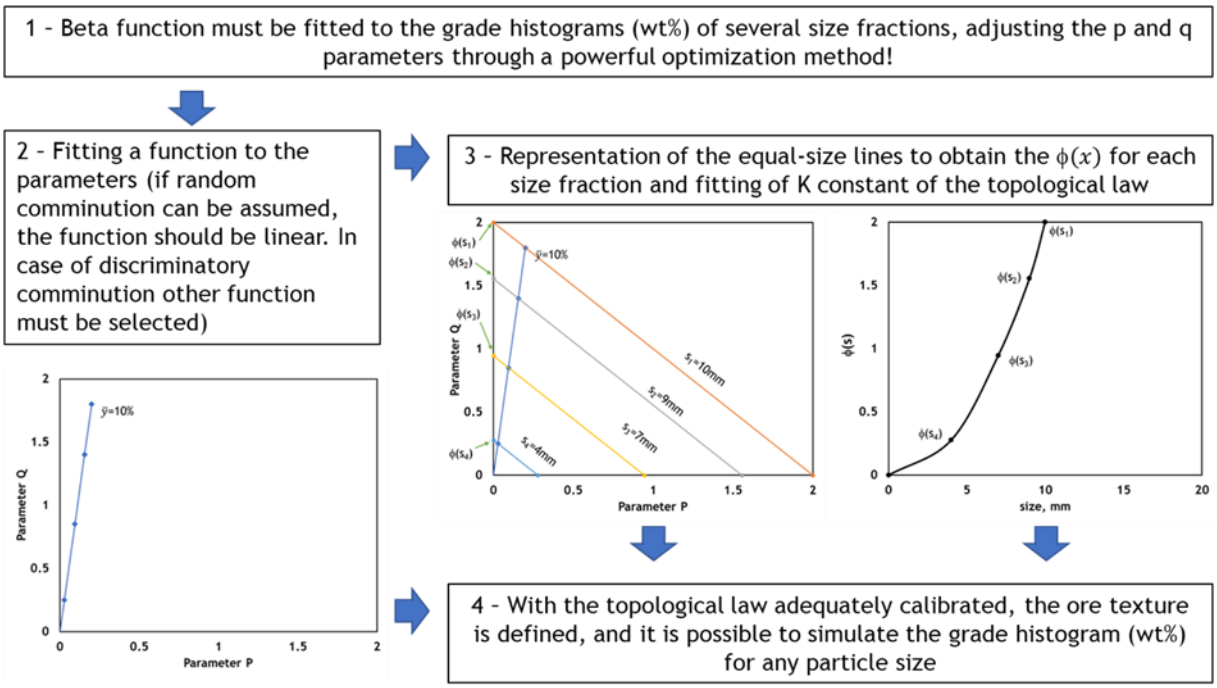

Fig. 13 – Application of Euler Beta Function to simulate grade histograms representing the evolution of liberation with decreasing size.

The main objective of this methodology is the definition of the ore texture typology, through the constant K, that allows for the application of the Beta function, having only as variable the particle size, since p and q were already calibrated during the procedure to

assess the ore typology. This means that it is possible to simulate the grade histogram (wt%) for any given size fraction, reducing the extra demand for mineralogical and chemical analysis.

As mentioned before, the authors demonstrated the applicability of this methodology in the case of random comminution. In the case of discriminatory comminution, the relation between p and q would not be linear, and probably the assumption $\phi(x) = p + q$ would not be verified. Thus, the representation of the p and q diagram would be an appropriate way to assess the comminution behaviour of a specific ore, including the extent of its non-random character.

Madureira, Machado Leite and Cavalheiro have exploited this methodology, however, at that time, the access to experimental grade histograms was a challenging task which has limited more in-depth investigation [5, 13, 15] for years. During this work, some grade histograms (wt%) will be generated, giving the opportunity to exploit this methodology for different case studies.

2.1.5 FINAL REMARKS ON MINERAL LIBERATION

The importance of mineral liberation and its impact on the efficiency of separation processes was discussed in this chapter. In short, the concept presented pretends to demonstrate that mineral liberation impacts in all mineral processing steps, with an emphasis on the comminution and mineral separation stages. Liberation degree increases with the decreasing particle size and comminution costs increase as well. The particle liberation size defines the suitable separation processes and over-grinding usually is harmful to the separation efficiency.

So, it is essential to understand if the main reason for the reduced separator performance is due to the low mineral liberation or due to the low efficiency of the applied equipment.

In this project, ultimate efficiency performance of pre-concentration at crushing sizes, when gangue minerals and host rock material are liberated, and of concentration at grinding sizes, after both valuable and gangue are liberated, will be assessed. For this purpose, mineral liberation data acquisition will be necessary to compute grade histograms that represent each ore case behaviour in each type of separation.

2.2 OVERVIEW OF MINERAL SEPARATION PROCESS – PHYSICAL SEPARATION

Previous reflections on mineral liberation lead to the idea that any Mineral Processing flowsheet can be thought as a sequence of separation sections, each one preceded by a comminution step aiming at generating the practical liberation level necessary to achieve the respective separation objectives. In this approach, the following main sections can be conceived:

- Pre-concentration at crushing sizes, taking advantage of early liberation of gangue minerals and host rock;
- Concentration, developed when valuable and non-valuables are both liberated. In this case, cleaning and/or scavenging operations are widely applied in recirculating circuits to give another chance to misplaced particles or after regrinding to improve liberation of locked particles (true middlings).

2.2.1 PRE-CONCENTRATION AT CRUSHING SIZES

It is possible to admit that one of the main challenges in the mining industry is the mineral processing of low-grade ores. This type of ores causes an increase in the processing plant throughput rates, due to the high quantity of material processed to obtain a concentrated product, which would result in higher energy consumption and operational costs.

It is known that crushing and milling could be considered the primary energy consumption processes in a processing plant. It has been referred that, on average, 44% of the total electricity consumption is dedicated to these activities (Fig. 14).

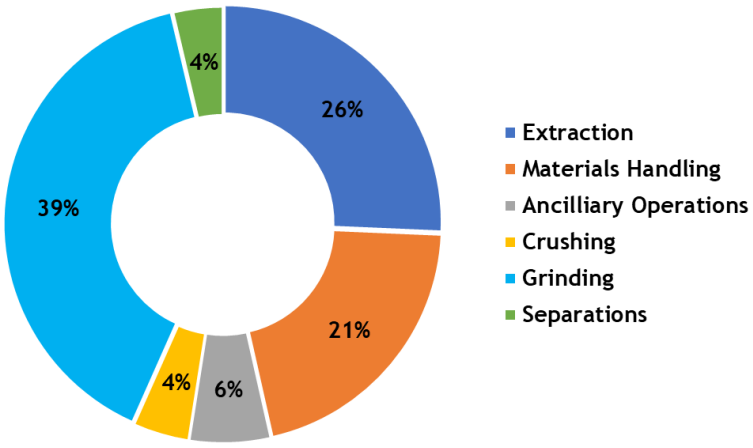

Fig. 14 - Energy consumption by mining stage [44].

Bond (1952), established an empirical equation (Eq. 9) for the required energy, per ton, crushing and milling (W), dependent on the difference between the d_{80} sizes of the feed (d_1) and of the final product (d_2). The working index (WI), is a characteristic of the mechanical properties of the material, which can be experimentally determined by a standard procedure. Significant reduction ratios between d_1 and d_2 could be an economy bottleneck for the subsequent separation steps [45-47].

$$W = 10 \times W_i \left(\frac{1}{\sqrt{d_1}} - \frac{1}{\sqrt{d_2}} \right) \quad \text{Eq. 9}$$

It is commonly accepted that the ore upgrading through coarse waste rejection (pre-concentration) is a viable solution for the discussed problem. In metallic mining, except iron mining, is common that 95-99% of processed material in the comminution stage contains no economic metal value, which means wasted energy. In addition, the reduction of material also represents a decrease in the processing plant capacity, and consequently, lower areas are required for the treatment plant facilities, and less operating costs will be necessary. Another critical issue is the reduction of disposal points along with the processing plant, which also reduces the operating costs related to the disposal of waste material in the tailings impoundment [45, 48, 49]. In these terms, pre-concentration is nowadays considered an exciting issue for the low-impact mining concept, in which a set of actions are promoted with the intent of reducing the impact of mining activities in the surrounding area.

In practical terms, a pre-concentration after the crushing stage can work in the range [50, 5] mm and rejects in de order of magnitude above 75% are often reported. In the case of Panasqueira mine (wolframite ore), mass rejection is of about 85%. This size range is usually achieved by coarse crushing in jaw and cone crushers. For the case of low-grade ores, as can be observed in Fig. 15, when gangue liberation occurs after the crushing circuit, pre-concentration can be applied to reject gangue material. In the case of high-grade ores, pre-concentration can be applied to produce a high-grade product, if valuables are liberated.

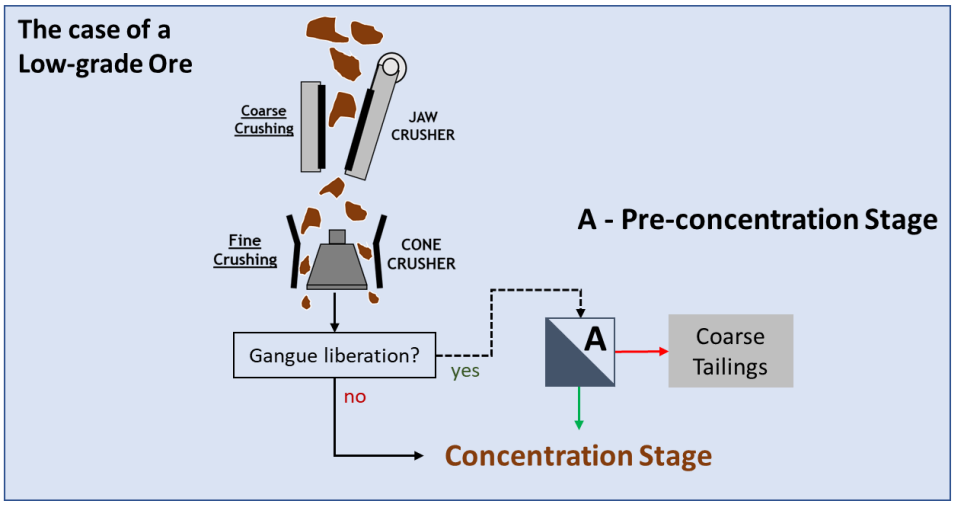

Fig. 15 - Crushing steps adequate for Pre-concentration.

Pre-concentration has found application in worldwide mines, being the main reason for the viability of many processing plants, namely when sublevel and caving mining methods and mechanization were adopted to exploit low-grade mineral deposits. Rejection of coarse uneconomical material produced in early comminution stages has been identified as a plausible operating alternative that can significantly increase energy efficiency and unit metal productivity [50, 51]. Unfortunately, pre-concentration cannot be applied in all mining projects, because its feasibility is dependent on the ore mineralogy, and consequently on the mineral liberation degree at coarse sizes.

2.2.1.1 MINERALOGY CONSTRAINTS AND CONTRAST PROPERTIES

As stated before, the relation between mineralogical features and the contrast property between valuable mineral and gangue are crucial for designing a suitable flowsheet. In the case of pre-concentration, the definition of the contrast property is even more complicated, because its intensity must be enough to allow for the differentiation between the particles to recover and the others to reject at a time when only non-valuables are free or nearly free. Table 2 presents the main contrast properties that can be applied in the pre-concentration step.

Table 2 – Main contrast properties and the applied separation process.

Contrast Property	Applied Technology	Example
Colour	Optical Electronic Sorting	Lepidolite vs Quartz
Density	Dense Media Separation X-ray Sorting Jigging with ragging bed	Wolframite or Cassiterite vs silicates
Magnetic susceptibility	Low-Intensity Magnetic Sep	Magnetite
Crushing behaviour	Scalping by Screening	Hydrothermal veins

A mineralogical study must be well conducted to identify the contrast property clearly, but the distribution of the valuable mineral in the host rock also plays a key role in the pre-concentration feasibility. Thus, if the valuable mineral occurs in fine grains and highly disseminated, the probability of a feasible pre-concentration is very low, because crushed particles will be very homogeneous in what concerns of its valuable mineral content. In the opposite side, if valuable mineral occurs in coarse grains and low dissemination, the feasibility of pre-concentration is higher. The crushing process will tend to produce two types of particles – particles with no valuable mineral content and particles with valuable mineral in a wide range of content. As the occurrence grain is coarser, the higher the grade contrast will be between these two types of particles. However, it is vital to notice that, even when fine dispersion occurs, if the intensity of contrast property is higher, it could be possible to separate non-valuable from valuable particles. Still, it also means that working size will be smaller and the mass rejection will be reduced.

2.2.1.2 THE IMPACT OF MINERAL LIBERATION ON PRE-CONCENTRATION FEASIBILITY

As previously discussed, mineral liberation is a key issue for any separation process. In the next paragraphs, the effect of mineral liberation in the pre-concentration stage is analyzed. Table 3 shows the most typical mineral textures that drive the pre-concentration feasibility.

Table 3 - Effect of mineral liberation on pre-concentration

Liberation in an early crushing stage	Macro-texture
Coarse-grained texture – **About 60% of the particles are pure gangue.** – **40% of mixed particles; rich middlings are dominant.** – **Pre-concentration would be feasible due to the high-contrast between valuable and non-valuable particles.**	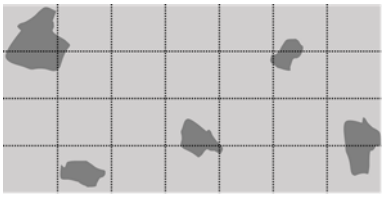
Fine and dispersive texture – **Only about 20% of particles are pure gangue.** – **Low-grade mixed particles are dominant.** – **Pre-concentration would be not recommended.**	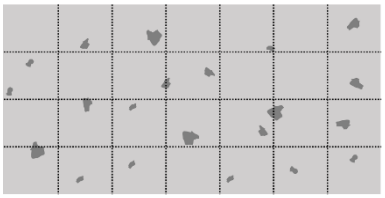
Fine and clustered texture – **About 60% of the particles are pure gangue.** – **40% of mixed particles; intermediate middlings are dominant.** – **Pre-concentration would be feasible, but high selectivity is required.**	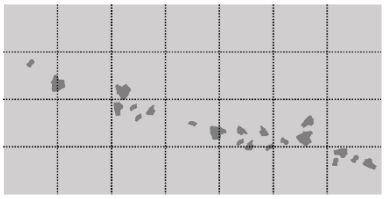
Mix of Coarse and Fine texture – **About 30% of the particles are pure gangue.** – **70% of intermediate and low-grade mixed particles.** – **Pre-concentration would be non-economic unless high selectivity is available.**	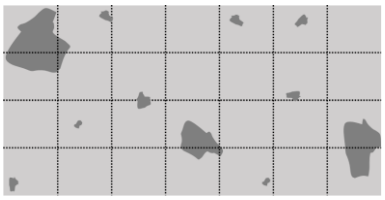

2.2.1.3 PRE-CONCENTRATION METHODS

As aforementioned, pre-concentration could be the key to the success of the mining exploitation of low-grade deposits. Some processes can be applied to reject gangue particles that are already liberated in the early steps of fragmentation. The most typical methods used in of pre-concentration, such as dense media separation, magnetic separation, jigging, size scalping by screening and electronic ore sorting are reviewed in

this section. Due to its rising relevance, a particular focus is given to the electronic sorting methods.

Heavy Media Separation

Heavy Media Separation is a method of separation of particles according their specific gravity (s.g) that corresponds to the practical implementation of the buoyancy principle using a fluid of intermediate density: particles of s.g above the s.g of the fluid sink, while those of density below will float and be discharged by overflow. Instead of using heavy liquids, in the industrial applications, the separation medium is a water suspension of an external heavy solid material, ground at very fine size and at high percent solids so that the suspension exhibits an apparent density enough to operate the desired separation, while maintaining the fluid rheological properties.

This type of separation is be called Heavy Medium Separation (HMS), but also as Dense Medium Separation (DMS) or Sink and Float process [1, 4].

Particles are introduced into the heavy-liquid medium with considerable downward momentum. The fluid body will constrain the particles to flow inside the separating vessel, at velocities that have effects on the separation [52]. The heavy medium used in industrial separations is a thick suspension, or pulp, of some heavy solid in water, which behaves as a heavy liquid, avoiding the application of the toxic and expensive heavy liquids applied in the laboratory. HMS offers some advantages over other gravity processes as it is able to make sharp separations in a wide range of cut-off densities with high efficiency, even in the presence of high percentages of near-density material, is able to deal in a very wide size range (from more than 30 mm to 5 mm) and density can be controlled and maintained under normal conditions for undefined periods [1], which makes the process very appropriate for Pre-Concentration purposes.

Equipment used in Heavy Media separation can work under gravity or in a centrifugal field (Table 4). Gravity separators can be of “tank” or of “drum” type and differences are related to the adopted solution for sink removal. The centrifugal solutions are based hydrocyclones of a traditional or more specific design.

Table 4 - Main types of heavy media separators.

Gravity heavy media separators		
Drum Type	Tank Type	
	Drewboy	Cones
The cylindrical rotating drum is used for mineral and coal separation. The float product overflows on the opposite side of the drum feed (Fig. 16).	Material is fed into the bath at one end and the floats scraped from the opposite end. The sinks are removed at the bottom by vanes.	Material is added to an agitated media. The floats overflow and the sink is removed from the bottom of the cone by pump or by an airlift.
Centrifugal dense medium separators		
Light particles ascend to the surface, while heavier particles sink to the bottom, due to the actuation of centrifugal acceleration. The particle separation rate depends on the magnitude of the gravitational and buoyant forces, which determine the capacity of the separating vessel.		

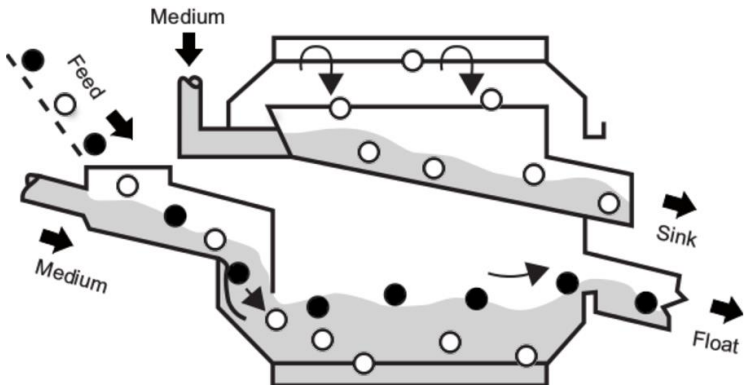

Fig. 16 - Heavy medium separators - Drum Separator[53].

Low-Intensity Magnetic Separation

Magnetic separation takes advantage of the magnetic susceptibility to separate magnetic from non-magnetic minerals. It could be applied for the concentration of magnetic minerals, magnetic contaminants removal and separation of other valuable minerals from the non-magnetic values.

When introduced in a divergent magnetic field, paramagnetic materials tend to concentrate the force lines of the external influencing field and are affected by forces

parallel to those lines in the direction of the growing field intensity. Conversely, diamagnetic material works in a reverse manner, but working forces are very weak and useless for technical purposes. In practical, paramagnetic and ferromagnetic materials are subjected to atractive magnetic forces, while diamagnetic particles are not influenced by the magnetic field and follow simple gravity trajectories[52, 54].

Magnetic separation can be carried out in wet or dry conditions, at different intensities and applying several equipment configurations [55]. Fig. 17 shows the classification of magnetic separators.

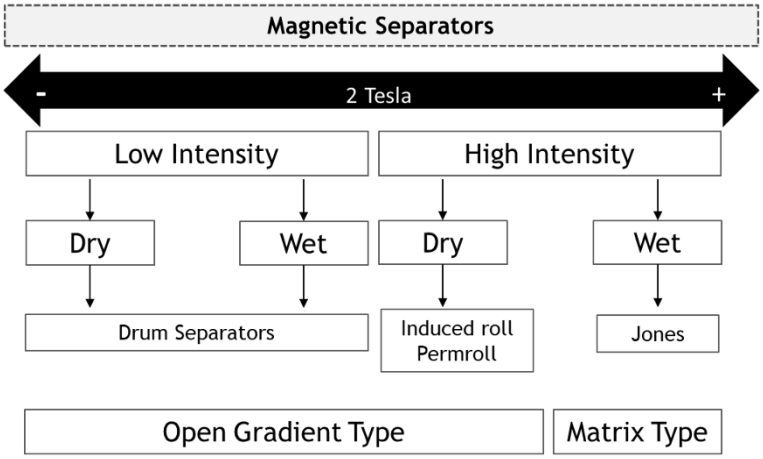

Fig. 17 - Classification of magnetic separators with examples.

Dry magnetic separators can be efficiently applied to particles above 5 mm, being adequate for pre-concentration purposes. Below 5 mm dry magnetic separators loose efficiency, being replaced by wet methods [52].

Dry drum separator is widely applied for magnetic separation, consisting of a rotating drum with several permanent magnets inside. It is very efficient for particles between 25 and 0.1 mm. The rotation speed can be varied, making possible to obtain a high-grade concentrate, when high speeds are applied and high metal recovery when low rotation speeds are employed [59]. Fig. 18 presents the examples of dry drums separators, with two different feed systems.

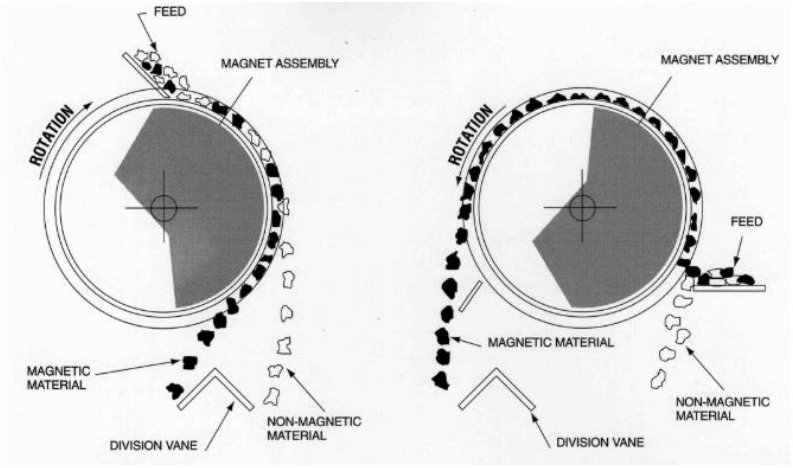

Fig. 18 - Dry low-intensity drum separator [56].

Dry low-intensity separators are indicated for the separation of ferromagnetic ores, being applied in the following processes:

- iron and steel slag treatment;
- production of calcined ilmenite, metal powder and high-grade metal concentrate;
- removal of ferromagnetic particles before high-intensity magnetic separation;
- control iron contamination in glass sand production [57].

Low-intensity magnetic separation only can be applied as a pre-concentration stage when a high magnetic permeability contrast between minerals is observed, which is the case of the ferromagnetic minerals, such as magnetite ores. According to that, efficient separation of weakly paramagnetic minerals only can be achieved by applying high-intensity magnetic fields, higher than 2 T and for treating high capacities matrix type separators are needed and, consequently, it is only available to work with fines sizes.

Permroll is a medium-intensity separator that can be applied in pre-concentration steps. This equipment is widely applied to process sand material for the glass industry, to upgrade wolframite and tin concentrate separately and phosphate rock. It consists of a roll separator made with rare earth elements new generation of permanent magnets, which are capable of generating magnetic fields slightly above 1 T. Permroll can separate highly magnetic mineral as well as weakly paramagnetic particles, due to the presence of a belt over the magnetic roll, avoiding the contact between the roll and the particles [1]. Feed rate, roller belt speed and splitter angle can be adjusted for different final productions. High feed rates and high roller speed will produce high-grade concentrates.

However, the angle/position of the splitter is the most important parameter that controls the concentrate grade [58].

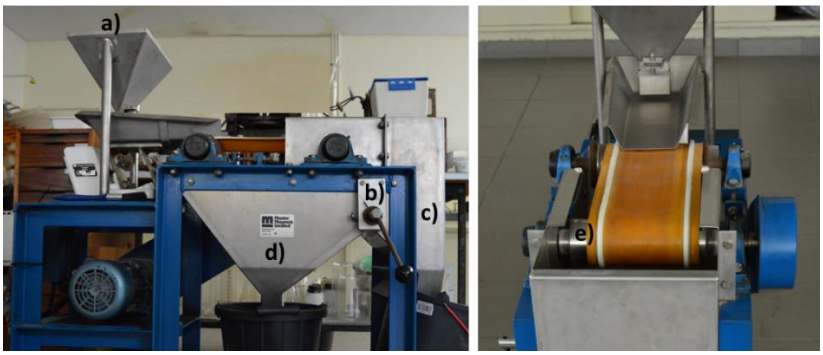

Fig. 19 - Permroll (National Laboratory of Energy and Geology, Portugal): a) feeder; b) angle splitter; c) non-magnetic fraction; d) magnetic fraction; e) roll permanent magnet under the belt.

Jigging

In low capacity mineral processing plants (below 80 t/h) the investment in a Heavy Media Separation is sometimes not profitable and in this case, Jigging has been an alternative for the Pre-Concentration.

A jig is a mechanical concentrator that operates a fluidized bed, whose stratification forms a sequence of layers that offer increasing resistance, from top to bottom, to the penetration of particles with density lower and size higher than those of particles that constitutes de bed. Descending particles exhibiting “penetrating energy”, given by their density and size, higher than the “potential energy” of the layer will be incorporated in the layer. To comply with the layer mass balance, at the same time particles belonging to the layer with the lowest “penetrating energy” will ascend in the fluidized bed.

Bed fluidization is achieved by means of a semi-stationary medium created by pulsating water currents that cross the bed, alternatively upwards and downwards. The bed can be defined as a mixture of solid and liquid, which is expanded when lessened by pulsation and compacted when grains have all settled back into positions so that the jig constitutes their entire support [1, 52].

The particles in the jigging bed can be defined as:

- sub interstitial particles can pass through the interstices of the bed without other than glancing contacts;

- super interstitial particles that are too large to penetrate the interstices without displacement of the bed particles;
- par-interstitial when penetrates the bed along interstitial passages without apparent displacement of the bed particles but stopping each time the bed compacts;
- low-density particles are discharged by overflow on the top of the jig, forming the tailings in the typical case of metallic ores;
- particles of high density are accumulated in the bottom-most layer of the jig to form de "concentrate on the screen" and are discharged intermittently or continuously by specific mechanisms.

In its basic design, the jigging bed is autogenous, i.e., it is formed by particles belonging to the ore itself. However, an external material is sometimes used to form a permanent filtration bed that remains at the bottom of the jig. In this case, the external bed, known as "ragging" takes the place of the "concentrate on the screen" and operates as a "filtering bed" that is only allowed to pass through particles that have density above a certain value, which is defined by the density and size of the ragging. This type of jigging is usually operated in a movable screen and has recently been upgraded in a model patented in Australia as the "inline pressure jig".

There are three main mechanisms inside the jig: vertical movement of the layers, penetration of a jig bed and sorting action in a jig bed. Fig. 20 shows the sequence of movements inside the jig.

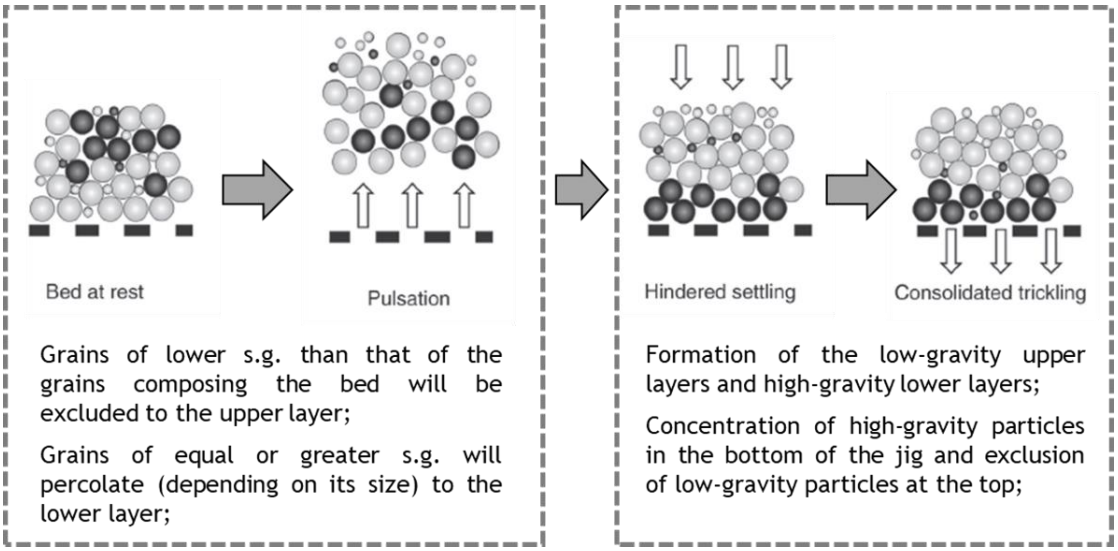

Fig. 20 - Movement sequences inside the Jig and concentration process adapted[4].

Table 5 shows the main types of jigs and bed movement characteristics.

Table 5 - The main types of jigs.

Type of Jig		Bed movement characteristics
The fixed-sieve dilating fluid is caused to pulsate while the bed is stationary	Plunger Jig	Water pulsation through the sieve is caused by reciprocation of a plunger
	Paddle Jig	The impulse comes from a paddle
	Air-pulsated Jig	The movement is due to alternate expansion and contraction of a confined body of air
	Diaphragm Jig	The plunger edges are sealed to the wall of the chamber by a flexible seal, allowing the lounger movement, but preventing water flow
	Pulsating Jig	Water comes to the underside of the screen from a closed chamber supplied with water through a pulsating valve
Movable-sieve - The bed moves in a stationary body of water		
Jigging with ragging - A thick bed of coarse heavy particles (ragging) is placed on a perforated horizontal jig screen. The heavier particles penetrate through the ragging and screen to settle down quickly as concentrate..		

As jigs can operate in the in size range between 20 and 5 mm, they could be applied as pre-concentrators at crushing sizes, being advisable to work with ragging. However, a high specific gravity contrast is required for efficient separation, because in this case, jigs are operating with free gangue and the valuables predominantly in locked particles.

Size Scalping by Screening

Scalping is a screening separation performed, by definition, at a very coarse cut-size (in the range [20, 100] mm), that can be applied after a primary crushing stage when the raw ore exhibits a size-related grade differentiation between lump fragments of the host rock and finer particles belonging the mineralized body. The process takes advantage of

petrological differentiations that occurs, for instance, when hydrothermal quartz veins are installed in siliceous schists or in quartzite, which translate in differences in hardness, friability and crushability.

The generated particles have varied sizes and shapes, allowing for their separation on vibrating screens. Applying the proper screen (by size or shape) it may be possible to reject by oversize a significant amount of barren rock, while the valuable mineral is concentrated in the undersize. This method can be economically efficient when applied to the pre-concentration at crushing sizes [1, 4, 52].

The generated particles own varied sizes and shapes, allowing for their separation on vibrating screens. The most typical example of using selective screening is in the processing of metallic minerals because its typical brittle character allows high-grade particles to concentrate in the finer fractions. The opposite may also happen when the valuable mineral is harder than the gangue minerals, producing concentrate in the higher size fractions [59].

Electronic Ore sorting

Preliminary ore sorting has been applied by handpicking for centuries, using visual observation of the mineralization on the surface of individual stone specimens [1, 60]. However, the technological evolution affords the opportunity to look faster and better than human observation, deeper than the surface and in spectral ranges invisible to the naked eye. Ore sorting has already been used in the mining industry, with some of the earliest application finding use in high-value products such as diamond. In general terms, ore sorting refers to the ability, based on analyzed characteristics determined by on-line sensors, to sort bulk feed material into two or more products. The sorting process starts with the material being fed to a conveyor belt. The particles go through the field of a sensor, which sends a signal to the processor, which decides if the particle should be accepted or rejected according to its properties. The processed signal is conducted to the sorting mechanism, which is programmed to generate the desired classes of particles (Fig. 21), being gangue rejection, high-grade product acceptance or rejection of products based on their contaminant level common applications of ore sorting [61-63].

The electronic sorting process can be described in three main stages:

- Singulation: each particle must be individually examined by the sensor, in a fast process to allow for adequate throughputs. Particles must be evenly distributed, in a single layer, across the conveyor belt. Once analyzed by the sensor, each particle maintain its known speed and position until it reaches the separation zone[64];
- Detection: the system is composed of the sensor and the processor, and it is dependent on the ore. The existence of a contrast property between the minerals to be separated is fundamental for the actuation of the sensor, which will send an electrical signal to the processor to decide if the particle will be accepted or not;
- Ejection: an air/mechanic ejector actuates over the particles according to the processor signal, performing the separation. This system must be fast and accurate;

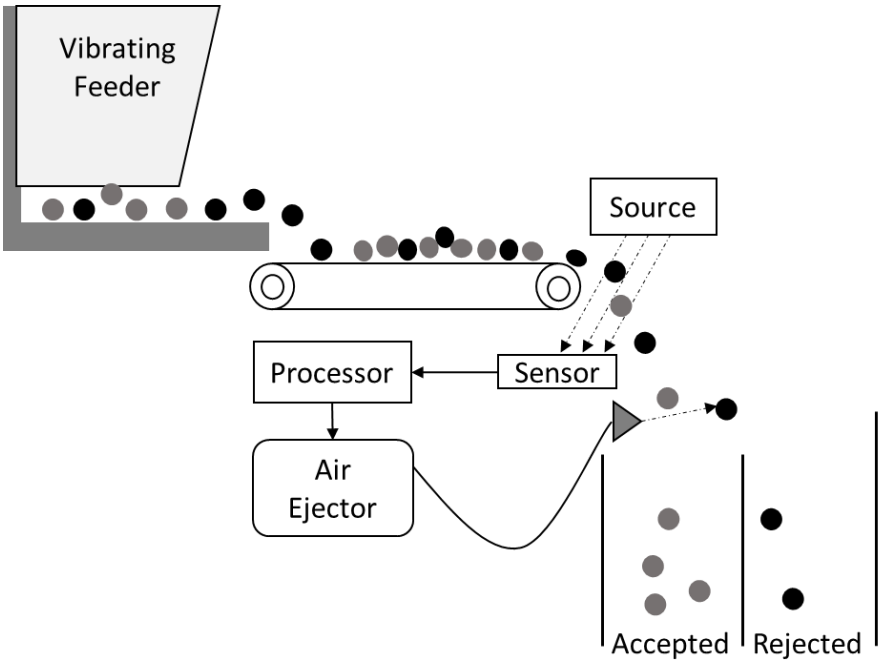

Fig. 21 - Ore Sorting schematic representation.

According to the contrast property of the minerals to be separated, it is possible to select the most appropriate sensor. The sensors can be classified related to the analyzed property: i) surface properties; ii) entire particle properties; iii) secondary properties as colour, reflection, brightness, electric conductivity, density, magnetic susceptibility, and radioactivity; iv) primary properties as chemical and mineral composition. There are several sensor technologies that can be applied to acquire useful particle information to

distinguish valuable and non-valuable particles [65]. Table 6 shows the most applied sensor technologies according to the identified mineral characteristics.

Table 6 - Minerals characteristics and applicable sensor technologies.

Minerals characteristics	Sensor technologies
Transmission of visible radiation, brightness, adsorption and reflection	Optical sensors
Transmitted X-ray radiation	X-ray Transmission
Reflection and adsorption of NIR-radiation	Near-Infrared (NIR)
Reflected X-ray fluorescence under X-ray radiation	X-ray fluorescence
Electrical conductivity and susceptibility	Inductive (metal detector)
Natural radioactivity	Radiometric
Monochromatic reflection/absorption and scattering of laser light	Laser Reflection/Scattering/Fluorescence
Heat conductivity and heat dissipation	Infrared CAMERA (IR)
Light absorption	Infrared Transmission (IRT)
Visible spectrum for transparent and opaque materials	Visible Light Spectrometry (VIS)

Ore sorters have a good prospective future, being effective to reduce the amount of material fed to the milling circuits and reject waste material, avoiding capital and operating expenses, which have been stated as central objectives of pre-concentration. Table 7 presents the main advantages and disadvantages of ore sorting.

Table 7 – Advantages and disadvantages of ore sorting [66].

Advantages	Disadvantages
Reduction of comminution and tailings disposal costs; Rejection of low-grade material; Higher mill feed grade which results in higher recoveries and higher concentrate production; Higher concentrate production and capability working in a wide size range 300-2 mm;	Better results with closely sized feed (top/bottom size 2:1 or 3:1) Coatings (slimes, dust) have an adverse effect on surface-based measurement Cost and noise of compressed air In optical sorting, belt and chute color must be carefully chosen to avoid interference in the process

2.2.2 CONCENTRATION AT GRINDING SIZES

Concentration of high-quality end products (e.g., high mineral/metal grade) is the most notable step in the mineral value chain, which only can be carried out after good levels of the liberation of valuable have been reached. As already mentioned, in general, long residence time comminution is necessary to fully liberate the valuable mineral from the host rock, which will come before the concentration final upgrading stage of the processing plant. This concentrate will be converted into metal in the smelters. Fig. 22 shows a schematic organization of a generic mineral processing diagram considering the interaction between the pre-concentration and concentration steps. Dashed lines represent the optional flows; for example, pre-concentration is only advisable if gangue liberation occurs.

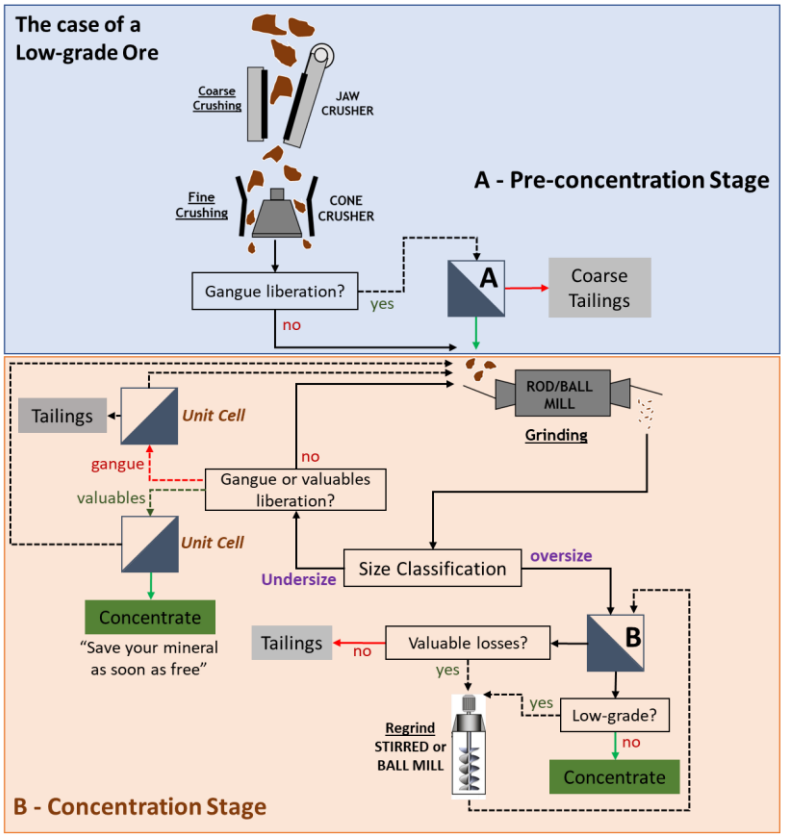

Fig. 22 – Generic Mineral Processing Diagram (adapted from [67]).

In most cases, concentration can be applied after coarse grinding or fine grinding, depending on the liberation size.

It is well known that as far as fine grinding is needed to improve liberation, it is likely that over-grinding will take place, which is a source of increasing energy costs and at the same time is responsible for losses in the finest size fractions (slimes production). Thus, grinding must be well designed to be a good balance between operational costs, mineral liberation and fines/slimes production [1]. The addition of a unit cell in the grinding circuit would be the key to avoid over-grinding. Furthermore, when the aim is to produce high-grade products, the grinding must be followed by a roughing stage and regrinding before a cleaning step. When the driving force is to reach high recovery levels, as the case of treating minerals of high market quotation (e.g. Gold), regrinding before the scavenging will be the choice. The different option for the concentration stage will be presented later.

Concentration is the decisive step on a mineral processing plant, and maybe the most complex, not due to the complexity of the concentration process, but due to its dependence on the precedent steps. In a preliminary phase of any mining project, it is necessary to study the concentration feasibility, to determine the characteristics of

concentrate that would be produced – recovery, grade, presence of contaminants, by-products production, etc. This is crucial for the project economic analysis, being decisive for the assessment of its viability. Several parameters must be carefully analyzed to assess concentration feasibility, mineral liberation, contrast property and the separation method that could be applied.

2.2.2.1 MINERALOGY AND CONTRAST PROPERTIES (NATURAL OR INDUCED)

In view of what has been said, grinding is the key to produce mineral liberation for a successful concentration process. For this objective, ore texture, seen as the "geometry" of the distribution of the valuable in the host rock, is a key issue that affects the liberation progress during the grinding stage. For example, facing a low-grade ore with valuables occurring in small grain size and very disseminated through the host rock will involve an extended grinding circuit, with high energy costs and high fines losses. Table 8 shows examples of different ore texture, averaging the same valuable mineral content and their impact on the liberation by comminution: examples are chosen to design a texture typology of binary ores; grade histograms are calculated as a result of random comminution, simulated by overlapping square grids upon each texture with a mesh of different sizes.

Table 8 - Impact of mineralogical characteristics in the mineral liberation.

Type of occurrence	Grade histogram after grinding	Comments
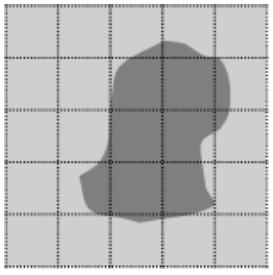	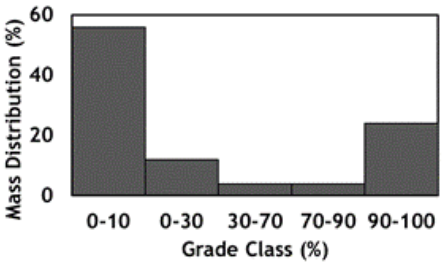	Coarse texture induces significant liberation, even after coarse grinding

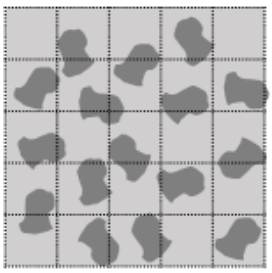

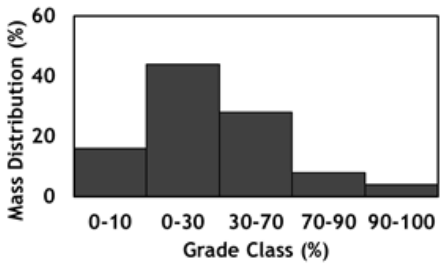

Disseminated texture after coarse grinding generates a non-liberated pattern

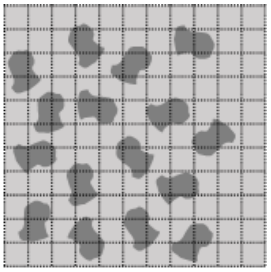

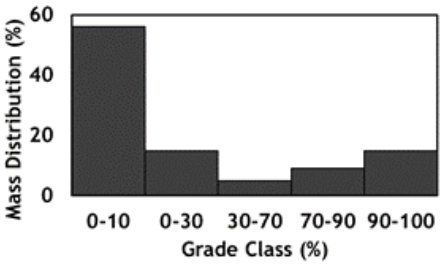

The finer the texture, the finer the grinding must be to achieve a desirable degree of liberation

It is possible to observe that coarse mineral occurrence leads to a noticeable level of liberation after coarse grinding (the pattern of grade histogram is of U-shape). When valuable mineral occurs in finer textures, more intense comminution is necessary to reach equivalent liberation levels.

It is also important to discuss the impact of the contrast property in the concentration step. Table 9 shows the available technology according to the contrast property. It is important to notice that, in some cases, the separation is based in a contrast property that is enhanced or even induced, when it is not natural of the minerals, by the application of chemicals to modify the particles' surface.

Table 9 - Contrast properties and the applied separation process.

Contrast Property	Applied Technology	Example
Magnetic Susceptibility	Magnetic Separation	Magnetite
Density	Gravity Separation	Wolframite
Electrical conductivity	Eletrostatic Separation	Cassiterite
Chemical Surface Modification (induced)	Flotation	Chalcopyrite

The first step is to identify the property that allows for the separation between valuable and non-valuable mineral. The intensity of the contrast between valuable and

gangue will determine the necessary degree of liberation that must be achieved: in the case of a sharp contrast full liberation would not be required, because, for instance, particles averaging 60% of valuables will be easily separated from a gangue particle. In the opposite case, a low contrast would require almost full liberation to produce efficient separations, unless middlings production would greatly increase, which would cause high recirculating ratios.

As a final remark, it can be said that ore texture and contrast property impact directly on the complexity of the concentration flowsheet, it being evident that fine textures and low contrast property lead to more complex diagrams, which are commented in next paragraph.

2.2.2.2 IMPACT OF MINERAL LIBERATION ON CONCENTRATION

As seen in previous paragraphs, the evolution of the various liberation patterns is intimately linked with ore texture and size range achieved by comminution. On the other hand, separation properties and contrast levels are crucial to define the concentration flowsheet. In other words, the generic flowsheets above presented will be decomposed in practical solutions to deal with very specific liberations patterns and the selected contrast properties. In this paragraph, some typical flowsheet options are a matter for reflection, having in mind that process optimization also includes the best decision about the structure of the flowsheet itself.

Before starting the following preliminary remarks could be drawn:

- Grinding all minerals to a fully liberated state is not mandatory to produce effective separations. A stagged process is always the solution, proceeding with successive fragmentation steps followed by separations until achieving the required concentrates under acceptable recovery, together with final tailings and middlings;
- Misplaced middlings can be recirculated back to the separator feed, to give misplaced particle another chance to be well separated;
- Truly locked middlings are also recirculated to the grinding circuits, always avoiding over-grinding as much as possible; sometimes, the excess of very fine particles makes back recirculation unsuitable and advises to use proper equipment adapted to deal with small size particles [3].

As stated above, the concentration stage must be adjusted according to the ore texture. Fig. 23 shows a concentration flowsheet that can be applied to a coarse mineralized ore, meaning that the liberation of valuable can occur at greater size particles. According to this, a unit cell must be included in the closed grinding circuit, following the old concept of mineral processing – "save your mineral as soon as free". The concentration stage must be designed to avoid regrinding, which can be included in the scavenging circuit to reduce mineral losses. It is advisable to recirculate the cleaning tailings, giving another opportunity to misplaced particles.

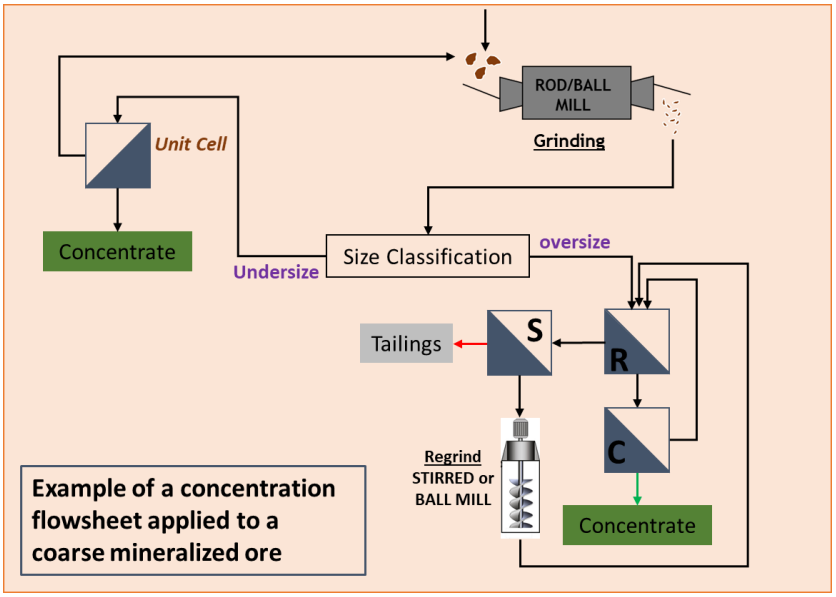

Fig. 23 – Concentration stage applied to a coarse mineralized ore.

Fig. 24 shows another example of processing flowsheet. In this case, the unit cell is included to reject tailing is the closed grinding circuit. Due to the clustered occurrence of valuables, it is expected that gangue starts to be liberated sooner than the valuables, being advisable to reject them as soon as possible, increasing the head grade of the material that goes to the concentration stage. The regrinding of the cleaning tailings and scavenging concentrates can be required to achieve valuables liberation and improve mineral recovery.

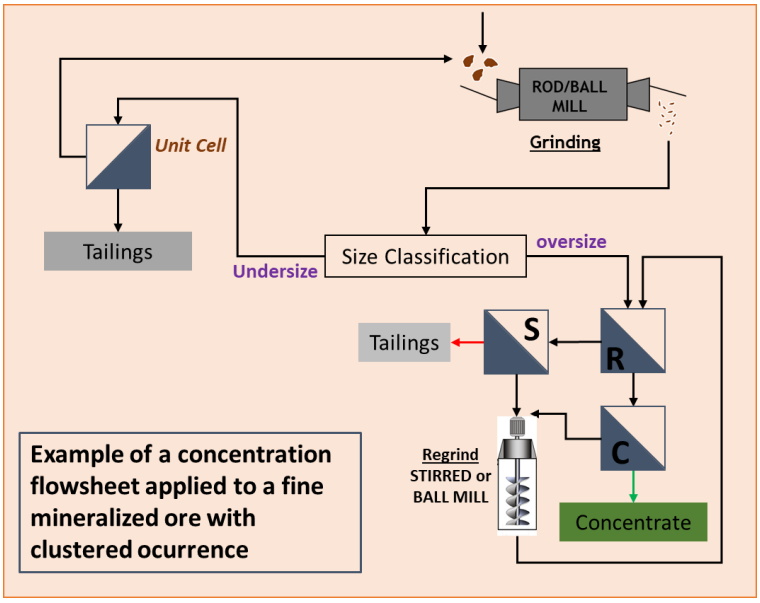

Fig. 24 - Concentration stage applied to a coarse fine mineralized ore with clustered occurrence.

Finally, a processing flowsheet for a fine and disseminated mineral texture is proposed in Fig. 25. In this case, a unit cell would not be recommended since it is expected that gangue and valuable would be liberated at very fine sizes. According to this, roughing tailing will be claimed in the scavenging to avoid mineral losses. The concentrates of both stages can be re-ground to achieve the adequate liberation of valuables to produce a high-grade concentrate.

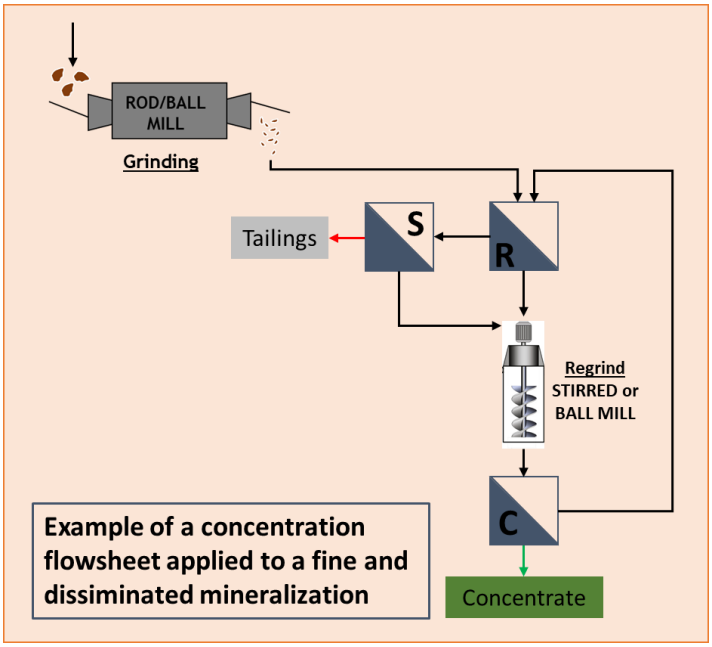

Fig. 25 - Concentration stage applied to a coarse fine and disseminated mineralized ore.

According to the liberation degree, the concentration flowsheet could be manipulated to maximize metal recovery and to reduce energy costs. Size reduction is the key for mineral liberation. However, it must be well coordinated with mineralogical characteristics and contrast property between valuable and gangue minerals, in order to identify which kind of flowsheet could be applied, i.e., according to the analysis of these properties it would be decided, for example, if it is possible to produce a coarse concentrate, or to reject coarse gangue particles before fine grinding.

2.2.2.3 CONCENTRATION METHODS

Concentration is the operation that ensures the final product meets the market requirements for the following metallurgical steps or of other manufacturing industries.

According to that, concentration techniques must be efficient and accurate to attain its objective: producing high-grade concentrates under high recoveries. In the next paragraphs, a brief review of the most applied concentration methods is presented. It should be highlighted that concentration fundamentals are the same as that applied in the pre-concentration, however, dealing with lower size particles (due to the persecution of mineral liberation).

Gravity Separation

The gravity concentration process is the second oldest beneficiation method known to humankind. It is a physical process that exploits the differences in density of minerals, being a cheap and environmentally friendly process. Concentration occurs applying gravity forces on particles, taking advantage of the resistance offered by uneven surfaces of rock or sediment to particle movement across them, against the push of flowing water, often reinforced by the inertia of suspended solids. Gravity separation may be thought as either as a concentration process in which minerals of different densities are separated according to the respective species or as a classification process in which minerals with the same density are separated according to size [52]. This description of the gravity concentration is in line with what was already said about jigging, in which a fluidized bed forms a sequence of stratified layers that offer increasing resistance, from top to bottom, to the penetration of particles with density lower and size higher than those of particles that constitute the bed.

Throughout history, different types of gravity separation devices have been utilized, taking advantage of the difference between valuables and gangue minerals' densities [68]. The most frequent gravity methods are described in Table 10.

Table 10 - Operating principles of the most applied gravity separators.

Separator	Operating principles
Shaking Tables	The fluidization of the bed is operated by a horizontal and asymmetric oscillatory mechanism of a flat table, in which a sequence of longitudinal rifles retain the bed; as bed stratifies, a cross-flow of water washes the upper layers towards the zone of tailings extraction, while the asymmetric oscillatory mechanism pushes the lower layers longitudinally towards the concentrate zone. An intermediate product is collected close the angle of the table as middlings. Table slope, stroke amplitude and frequency, and splitter positions are adjusted as needed. Different riffle height can be used [1].
Sluices and Spirals	Sluices are primaeval gravity separators; the slurry is introduced at the top of the channel: water flowing turbulence vibrates the bed and promotes its fluidization and stratification according to particles densities and size; during the process, a layer of dense particles is accumulated on the bottom of the channel while heavy particles are washed continuously towards the end of the channel. A spiral is a coiled channel around a vertical axis, in which centrifugal actions spread the pulp down and similar fluidization and stratification occur; light particles are radially washed by centrifugal forces, while heavy particles remain in internal positions and are discharged through holes located at the bottom of the channel.
Pinched Sluices and Reichert cones	In the pinched sluice the slurry is fed on the top edge as a monolayer; due to the pinching of the channel heavy particles always travel on the bottom of the flowing film, while light particles tend to climb to the top of the stratification. A narrow transversal opening placed at the end of sluice, allows for the concentrate collection, while tailings pass over the slot and are discharged at the end of the sluice. Reichert Cones are pinched sluices of revolution; the modern technical realization is composed by a superior cone with the apex at the top, used to spread the slurry down to form the monolayer on the lower edge and an inferior cone, with the apex at the bottom, on which is produced the separation effect. A series of cones are required for adequate separation efficiency [1].

Centrifugal	Operate at high rotation speeds in order to reach high G levels, more adequate to process fine material, unrecoverable using the other methods. - Knelson concentrator is a rotating inverted cone with fluidization holes that allow for the water inlet and consequent water fluidization. The fluid will collide with feed slurry, pushing light particles to the central zone of the cone, while heavier particles will be captured in the rings placed in the cone inside the surface. Lighter particles will be displaced over the top of each ring, producing a continuous tails stream to overflow the inner bowl [69]. - Falcon is fed in the central zone. The rotation movement will push the heavier particles to the cone wall, creating two sections, a lower high-density layer and an upper low-density layer. Heavy particles will percolate the layers. The upper layer will be progressively removed by the cone upper zone, caused by water injection[70].

a)  b)  c) 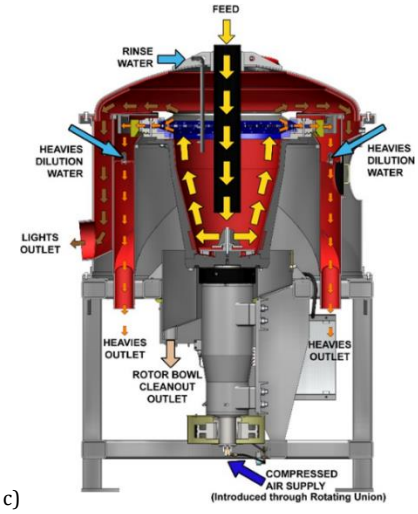

Fig. 26 – Gravity concentrators a) shaking table; b) Humphrey spiral; c) Falcon[71].

Froth Flotation

Froth Flotation allows for minerals separation accordingly with their natural affinity to water (hydrophilic character) or to air (aerophilic character); when both types of particles are present in a water slurry in which air bubbles are generated, aerophilic particles will attach to bubbles and will be collected on a froth that forms on the top of the cell, while hydrophilic particles will be maintained in suspension by an agitator. It is a physical-chemical process that occurs in the interfaces of an aqueous medium with the surface of a solid mineral, in the presence of a gaseous phase. In a simplified way, it occurs by attachment and aggregation between air bubbles and mineral particles, followed by its levitation and transference to a froth phase, which will allow for the collection of a float

product [1, 72, 73]. Aerophilic particles have no affinity to water, such as it naturally occurs with sulphide minerals, which allows for the attachment of particles surface to air bubbles. On the other hand, hydrophilic particles, such as silicates in general, have an affinity to water, which means that they cannot be attached [74]. Fig. 27 presents the main components of a flotation system [75].

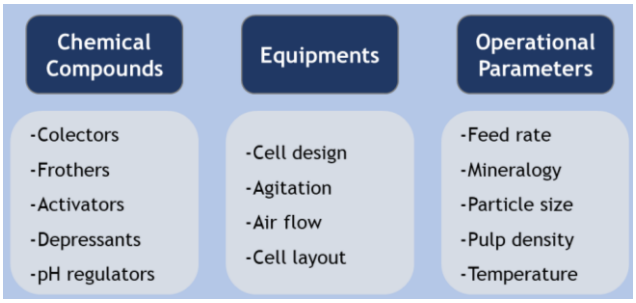

Fig. 27 - Components of a flotation system.

Chemical reagents can be used to enhance, reduce or induce the aerophilic character of specific minerals present in the pulp, playing a key role in the selectivity of froth flotation by changing the natural surface properties of minerals. Table 11 presents the principal action of the reagents applied in flotation.

Table 11 - Main reagents applied to the flotation.

Reagent	Effect
Collectors	Actuate on the surface of valuable minerals, promoting its flotation.
Frothers	Contribute for the stabilization of air bubbles, and for the formation of a froth layer in the top of the flotation cell.
Depressants	Actuate over the surface of the gangue particles, avoiding their activation.
Activators	In general, are applied to prepare the mineral surface to the action of collectors and to neutralize the depressants' function if needed
pH Regulators	Pulp alkalinity plays a significant role in flotation. The selectivity between different minerals is dependent on the pH, i.e., different minerals float at different pH levels. Normally, the pH is chosen according to the stability of the valuable mineral in the Eh/pH diagram.

Flotation cells are composed by an agitator to maintain the particles in suspension and enable the contact between particles and air bubbles. The existence of an air inlet is also fundamental to produce air bubbles. As stated above, valuable particles will attach and aggregate to air bubbles, being carried to the top of the cell, where a froth layer is generated. The froth phase keeps the valuable particles, while gangue particles are drained back to the pulp. A concentrated product is collected at the top of the cell. Tailings are removed from the bottom of the cell. Fig. 28 shows a simplified scheme of a flotation cell.

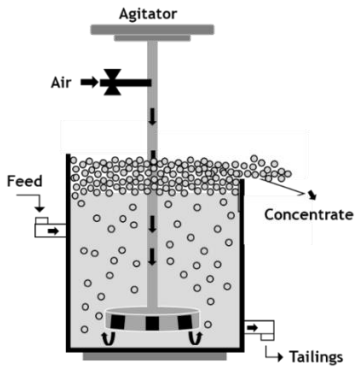

Fig. 28 - Scheme of a flotation cell.

Froth flotation is one of the more frequently applied methods in mineral processing, being preferentially carried out on particles between 0.3 and 0.010mm. Levitation by air bubbles of particles larger than 0.3 mm is difficult, while efficiency is reduced for particles lower than 0.010 mm due to lower probability of collision to the air bubbles [76, 77].

Magnetic Separation

The principles of magnetic separation were already discussed in a previous paragraph for its application in pre-concentration. At that time, a special focus was given to low/medium intensity dry magnetic methods, which are more suitable to deal with ferromagnetic minerals at coarse sizes.

The use of magnetic separation in the concentration stage, working in size range below 5 mm and mainly below 1 mm, has a wider spectrum of application. Wet low-intensity magnetic drums are applied to upgrade final magnetite concentrates, after coarse/fine grinding. Dry high intensity induced roll separators can be used to recover valuable paramagnetic minerals and to remove penalizing minerals in the processing of

sand for the glass industry. Wet high intensity and high gradient matrix separators are used for hematite concentration after very fine grinding and as magnetic filters to improve the final quality of non-metallic products, as in the case of china clay. Wet magnetic separators can be classified as low intensity and high intensity, according to its application.

Table 12 – Description of wet magnetic separators [1, 78, 79].

	Low Intensity	High Intensity
Equipment	Dry/Wet drum open gradient separators	Dry Drum open gradient separators Wet Matrix separator
Working Principles	The magnetic field is created by a permanent magnet. Forces acting on particles are the resultant of the influence of both the Gravity and the Magnetic fields: magnetic particles are attracted to the drum surface, being transported to the concentrate collection zone; tailings follow the gravity trajectory alone, being discharged in the tailings compartment. (Fig. 29).	The magnetic field is created by an electromagnetic coil. A steel mainframe is used to condense the force lines of the field to produce an open gradient field at specific point where the separation will be done in dry mode, or to produce a high volumetric gradient inside a metallic matrix in wet mode: - Dry open gradient separators operate under the same principle of low-intensity dry Drums; - In wet matrix separators, the pulp is fed to a matrix under the influence of the magnetic field; magnetic particles are retained inside the matrix by magnetic forces, while non-magnetics are washed away to the tailings box; the matrix is removed from the influence of the magnetic field and magnetics are washed. - In cryogenic type matrix separators, the magnetic field is generated by an electromagnetic coil made with superconductors that are able to achieve fields above 2,5 T (Fig. 30).

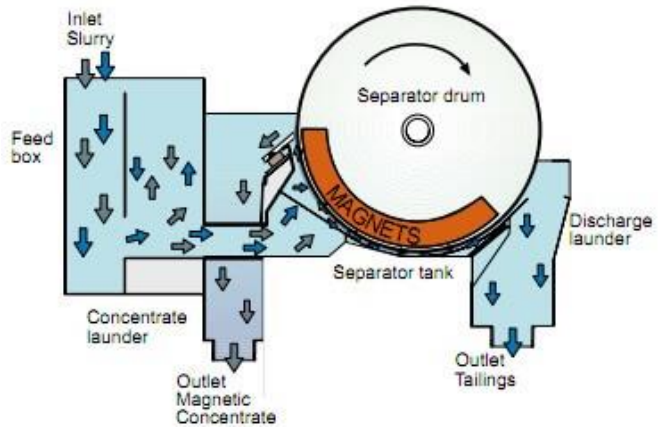

Fig. 29 - Wet low-intensity drum separator[80].

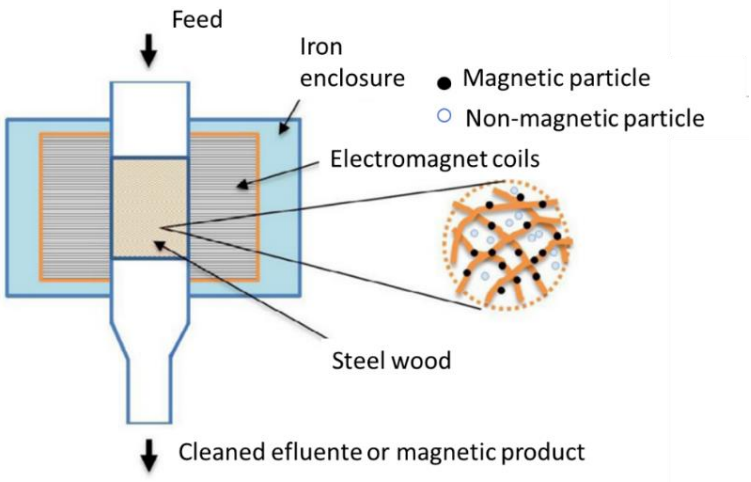

Fig. 30 – High gradient magnetic separator [81].

Electrostatic Separation

Electrostatic separation can be defined as a separation of solid species by means of the electric forces that act on charged or polarized bodies [82]. These forces are generated by the action of an electrostatic field on a charged particle. Consequently, the existence of a source of electric potential to generate the electrostatic field is fundamental [83]. The Separation in an electrostatic separator involves three sequential phases: i) differential charging of the particles; ii) dynamics of the particles on a grounded surface; iii) dynamics of the particles if they leave the surface [84]. Electrostatic separations can be classified as an electrophoresis method when charged particles are involved, and as a dielectrophoresis method, when it involves uncharged particles.

The electrophoresis separation requires a high-intensity field and pre-charging of the particles. The particle charging can be carried out by ion bombardment (corona), induction and friction (tribo effect), originating different types of separators: high tension, electro-static and triboelectric, respectively.

- High tension separators are the more frequently applied in the mining industry. A grounded rotor carries the feed into a corona field where particles are charged by ion bombardment. Conducting particles release to the rotor received negative ions and when they leave the corona field, they are not charged or are only weakly charged according to their conductive character. Non-conducting particles receive a negative charge and after leaving the corona field, they hold the negative ions, for the longest time the more insulating they are. Under the electrostatic field, conducting particles will further be attracted away from the rotor, while non-conducting remain held to the rotor until their negative charge slowly dissipates or are mechanically removed from the rotor
- Static field separators are different from the previous one, due to the particle charging occurs only from a static field. A rotor or a stationary surface can be used as a grounded surface.
- In triboelectric separators, particle/particle and/or particle/surface contacts are responsible for the particles charging. A vibrating bed, a fluidized bed, or a pneumatically conveyed stream of particles can be used to generate the contacts. When particles run between two plate electrodes, they are separated according to the acquired charge.

Finally, dielectrophoresis involves the movement of a neutral particle in a non-uniform electric field. The field moves in the direction of the highest field intensity polarizing the particles, while nonpolarized particles remain unaffected. The practical application of this method is limited [85].

Fig. 31 presents the main types of electrostatic separators discussed.

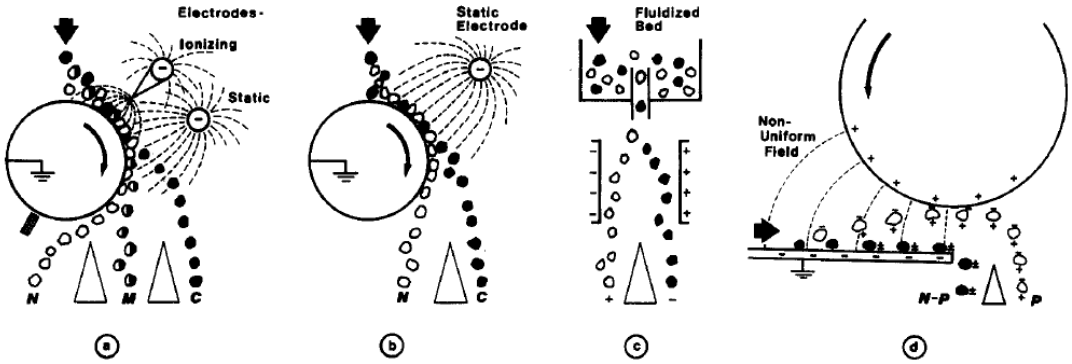

Fig. 31 - The main types of electrostatic separators: a) high tension; b) static field; c) triboseparator; d) dielectrophoretic [84].

2.3 ASSESSMENT OF SEPARATION EFFICIENCY USING UPGRADING CURVES

Once liberation is established in practical terms, the separation efficiency is still dependent on the other three important factors: the separation contrast property and its correlation with the metal grade, the separator technical performance and target metallurgical ratios such as final concentrate grade and recovery. Differences in particle size, shape, density, magnetic susceptibility, electrical conductivity and surface properties are usually exploited to ensure the separation between different minerals.

It is well established that the overall efficiency of complex processes is calculated as the product of the partial efficiencies of each of the components influencing the process. So, in the view of the above, the overall separation efficiency (E_g), is expressed by the product between the liberation efficiency (E_l) (full liberation meaning 100% efficiency) and technical efficiency (E_t) that depends on the technology and equipment configuration (Eq. 10).

$$E_g = E_l \times E_t \qquad \text{Eq. 10}$$

The liberation efficiency, as already discussed, depends on the ore mineralogy and texture and on the comminution that produces the optimal liberation by size reduction. The technical efficiency is a complex function of the contrast property (sharp contrast will allow for successful separations), equipment technical features and the operating conditions. For example, apparent medium density, working pressure and apex size in a

heavy medium cyclone and the stroke frequency, table slope and water flow in a shaking table, are important operational variables that control the efficiency of the separation.

It is well known that the success of any industrial process is highly dependent on the efficiency of the process and, normally, it is expected that efficiency is expressed quantitatively and preferably by a single number. Concentrate grade and recovery are always important terms to take into consideration in efficiency assessment, but a conflicting criterion emerges, i.e., an infinite number of combinations of grade and recovery would result in the same value [86]. Due to that, the use of graphic approaches is recommended that can give a qualitative approach of the separation performance based on the shape of separation curves, or in the case of insufficient data, based on the position of experimental points [79, 87].

In a separation process, the feed is separated into at least two products, presenting quantitative and/or qualitative differences, in at least one property [79].

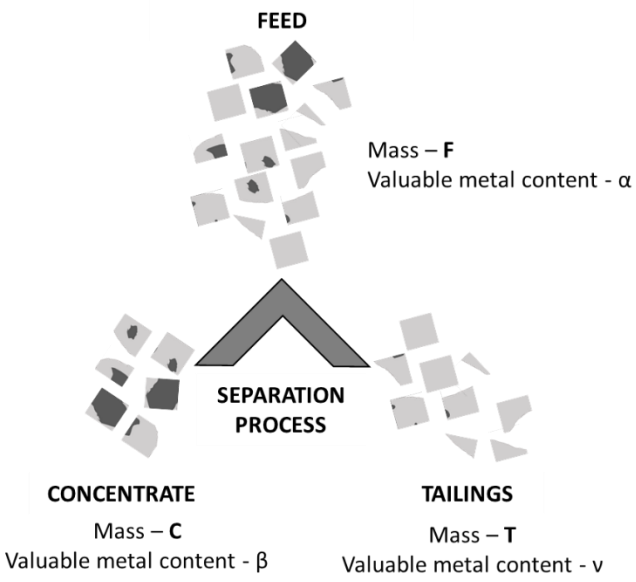

Fig. 32 - Separating process into two products.

The concentrate is the product of interest with a high mineral/metal grade (β), while tailings are normally rejected due to its low grade (ν). The feed is characterized by its mass flow and grade (metal/mineral content). These values are used to compute two important parameters to characterize the separation: Yield (γ) and Recovery (ε): Yield is the percentage of total mass (or mass flow) recovered in the concentrate (Eq. 11);

Recovery is the percentage of mineral/metal recovered in the concentrate (Eq. 12) [1, 3, 79].

$$\gamma = \frac{C}{F} \times 100 \qquad \text{Eq. 11}$$

$$\varepsilon = \frac{C \times \beta}{F \times \alpha} \times 100 \qquad \text{Eq. 12}$$

These equations can be applied to the case where more than two products are obtained, which may occur when middlings products are collected or when there is more than one valuable mineral.

Yield and Recovery combined with the mineral grade are important parameters to assess separation efficiency since they are used to calculate the graphical representations above mentioned, as suitable ways to assess separation efficiency. On account of this, those graphical representations are called upgrading curves and are applied to evaluate and compare the efficiency of different separations. Several upgrading curves have been developed, as Henry's, Mayer's, Halbich's, Fuerstenau's, Stepinski's, Dell's, Hall's, Luszczkiewicz's and Mayer-Drzymala-Tyson-Wheelock Curves. The objectives of these representations are similar, and each one is applied according to the aim of the analysis itself. For example, Fuerstenau curve could be an important tool for the analysis of the selectivity in flotation, because it relates de recovery of target mineral in the flotation concentrate and the recovery of unwanted minerals in the flotation tailings, giving an accurate understanding about the selectivity of the process between those minerals [88].

For the purpose of this work, Henry, Fuerstenau and Mayer upgrading curves will be deeply studied.

2.3.1 HENRY UPGRADING CURVE (WASHABILITY CURVE)

The Henry curve, also called Washability curve due to its application in coal processing, relates the yield obtained for different cut-grades. From the Henry curve, two auxiliary curves are derived, the Concentrates Curve (Yield vs Concentrate average grade) and Tailings Curve (Yield vs Tailings average grade), which are used to assess the evolution of concentrate and tailings grade according to the applied cut-grade, as it is

possible to observe in Fig. 33 [89, 90]. Cumulative Yield is represented in the vertical axis, the horizontal axis being used to represent separation cut-grade, concentrates average grade and tailings average grade, respectively for each curve. When used in coal processing, a sample of the ore feed is separated into several products by applying heavy liquids with different density; products are chemically assayed to determine the ash content; cumulating all products successively, the washability curve is developed, relating yield and ash content [90].

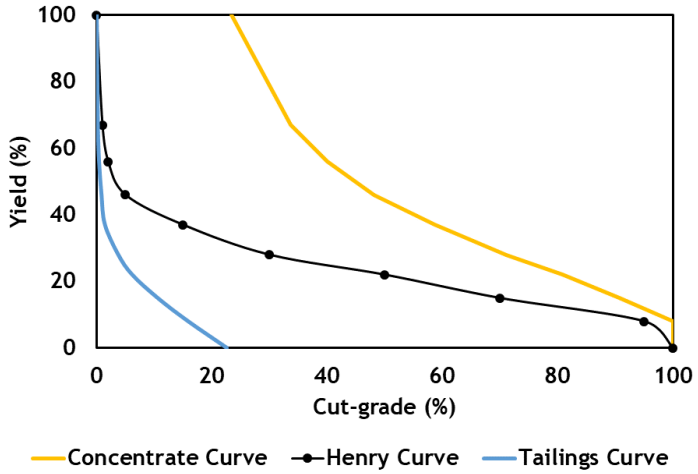

Fig. 33 – Henry curves representation and ideal upgrading and non-upgrading curves identification.

The typical Henry curve representation, shown in Fig. 33, can also include a non-upgrading line and an ideal upgrading line. The former is the limit of no upgrading, which means that no separation occurs, i.e., the valuable content of the concentrate is equal to the feed average metal/mineral content, for any yield. In contrast, the ideal upgrading line represents a perfect separation of a completed liberated ore, which means that the concentrate contains only particles with 100% of valuable. Fig. 34 presents the representation of the Henry curve and the corresponding ideal and non-upgrading curves.

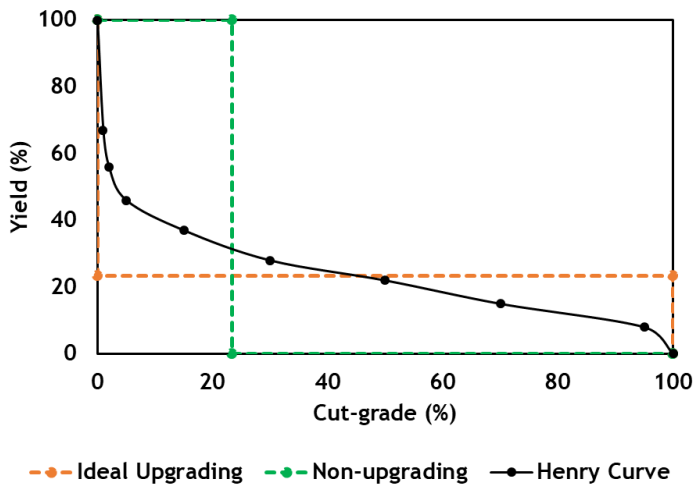

Fig. 34 – Representation of Henry curve and ideal upgrading and non-upgrading indicators.

Now, it is possible to assess the separation efficiency comparing the Henry curve representation with the ideal upgrading and non-upgrading curves. When the Henry curve approaches the "shape" of the ideal upgrading curve and moving away from the "shape" of the non-upgrading curve, the separation becomes more efficient. Fig. 35 shows two examples of separation that were carried out under different efficiencies. It is observed that separation A is more efficient due to its proximity to the ideal upgrading curve. In the opposite direction, separation B is closer to the non-upgrading behaviour, meaning lower separation efficiency.

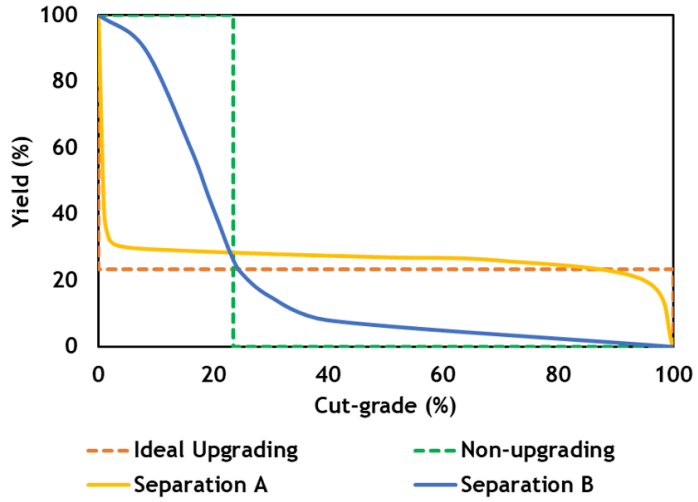

Fig. 35 – Comparison between two different separations using the Henry curve representation.

As mentioned before, Henry curve relates Yield and Cut-grade, being a direct way to understand the % mass that can be rejected at a given cut-grade. It can be a very useful

tool to analyze separation efficiency, for instance, in the case of pre-concentration at crushing sizes. Generally speaking, pre-concentration is feasible when a high % mass can be rejected with low associated losses (high recovery), e.g., a low cut-grade it able to reject a significant amount of material (low yield). In terms of Henry curve, this behaviour corresponds to a curve very close to the y-axis– separation A presented in Fig. 35.

It seems that Henry curve could be a very useful tool to assess the efficiency and feasibility prediction of the separation. However, it is fundamental to consider that it is very difficult to obtain adequate data to build those curves. The determination of the cut-grade applied in a separation process is a difficult task, and this is the main reason for the oversight of this upgrading curve for a long time. However, as will be shown in the thesis, the continuous developments of image analysis and analytical systems for quantitative mineralogy could allow for the obtention of grade histograms that would be adequate data to build the Henry curve representation properly.

2.3.2 MAYER UPGRADING CURVE

Mayer curve, (Fig. 36) relates the Yield (γ) and metal/mineral Recovery (ε), represented in the horizontal and vertical axes, respectively. Working Eq. 11 and Eq. 12, it is easy to mathematically describe the relationship between Yield and Recovery (Eq. 13).

$$\varepsilon = \frac{C \times \beta}{F \times \alpha} \times 100 = \gamma \times \frac{\beta}{\alpha} \times 100 \qquad \text{Eq. 13}$$

This means that, in Mayer representation, the slope of the line that joins the origin to the point that represents the separation is the upgrading ratio between concentrate grade and feed grade: $\left[\frac{\beta}{\alpha}\right]$. Graphically it means that high slopes are a consequence of a faster increase of the recovery when compared to the yield, which commonly occurs at the very beginning of the separation process because only high-grade particles (high liberated particles) are being collected in the concentrate.

As in the case of Henry curve, Mayer Diagram would be completed with the representation of ideal upgrading and non-upgrading lines. The first one represents the perfect separation of a fully liberated ore. In contrast, the second one represents the non-

separation, where the generated products present similar metal/mineral content and equal to feed.

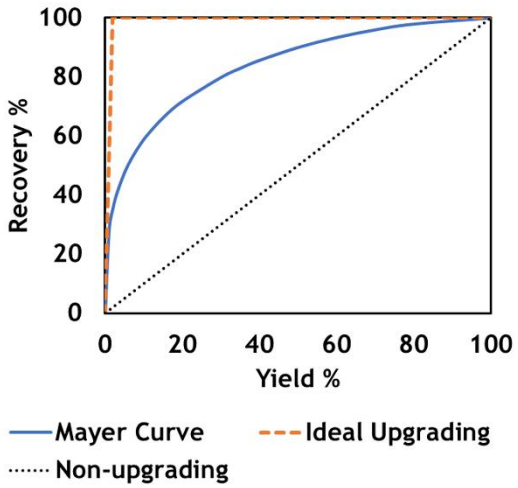

Fig. 36 – Mayer curve representation and ideal upgrading and non-upgrading curves identification.

Using the same concept applied for the Henry curve, separation efficiency can be evaluated by the distance between the Mayer Curve and the Ideal upgrading line. Thus, when the Mayer curve approaches the ideal upgrading line, it means that the upgrading process is more efficient. Lower separation efficiency occurs when the upgrading curve moves towards the non-upgrading line [79, 87]. A comparison between two different separations is presented in Fig. 37, where it is possible to observe that separation B was carried out under a higher efficiency than separation A.

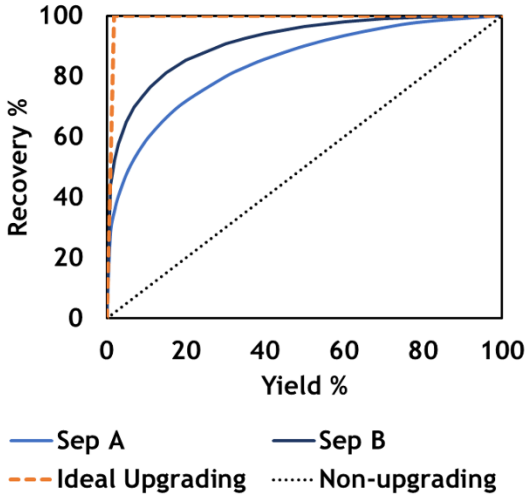

Fig. 37 - Comparison between two separations using the Mayer Diagram.

The Mayer curve is widely applied to assess the separation performance and to compare different separation methods or different configuration/parameters of the same process. It is straightforward to compute and allows for a quick reading of the yield, recovery and gives an adequate graphical view of the upgrading efficiency.

Other important information that can be taken from the Mayer Diagram is the % mass of fully liberated particles, i.e., particles 100% and 0 % content on target mineral, respectively. In fact, it starts from the point [0,0], where the experimental Mayer curve overlaps the ideal upgrading line, meaning that the concentrate is composed only by particles of 100% content (full liberation of target mineral). Thus, the yield at which the overlapping ceases is exactly the amount of full liberated particles. Any other separation showing higher yield and recovery is recovering non-liberated particles of intermediate grade. At the point where Mayer curve and Ideal upgrading line join again, the complement of the yield corresponding to the intercept gives the number of particles wit 0% grade. Fig. 38 presents this analysis – the feed averaging 10% target mineral can be described as composed by three fractions; 5% of liberated mineral (100% mineral); 18% of liberated gangue (0% mineral) and 77% of locked middlings averaging 6,5% mineral (calculations are easily done).

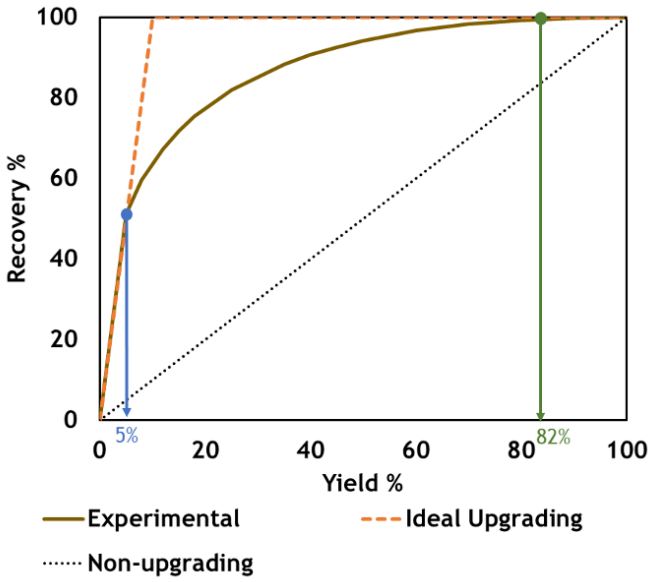

Fig. 38 - Identification of the intersection zones between Mayer curve and ideal upgrading line.

The example demonstrates the usefulness of knowing a Mayer representation. However, its acquisition with adequate accuracy to be helpful for flowsheet simulations is a very difficult task, as it requires access to a considerable set of experimental data. In chapter 5, the application of wise mathematical models to a scarce set of data for generation of Mayer representations, with a high level of discretization, will be presented.

2.3.3 FUERSTENAU UPGRADING CURVE

The Fuerstenau curve relates to the recoveries of a component or components in different products [88, 91]. For example, assuming a binary ore composed by the target mineral and gangue, the Fuerstenau curve represents the recovery of the target mineral in the concentrate ($\varepsilon_{1,c}$) against the recovery of gangue in the tailings ($\varepsilon_{2,t}$), as can be seen in Fig. 39, following Eq. 14 and Eq. 15.

In addition, the author proposed a methodology to assess the separation quality, based on a selectivity index (factor F), which is obtained by the intersection of the Fuerstenau curve with the line $\varepsilon_{1,c} = \varepsilon_{2,t}$. The separation criteria are presented in Table 13.

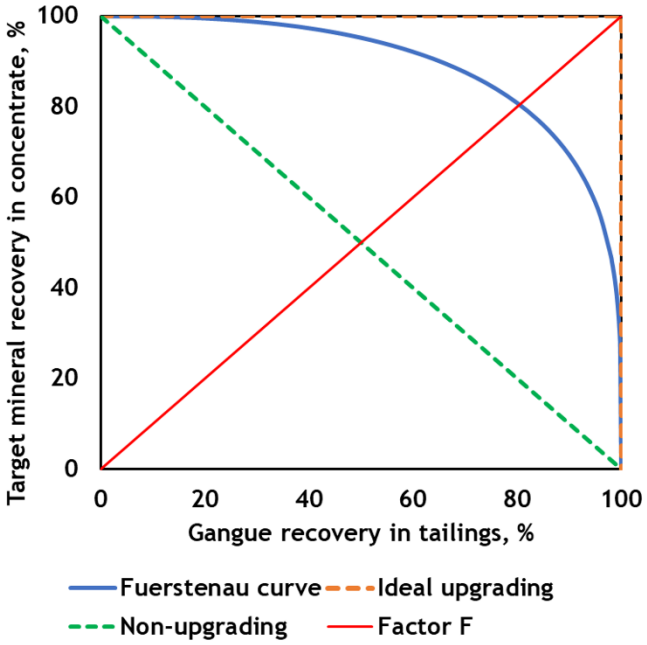

Fig. 39 - Representation of Fuerstenau curve.

$$\varepsilon_{1,c} = \gamma \times \frac{\beta}{\alpha} \times 100 \qquad \text{Eq. 14}$$

$$\varepsilon_{2,t} = (100 - \gamma) \times \frac{100 - \nu}{100 - \alpha} \times 100 \qquad \text{Eq. 15}$$

Table 13 – Separation criteria applied to Fuerstenau curves.

Selectivity Index	Degree of separation
50-60	no separation
60-70	weak separation
70-80	medium separation
80-90	good separation
90-99	very good separation
100	ideal separation

It is also possible to compare the target element recovery in concentrate and the recovery of an unwanted mineral in tailings, which can be very useful to study the selectivity on flotation. This Fuerstenau upgrading curve would be a good choice in specific situations, for instance, as in the case of differential flotation of Cu-Zn complex sulphides, allowing for the assessment of flotation selectivity comparing the recovery of copper in the concentrate and the recovery of zinc in the tailings.

As in the case of the Mayer curve, it is possible to identify two intersection points, as can be seen in Fig. 40. The first one occurs when the target mineral recovery in the concentrate is 100%, meaning that tailings are composed only by 0% grade particles. Similarly, in the reverse case, when the gangue recovery in tailing is 100%, it means that the concentrate is totally composed of particles 100% grade. In this example, it is realized that 22 % the gangue is full liberated (0% grade) and 50% of the target mineral is also full liberated (100% grade). Conversely to the Mayer curve, the simple observation of Fuerstenau curve does not allow for the determination of the number of particles of 0% and 100% grade, it only provides the percentage of the target mineral that occurs in 100%

grade particles and the percentage of gangue that occurs in 0% grade particles. The computation of the mass of particles in each grade fraction would imply data manipulation and assess to the feed grade, which is not provided by the graphical representation. Once feed average grade is known, it is possible to calculate the % mass of mineral and gangue, respectively, fully liberated, however the manipulation of equations Eq. 16 and Eq. 17 is a little more laborious.

Eq. 18, considering ε=50% and β=100% and α=10%, will result in γ=5%. Eq. 19, considering ε=22% and ν=0% and α=10%, will result in γ=80.2%. Those calculations allow determining that the ore is composed by 5% of liberated mineral (100% mineral), 19.8% of liberated gangue (0% mineral) and 75.2% of locked middlings averaging 6.7% mineral.

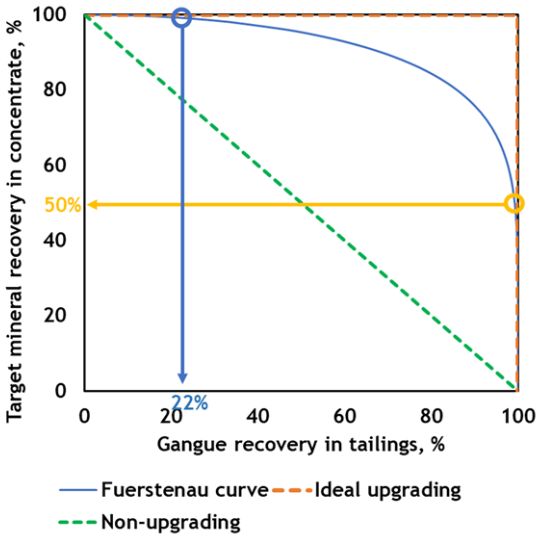

Fig. 40 – Identification of the intersection zones between the Fuerstenau curve and ideal upgrading.

The problem of experimental data insufficiency identified in the case of the Mayer curve remains applicable for the Fuerstenau curve. However, for the Fuerstenau curve, J.Drzymala and H. Ahmed have proposed the adjustment of mathematical equations to experimental data, finding several equations that can fit experimental data with great confidence [92].

2.3.4 GRADE AND RECOVERY UPGRADING CURVE

Another widely applied upgrading curve is the Grade and Recovery, which relates the mineral grade and recovery, as can be observed in Fig. 41.

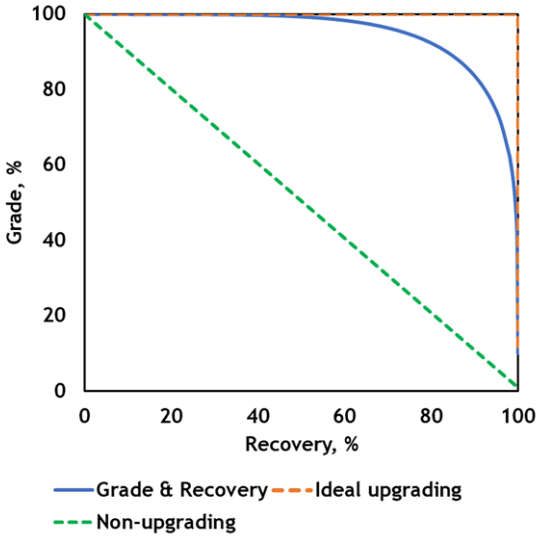

Fig. 41 - Grade and Recovery upgrading curve.

Following the same approach used for Mayer and Fuerstenau graphical representations, the ideal upgrading and non-upgrading lines can be added to frame the Grade and Recovery curve. The separation is more efficient when the curve is closer to the ideal upgrading and far from the non-upgrading. As in the two previous cases, the intersections of the Grade and Recovery curve with the Ideal Upgrading provide some important figures concerning the ore liberation (Fig. 42).

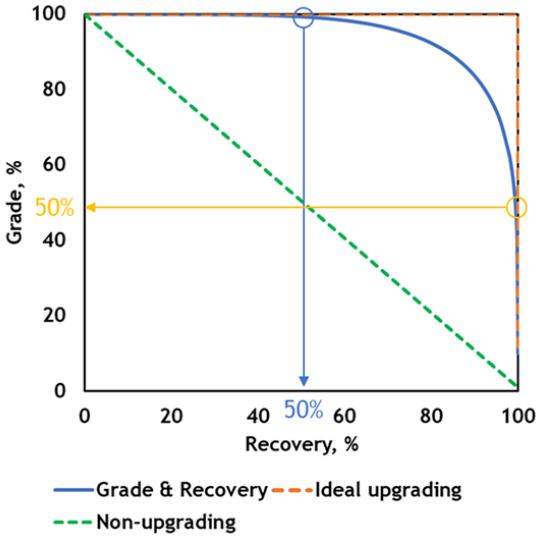

Fig. 42 - Identification of the intersection zones between Grade and Recovery curve and ideal upgrading.

The intersection with the maximum grade line provides the quantity of target mineral present in 100% grade particles, 50% in this case. The second can be read in the maximum recovery line as the concentrate grade when 100% recovery is achieved. As in the case of the Fuerstenau curve, the mass of particles with grade 100% and 0% is not directly obtained from the graphical representation, being required to apply mathematical operations, using the previously presented Eq. 13, which also requires the feed grade (for demonstration purposes, 1% was assumed as feed grade). For this case, the operations are the following:

$$\varepsilon = \gamma \times \frac{\beta}{\alpha} <=> \gamma = \varepsilon \times \frac{\alpha}{\beta} = 0.5 \times \frac{0.1}{1} = 5\%$$

$$\varepsilon = \gamma \times \frac{\beta}{\alpha} <=> \gamma = \varepsilon \times \frac{\alpha}{\beta} = 1 \times \frac{0.1}{0.5} = 20\%$$

According to this, it is possible to determine that 5% mass corresponds to 100% grade particles and 20% corresponds to 0% grade particles.

FINAL REMARKS

Graphical representations are very common in Mineral Processing as adequate tools to evaluate process performance, separation efficiency and forecasting scenarios for flowsheet structure and parameters optimization.

However, when considering overall separation efficiency, as proposed in section 2.3 of this Chapter, the direct use of plotted experimental data in Mayer, Fuerstenau or Grade vs Recovery representations do not allow to distinguish between the liberation efficiency (E_l) and technical efficiency (E_t). For instance, it will be difficult to realize if a worse separation performance was due to an ineffective application of the separation technique, or because the degree of liberation was not enough for the desired successfulness of the separation.

The following challenge was accepted for the present thesis: development of a methodology to assess separation efficiency, based on an integrated comprehension of the process, allowing for the distinction between two components of the overall efficiency as described in Eq. 10.

NOMENCLATURE AND GLOSSARY

C_t	Grade distribution given the size and the ore averaging grade	
g	Grade	
g_0	Ore average grade	
s	Particles size	mm
C_{pq}	Beta function constant	
p,q	Beta function parameters	
$\bar{y}$	Average grade of a certain size fraction	
y^*	Average grade of the ore	
$\phi(s)$	Topological law (function of size)	
K	Topological constant	
d_{80}	80% passing material coefficient	mm
d_1	80% passing coefficient of the feed material	mm
d_2	80% passing coefficient of the crushing product	mm
W	Energy required for crushing and milling per tonne	kWh/t
W_i	Working index	kWh/t
E_g	Overall separation efficiency	
E_l	Liberation efficiency	
E_t	Technical efficiency	
F	Mass of feed	g
C	Mass of Concentrate	g
T	Mass of tailings	g
α	Valuable mineral/metal grade of feed	
β	Valuable mineral/metal grade of concentrate	
ν	Valuable mineral/metal grade of tailings	
γ	Yield	
ε	Recovery	

REFERENCES

1. Wills, B.A., *Minerals Processing Technology*. Five ed. 1992: Pergamon Press.
2. Guilbert, J.M. and C.F. Park, *The Geology of Ore Deposits*. 1986: W.H. Freeman.
3. Pryor, E.J., *Mineral Processing*. 1960, London: Mining Publications.
4. Gupta, A. and D. Yan, *Mineral Processing Design and Operation*. Second Edition ed. 2015: Elsevier.
5. Machado Leite, M.R., *Liberation by size reduction. Consequences and improvements on flotation kinetics*, in *Innovations in Advanced Flotation Technology*, N.A. SERIES, Editor. 1992, Kluwer Academic Publishers. p. 149-170.
6. Mariano, R.A., C.L. Evans and E. Manlapig, *Definition of random and non-random breakage in mineral liberation - A review.* Minerals Engineering, 2016. **94**: p. 51-60.
7. Gray, P.M.J., *Matallurgy of the complex sulphide ores.* Mining magazine, 1984. **315**.
8. Gaudin, A.M., *Principles of Mineral Dressing*, ed. McGraw-Hill. 1939, New York, United States.
9. Gay, S.L., *Simple texture-based liberation modelling of ores.* Minerals Engineering, 2004. **17**: p. 1209-1216.
10. Ueda, T., T. Oki and S. Koyanaka, *Stereological correction method based on sectional texture analysis for the liberation distribution of binary particle systems.* Advanced Powder Technology, 2017. **28**.
11. King, R.P., Schneider, C.L.,, *Stereological correction of linear grade distributions for mineral liberation.* Powder Technology, 1998. **98**: p. 21-37.
12. Bonifazi, G. and P. Massacci, *Ore modelling by minerals topological evaluation.* Minerals Engineering, 1995. **8**(6): p. 649-658.
13. Cavalheiro, A., *Libertação de minério por cominuição - Modelo matemático*, 1984. *Departamento de Engenharia de Minas*,Universidade do Porto, PhD Thesis
14. King, R.P., *A model for the quantitative estimation of mineral liberation by grinding.* International Journal of Mineral Processing, 1979. **6**(3): p. 207-220.
15. Madureira, C.M.N., M.R. Machado Leite, A. Cavalheiro and J. Silva, *Size, Grade and Liberation: a stochastic approach to the fundamental problem of mineral processing*, in *XVI International Mineral Processing Congress*, E.S. Publisher, Editor. 1988: Stockholm.

16. Resabal, V., E.V. Manlapig, C.L. Evans and E.M. Wightman. *A method using 2-D images of particles obtained from SEM-based image analyisis sytem to model mineral liberation in regrind stirred mills*. in *Process Mineralogy '14*. 2014. Cape Town.
17. Guimarães, C. and F. Durão, *2D Simulation Model of mineral particles yielded by discriminatory size reduction.* Minerals Engineering, 2003. **16**: p. 1339-1448.
18. King, R.P., *A model for the quantitative estimation of mineral liberation by grinding*, in *Progress Report No. 1*. 1977, University of Witwatersrand.
19. Fandrich, R., Y. Gu, D. Burrows and K. Moeller, *Modern SEM-based mineral liberation analysis.* Internation Journal of Mineral Processing, 2007. **84**: p. 310-320.
20. Miller, P.R., A.F. Reid and M.A. Zuiderwyk, *QEM*SEM image analysis in the determination of modal assays, mineral associations and mineral liberation*, in *CIM-XIV International Processing Congress*. 1982: Toronto, Canada.
21. Gu, Y. and T. Napier-Munn, *JK/Philips mineral liberation analyzer - an introduce*, in *Minerals Processing '97 Conference*. 1997: Cape Town.
22. Pascoe, R.D., M.R. Power and B. Simpson, *QEMSCAN analysis as a tool for improved understanding of a gravity separator performance.* Minerals Engineering, 2007. **20**: p. 487-495.
23. Reichert, M., C. Gerold, A. Fredriksson, G. Adolfsson and H. Lieberwirth, *Research of iron ore grinding in a vertical-roller-mill.* Minerals Engineering, 2014. **73**: p. 109-115.
24. Leibner, T., K. Bachmann, J. Gutzmer and U.A. Peuker, *MLA-base partition curves for magnetic separation.* Minerals Engineering, 2016. **94**: p. 94-103.
25. Wielen, K.P. and G. Rollinson, *Texture-based analysis of liberation behaviour using Voronoi tessellations.* Minerals Engineering, 2016. **89**: p. 93-107.
26. Guimarães, C. and F. Durão, *Application of a cellular automata based simulation model of size reduction in mineral processing.* Minerals Engineering, 2007. **20**: p. 541-551.
27. Government of Western Australia - Department of Mines, I.R.a.S. 2019 [cited 2019 July]; Available from: http://www.dmp.wa.gov.au/Geological-Survey/HyLogger-spectral-scanner-1396.aspx.
28. Antonov, A. and L. Linsen, *Interactive visual analysis and classification of hyperspectral imaging data.* Journal of Computational Science, 2018. **26**: p. 13-21.

29. Tusa, L., L. Andreani, M. Khodadadzadeh, C. Contreras, P. Ivascanu, R. Gloaguen and J. Gutzmer, *Mineral Mapping and Vein Detection in Hyperspectral Drill-Core Scans: Application to Porphyry-Type Mineralization.* Minerals, 2019. **9**(2).
30. GEOTEK. 2018 [cited 2018 December]; Available from: https://www.geotek.co.uk/2018/01/24/development-of-vnir-swir-hyperspectral-mscl/.
31. Koch, P.-H., C. Lund and J. Rosenkranz, *Automated drill core mineralogical characterization method for texture classification and modal mineralogy estimation for geometallurgy.* Minerals Engineering, 2019. **136**: p. 99-109.
32. Turner, D., B. Rivard and L. Groat. *Rare earth element ore grade estimation of mineralized drill core from hyperspectral imaging spectroscopy*. in *2014 IEEE Geoscience and Remote Sensing Symposium*. 2014.
33. Simpson, M., *Reflectance spectrometry [SWIR] of alteration minerals surrounding the Favona epithermal vein. Waihi vein system, Hauraki Goldfield*. 2015.
34. Wang, L. and C. Zhao, *Hyperspectral Image Processing*. Springer-Verlag Berlin AND Heidelberg Gmbh & Colorado. KG, Springer-Verlag Berlin AND Heidelberg Gmbh & Colorado. K. 2016: Berlin.
35. Farooq, A. *Pixel Purity Index Algorithm and n-Dimensional Visualization for ETM + Image Analysis : A Case of District Vehari*. 2013.
36. Shukla, A. and R. Kot, *An Overview of Hyperspectral Remote Sensing and its applications in various Disciplines.* 2016, 2016. **5**(2): p. 6.
37. Gay, S.L. and R.D. Morrinson, *Using two dimensional sectional distributions to infer three dimensional volumetric distributions - Validation using tomography.* Part. Syst. Charact., 2006. **23**: p. 246-253.
38. Spencer, S. and D. Sutherland, *Stereological correction of mineral liberation grade distributions estimated by single sectioning of particles.* Image Anal. Stereology, 2000. **19**: p. 175-182.
39. Ueda, T., T. Oki and S. Koyanaka, *Stereological bias for spherical particles with various particle compositions.* Advanced Powder Technology, 2016. **27**(4): p. 1828-1838.
40. Zhang, J. and N. Subasigne, *Extraction ore texture information using image analysis.* Mineral Processing and Extractive Metallurgy, 2012. **121**(3).

41. Barbery, G., *Measurement, Simulation and Practical Use in Mineral Processing*. Les Editions GB. 1991, Canada.
42. Barros, E., *Modelagem fenomenológica da flutuação por espumas*, 1995. *Faculty of Engineering*,University of Porto, Master
43. Barros, E., M.R. Machado Leite and A. Cavalheiro, *The use of microscopy data for flotation process control by means of a liberation model.* CIM Bulletin, 2000: p. 4.
44. BCS, I., *Mining Industry Energy Bandwidth Study*, I.T. Program, Editor. 2007, U.S. Department.
45. Lessard, J., Bakker, J., McHugh, L.,, *Development of ore sorting and its impact on mineral processing economics.* Minerals Engineering, 2014. **65**: p. 88-97.
46. Bond, F.C., *Crushing and Grinding Calculations.* Allis-Chalmers Manufacturing Company, 1961: p. 16.
47. de Bakker, J., *Energy use of fine grinding in mineral processing.* Metallurgical Material Tansactions, 2014: p. 8-19.
48. Powel, M.S. and A.R. Bye, *Beyond Mine-to-Mill - Circuit design for energy efficient resource utilisation*, in *AusIMM Tenth Mill Operators' Conference*. 2009: Adelaide. p. 357-364.
49. Bearman, R.A., *Step change in the context of comminution.* Minerals Engineering, 2013. **43-44**.
50. Carrasco, C., L. Keeney and S.G. Walters, *Development of a novel methodology to characterise preferential grade by size deportement and its operational conditions.* Minerals Engineering, 2015. **91**: p. 100-107.
51. Bowman, D.J. and R.A. Bearman, *Coarse waste rejection through size based separation.* Minerals Engineering, 2014. **62**: p. 102-110.
52. Taggart, A.F., *Hanbook of Mineral Dressing*, ed. W.E.H. Series. 1945.
53. Meyer, E.J. and I.K. Craig, *Dynamic model for a dense medium drum separator in coal beneficiation.* Minerals Engineering, 2015.
54. Lopes, V., *Caracterização experimental de sistemas particulados e quantificadores de operações de concentração em processamento de minérios.*, 2015. *Mining Department*,University of Porto, Master
55. Dobbins, M., J. Domenico and P. Dunn, *A discussion of magnetic separation techniques for concentrating ilmenite and chromite ores*, in *6th International Heavy Minerals Conference*, T.S.A.I.o.M.a. Metallurgy, Editor. 2007: South Africa.

56. industries, A. *Magnetic Separation*. 2017 [cited 2017 24th October]; Available from: https://allmag.co.za/drum-separators.
57. Corporation, M. *Metso Mining*. 2017 [cited 2017 24th october]; Available from: www.mtso.com/products/separation/lims-dry-drum/.
58. Koca, H., S. Koca and O.M. Kockar, *Uprgrading of Kutahya region lignites by mild pyrolysis and high intensity dry magnetici separation.* Minerals Engineering, 2000. **13**(6): p. 657-661.
59. Zuo, W., Fengnian, S., Manlapig, E.,, *Pre-concentration of copper ores by high voltage pulses. Part 1: Principle and major findings.* Minerals Engineering, 2015. **79**: p. 306-314.
60. Newton, J., *Extractive Metallurgy*. 1959: Wiley.
61. Cutmore, N.G., Liu, Y., Middleton, A.G.,, *Ore characterisation and sorting.* Minerals Engineering, 1997. **10**: p. 421-426.
62. Tomra. *Diamonds*. 2013 [cited 2016; Available from: www.tomra.com.
63. Von Ketelhodt, L., *Sensor based sorting: new developments*, in *Mintek 75th Anniversary Conference*. 2009.
64. Barton, P.J. and H. Schmid, *The application of Laser/Photometric sorting techniques to ore sorting processes*, in *12th Internationa Mineral Processing Congress*. 1977.
65. Knapp, H., K. Neubert, C. Schropp and H. Wotruba, *Viable Applications of Sensor-Based Sorting for the Processing of Mineral Resources.* ChemBioEng Reviews 2014. **1**: p. 86-95.
66. Fitzpatrick, R., Pascoe, R.D., Glass, H.J.,. *Automated/sensor based sorting research at camborne school of Mines*. in *MES Mineral Processing Symposium 2015*. 2015.
67. Machado Leite, M.R. and A. Futuro, *Generic Mineral Processing Diagram*. 2013, Faculty of Engineering of University of Porto: Mineral Processing Course.
68. Abols, J.A. and P.M. Grady, *Maximizing Gravity Recovery through the Application of Multiple Gravity Devices*, G. Systems, Editor.: Vancouver, Canada.
69. Ancia, P., J. Frenay and P. Dandois, *Comparison of the Knelson and Falcon centrifugal separators*, in *Mozley International Conference*. 1997: Falmouth.
70. Laplante, A.R., M. Buonvino, J. Robitaille and K. Mikulash. *The Falcon Concetrator*. in *25th Annual Canadian Mineral Processor Conference*. 1993. Ottawa.
71. Commons, W. *Falcon Continuous Concentrator*. 2011 [cited 2020; Available from: https://commons.wikimedia.org/wiki/File:Falcon_Continuous_Concentrator.jpg.

72. Kowalczuk, P.B. and J. Drzymala, *Selectivity and power of frothers in copper ore flotation.* Physocochemical Problems of Mineral Processing, 2017. **53**(1): p. 515-523.
73. Sousa, R., A. Futuro, C. Setas Pires and M. Machado Leite, *Froth Flotation of Aljustrel Sulphide Complex Ore.* Physocochemical Problems of Mineral Processing, 2016. **53**(2): p. 758-769.
74. Fuerstanau, M.C., J.D. Miller and M.C. Kuhn, *Chemistry of Flotation.* Society of Mining Engineers, 1985: p. 1-14.
75. Klimpel, *The influence of frother structure on industrial coal flotation, high efficiency coal preparation*. Society for Mining, Metallurgy, and Exploration. 1995, Littelon, (EUA).
76. Fuerstanau, M.C. and R.H. Urbina, *Flotation Fundamentals*, ed. M.D. Inc. 1987, New York and Basel.
77. Sousa, R., *Estudo da Flutuação de Minérios de Sulfuretos Maciços - Aljustrel*, 2014. *Engenharia de Minas*,Faculdade de Engenharia da Universidade do Porto, Master
78. Sierra, C., J. Martínez, J.M. Menéndez-Aguado, E. Afif and J.R. Gallego, *High intensity magnetic separation for the clean-up of a site polluted by lead metallurgy.* Journal of Hazardous Materials, 2013. **248**: p. 194-201.
79. Drzymala, J., *Mineral Processing - Foundations of theory and practice of minerallurgy*, ed. W.U.o. Technology. 2007.
80. Metallurgist. *Wet High Intensity Magnetic Separation*. 2017 [cited 2020; Available from: https://www.911metallurgist.com/whim-wet-high-intensity-magnetic/.
81. Ge, W., A. Encinas, E. Araujo and S. Song, *Magnetic matrices used in high gradient magnetic separation (HGMS): A review.* Results in Physics, 2017. **7**: p. 4278-4286.
82. Inculet, I.I., G.S.P. Castle and J.D. Brown, *Electrostatic separation of plastics for recycling.* Part Sci. Technology, 1998. **16**: p. 91-100.
83. Inculet, I.I., *Electrostatic Mineral Separation*, ed. D.J.F. Hughes. 1984: Research Studies Press.
84. Kelly, E.G. and D.J. Spottiswood, *The theory of electrostatic separations: a review part III. The separation of particles.* Minerals Engineering, 1988. **2**: p. 337-349.
85. Jordan, C.E., *A continuos dielectric separator for mineral beneficiation.* US Bureau of Mines, Report of Investigations, 1979. **8437**.
86. Kelly, E.G. and D.J. Spottiswood, *Introduction to mineral processing*. 1982: Wiley.

87. Sousa, R., B. Simons, K. Bru, A.B. de Sousa, G. Rollinson, J. Andersen, M. Martin and M. Machado Leite, *Use of mineral liberation quantitative data to assess separation efficiency in mineral processing – Some case studies.* Minerals Engineering, 2018. **127**: p. 134-142.
88. Dryzmala, J., *Atlas of upgrading curves used in separation and mineal science and technology.* Physocochemical Problems of Mineral Processing, 2006. **40**: p. 19-29.
89. Henry, *Le lavage des charbons.* Revue Universelle, 1905. **V**: p. 274.
90. Dryzmala, J., *Atlas of upgrading curves used in separation and mineral science and technology (Part II).* Physocochemical Problems of Mineral Processing, 2007. **41**: p. 27-35.
91. Fuerstenau, D.W., *Coal surface control for advanced fine coal flotation*. 1988-1992, University of California, University of Columbia, University of Utah and Praxis Engineers Inc: California.
92. Drzymala, J. and H.A.M. Ahmed, *Mathematical equations for approximation of separation results using the Fuerstenau upgrading curves.* International Journal of Mineral Processing, 2005. **76**(1): p. 55-65.

3 Materials and Methods

3.1 BASICS OF THE PURPOSED METHODOLOGY

As mentioned before, the focus and the principal aim of this work was the development of a novel approach to assess the efficiency of Separation in mineral processing – Pre-concentration and Concentration. This was highly stimulated by the immensity of experimental data generated during the execution of the FAME project, which became a challenge for the development of a new vision for data analysis. The conventional comparison between upgrading curves is made to obtain information about the overall efficiency of the separation. However, it is not possible to distinguish the reasons behind the separation inefficiency, that can be caused by the lack of liberation or by technical problems related to the tuning of the separator. In line with this, a new methodology for separation efficiency assessment was developed to be applied to two FAME case studies – scheelite ore from São Pedro das Águias skarn deposit and lepidolite ore from Alvarrões pegmatite, both in Beira Alta region in Portugal.

The main steps of this work are presented in Fig. 43, where it is possible to observe that the methodology to assess separation efficiency can be split into two main parts.

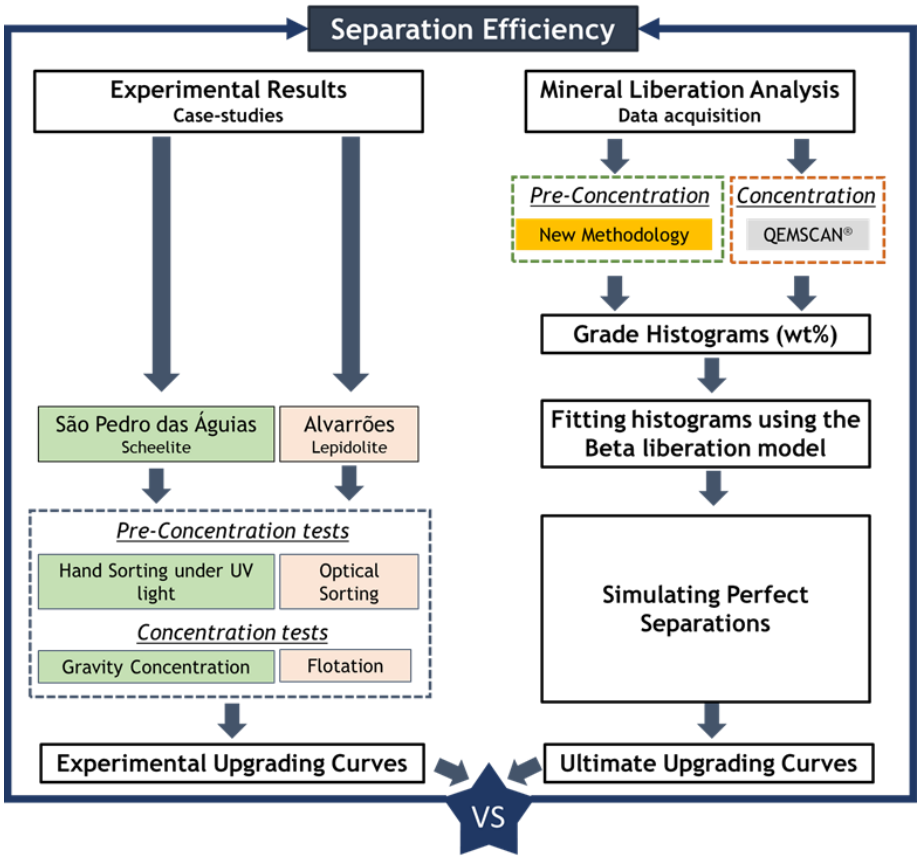

Fig. 43 – Description of the working methodology.

The first part corresponds to the experimental results of testwork carried out in the framework of the FAME project, involving pre-concentration and concentration in both studied cases. It is important to highlight that, although the experimental work was a very laborious and time-consuming task, the experimental results are only an input to demonstrate the methodology developed in this thesis. For this reason, it was decided to present the experimental results as case studies.

The second part corresponds to the conception and development of a new approach to assess the separation efficiency. In general terms, the procedure involves the definition of an Ultimate Upgrading Curves (UUC) [1, 2] that is calculated through the simulation of perfect separations using the feed grade histograms (wt%) acquired by quantitative mineralogical analysis. This second part is the focus of the thesis, and all steps are carefully explained:

i. Mineral Liberation Analysis: It is fundamental to have access to mineral liberation analysis. In the case of concentration, QEMSCAN® and MLA technologies are now available to provide reliable data concerning mineral distribution in ore textures and in single particles. Conversely, for the case of pre-concentration at crushing sizes, the access of similar type of data has been a critical issue since at the start of this project the existing technologies were not able to characterize ore macro-textures and coarse particles (25-6 mm). Thus, a new approach was developed to access the data required for the case of pre-concentration (mineral liberation analysis of coarse particles). Currently, hyperspectral data are being developed for the analysis of drill cores, and it appears that these new methodologies are very promising.

ii. Grade Histograms (wt%): Once access to mineral liberation analysis was granted, it was possible to compute the grade histograms (wt%), giving access to the mass distribution by grade class. Grade histograms are presented in this thesis as an adequate descriptor of mineral liberation;
    - At this stage, Mineral Liberation analysis of sawn cuts of lump rock specimens give important prior knowledge about ore macro texture useful to design mineral processing solutions and to conduct experimental testwork;

iii. Fitting Grade Histograms (wt%): In this step, the adjustment of the Beta Law Liberation Model [3] to the grade histograms (wt%) is used in two ways: data validation by direct comparison between experimental and predicted grade histograms, and smoothing of raw data to reduce noise that sometimes affects mineralogical data due to representativeness difficulties;

iv. Simulating Perfect Separations: The application of partition functions represented by the Heaviside function to smoothed grade histograms (wt%) is used to simulate perfect separation scenarios; in this context, partition function represents the (grade) fractional recovery in the concentrate;
v. Computation of Ultimate Upgrading Curves: Converting the perfect separation scenarios into upgrading curves allowed for the acquisition of the UUC, which describes the mineralogical limit of the separation performance, i.e., its maximum potential allowed by the ore liberation degree;
vi. Assessment of separation efficiency: The comparison between the experimental upgrading curve with the UUC, representing the limit of the separation given by the liberation degree, allows for distinguishing the technical separation inefficiency induced by the applied separation technology from the inefficiency induced by the lack of liberation.

Although the main objective of this methodology was to assess the separation efficiency, it was found that UUC can also be used as a simulator to predict the separation feasibility giving the opportunity to predict different separation scenarios, for example, in the case of pre-concentration at crushing sizes, aiming at rejecting barren rock in the early stages of the comminution flowsheet, a simulator based on the UUC can be used to define the most suitable size range and to predict the viability of pre-concentration during the pre-feasibility studies.

As it will be discussed in Chapter 5, sliding the Partition Curve under the feed grade histogram (wt%) gives rise to a more densely discretized upgrading curve fitted to raw data. The interpretation of the Partition Curves parameters itself also enables some conclusions regarding the efficiency of the process. Furthermore, the application of the fitted partition curves to the feed grade histogram (wt%) gives the opportunity to predict the concentrate grade histograms (wt%).

In summary, the focus of this work was to assess the separation efficiency of Pre-concentration at crushing sizes and Concentration at grinding sizes. This was accomplished by following the above-mentioned steps, in which the Ultimate Upgrading Curve and its comparison with Experimental Upgrading Curve is the main contribution of the thesis for a better interpretation of separation performance (efficiency and prediction of separation scenarios).

3.2 SAMPLES DESCRIPTION – GEOLOGY AND MINERALOGY

3.2.1 SÃO PEDRO DAS ÁGUIAS ORE

São Pedro das Águias deposit is a skarn deposit situated in the Central Iberian Zone, of the Iberian Variscan Belt, located in Tabuaço, in the north-central region of Portugal [4]. The skarn bodies are situated in the contact of the Variscan age Armamar-Tabuaço granitoid intrusion with carbonate-rich units in Douro Valley Schist-Greywacke Complex. There are three locally described facies to the skarn mineralization: i) The Upper Carbonate Horizon which is classified as being separate from the skarn; ii) The Main Skarn Zone is characterized by a "greyish white rock with a blueish-pink hue" that is either weakly banded with black porphyroblasts or blocky; iii) The Lower Skarn Zone is considered to be me more typical of classic skarns and is characterized by alternating zones of prograde mineralogy with retrograde mineralogy.

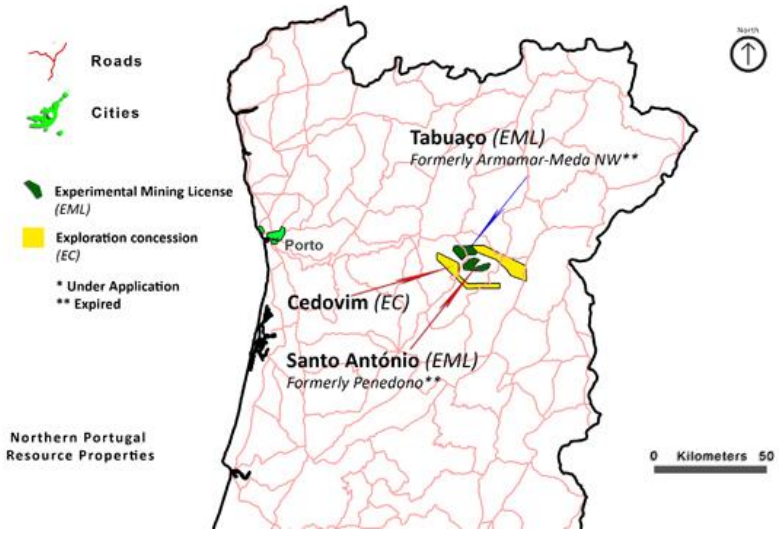

Fig. 44 – Identification of Tabuaço deposit [5].

The Tabuaço skarns (Fig. 45) are composed of variably banded sodic plagioclase, K-feldspar, vesuvianite, epidote, zoisite/clinozoisite, diopside, garnet (grossular), hornblende, tremolite-actinolite, quartz, sericite, calcite, fluorite, apatite and scheelite. The high scheelite ($CaWO_4$) grade coupled with a low sulphide abundance and low heavy metal content contributes to the high quality of this ore, making it highly prospective for the development of high-grade products [5].

Fig. 45 – Photo of the mineralized skarn outcrop [5].

3.2.2 ALVARRÕES ORE

Alvarrões deposit is located in Gonçalo, south of Guarda (Central Portugal), inserted in the Central Iberian Zone. A granitic pegmatite can be found, occurring in the western extreme of the European Variscan Belt. Alvarrões pegmatite occurs as sills and is hosted by a synorogenic Variscan porphyritic biotite granite (Beiras granite or Guarda granite) [6].

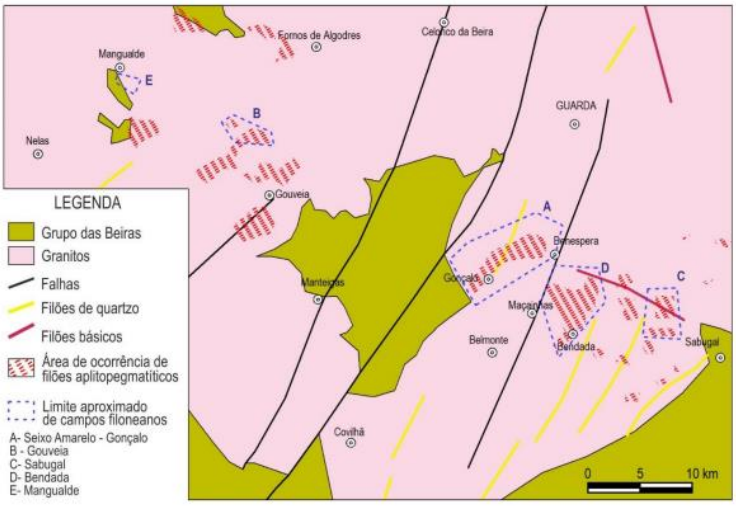

Fig. 46 - Simplified Geological Map of the Guarda region [7].

The Alvarrões ore presents pegmatitic and aplitic components, with lepidolite, albite, Li-muscovite, quartz and K-feldspar as major minerals, and montebrasite, topaz, cassiterite, columbo-tantalite, beryl, and zircon as minor minerals. Lepidolite is the most

abundant lithium mineral in both pegmatitic and the aplitic components. In the pegmatitic component, lepidolite occurs mainly as a medium to coarse-grained (> 500 μm), whereas in the aplitic component it frequently forms aggregates and is fine-grained (60 μm-250 μm) to very fine-grained (≤ 60 μm).

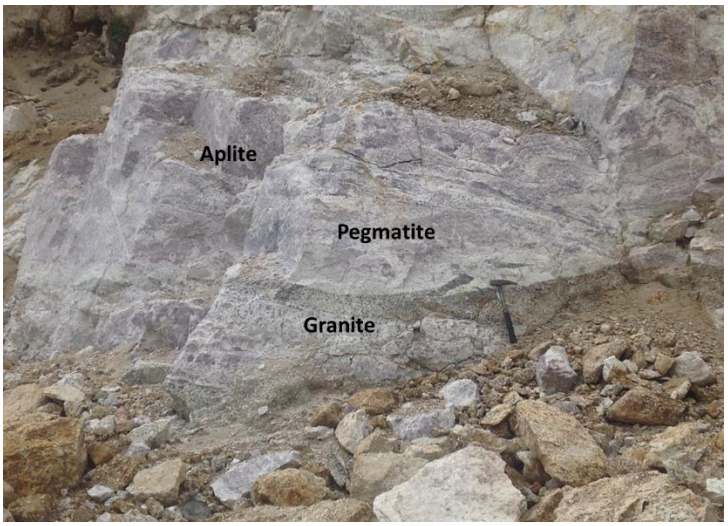

Fig. 47 - Alvarrões open pit [8].

3.3 SAMPLE CHARACTERIZATION AND PREPARATION

The success of the aforementioned methodology depends on the access to some ore properties such as the average grade, comminution behaviour and grade and size distributions. It was also required to prepare samples for the mineral liberation analysis of both studied ores at pre-concentration and concentration size ranges.

According to preliminary studies developed by FAME team, namely in what concerns the texture and grain size occurrence of the respective valuables, it was well established that scheelite from São Pedro das Águias would be mainly concentrated by gravity methods, while froth flotation would be the concentration method for lepidolite recovery in the case of Alvarrões. Bearing this in mind, the first attempt to study both ores consisted in a primarily fine crushing to minus 3.35 mm, followed by size analysis in order to obtain narrow sized sub-samples for characterization purposes - chemical assay and mineral liberation analysis. In a second step, a similar approach was applied to study the pre-concentration stage using another feed sample. This material was coarse crushed at

minus 16mm and 19mm, in the cases of scheelite and lepidolite ore, respectively, followed by size and grade analysis.

A brief description of these tasks is presented in the following sections.

3.3.1 CONCENTRATION

3.3.1.1 SÃO PEDRO DAS ÁGUIAS ORE

A sample from the São Pedro das Águias deposit was used to study the concentration stage. Material was crushed in Jaw Crusher, single toggle, 5"x6", 4 kW, 325-375 RPM (Denver), followed by a cone crusher (8" - No. 12 Gyratory Crusher, 1.1 kW, Denver - Symons type) and a roll crusher (6" Dual Roll Crusher, 10"Dx6"L, 2.2 kW, Denver) to obtain a minus 3.35 mm material, as shown in Fig. 48.

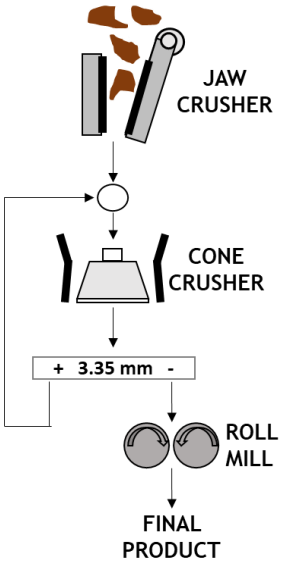

Fig. 48 – Comminution diagram applied in the study of the concentration stage.

The comminution product was size classified for determination of particle size distribution and then chemical assayed by XRF to obtain the metal and grade (WO_3) distribution by size class (Fig. 49).

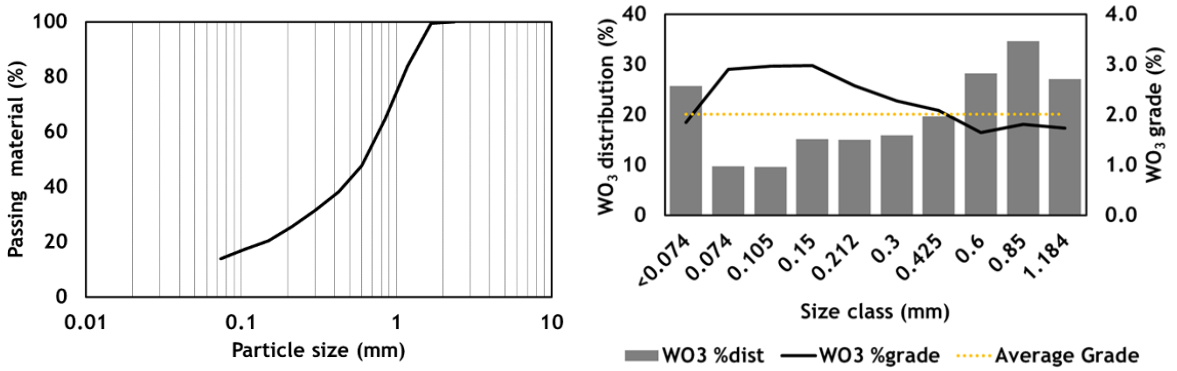

Fig. 49 - Particle size distribution (left) and metal and grade (WO_3) distribution by size class (right) - Grinding of São Pedro das Águias ore.

Size and WO_3 grade distribution point to some discriminative comminution due to the brittle character of scheelite, WO_3 grade being slightly higher in the [0.074, 0.300]mm size range. The average sample grade was determined as 2% WO_3.

In the case of São Pedro das Águias the application of gravity concentration methods is justified by the contrast of specific gravity between scheelite and gangue minerals. However, as it has been well established for a long time by the Taggart criterion (Eq. 20), the separation efficiency also depends on particle size, which suggests that feed must be previously classified according to that criterion to enhance separation efficiency.

$$\frac{l_2}{l_1} = \sqrt{\frac{d_1 - \rho_{fluid}}{d_2 - \rho_{fluid}}} \qquad \text{Eq. 20}$$

Where d_1 is the density and l_1 the size of scheelite particles and d_2 is the density and l_2 the size of quartz particles. When shaking tables and spirals are used, this previous classification, instead of sieving, is properly processed by hydrosizing (elutriation).

For the purpose of performing that preliminary classification of São Pedro das Águias ore, a batch elutriation device was specifically developed. As shown in Fig. 50, inside a sedimentation cone, a teetered bed was created by upward rinsing water, flowing through a perforated plate at the bottom of the cone. The sample was fed into the elutriator and while the rinsing water flows at low pressure, the finer fraction, with size below approximately 0.075mm, is collected in the overflow. After a certain lapse of time, the rinsing water was regulated to a higher pressure, forcing the overflow of an

intermediate fraction, approximately in the size range 0.075/0.212 mm, while the coarsest fraction, approximately above 0.212 mm, remained inside the sedimentation cone and was discharged by underflow at the end of the test.

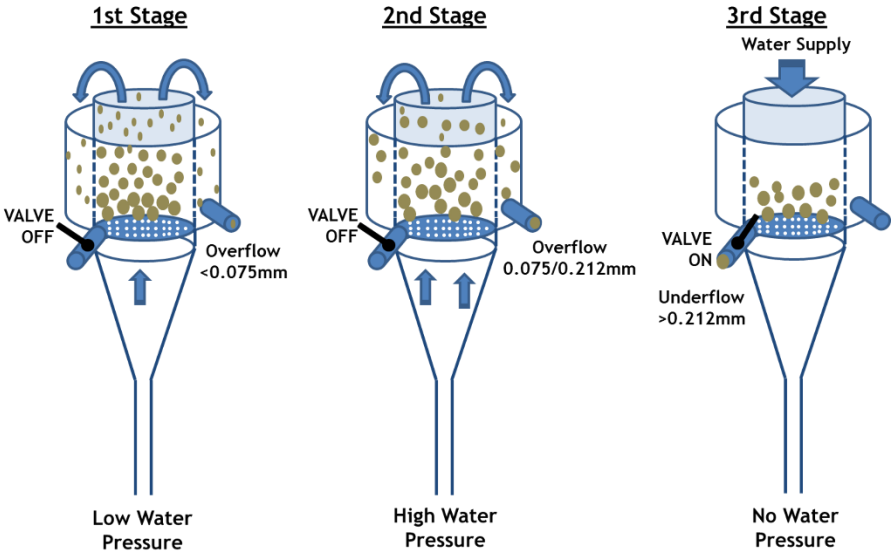

Fig. 50 – Batch elutriator device applied in the São Pedro das Águias hydrosizing.

Table 14 shows the sample identification and the average grade of each size fraction.

Table 14 – São Pedro das Águias samples after hidrosizing

Sample ID	Mass (%)	Grade
SPA [cutsize=0.212mm]	64.50	1.87 %WO_3
SPA [cutsize=0.075mm]	23.16	1.89 %WO_3

The fraction <0.075mm is not suitable for the traditional gravity concentration methods – spirals and shaking tables, being disregarded for the purpose of this study. A sample of each size fraction was used for mineral liberation analysis, and the remaining material was preserved for the experimental testwork.

3.3.1.2 ALVARRÕES ORE

The same procedure as that applied to grind the São Pedro das Águias sample was applied to Alvarrões (Fig. 48). Products were then size classified, and each size fraction

was chemically assayed for Li by Atomic Adsorption Spectrometry (AAS). The particle size analysis and Li grade distribution can be observed in Fig. 51.

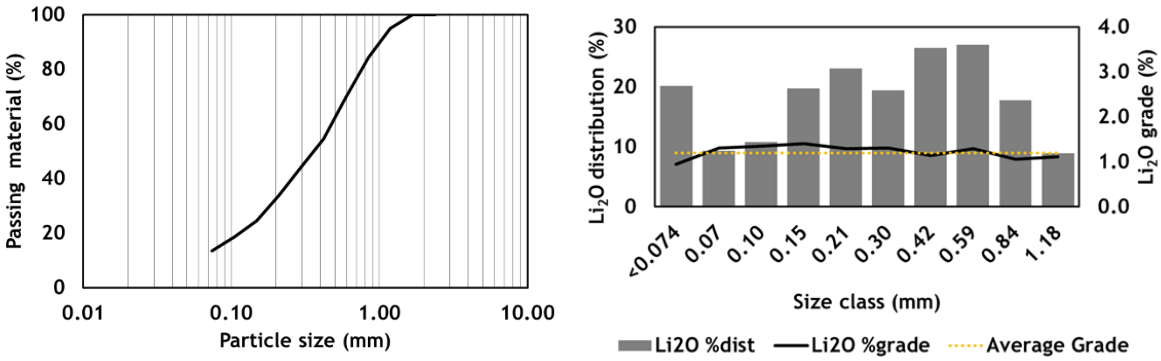

Fig. 51 - Particle size distribution (left) and metal and grade (Li_2O) distribution by size class (right) - Grinding of Alvarrões ore.

Consistency of Li_2O grade in the different size fractions points out for the random nature of comminution at crushing level. However, a small peak of Li_2O grade around 150 µm along with a slight decrease of Li grade in the lowest size is compatible with the lamellar character of Lepidolite due to its cleavage, which allows assuming that lepidolite exhibits a lower size reduction ratio compared with gangue minerals. The average grade of the sample is 1.83 %Li_2O.

In the case of Alvarrões ore, the most promising mineral processing technique is froth flotation, which is efficient for particle sizes in the range of 0.500/0.060 mm. According to that, the product of the roll crusher was then milled using a rod mill to produce particles suitable for flotation. The material was then deslimed to remove particles below 0.060mm, which are harmful to flotation performance. A sample of the hydrocyclone underflow was sent for mineral liberation analysis by QEMSCAN® and the remaining material was used in batch flotation tests (Fig. 52).

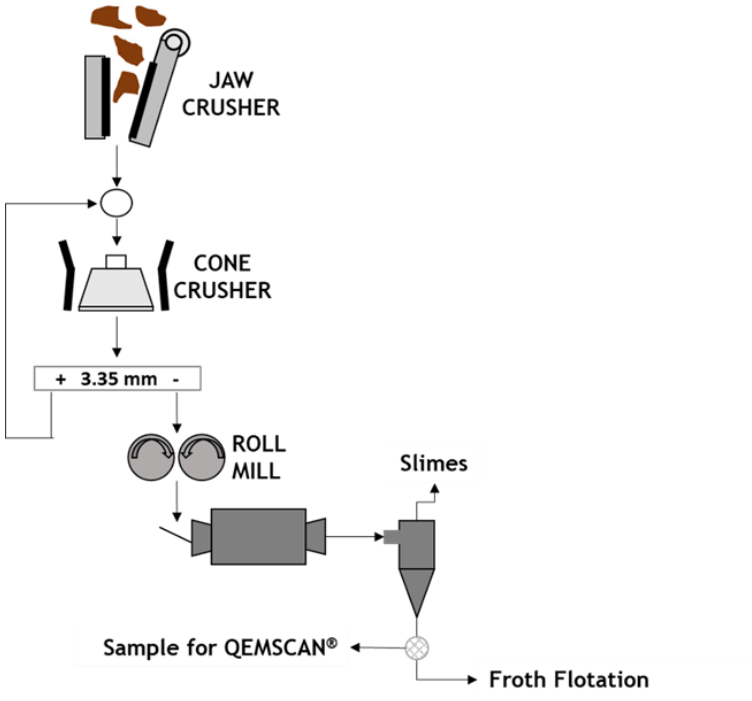

Fig. 52 - Processing diagram applied to the concentration test of Alvarrões ore.

3.3.2 PRE-CONCENTRATION

3.3.2.1 SÃO PEDRO DAS ÁGUIAS

A set of drill cores were collected from the São Pedro das Águias deposit (Fig. 53). A sample was preserved for macrotexture assessment purposes. The remaining material was crushed to produce particles adequate for the pre-concentration studies using a Jaw Crusher, single toggle, 5"x6", 4 kW, 325-375 RPM (Denver) to produce a minus 16 mm product, being the applied procedure presented in Fig. 54.

Fig. 53 – Examples of drill cores collected from São Pedro das Águias deposit.

The jaw crusher product was size classified using a classic sieving device and size fractions were chemically assayed to determine the WO_3 grade distribution along with size, which is shown in Fig. 55.

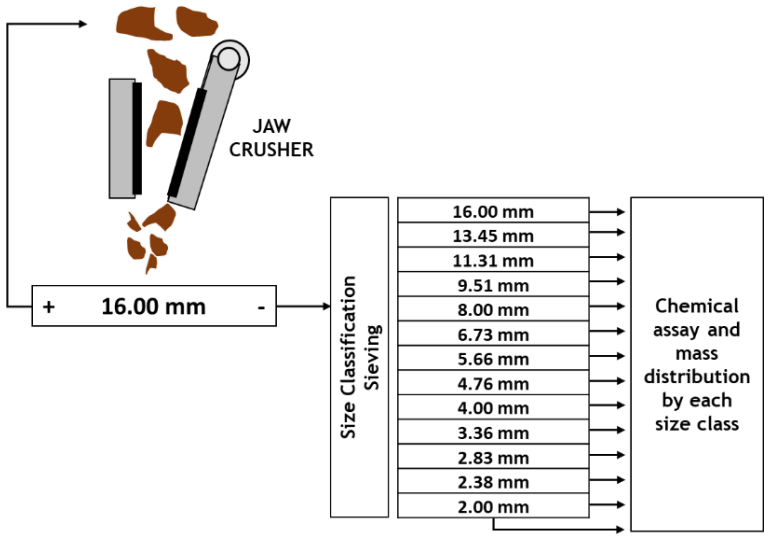

Fig. 54 - Coarse comminution diagram applied to São Pedro das Águias ore - Coarse crushing, size classification and chemical assay.

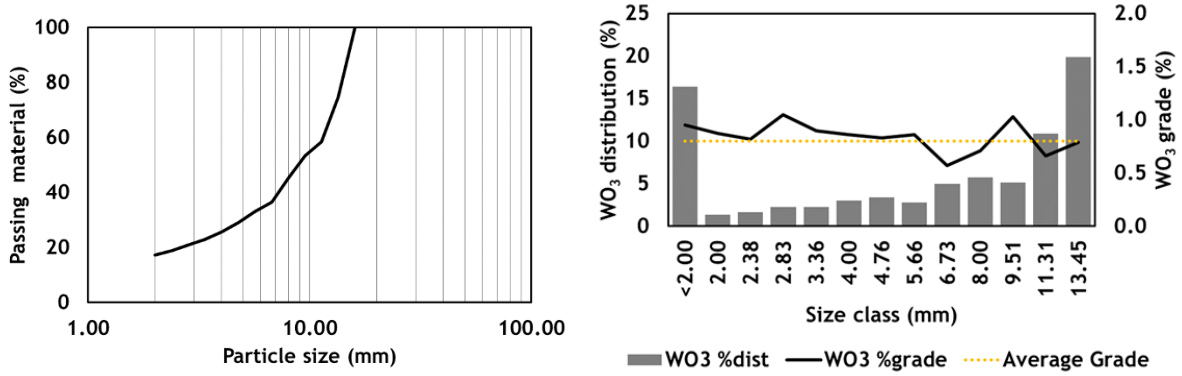

Fig. 55 - Particle size distribution (left) and metal and grade (WO_3) distribution by size class (right) - Coarse crushing of São Pedro das Águias ore.

The grade distribution points out for a slight variation with size, being an important indicator of the almost random character of the comminution at the crushing stage. The sample average grade is 0.80 %WO_3.

Pre-concentration of São Pedro das Águias ore was studied in the size range 16/6.7mm, so samples of this size fraction were preserved for the mineral liberation analysis and for experimental testwork.

3.3.2.2 ALVARRÕES ORE

In the case of Alvarrões, a set of hand samples was collected from the mine site. A sub-sample was saved for the macrotexture assessment and another sub-sample was coarsely crushed following a similar procedure as that applied to São Pedro das Águias sample, with the exception that in this case the top size was defined as 19 mm rather than 16 mm.

Fig. 56 – Hand sample (left) collected from Alvarrões deposit (right).

The final product was size classified and then chemical assayed by AAS for Li. The particle size distribution and the Li_2O grade distribution along size can be observed in Fig. 57.

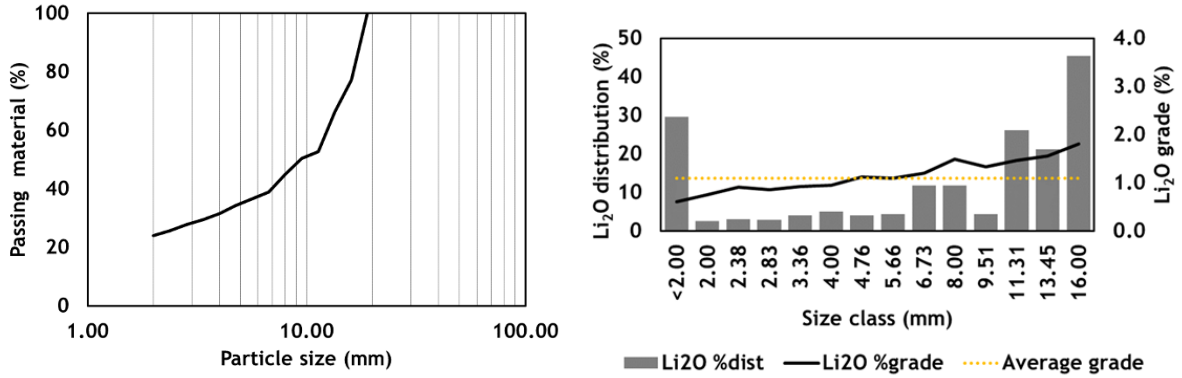

Fig. 57 - Particle size distribution (left) and metal and grade (Li_2O) distribution by size class (right) - Coarse crushing of Alvarrões ore.

It is possible to observe that the Li_2O grade remains practically constant along with the size classes, which is an indicator of random comminution at the crushing stage. The average grade of this sample is 1.9 %Li_2O.

In the case of Alvarrões ore samples of the size range 19/6.7 mm were saved for the mineral liberation analysis and for experimental testwork.

3.4 OVERVIEW OF EXPERIMENTAL TESTWORK – CASE STUDIES

According to the proposed methodology, the accomplishment of the main objective of this project requires experimental data obtained from real separations. These results are fundamental to demonstrate the applicability of the developed methodology for separation assessment, being considered as an important input for this work. However, it must be clear that the objective of this thesis is not to study the separation processes themselves as applied to each studied ore, but rather to validate the developed approach to assess separation feasibility and efficiency. Therefore, experimental results on Concentration and Pre-concentration are presented in the following sections as case studies.

3.4.1 CONCENTRATION TEST

3.4.1.1 GRAVITY CONCENTRATION OF SÃO PEDRO DAS ÁGUIAS ORE

Taking advantage of density contrast between scheelite and gangue minerals, gravity separation tests were carried out using a Wilfley shaking table equipped with a 130 cm long and 56 cm wide fibreglass deck, adjusted to around 230 rpm (dial position 6) stroke speed and a stroke length of 20 mm. Fig. 58 shows the results of shaking table tests.

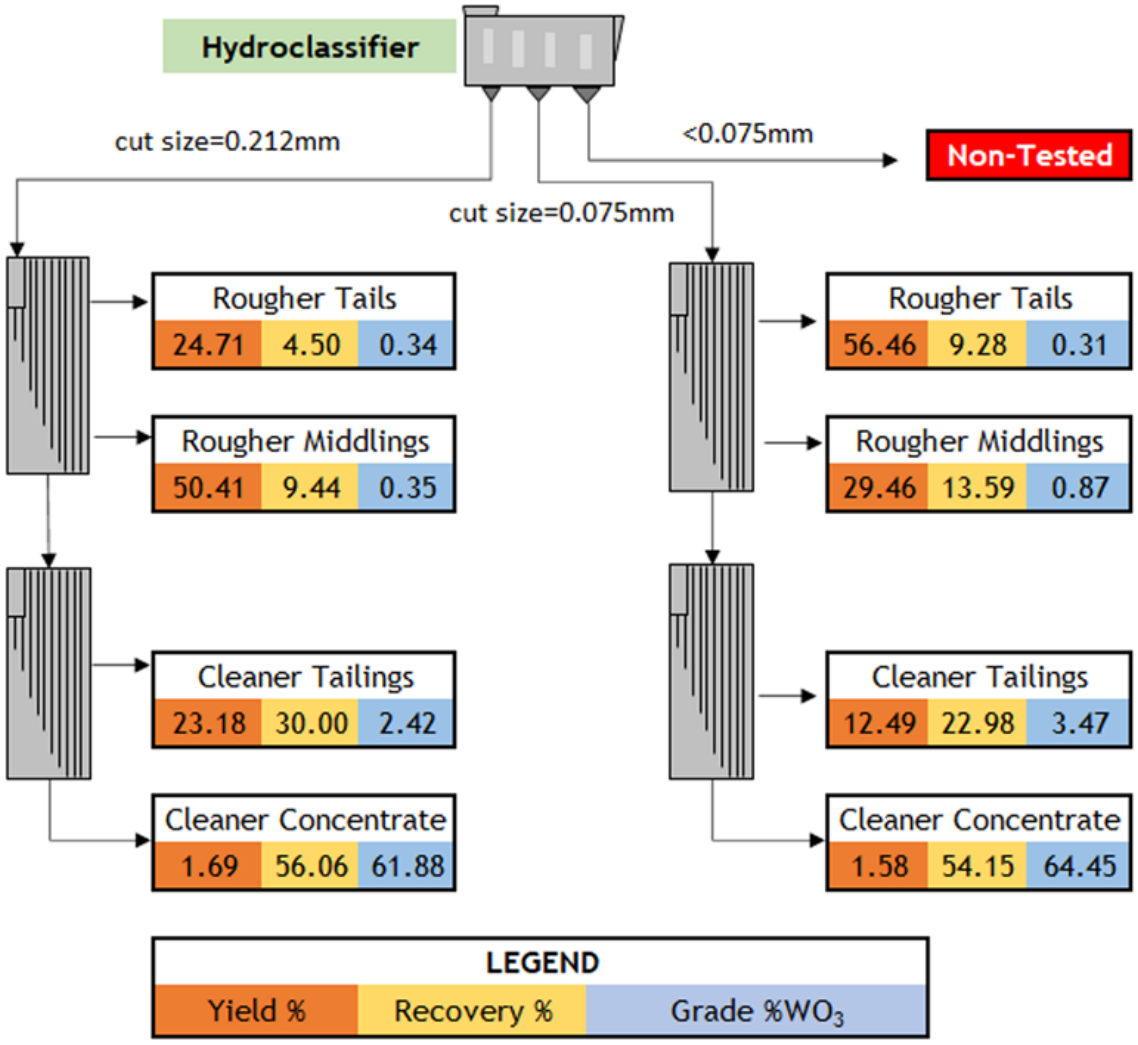

Fig. 58 - Gravity concentration of São Pedro das Águias ore using Wilfley shaking table.

Wilfley shaking table produced high-grade concentrates, at around 61-65 WO_3%, under-recoveries of about 55%, for both size fractions, meaning that a good liberation level was achieved and traditional gravity methods are a viable option for the final concentration stage of São Pedro das Águias ore.

These data can be handled to obtain results of different separation scenarios, depending on the application of specific cut-points. In Fig. 59 is observed an example of a separation carried out using a shaking table to recover heavy minerals, in which three products were collected: the leftmost collection zone collects a high-grade product, while the rightmost collects a low-grade product (if the valuable mineral is a high-density mineral).

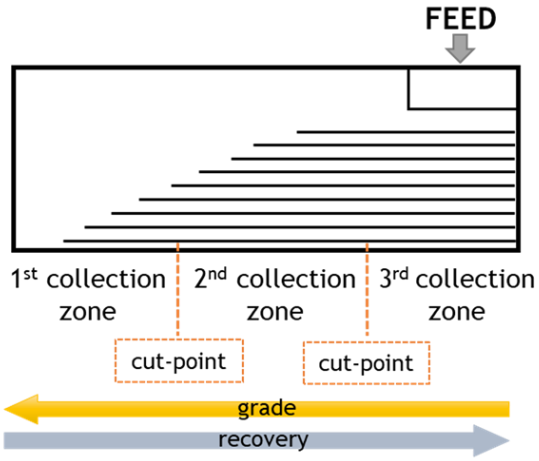

Fig. 59 – Definition of collection zones in a Wilfley shaking table.

The three collected products can be re-arranged to simulate two distinct separations: In the first cut-point, the concentrate is composed by the material collected in the 1st zone, and the tailings by the material collected in the 2nd and 3rd zones. In the second cut-point, the concentrate is composed by the material collected in the 1st and 2nd zones and the tailings were collected in the 3rd zone. According to this, the 1st cut-point produces a concentrate with higher grade and lower recovery, while the 2nd cut-point produces a concentrate with lower grade and higher recovery. Following this pattern, data collected in the experimental testwork with São Pedro das Águias ore can be re-arranged as in Table 15:

- 1st cut-point: Concentrate = cleaner concentrate; Tailings = cleaner tailings + rougher middlings + rougher tailings;
- 2nd cut-point: Concentrate = cleaner concentrate + cleaner tailings; Tailings =rougher middlings + rougher tailings;
- 3rd cut-point: Concentrate = cleaner concentrate + cleaner tailings + rougher middlings; Tailings = rougher tailings;

Table 15 – Results of different gravity concentration scenarios of São Pedro das Águias ore.

Wilfley cs=0.212mm				Wilfley cs=0.075mm			
Cut-point	**Yield %**	**Recovery %**	**Grade %**	**Cut-point**	**Yield %**	**Recovery %**	**Grade %**
1st cut-point	1.69	56.06	61.88	1st cut-point	1.58	54.15	64.45
2nd cut-point	24.88	86.07	6.47	2nd cut-point	14.08	77.13	10.34
3rd cut-point	75.29	95.51	2.37	3rd cut-point	43.54	90.72	3.93

3.4.1.2 FROTH FLOTATION OF ALVARRÕES ORE

Froth flotation is generally considered a promising concentration method to produce high-grade lepidolite concentrates[9]. According to this, several batch flotation tests using a traditional Denver laboratory cell were carried out to set the optimal conditions for lepidolite flotation. Finally, a kinetic flotation test was conducted in a Leeds open-top laboratory flotation machine with a 3.0 L cell, using the following optimal conditions:

- d_{80}=0.300 mm size after lab milling of 1 kg sample at 15 minutes of residence time
- pH was maintained at 3;
- Collector Flotigam EDA (from Clariant®) was added at a dosage of 150 g/t;
- Pulp density was 25%;
- Impeller speed of 1000 rpm;
- Airflow rate of 7.5 L/min;

Table 16 – Results of kinetic batch flotation test – Alvarrões ore.

	Yield	Li_2O	
Time (s)	%	%grade	%dist
0	0.00		0.00
20	7.81	4.10	27.33
40	5.92	3.44	17.36
60	4.58	3.23	12.61
90	4.24	3.01	10.89
180	3.91	2.58	8.60
Sink	73.55	0.37	23.22
Feed		1.17	

The results achieved in the kinetic tests showed that it is possible to obtain a high-grade concentrate (4.10 %Li_2O), however, this value is far from the theoretical Li_2O content of lepidolite (7.70 %Li_2O) and the recovery was only 27.3%. Another interesting fact is that with the increase of recovery, the grade remains practically constant, suggesting that lepidolite is floating together with gangue minerals. This phenomenon was carefully discussed in the manuscript "Flotation of lithium ores to obtain high-grade Li_2O concentrates. Are there any mineralogical limitations?"[10], showing the existence

of very fine inclusions of quartz and albite inside the lepidolite, meaning that lepidolite cannot be fully liberated at the flotation size range. In line with this, the target grade for a lepidolite concentrate of Alvarrões ore deposit must be of about 4.5% Li_2O.

As in the case of concentration tests of São Pedro das Águias ore, results of the kinetic flotation test of Alvarrões ore can be converted into several separation scenarios accordingly with accumulated flotation time: high-grade particles are recovered in the first flotation period: over time middlings starts floating and recovery increases while froth average grade decreases with the time; and successively different cut-points can be obtained by changing the froth collection time. In the case of the flotation test carried out with Alvarrões ore, the following cut-points can be presented:

- 1st cut-point: Concentrate = Froth collected in 0 – 20 s; Tailings = froth collected in 20-180 s + sink;
- 2nd cut-point: Concentrate = Froth collected in 0 – 40 s; Tailings = froth collected in 40 -180 s + sink;
- 3rd cut-point: Concentrate = Froth collected in 0 – 60 s; Tailings = froth collected in 60 -180 s + sink;
- 4th cut-point: Concentrate = Froth collected in 0 – 90 s; Tailings = froth collected in 90 -180 s + sink;
- 5th cut-point: Concentrate = Froth collected in 0 – 180 s; Tailings = sink;

The separation scenarios can be observed in Table 17.

Table 17 - Results of different concentration scenarios of Alvarrões ore by flotation.

cut-point	Yield %	Recovery %	Grade %
1st cut-point	7.81	27.33	4.10
2nd cut-point	13.73	44.69	3.82
3rd cut-point	18.30	57.30	3.67
4th cut-point	22.54	68.19	3.55
5th cut-point	26.45	76.78	3.40

The growing interest in lithium as the key for the energy transition program draw special attention for the Portuguese lithium deposits and for the work carried out in the framework of the FAME project. This interest triggered the desire to move on to the pilot plant trials, demonstrating the feasibility of producing lepidolite concentrates from the Alvarrões ore. Thus, the LNEG pilot plant facilities were adjusted to carry out pilot plant

trials to demonstrate the production of lepidolite concentrates by froth flotation. Fig. 60 and Fig. 61 shows the quantitative flowsheet obtained in two different trials carried out in the pilot plant. In the first test, the froth flotation stage was designed with a conventional scavenging-roughing-cleaning process, generating a concentrate with 3.87 %Li_2O under recovery of about 25%. Based on these results, a different flotation cell configuration was tested with all cells producing concentrates. This modification allowed for increasing the recovery to 82.50% with a concentrate grade of 2.71 %Li_2O that should be upgraded in a cleaner step. However, problems related to the froth freezing put technical difficulties to froth handling that were not solved during the project life-time.

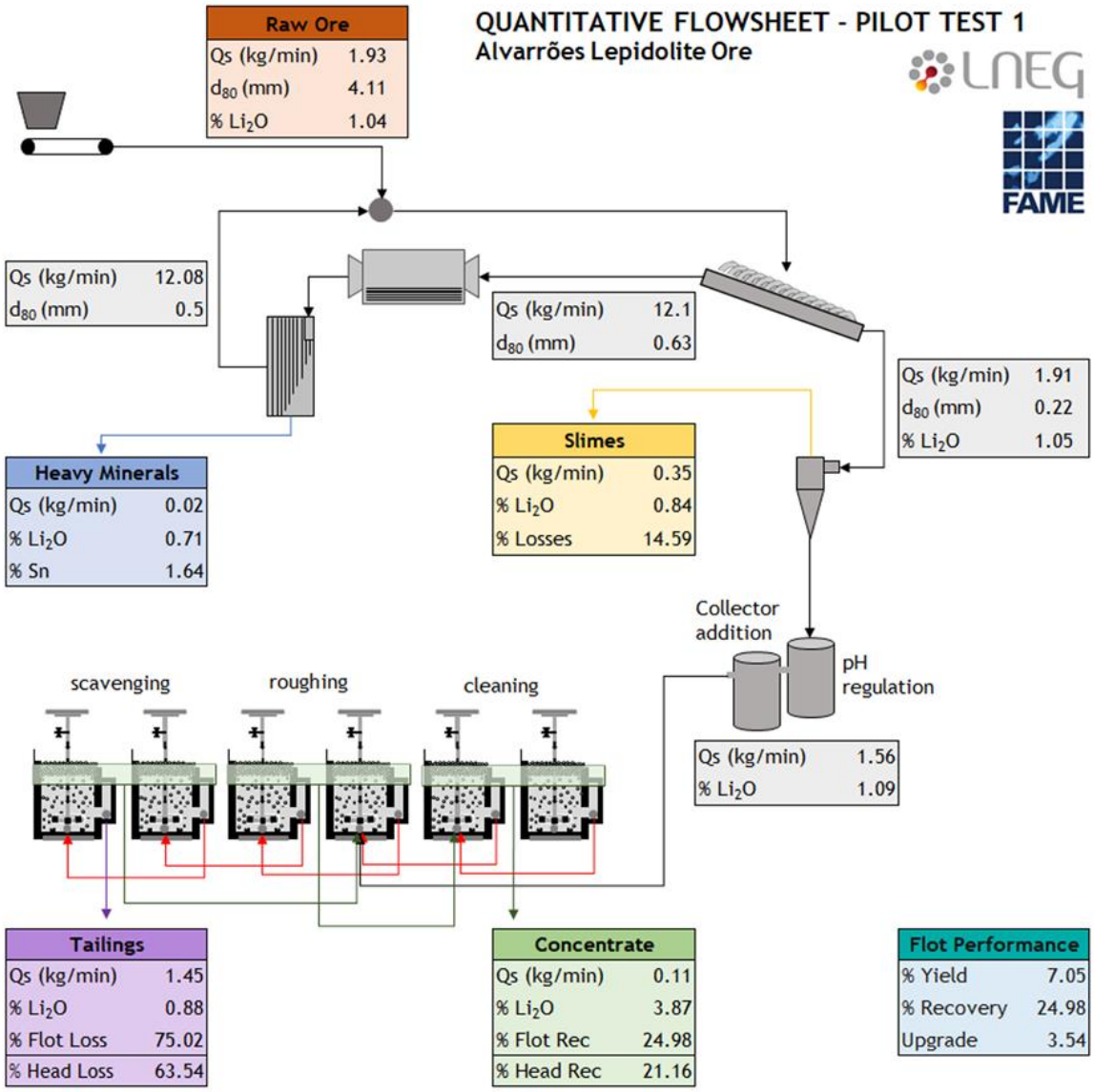

Fig. 60 - Quantitative flowsheet of pilot plant test 1.

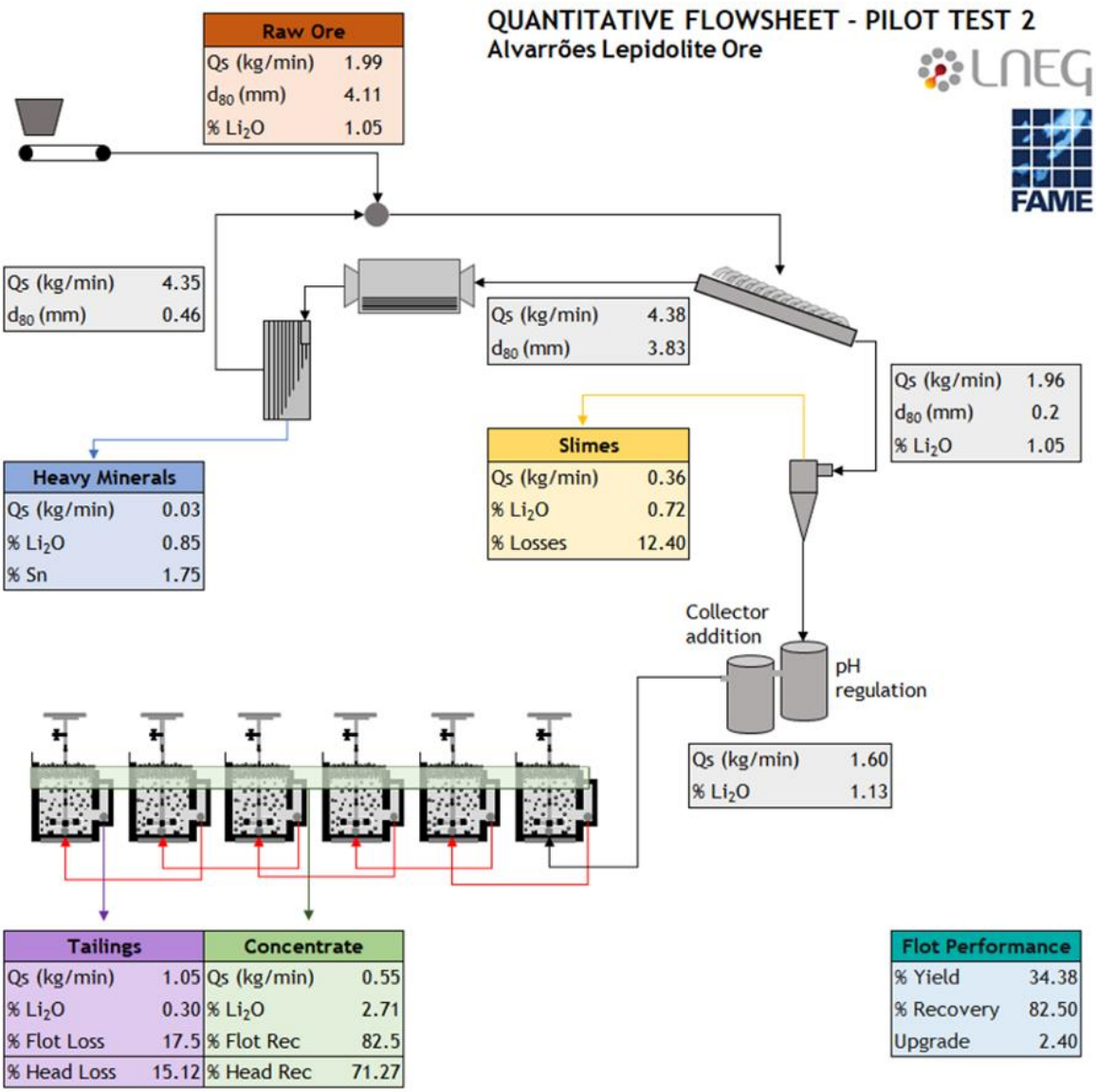

Fig. 61 - Quantitative flowsheet of pilot plant test 2.

Each pilot plant trial generated only two products (concentrate and tailings), meaning that only one cut-point was applied and that only one separation scenario can be assessed. This is precisely the reason behind the inclusion of the results of pilot plant tests in this thesis, as the quantity of available data is reduced, the methodology must be adjusted to be successfully applied.

As the procedure was deeply described for the cases of gravity tests on São Pedro das Águias ore and batch flotation test with Alvarrões ore, the application of the methodology for the case of flotation pilot plant tests are presented in annexe A1.1.

3.4.2 PRE-CONCENTRATION TESTS

3.4.2.1 HAND SORTING OF SÃO PEDRO DAS ÁGUIAS ORE

According to the properties of São Pedro das Águias ore, the adequate methods for a pre-concentration step aiming at distinguishing between the mineralized zone and the host rock are Heavy Media Separation (HMS) and Electronic Sorting due to the high scheelite specific gravity (6.12). In the framework of FAME project, it was decided to test an electronic sorting method as an alternative to HMS, as these techniques are gaining competitiveness in the field of mineral processing. For this purpose, X-Ray Transmission sorting or optical sorting under UV light could be chosen. Unfortunately, none of both possibilities were available. However, as the objective is to test a methodology to assess separation efficiency, it was decided to carry out a hand-sorting separation by visual inspection under UV light trying to simulate the operation of sorting device working under UV light. Three products were collected: i) Concentrate (high quantity of scheelite); ii) Middlings (low quantity of scheelite) and iii) Tailings (no visible scheelite), as can be observed in Fig. 62.

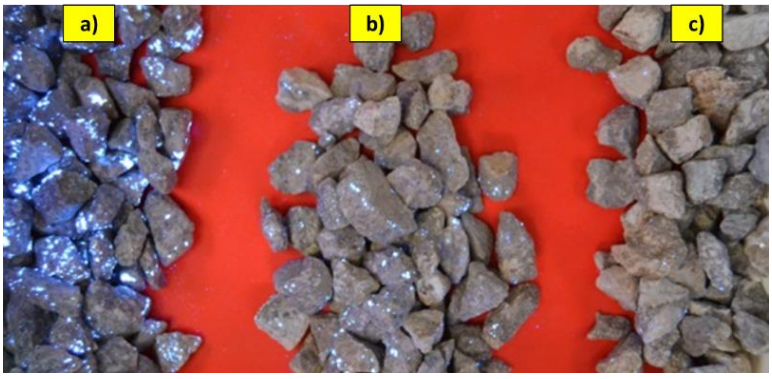

Fig. 62 - Result of hand-sorting separation under UV light: a) concentrate, b) middlings and c) tailings.

Table 18 shows the results of hand-sorting separation. All products were weighed and chemically assayed at full quantitative mode (WDS) by X-ray fluorescence (Philips – PW 2404 X-ray Spectrometer), at LNEG facilities.

Table 18 - Results of hand-sorting separation.

	Yield	WO_3	
	%	%grade	%dist
Concentrate	25.56	2.90	84.52
Middlings	31.65	0.40	14.52
Tailings	42.80	0.02	0.02
Feed		0.88	

Based on the experimental results, it is possible to draw the following conclusions:

- With a rejection of almost 43% of processed material, the average grade was increased from 0.88 % to 1.52 %WO_3, under a metal recovery of around 99%
- If middling are disregarded from the concentrate, a high-grade concentrate averaging 2.90 %WO_3 was obtained, however with 15% of metal losses;

These results mean that the hand-sorting was efficient to recognize the presence of scheelite in mixed particles;

As in the case of concentration tests, experimental data of pre-concentration can be handled to present the results of different separation scenarios adopting different cut-points (Table 19).

Table 19 - Results of different pre-concentration scenarios of São Pedro das Águias ore

	Yield	Recovery	Grade
	%	%	%
1st cut-point	25.56	84.52	2.90
2nd cut-point	57.20	99.08	1.52

3.4.2.2 OPTICAL SORTING OF ALVARRÕES ORE

In the case of lepidolite from Alvarrões, HMS and X-Ray Transmission sorting are not feasible for pre-concentration due to no contrast density in the case of HMS and the transparency of Li under X-Ray. However, the contrast colour between the purple lepidolite and the whitish gangue minerals is appropriate for an optical sorting technique under visible light.

Thus, during the FAME project, a coarse crushed sample of the Alvarrões Li ore was sent to an external laboratory to perform some tests in an optical sorter. The separation was performed in two steps: in the first one, the separator was calibrated to accept a rich lepidolite concentrate; the rejected was subjected to a second scavenger step adjusted to accept a middling lepidolite product and to reject a tailings fraction composed by particles with almost no lepidolite content. The objective of the first step was to assess the possibility of producing a high-grade marketable product that can be directly sent to a Li conversion plant. The second step was designed to evaluate the possibility of rejecting gangue in an early stage of the comminution flowsheet. Three fractions were obtained: concentrate, middlings and tailings, as can be seen in Fig. 63.

a)  b)  c) 

Fig. 63 - Products of optical separation at Mogensen: a) Concentrate; b) Middlings; c) Tailings.

Table 20 shows the results of optical sorting applied to the size range [19/6.3] mm. All products were weighed and chemically assayed by atomic absorption spectroscopy (AAS), at LNEG facilities.

Table 20 - Result of optical sorting of Alvarrões ore.

	Yield	**Li_2O**	
	%	**%grade**	**%dist**
Concentrate	39.60	2.80	50.66
Middlings	22.40	1.83	18.78
Tailings	38.00	1.76	30.55
Feed	100.00	2.19	

Based on the experimental results, the following conclusions can be drawn:

- In the first step, the optical sorter was able to generate a concentrate with 2.8% Li_2O, with a recovery of about 51% and producing a reject of about 1.79% Li_2O.

- In the second step, the Li_2O content of the accepted material was 1.83% and the rejected material was 1.76%;
- The optical sorter was not able to generate a high-grade product close to the 4.5 %Li_2O;
- Regarding the possibility of gangue rejection, the separation was also unsuccessful. The mass rejection of 38% is an interesting figure, but losses of about 30 %Li_2O would make the solution economically non-viable;

Similarly to the previous case, results of Alvarrões pre-concentration optical ore sorting can be converted into different separation scenarios, following the two available cut-points (Table 21).

Table 21 - Results of different pre-concentration scenarios of Alvarrões ore.

	Yield %	**Grade %**	**Recovery %**
1st cut-point	39.60	2.80	50.66
2nd cut-point	22.40	2.45	69.44

NOMENCLATURE AND GLOSSARY

l_1	Size of dense particles	-
l_2	Size of light particles	
d_1	Density of dense mineral	
d_2	Density of light mineral	
ρ_{fluid}	Density of the separation fluid	kg/m^3
Q_s	Solid troughput	kg/min
d_{80}	80% passing size	mm

REFERENCES

1. Sousa, R., A. Futuro, A. Fiúza and M.M. Leite, *Pre-concentration at crushing sizes for low-grade ores processing – Ore macro texture characterization and liberation assessment.* Minerals Engineering, 2020. **147**: p. 106156.
2. Sousa, R., B. Simons, K. Bru, A.B. de Sousa, G. Rollinson, J. Andersen, M. Martin and M. Machado Leite, *Use of mineral liberation quantitative data to assess separation efficiency in mineral processing – Some case studies.* Minerals Engineering, 2018. **127**: p. 134-142.
3. Madureira, C.M.N., M.R. Machado Leite, A. Cavalheiro and J. Silva, *Size, Grade and Liberation: a stochastic approach to the fundamental problem of mineral processing*, in *XVI International Mineral Processing Congress*, E.S. Publisher, Editor. 1988: Stockholm.
4. Gomes, G.L., *Spatial simulation of the W-Sn ore grades of São Pedro das Águias skran mineral deposit (Tabuaço, northern Portugal)*, 2016. *Geological Engineering*,Universidade Nova de Lisboa, Mestre
5. Colt Resources Inc., *Tungsten Mineralization in Portugal - The case of the São Pedro das Águias Deposit*, in *Mineral resource assessment workshop: Assessment of the tungsten potential in Greenland*. 2013: Copenhagen.
6. Ramos, J.M.F., *Locality nº5: Seixo Amarelo-Gonçalo rare element aplite-pegmatite field.*, in *GRANITIC PEGMATITES: THE STATE OF THE ART - FIELD TRIP GUIDEBOOK. MEMÓRIAS N. º 9*, A.L.a.E.R.R. (Eds.). Editor. 2007, Departamento de Geologia da Faculdade de Ciências University of Porto.
7. Português, G., *Relatório do Grupo de Trabalho "Lítio"*, S.d.E.d. Energia, Editor. 2017.
8. Ramos, V. and R. Sousa. *Portuguese Potential as European Li Supplier*. in *FAME Closure Conference*. 2018. London.
9. Sousa, R., V. Ramos, A. Guedes, F. Noronha, A. Botelho de Sousa, M.R. Machado Leite, R. Seltmann and A. Dolgopolova, *The Alvarrões-Gonçalo Li project: an example of sustainable lithium mining.* Advances in Geosciences, 2018. **45**: p. 1-5.
10. Sousa, R., V. Ramos, A. Guedes, A. Botelho de Sousa, F. Noronha and M. Machado Leite, *Flotation of lithium ores to obtain high-grade Li2O concentrates. Are there any*

mineralogical limitations? International Journal of Mining, Materials, and Metallurgical Engineering, 2019. **5**: p. 7-18.

4 DATA ACQUISITION

4.1 THE IMPORTANCE OF MINERAL QUANTITATIVE DATA

Mineralogical studies are fundamental to identify and characterize the ore paragenesis and texture, and to predict mineral liberation. This data is fundamental for the optimization of the comminution and mineral separation stages, providing key figures about the nature of separation inefficiencies, i.e., if the inefficiencies are related with low mineral liberation, requiring the adjustment of the comminution stage, or if it is related with technical issues, requiring the adjustment of the separation technology/process[1-4].

For the purpose of this work, mineral liberation analysis at concentration and pre-concentration stages must be carried out. The acquisition of mineral liberation analysis of fine particles, in the case of concentration, was carried out by scanning electron microscopy with automated mineralogy, using the QEMSCAN® technology. These systems are able to generate statistically valid information of modal compositions, mineral liberation and particle shapes [5-7]. As already mentioned, the MLA systems SEM-based are not feasible to work with the coarse sample specimens and size particles, as required to acquire mineral liberation analysis at pre-concentration sizes. Notwithstanding the emerging of hyperspectral imaging methods for mineral mapping, technologies to develop mineral liberation analysis at coarse particle size are not very accessible [8-11]. At the beginning of the presented work, the offer of this new technology was very scarce. Thus, a straightforward and simplified methodology, to acquire some quantitative mineralogical data for application to coarse sized samples and individual particles, was conceived and developed.

This chapter aims at presenting the adopted and developed procedures for mineral liberation analysis in the grinding and crushing steps to generate data that allow the computation of the grade histograms (wt%) that will be used to characterize the feeding of the concentration and pre-concentration stages, respectively.

4.2 MINERAL LIBERATION ANALYSIS AT GRINDING SIZES

Sub-samples of São Pedro das Águias and Alvarrões were sent to Camborne School of Mines, to be analyzed in a QEMSCAN® 4300 and to produce the required mineral liberation analysis. Then, quantitative mineralogical data obtained from QEMSCAN®

could be applied to compute the grade histograms (wt%), which is a robust descriptor of the liberation state of a given mineral system, and fundamental to assess the mineral separation efficiency. The QEMSCAN® procedure and the data treatment to assess the grade histograms (wt%) is discussed in the next sections.

4.2.1 QEMSCAN® METHODOLOGY – SAMPLE PREPARATION AND OUTPUTS

Samples of São Pedro das Águias size fractions (SPA[cutsize=0.212] and SPA[cutsize=0.075]) and Alvarrões ore after grinding and desliming, were analyzed by QEMSCAN®. In a simplified way, particles are scanned with an electron beam at a pre-determined resolution; X-ray spectra and backscattered electron signals are collected and compared to a database of known minerals (and other chemical phases). The mineralogical phases are then identified, and the surface spatial distribution of minerals is calculated. To ensure accurate mineral identification, QEMSCAN® is cross-checked with optical microscopy. The modal mineralogy, calculated chemical composition and grade, mineralogical association and liberation data can then be evaluated in the context of products chemical assays to inform about losses during mineral processing [12].

The preparation procedure was the following:

- Polished sections (30 mm diameter epoxy resin mounts) were prepared;
- Sample quantity was randomly reduced for analysis by coning and quartering;
- A mix of the sample with pure carbon powder (to ensure good particle separation and reduce settling) was mounted in cold epoxy resin (Epofix) into plastic moulds and left to cure;
- The samples were then labelled and encased in Araldite resin, producing a 30 mm diameter block with a thickness of approximately 15 mm.
- The blocks were polished to a 1 μm finish using diamond media and carbon-coated to 25nm.
- The mixture of graphite and sample creates a viscous fluid that is evenly mixed, and so, the settling issue is reduced as much as possible [6].

Then, using a Zeiss EVO® 50 scanning electron microscope instrument, fitted with four light elements Bruker Xflash® silicon drift energy-dispersive X-ray detectors and an electron backscattering detector it was possible to carry out the analysis, following the next steps:

- The system relies on the collection of spatially resolved X-ray spectra and BSE within a specified area of the sample, which is compared to a database of known minerals;
- An essential component of QEMSCAN® analysis is the development of the mineral list, known as species identification protocol (SIP) using these X-ray spectra and BSE signals.
- In this study, the analyses were carried out in field scan mode, with X-ray and BSE data collected every 10 μm on the polished block [13].
- The fieldscan analytical mode allows for the collection of compositional data in a predefined grid across the sample surface, producing a visual representation of the distribution of minerals (mineral map), as well as quantitative data.
- Species Identification Protocols were developed in-house tailored to the two different reference ores to ensure correct identification of the target minerals in each case.
- QEMSCAN® mineral identification was cross-checked by optical microscopy and manual SEM on thin polished sections.

As QEMSCAN® works with mineral mapping, the grade is always referred to as mineral grade (that by stoichiometry can be converted in metal grade).

Since São Pedro das Águias scheelite ore is a low-grade ore, a substantial number of particles with grade close to 0% would be generated after grinding. According to this, it is adequate to discretize the grade classes near to 0%0-10% grade into 5 classes. A similar approach was applied to the range of 90-100% since the generation of some high-grade particles was also expected.

Table 22 shows the distribution of scheelite in the several mineral grade fractions for the two samples of São Pedro das Águias (we should remember that each sample was obtained by elutriation of the fine crushed material), given by QEMSCAN®. For better readability of the graphical representation presented in Fig. 64, discretized grade fractions between 0-10% and 90-100% were merged again in the respective single fractions 0-10% and 90-100%. However, all mathematical manipulations were performed with more discretized grade classes.

Table 22 – Scheelite distribution by grade class in the São Pedro das Águias samples.

Grade Class (%)	SPA [cs=0.212]	SPA [cs=0.075]
0-2	0.28	1.68
2-4	0.20	0.57
4-6	0.08	0.13
6-8	0.01	0.25
8-10	0.30	0.21
10-20	0.86	0.59
20-30	0.16	7.75
30-40	0.48	0.36
40-50	0.00	0.96
50-60	0.18	0.13
60-70	0.28	0.64
70-80	0.04	1.27
80-90	1.50	4.81
90-92	0.03	0.51
92-94	7.86	1.19
94-96	1.43	2.23
96-98	12.43	13.95
98-100	73.90	62.77

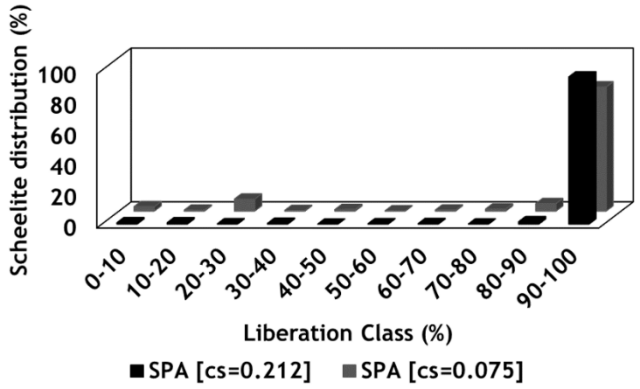

Fig. 64 – Scheelite distribution in each grade fraction.

Similar data was generated for the Alvarrões ore. In this case, as for an average head grade of 1%, Li_2O lepidolite represents 12.99% mass of the ore, the discretization of the extreme grade classes was not required. Table 23 and Fig. 65 shows the distribution of Lepidolite in the several mineral grade fractions of the Alvarrões milled sample, given by QEMSCAN®.

Table 23 - Lepidolite distribution by grade class in the Alvarrões sample.

Grade Class	Lepidolite distribution (%)
0-10	4.05
10-20	2.36
20-30	2.11
30-40	1.6
40-50	1.14
50-60	1.58
60-70	1.64
70-80	3.31
80-90	4.29
90-100	77.91

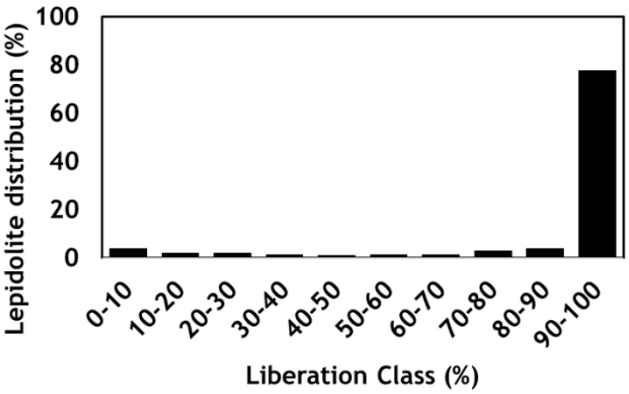

Fig. 65 – Lepidolite distribution in each grade fraction.

4.2.2 ACQUISITION OF GRADE HISTOGRAMS (WT%)

As mentioned before, QEMSCAN® mineral liberation analysis is fundamental to build the grade histograms (wt%), computed as the mass distribution in each (mineral) grade fraction.

Thus, QEMSCAN® data can be read as the percent mass of mineral in each grade class and is equivalent to mineral recovery (ε_i) that can be converted into total mass distribution, equivalent to yield (γ_i), both referring to the respective grade class, considering the ore head mineral grade (α) and assuming that the mineral grade of each

fraction (β_i) is given by the mid-value of the grade interval. This relationship is represented by Eq. 21.

$$\gamma_i = \varepsilon_i \times \frac{\alpha}{\beta_i} \qquad \text{Eq. 21}$$

The yield (γ_i) calculated for each mineral grade class, is the mass distribution which is referred to as the mineral grade histogram (wt%). However, to solve this approach conveniently, a final problem arises: assuming for the grade of each fraction (β_i) the mid-value of each grade interval it is necessary to define a slack variable that ensures the closing of the global mass balance. Thinking on this problem it was realized that for the grade of class nº 1 (β_1), corresponding to 0-2% and 0-10%, respectively for São Pedro das Águias and Alvarrões, it should not be recommended the use of the mid-value of the interval, because in those classes there will exist significant amount of particles of almost 0% grade. According to this, the grade of class nº 1 (β_1) was elected as the slack variable which determination should meet the following mass balance Eq. 22:

$$\sum_{i=1}^{n} \gamma_i = \sum_{i=1}^{n} \varepsilon_i \times \frac{\alpha}{\beta_i} = 1 \qquad \text{Eq. 22}$$

Once established the average grade of the first-class, it was possible to compute the grade histograms (wt%) for both case studies.

For the case of two samples from São Pedro das Águias, Table 24 shows the representation of QEMSCAN® raw data (Fig. 66), the calculated values of the mass distribution by mineral grade fraction – Grade Histogram (wt%) (Table 25) and the corresponding graphical representations (Fig. 67) to the two studied samples. A similar procedure is applied for the case of Alvarrões, as can be seen in Table 26.

Table 24 – Acquisition of grade histogram (wt%) using QEMSCAN® data- São Pedro das Águias.

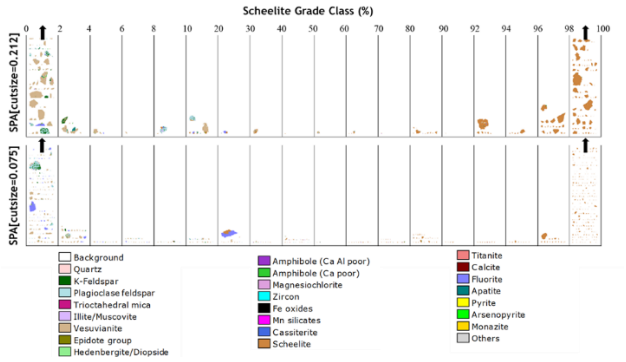

Fig. 66 – Particles distribution obtained by QEMSCAN® - São Pedro das Águias samples (extreme values are not fully represented in the plot area).

Table 25 – Mass distribution (%) by grade fraction – Grade Histogram (wt%).

Grade Class	0-10	10-20	20-30	30-40	40-50	50-60	60-70	70-80	80-90	90-100
SPA[cs=0.212]	97.30	0.11	0.12	0.09	0.08	0.07	0.07	0.08	0.11	1.97
SPA[cs=0.075]	97.84	0.10	0.11	0.08	0.07	0.07	0.07	0.08	0.10	1.47

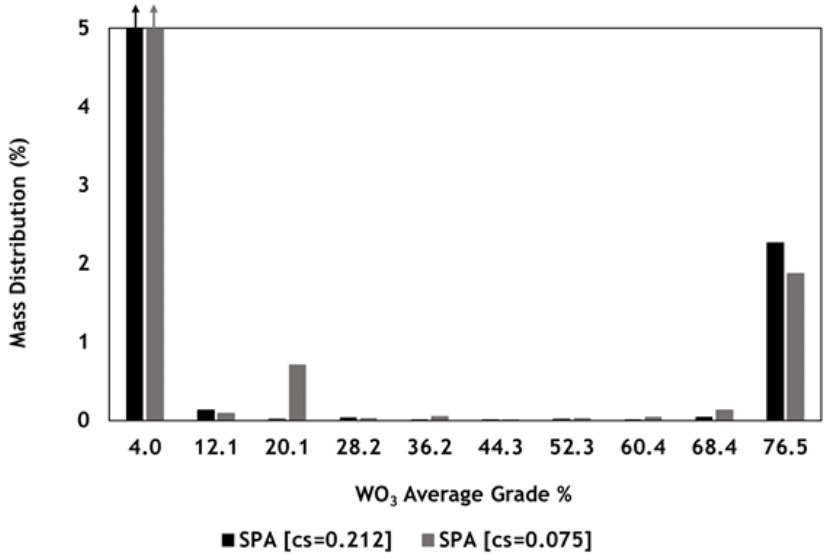

Fig. 67 – Mineral Grade Histogram (wt%) - São Pedro das Águias.

As it is possible to observe, both size fractions of São Pedro das Águias are well liberated, which is confirmed by the U-shape of the grade histogram (wt%). The amount of high liberated scheelite is higher in the greater size fraction, which can be due to the principle of equal settling, meaning that particles with different densities can exhibit the same settling velocity depending on the particle size. Due to the high specific gravity of

scheelite, it is possible that fine particles with high scheelite grade show similar settling behaviour as that of large particles with low scheelite grade and consequently low density.

Table 26 - Acquisition of grade histogram (wt%) using QEMSCAN® data- Alvarrões.

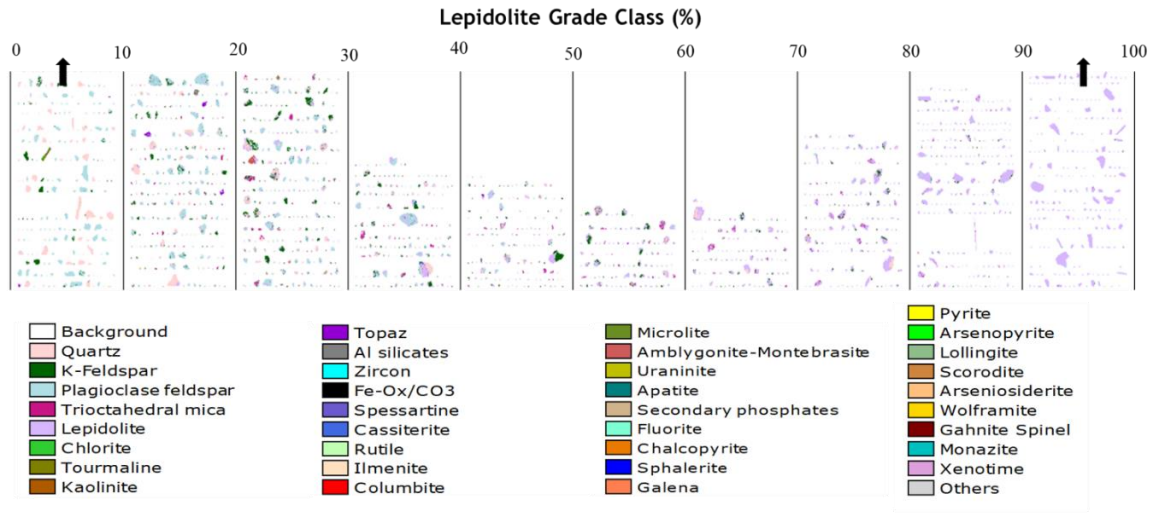

Fig. 68 – Particles distribution obtained by QEMSCAN® - Alvarrões sample (extreme values are not fully represented in the plot area).

Table 27 - Mass distribution (%) by grade fraction – Grade Histogram (wt%).

Grade Class	0-10	10-20	20-30	30-40	40-50	50-60	60-70	70-80	80-90	90-100
Alvarrões	81.73	2.24	1.20	0.65	0.36	0.41	0.36	0.63	0.72	11.69

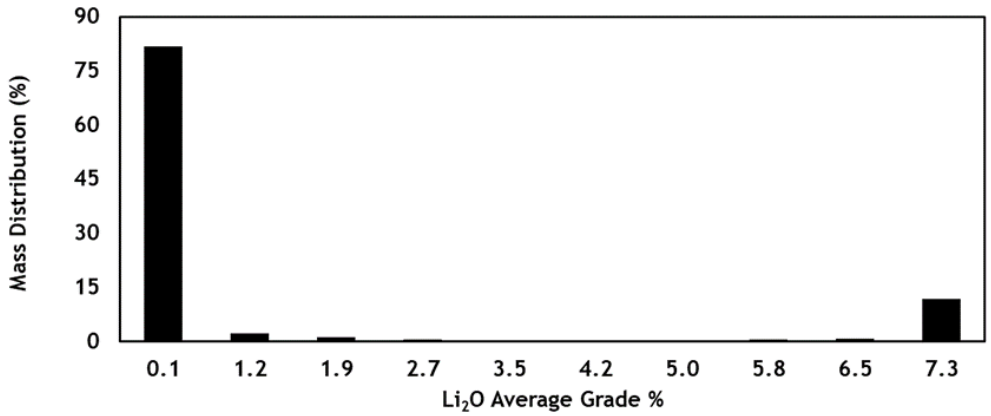

Fig. 69 – Mineral Grade Histogram (wt%) – Alvarrões.

Concerning the Alvarrões grade histogram (wt%) represented in Fig. 69, it is also observed a high liberation degree, confirmed by the U-shape histogram, meaning a high absence of particles in the intermediate grade classes.

4.2.3 FITTING HISTOGRAMS USING BETA LAW LIBERATION MODEL

In Chapter 2, Euler's Beta function (or Beta Law) was introduced as an appropriate mathematical/Statistical descriptor of liberation, that can be easily adjusted to real grade histograms (wt%), using only two parameters (P and Q). Moreover, the adjusted parameters can be interpreted according to the liberation degree of the mineral system. For the purpose of a qualitative validation of the experimental grade histograms (wt%) determined with data gathered with QEMSCAN® and also to reduce noise that sometimes affects mineralogical data due to sampling lack of representativeness, the generated histograms were fitted using the liberation model. It should be mentioned that p and q parameters were fitted using the Levenberg-Marquardt optimization algorithm. The goodness-of-fit was evaluated through the chi-squared test.

Starting by the case of São Pedro das Águias, P and Q parameters were adjusted to obtain the grade histograms (wt%) predicted by the Beta liberation model that better fit the experimental grade histograms. Fig. 70 shows the comparison between the grade histograms (wt%) acquired based on QEMSCAN® data and the beta law prediction for both size fraction of São Pedro das Águias ore.

a)

	1	3	5	7	9	15	25	35	45	55	65	75	85	91	93	95	97	99
QEMSCAN®	97.35	0.155	0.039	0.003	0.076	0.133	0.015	0.032	1E-04	0.008	0.01	0.001	0.041	7E-04	0.196	0.035	0.298	1.734
Beta law	96.87	0.21	0.10	0.07	0.05	0.11	0.12	0.09	0.08	0.07	0.07	0.08	0.11	0.09	0.04	0.05	0.08	1.71

b)

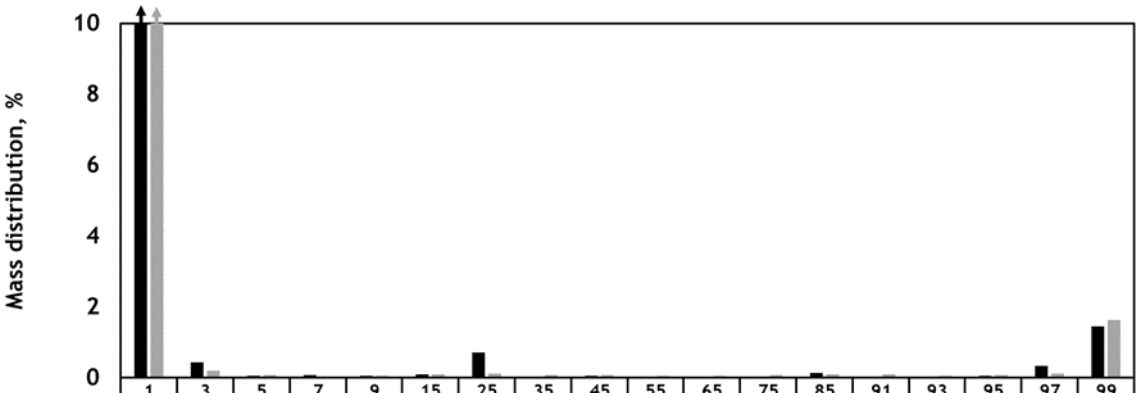

	1	3	5	7	9	15	25	35	45	55	65	75	85	91	93	95	97	99
QEMSCAN®	96.45	0.432	0.061	0.081	0.053	0.09	0.709	0.023	0.049	0.006	0.022	0.039	0.129	0.013	0.029	0.054	0.329	1.449
Beta law	97.00	0.20	0.08	0.04	0.05	0.10	0.11	0.08	0.07	0.06	0.06	0.08	0.10	0.08	0.06	0.08	0.11	1.63

Fig. 70 - Comparison between grade histograms (wt%) acquired using QEMSCAN® data and those predicted by Beta Law – São Pedro das Águias: a) SPA[CS=0.212mm]; b) SPA[CS=0.075mm].

P and Q values were (0.0019; 0.0833) and (0.0018; 0.1029) respectively for both size fractions. Both these values are substantially below 1, which, according to the Beta liberation model, points out for a high liberation degree of the ore, confirmed by the grade histograms (wt%). Q is significantly above P, which is due to the very low average samples grade.

Chi-squared test was applied to both size fractions, obtaining X^2 values of 2.56 and 2.69, respectively. For a significance level of 5%, considering 17 degrees of freedom, the theoretical X^2 is 27.59. According to this, as all computed values are substantially above, so it is possible to confirm the feasibility of using the Beta law to fit the obtained grade histograms (wt%).

The same process was applied to the Alvarrões ore. Fig. 71 shows the comparison between the grade histograms (wt%) calculated with QEMSCAN® data and the prediction of Beta law liberation model.

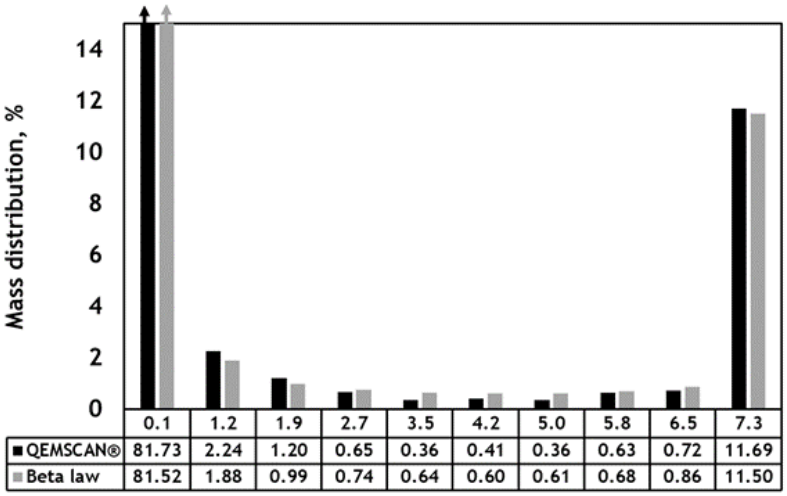

	0.1	1.2	1.9	2.7	3.5	4.2	5.0	5.8	6.5	7.3
QEMSCAN®	81.73	2.24	1.20	0.65	0.36	0.41	0.36	0.63	0.72	11.69
Beta law	81.52	1.88	0.99	0.74	0.64	0.60	0.61	0.68	0.86	11.50

Fig. 71 - Comparison between grade histograms (wt%) acquired using QEMSCAN® data and those predicted by Beta Law – Alvarrões ore.

P and Q values were 0.019 and 0.44, respectively. These values are both substantially below 1, pointing out for a high liberation degree of the ore, and Q > P but under a ratio lower than in the case of São Pedro das Águias, which is compatible with the lepidolite grade in the range of 25% much higher than the case of scheelite grade.

A chi-squared test was applied, obtaining X^2 values of 0.44. For a significance level of 5%, considering 9 degrees of freedom, the theoretical X^2 is 16.92, which is higher than the experimental value. So, it is possible to confirm the feasibility of using the Beta law to fit the obtained grade histograms (wt%).

4.3 MINERAL LIBERATION ANALYSIS AT CRUSHING SIZES

A straightforward methodology was developed to acquire quantitative mineralogical data of macro-textures or particles in the pre-concentration size range, based on image analysis algorithms that segments pixels in digital images based on colour (RGB colour scale). The objective is to compute the grade histograms based on the analysis of digital images of sawing cuts of hand samples (macro-textures) and sets of broken particles.

4.3.1 MINERAL QUANTITATIVE DATA ACQUISITION

4.3.1.1 MACRO-TEXTURE EVALUATION

In the case of São Pedro das Águias scheelite ore, scheelite fluorescence under UV light allows for the visual distinction between the valuables and gangue minerals. Thus, to assess the ore macro-texture, a set of photos of half drill-cores were taken under UV light. Fig. 72 shows an example of a drill-core photo under daylight and UV light, where it is possible to distinguish scheelite from the other gangue minerals.

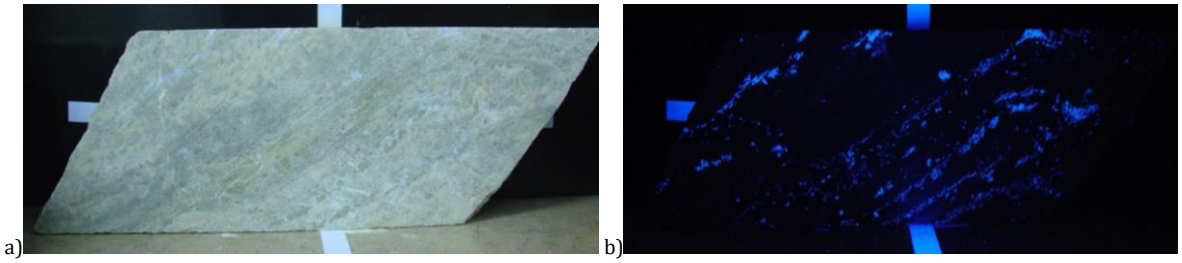

Fig. 72 - Example of Sample A photos a) at daylight; b) under UV light.

Several photos were cropped to obtain images without any background. Then a Matlab® algorithm was developed to convert the images into binary digital textures. For that purpose, the Matlab® command im2bw(f, level) was applied, where *f* is the image to be converted and *level* the parameter that controls the conversion of each pixel value (in the red-green-blue (RGB) scale) to a 0 or 1. The converted image replaces all pixels in the photo with luminance greater than level with the value 1 (white) and replaces all other pixels with the value 0 (black), as can be observed in Fig. 73.

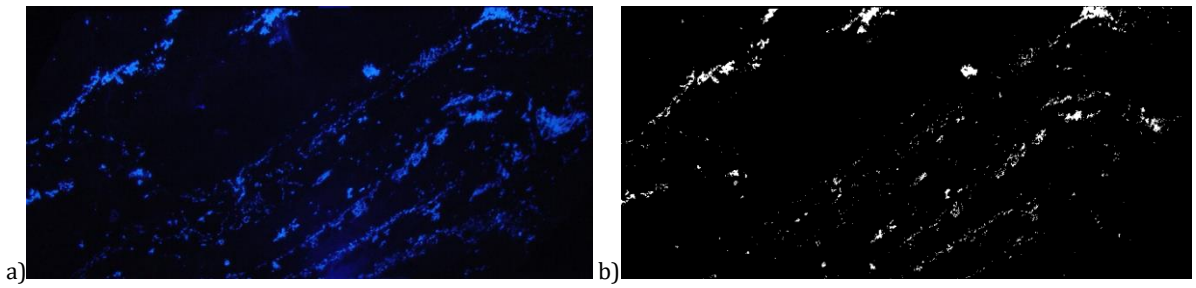

Fig. 73 – Conversion of a drill core photo (a) to a binary digital image (b).

Several photos of half drill cores were placed side by side to build a long drill core, simulating a representative sample of a scheelite distribution in a mineralized zone of São

Pedro das Águias ore deposit. An extract of the final macro-texture can be observed in Fig. 74.

a)

b)


Fig. 74 - Extract of São Pedro das Águias macro-texture: a) set of photos under UV light; b) Conversion to a binary image.

Then, the created algorithm is able to quantify the number of white and black pixels(px), which allowed for the calculation of the scheelite surface grade, according to Eq. 23.

$$\%scheelite\ (area) = \frac{counted\ white\ px}{counted\ total\ px} \qquad \text{Eq. 23}$$

However, the objective is to calculate scheelite mass grade, which means that it is necessary to multiply the number of white pixels by scheelite density and the number of black pixels by the gangue average density. Thus, it is possible to obtain the weight of each pixel and, consequently, it is possible to calculate the scheelite mass grade and the particle mass according to Eq. 24 and Eq. 25.

$$\%scheelite\ (mass) = \frac{(counted\ white\ px) \times \rho_{scheelite}}{(counted\ white\ px) \times \rho_{scheelite} + (counted\ black\ px) \times \rho_{gangue}} \qquad \text{Eq. 24}$$

$$particle\ mass = (counted\ white\ px) \times \rho_{scheelite} + (counted\ black\ px) \times \rho_{gangue} \qquad \text{Eq. 25}$$

Knowing the average grade of the São Pedro das Águias ore, obtained during the sample characterization procedure, it was possible to adjust the level of Matlab® command to meet the ore average grade. Table 28 shows the analysis of the *level* of the Matlab® command *im2bw* to calibrate the developed algorithm, according to the ore average grade. For the studied sample, a level of 0.35 was selected.

Table 28 - Determination of level for binary conversion.

Level	Scheelite (%)	WO_3 (%)
0.4	0.55	0.44
0.3	1.13	0.91
0.35	**0.99**	**0.80**

A similar procedure was applied to the lepidolite ore from the Alvarrões. In this case, the analysis was carried out with hand-samples collected at the mine site, instead of using half drill core samples. A set of samples were sawn to produce flat surfaces and photographed, as illustrated in Fig. 75 and placed side by side to simulate a cross-section of a mineralized pegmatite sill.

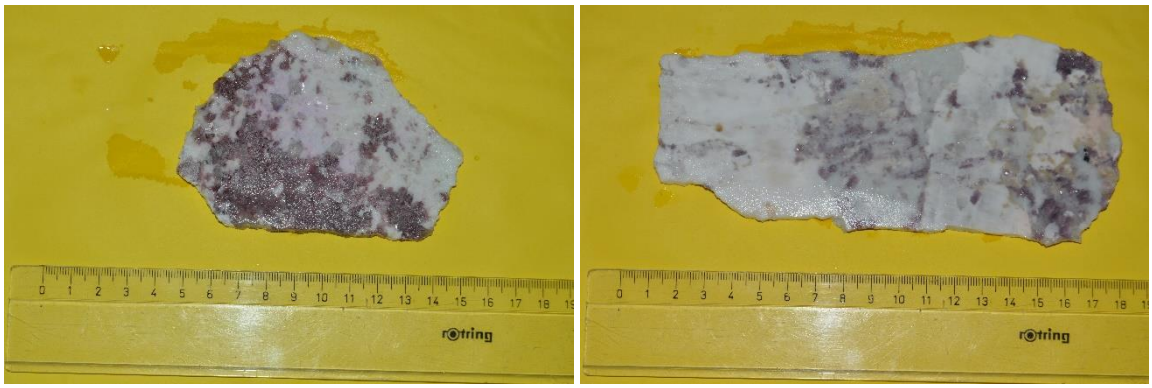

Fig. 75 - Photos of sawn hand sample from Alvarrões deposit.

Then, a Matlab® algorithm was developed to generate a digital texture where it is possible to distinguish Lepidolite from non-lepidolite pixels.

In the case of Alvarrões ore, the problem is more complex than in the case of scheelite from São Pedro das Águias, because the distinction between lepidolite and gangue minerals is based on a weaker signal obtained under visible light. It is an easy task for the human eye, but slightly complex for electronic devices.

First, it is imperative to find a way to characterize the lepidolite color, which can be done invoking the RGB color model. RGB is a color classification based on the red, green and blue light, which can be combined to reproduce a broad set of colors. Its main objective is to allow the representation of images in electronic systems. Each color

component (Red, Green and Blue) is represented on a scale between 0 and 255, which means that each image pixel is defined by three levels of color organized in a 3-D array.

The challenge was to determine the lepidolite RGB values which allow for the distinction between lepidolite pixels and gangue pixels. According to this, some pieces of Lepidolite were collected from the macro-texture photos, as illustrated in Fig. 76.

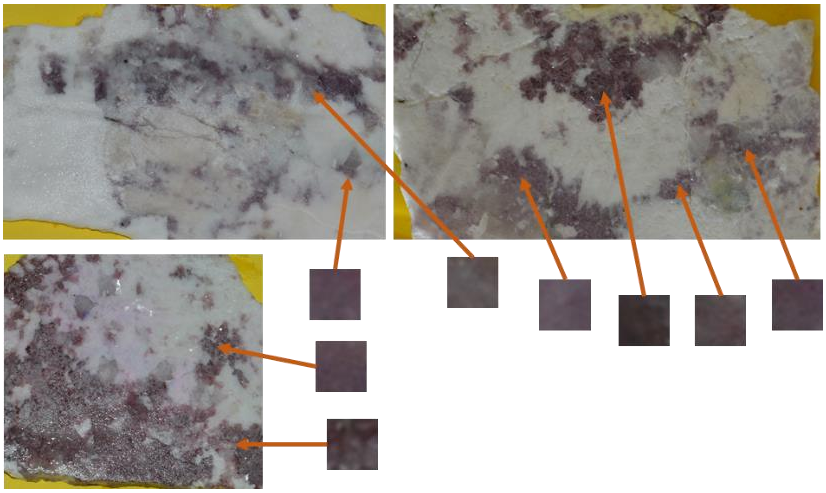

Fig. 76 – Collection of lepidolite standards.

Using these images and applying machine-learning techniques[14, 15], the algorithm was able to establish the range on the RGB scale that corresponds to Lepidolite. The study of the standards led to the definition of following ranges: i) red level between 48 and 134; ii) green level between 42 and 122; iii) blue level between 44 and 126. According to this, each px is classified as an LPD px if the three values of the RGB array meet the three previous intervals.

Eq. 24 can then be applied to compute the average grade of the digital image, considering the lepidolite and gangue minerals specific gravity (ρ) - 2.8 kg/m^3 in the case of Lepidolite and 2.6 kg/m^3 in the case of gangue minerals (mainly composed by quartz and feldspar). In this sense, a parameter L was added to the algorithm, increasing or reducing the length of the RGB intervals, according to the average ore grade.

The average ore grade determined in the coarsest size fraction after the coarse crushing of the size fraction 19.3/6.7mm is 1.97% Li_2O which corresponds to 25.6% Lepidolite. Applying the abovementioned intervals, the estimated average grade was computed as 28% Lepidolite. Then, the algorithm started to reduce the intervals until

obtaining a texture grade close to the objective. Table 29 presents the results of this process and Fig. 77 shows the procedure to obtain the final binary texture.

Table 29 – Calibration of RGB ranges according to Lepidolite average grade.

Parameter L	Colour level ranges			% Lepidolite	%Li_2O
	Red	Green	Blue		
0	48-134	42-122	44-126	29.3%	2.26
1	49-133	43-121	45-125	28.1%	2.16
2	50-132	44-120	46-124	27.2%	2.09
3	51-131	45-119	47-123	26.4%	2.03
4	**52-130**	**46-118**	**48-122**	**25.6%**	**1.97**

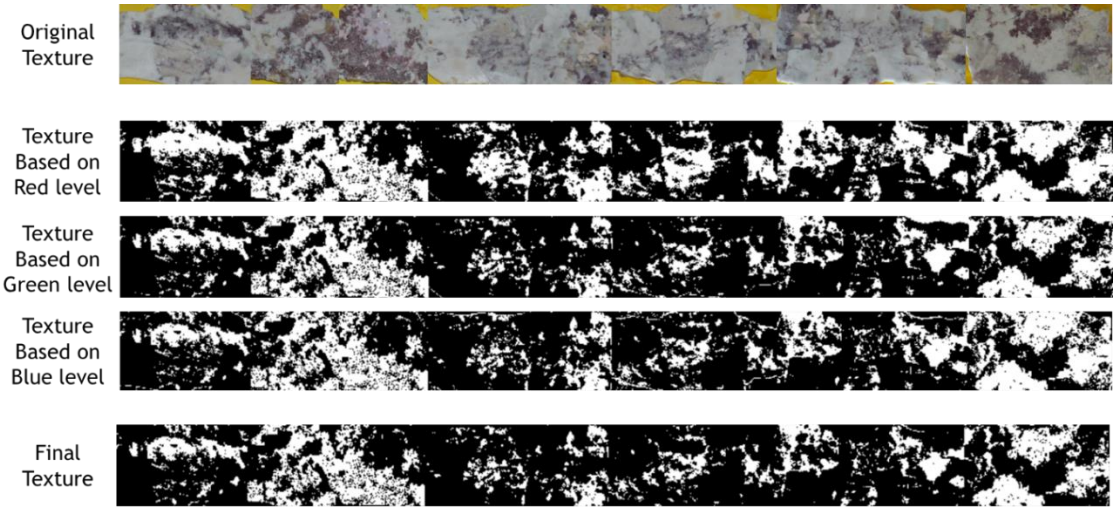

Fig. 77 – Representation of the main steps of the macro-texture generator algorithm.

At this point, even recognizing limitations in the methodology, such as low image resolution, the objective of producing a digital image representative of the ore macro texture seems to have been accomplished. It is not a real macro-texture image, but it is adjusted to the average ore grade and is composed by a series of real ore textures, which guaranty a certain level of representativeness of the spatial distribution of the valuable mineral.

4.3.1.2 BROKEN PARTICLES EVALUATION

As an alternative to the acquisition of mineral liberation analysis using digital macro-textures, mineral liberation analysis was directly applied to broken particles. Thus,

samples of the coarser size fractions were collected during the crushing stage. In the case of São Pedro das Águias, particles from each size fraction (16/13.5; 13.5/11.3; 11.3/9.5; 9.5/8.0; 8.0/6.7mm) were arranged in a grid to be photographed under UV light, as can be observed in Fig. 78. Due to the shadows caused by the particle irregularities, it was fundamental to use an image edition software to identify the boundaries of the particles and colour the background with a single tone colour as can be observed in Fig. 79 a).

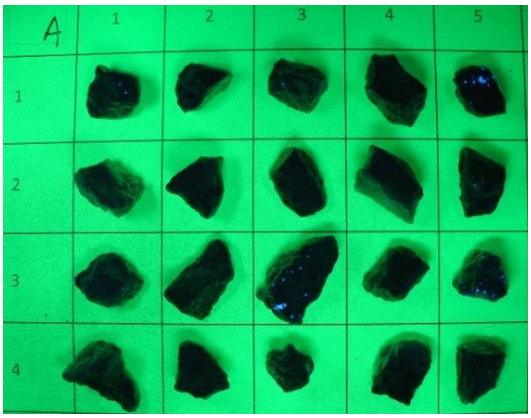

Fig. 78 - Particles arranged in a grid photographed under UV light.

After the photo's edition, a Matlab® algorithm was developed to convert the photos into digital textures, as it is possible to observe in Fig. 79. More examples are shown in the annexe A1.2.

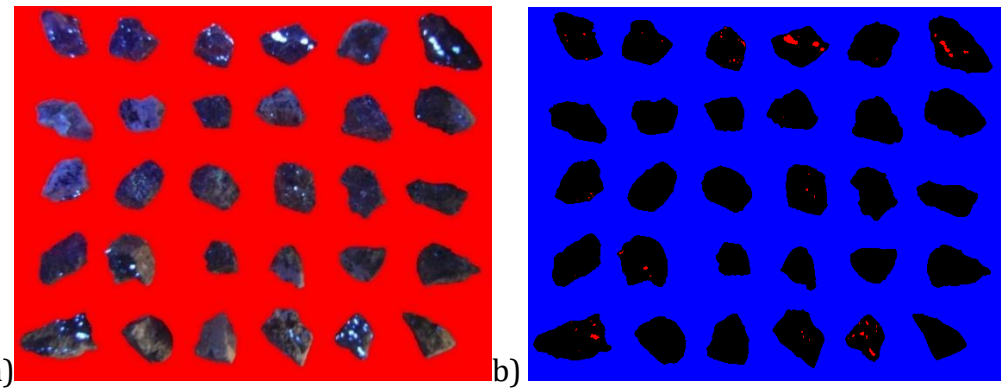

Fig. 79 – a) Photo of broken particles under UV light; b) Digital conversion of broken particles (red pixels represent scheelite pixels).

Then, based on the same methodology presented for macro-texture, the grade of each particle was calculated according to Eq. 24. The level was calibrated to adjust the grade of each size fraction to the chemical assays determined in the ore characterization

procedure. Table 30 shows the quality of the adjustment between real values and those calculated with data determined by image analysis of the particles observed under UV light using the developed algorithm.

Table 30 - Comparison between chemical assay and Matlab® calculated grades for each size fraction.

Size Fraction (mm)	Chemical Assay (XRF)		Matlab® calculation	
	%Scheelite	%WO_3	%Scheelite	%WO_3
16/13.5	0.987	0.794	0.974	0.754
13.5/11.3	0.814	0.656	0.801	0.650
11.3/9.5	1.284	1.034	1.287	1.036
9.5/8.0	0.877	0.706	0.871	0.701
8.0/6.7	0.705	0.567	0.699	0.563

Data obtained with this methodology was furtherly used to compute the grade histograms (wt%) given the respective size fraction.

In the case of Alvarrões ore, a similar procedure was applied using particles of each size fraction (19.3/16, 16/13.5, 13.5/11.3, 11.3/9.5, 9.5/8.0 and 8.0/6.7 mm) collected during the crushing stage and mounted in a regular grid and then photographed under daylight with a conventional camera. Photos were processed using the same image software and the Matlab® algorithm to convert photos into digital textures, recognizing the lepidolite pixels (red pixels) in each particle (Fig. 80). More examples are shown in the annexe A1.2.

a) 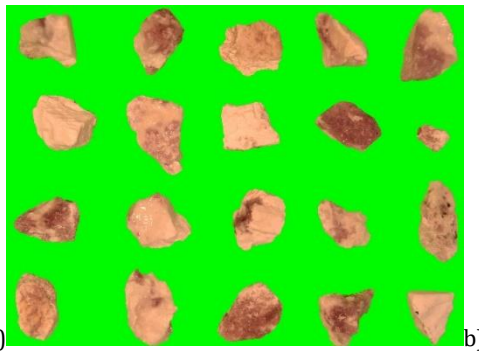 b) 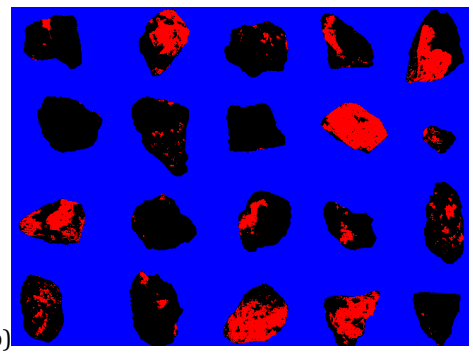

Fig. 80 - Conversion of photos of broken particles(a)) into digital textures (b)).

As in the case of scheelite, Table 31 shows the quality of the adjustment between real values and those calculated with data determined by image analysis of the particles observed under visible light using the developed algorithm.

Table 31 - Comparison between chemical assay and Matlab® calculated grades for each size fraction.

Size Fraction (mm)	Chemical Assay (AAS)		Matlab® calculation	
	%Lepidolite	%Li_2O	%Lepidolite	%Li_2O
19.3/16	27.3	2.10	27.8	2.14
16/13.5	25.9	2.00	26.2	2.02
13.5/11.3	25.1	1.93	25.9	2.00
11.3/9.5	25.7	1.98	28.3	2.18
9.5/8.0	26.2	2.02	28.6	2.20
8.0/6.7	27.4	2.11	27.1	2.09

Again, even being aware of the methodology limitations, which is more evident in the image analysis of broken particles due to the boundaries between particle and background, the calibration of the algorithm according to the average grade of each size fraction and the use of real textures representative of the ore are fundamental issues to have confidence in the obtained data.

4.3.2 GRADE HISTOGRAMS (WT%)

The proposed methodology allowed for the acquisition of quantitative mineralogical data based on an image analysis procedure that can be applied to macro-textures and broken particles. In the case of broken particles, grade histograms (wt%) for a given size fraction are easily calculated by automated particle-by-particle pixel counting on the digital images. In the case of the macro-texture, grade histograms (wt%) can be accomplished by applying a random comminution algorithm, that generates particles from the digital macro-texture with any desired size. Particles generated are then analyzed for grade determination by automated particle-by-particle pixel counting to obtain the grade histogram (wt%). This procedure is described in the next section.

4.3.2.1 ACQUISITION OF GRADE HISTOGRAMS OF PARTICLES GENERATED BY RANDOM COMMINUTION OF AN ORIGINAL ORE MACRO TEXTURE

The random comminution simulator is based on the overlapping of square masks under the acquired digital macro-texture. At each iteration, a particle is generated, with the desired size, collecting and storing the pixels information of each one. Then, by pixel counting and applying the formula presented in the Eq. 24, it is possible to calculate the grade of each particle. In the case of São Pedro das Águias, square grids of 15, 12, 10, 9 and 7 mm side, respectively, were adopted to compare with the size fractions used in the characterization of the broken material at minus 16 mm ([16/13.5]mm; [13.5/11.3]mm; [11.3/9.5]mm; [9.5/8.0]mm and [8.0/6.7] mm). The procedure is illustrated in Fig. 81.

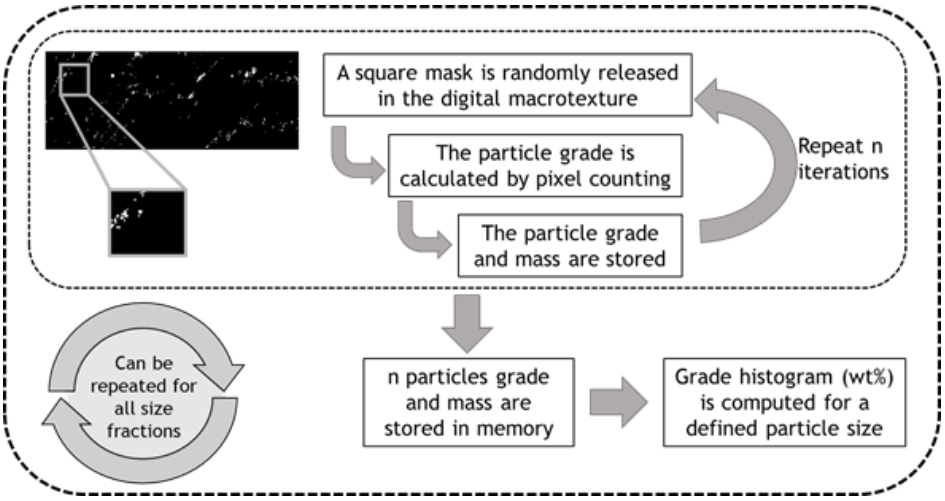

Fig. 81 – Procedure to generate grade histograms (wt%).

The application of the previous methodology allowed for the computation of the grade histograms (wt%) for all size fractions. Histograms were generated in some narrow size fractions to assess the evolution of the liberation degree. The grade histogram (wt%) of a broader size range 19.3/6.7 mm can be computed, considering the size composition of the crushed product of São Pedro das Águias ore to minus 16 mm, accordingly with Eq. 26 [1, 2, 16].

$$G_i(x) = \sum_j C_{i,j}(x,y) = \sum_j \left[B_{i,j}(x|y) \times A_j(y)\right] \quad \text{Eq. 26}$$

Where, $C_{i,j}(x,y)$ is the joint grade and size histogram, $B_{i,j}(x|y)$ is the conditional histogram of grade x given in the size y (i.e., grade histogram of a narrow size fraction of

size y), $A_i(y)$ is the marginal size histogram and $G_i(x)$ is the marginal grade histogram that represents the grade histogram of a broader size range.

Fig. 82 shows all the obtained histograms.

Random comminution of a digital ore macro-texture	São Pedro das Águias

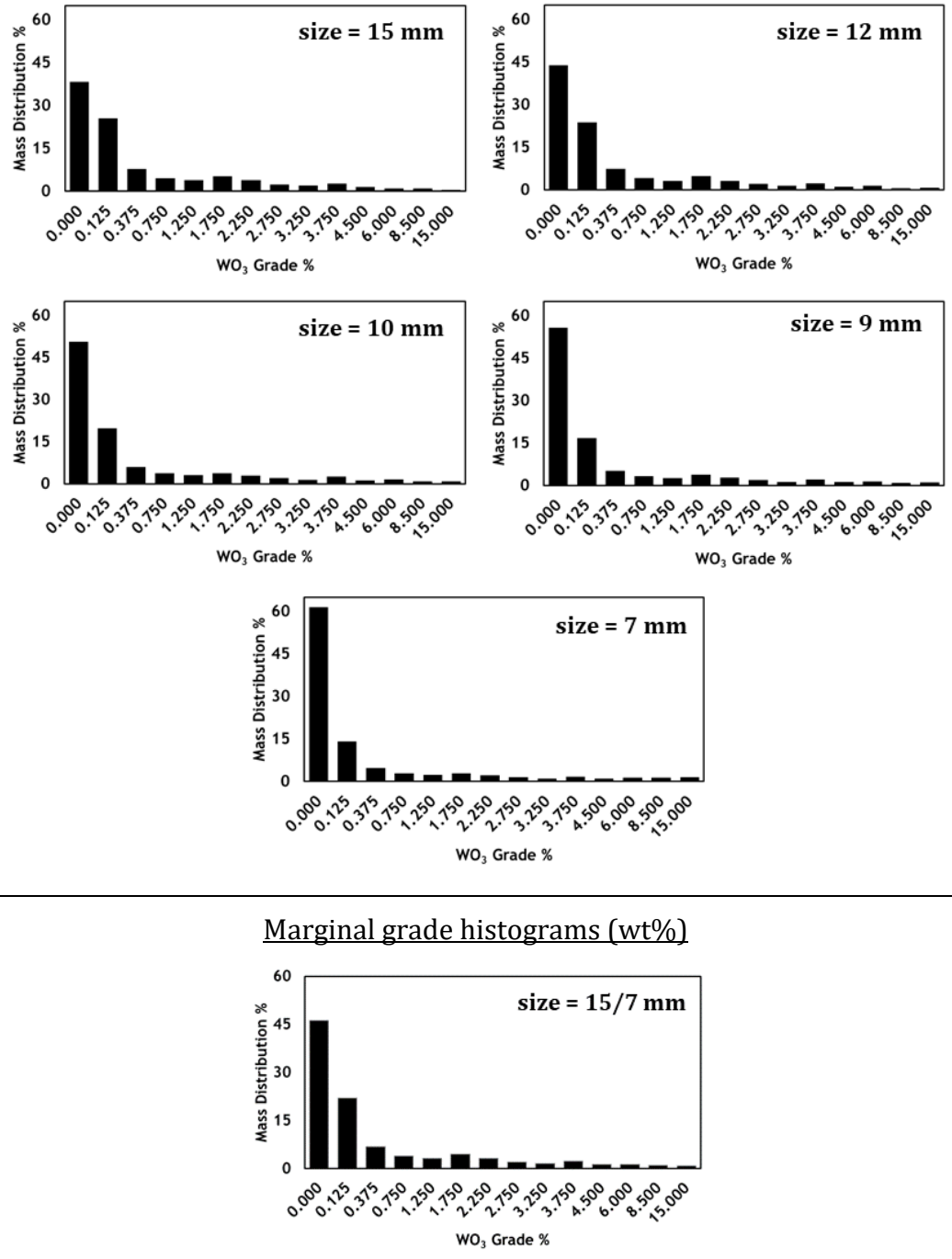

Fig. 82 - Grade histograms (wt%) of particles generated by random comminution of an original ore macro-texture – São Pedro das Águias case.

As expected, the liberation degree is higher in the finer size classes, which can be observed by the increase of 0% WO_3 particles with decreasing size, with the corresponding decrease of the mass in the middlings grade classes.

A similar procedure was applied to the acquired macro-texture of Alvarrões ore (Fig. 83). In this case, using square masks of 18, 15, 12, 10, 9 and 7 mm side, respectively, to compare with size fractions of [19.3/16] mm; [16/13.5]mm; [13.5/11.3]mm; [11.3/9.5]mm; [9.5/8.0]mm and [8.0/6.7]mm used in the characterization of the crushed material at minus 16 mm.

Random comminution of a digital ore macro-texture	**Alvarrões**

Grade histograms (wt%) by size fraction

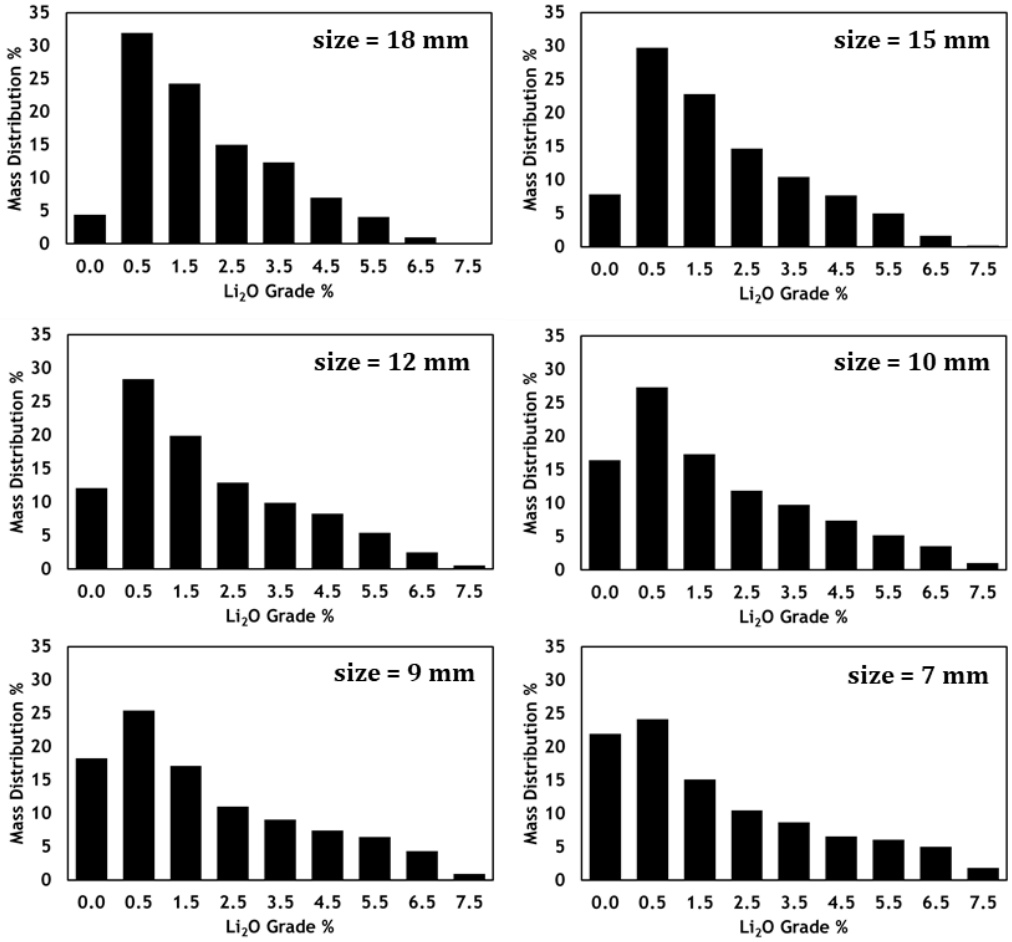

Marginal grade histograms (wt%)

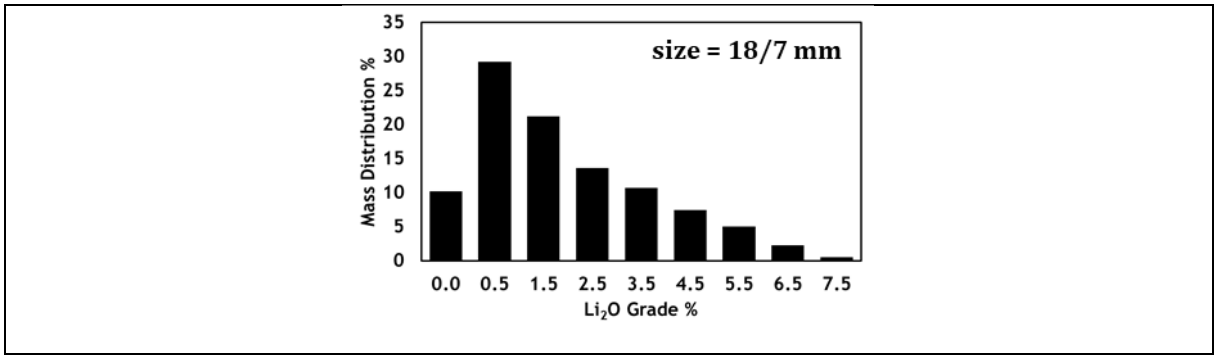

Fig. 83 - Grade histograms (wt%) of particles generated by random comminution of an original ore macro-texture – Alvarrões case.

4.3.2.2 ACQUISITION OF GRADE HISTOGRAMS OF BROKEN PARTICLES

As already mentioned, in the case of broken particles, grade histograms (wt%) for a given size fraction are easily calculated by automated particle-by-particle pixel counting on the digital images. This procedure is simpler because it only requires the computation of the particle grade by pixel counting and the corresponding storage of the grade and mass of each particle. A set of particles of each studied size fraction were photographed, converted into digital images for grade and mass calculation, and then the grade histogram (wt%) of each given size fraction was computed.

The acquisition of broken particles grade histograms is summarized in Fig. 84 and Fig. 85 for the cases of São Pedro das Águias and Alvarrões, respectively.

Broken Particles	São Pedro das Águias

Grade histograms (wt%) by size fraction

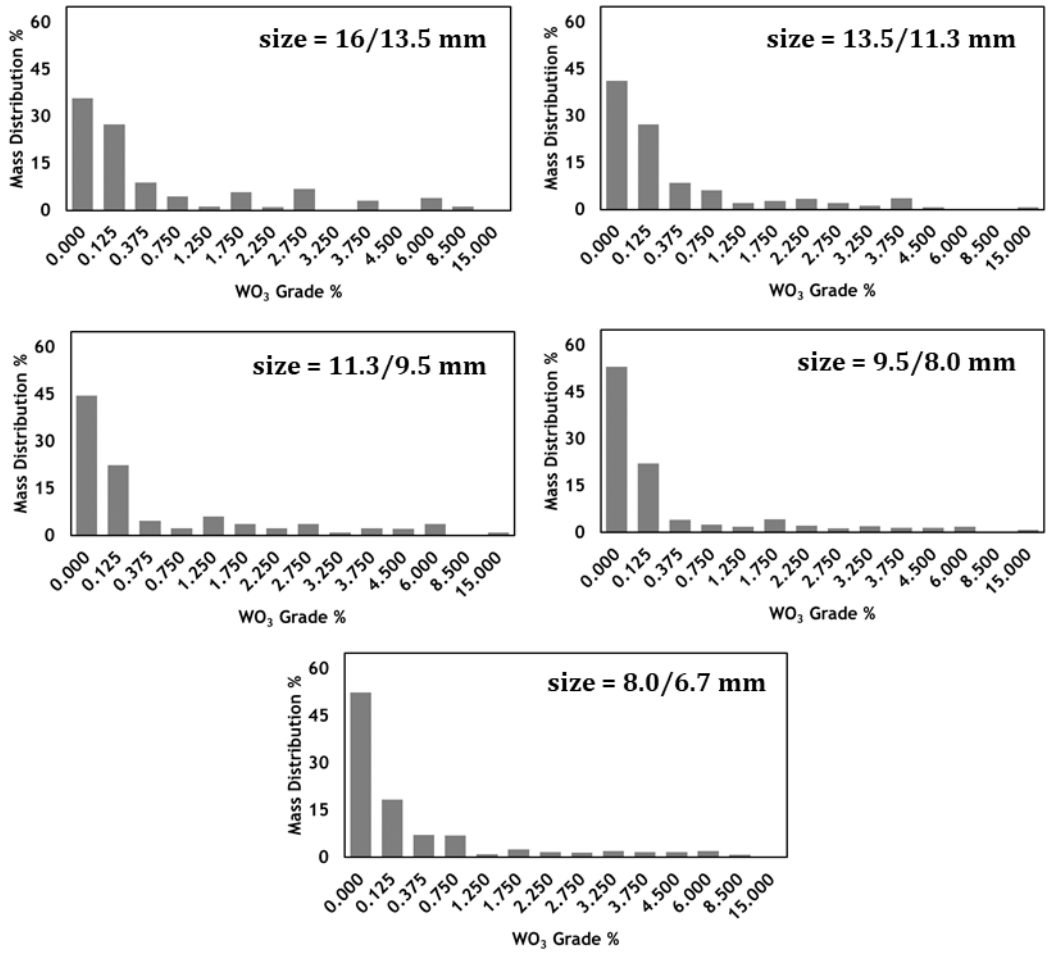

Marginal grade histograms (wt%)

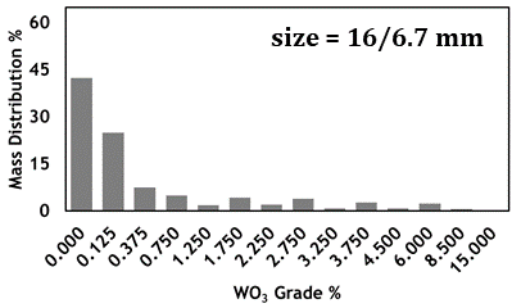

Fig. 84 - Grade histograms (wt%) of broken particles – São Pedro das Águias case.

Broken Particles	Alvarrões

Grade histograms (wt%) by size fraction

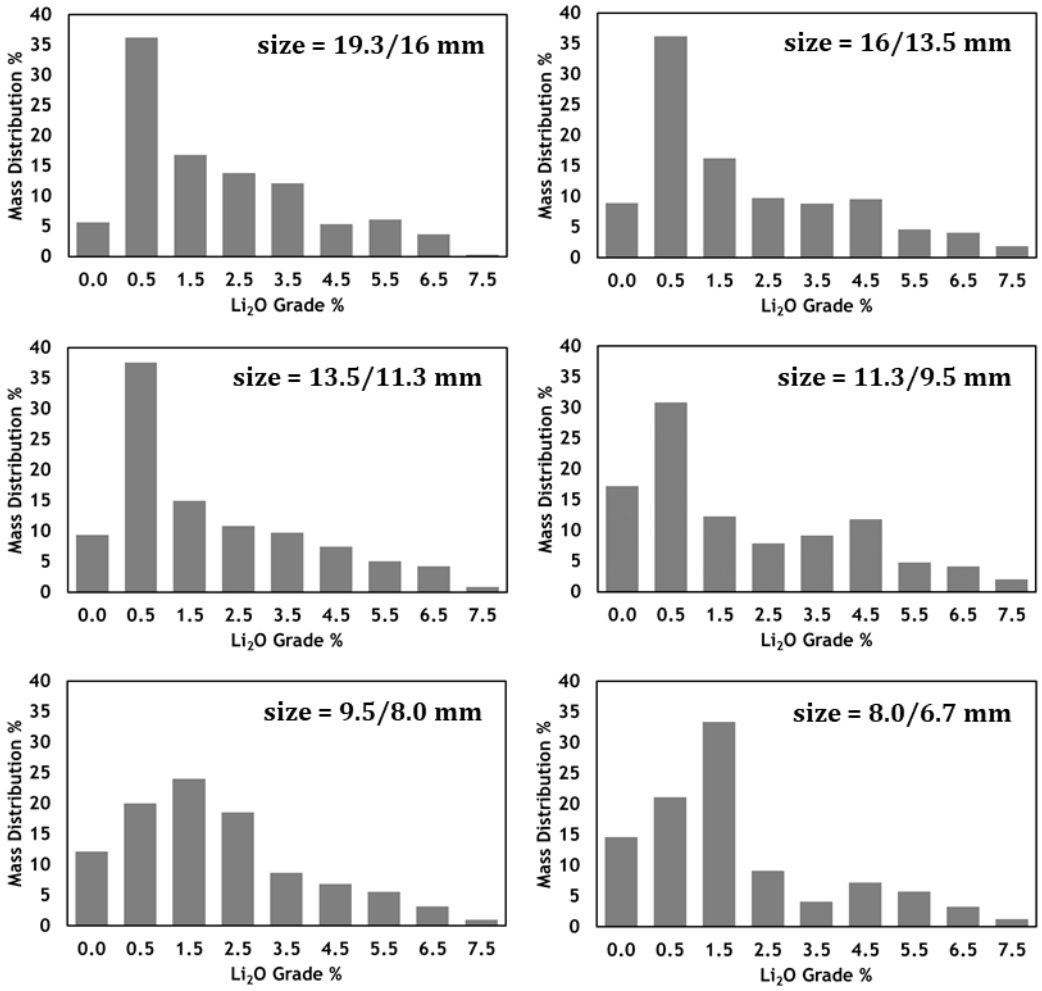

Marginal grade histograms (wt%)

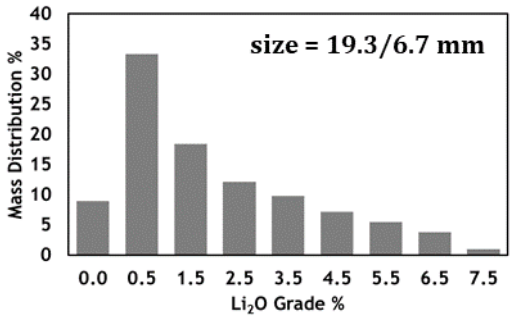

Fig. 85 - Grade histograms (wt%) of broken particles – Alvarrões case.

4.3.2.3 COMPARISON BETWEEN GRADE HISTOGRAMS GENERATED BY RANDOM COMMINUTION OF A DIGITAL TEXTURE AND BY ANALYSIS OF DIGITAL IMAGES OF BROKEN PARTICLES

As mentioned before, the presented methodology exhibits some weaknesses concerning the image resolution, which means that, for example, a fine inclusion of gangue minerals inside the valuable mineral grain would not be easily detected. In São Pedro das Águias case, scheelite fluorescence can produce a shadow effect around the valuable minerals inducing overcounting; in Alvarrões case lepidolite colour variability is responsible for a weak contrast with gangue minerals. According to this, although the adjustment of the algorithm with the average grade of each ore is fundamental to validate the applicability of the methodology, the agreement between the data produced by random comminution of digital images of macro-textures and by analysis of digital images of broken particles is crucial for the acceptance of the methodology.

Fig. 86 shows the comparison between grade histograms (wt%) of São Pedro das Águias, obtained for all studied size fractions and for a broader size fraction, based on image analysis of macro-texture randomly comminuted and of broken particles.

Globally, the comparison showed a good similarity. However, it should be highlighted that in size range 8/6.7 mm, the macro-texture procedure defined a higher quantity of 0 %WO_3 particles when compared with the broken particles' procedure. This difference is balanced in the next grade fraction (0.125 %WO_3), in which the quantity of particles is higher for the broken particles' approach than for the macro-texture approach.

Discrepancies between both approaches can be due to the fact that the random comminution algorithm applied to macro-texture allowed for the generation of an almost infinite number of particles (at least 5000 were generated in this work), while in the case of broken particles analysis, only approximately 100 particles were photographed for each size fraction, which points out to problems of representativeness when using this methodology.

Random Comminution vs Broken Particles	São Pedro das Águias

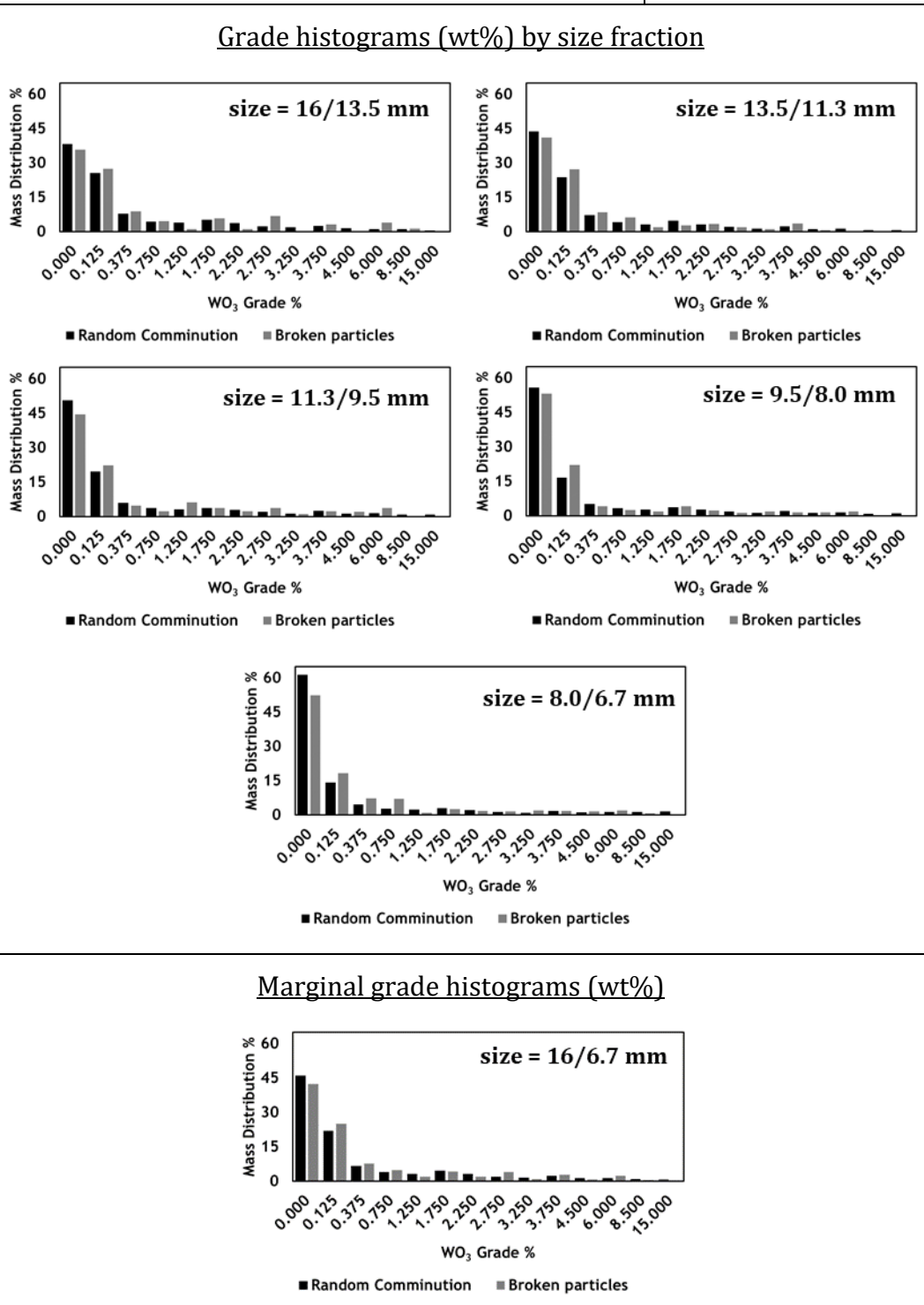

Fig. 86 - Comparison Between Grade Histograms generated by Random Comminution of a digital texture and by Analysis of digital images of Broken Particles – São Pedro das Águias case.

The same approach was carried out for the case of Alvarrões ore, as can be observed in Fig. 87.

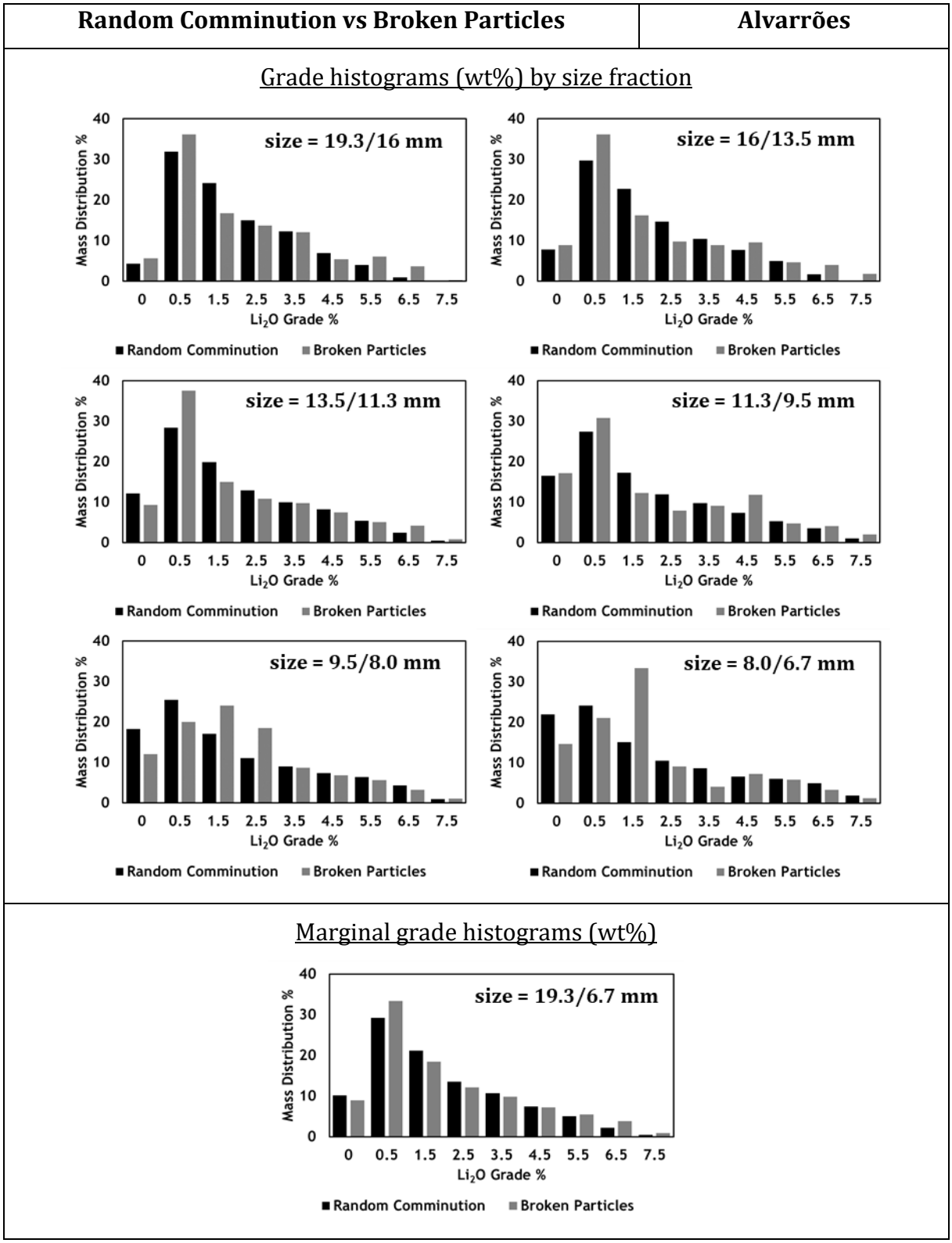

Fig. 87 - Comparison Between Grade Histograms generated by Random Comminution of a digital texture and by Analysis of digital images of Broken Particles – Alvarrões case.

Comparing the histograms of each size fraction, it is possible to observe some differences that are more evident in the lower size fractions. As in the case of São Pedro das Águias, the lack of representativeness in the case of the analysis of broken particles would be the major weakness of the methodology. This is indicated by the irregularity of the histograms, for example, the grade fraction 2.5 %Li_2O is practically constant in size range 19/9.5mm, presenting an unexpected growth in the lower size fractions.

Although the existence of some discrepancies in the individual histograms, a good similarity between the marginal grade histograms (wt%) of both approaches is observed, supporting the accuracy of the presented methodology.

In summary, in the case of São Pedro das Águias the comparison between two approaches showed a great consistency of the data, giving the confidence to validate the grade histograms (wt%) as representative of the ore mineral liberation. In the case of Alvarrões, there are some discrepancies between both approaches, requiring a more carefully data validation, in which Beta liberation model could play a fundamental role.

4.3.3 FITTING GRADE HISTOGRAMS (WT%) USING BETA LAW LIBERATION MODEL

Following the same procedure used to smooth the grade histograms acquired with QEMSCAN® data in the case of concentration sizes, the Beta Law liberation model was also fitted to all histograms generated to study the pre-concentration at crushing sizes. It is expected that Beta law would reduce the noise caused by the lack of representativeness, mainly in the case where grade histograms were generated with data gathered by pixel counting in a scarce number of digital images of broken particles.

4.3.3.1 GRADE HISTOGRAMS OF PARTICLES GENERATED BY RANDOM COMMINUTION OF DIGITAL MACRO-TEXTURES

This paragraph reports the application of the abovementioned procedure to determine the P and Q parameters that fit Beta Law model prediction to grade histograms (wt%) generated by random comminution.

Fig. 88 shows a graphical comparison of the adjustment for all grade histograms (wt%) of each size fraction and for the broader size fraction, for the case of São Pedro das Águias (crushing stage).

Fitting Beta to Random Comminution data	São Pedro das Águias

Grade histograms (wt%) by size fraction

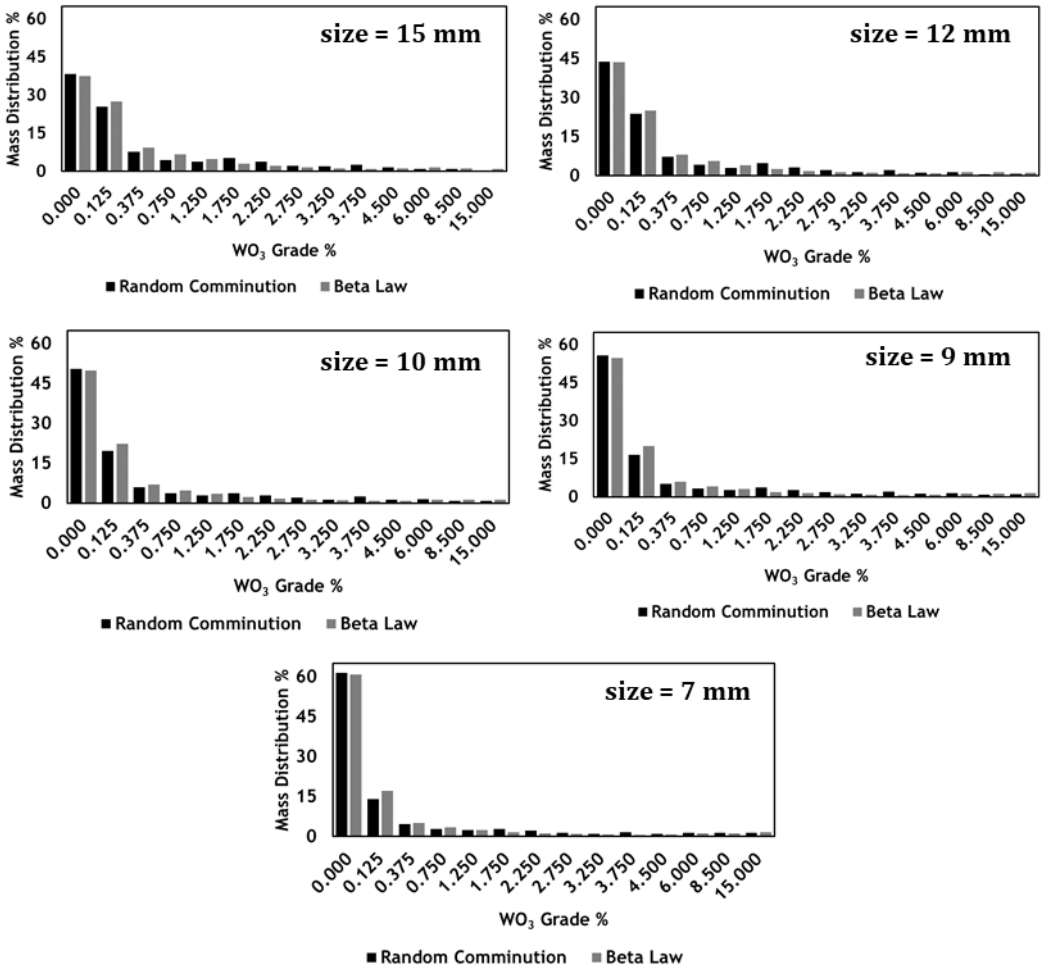

Marginal grade histograms (wt%)

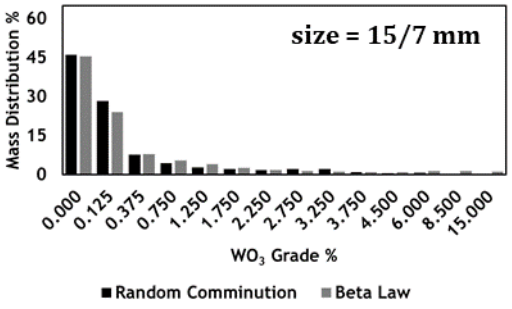

Fig. 88 - Fitting Beta Law Liberation Model to Grade Histograms (wt%) obtained by Random Comminution of digital textures – São Pedro das Águias case.

It is possible to observe that the grade histograms (wt%) predicted by the Beta law fit nicely to those obtained using the random comminution model of the macro-texture. Goodness-of-fit was assessed by a chi-squared test to determine whether there is a significant difference between the observed and the predicted grade histograms (wt%). Table 32 shows the X^2 values computed for the case of São Pedro das Águias ore.

Table 32 – Results of Chi-squared test applied to the fitting of São Pedro das Águias grade histograms (wt%) acquired by random comminution.

size (mm)	16/13.5	13.5/11	11/9.5	9.5/8	8/6.3
X^2	3.71	2.90	2.39	2.99	1.98

For a significance level of 5% and considering 13 degrees of freedom, the theoretical X^2 is 22.36. According to this, as all computed values are substantially below 22.36, so it is possible to confirm the feasibility of using the Beta law to fit the obtained grade histograms (wt%).

The same procedure was applied to the data generated during the analysis of Alvarrões macro-texture, as can be observed in Fig. 89.

Fitting Beta to Random Comminution data	Alvarrões

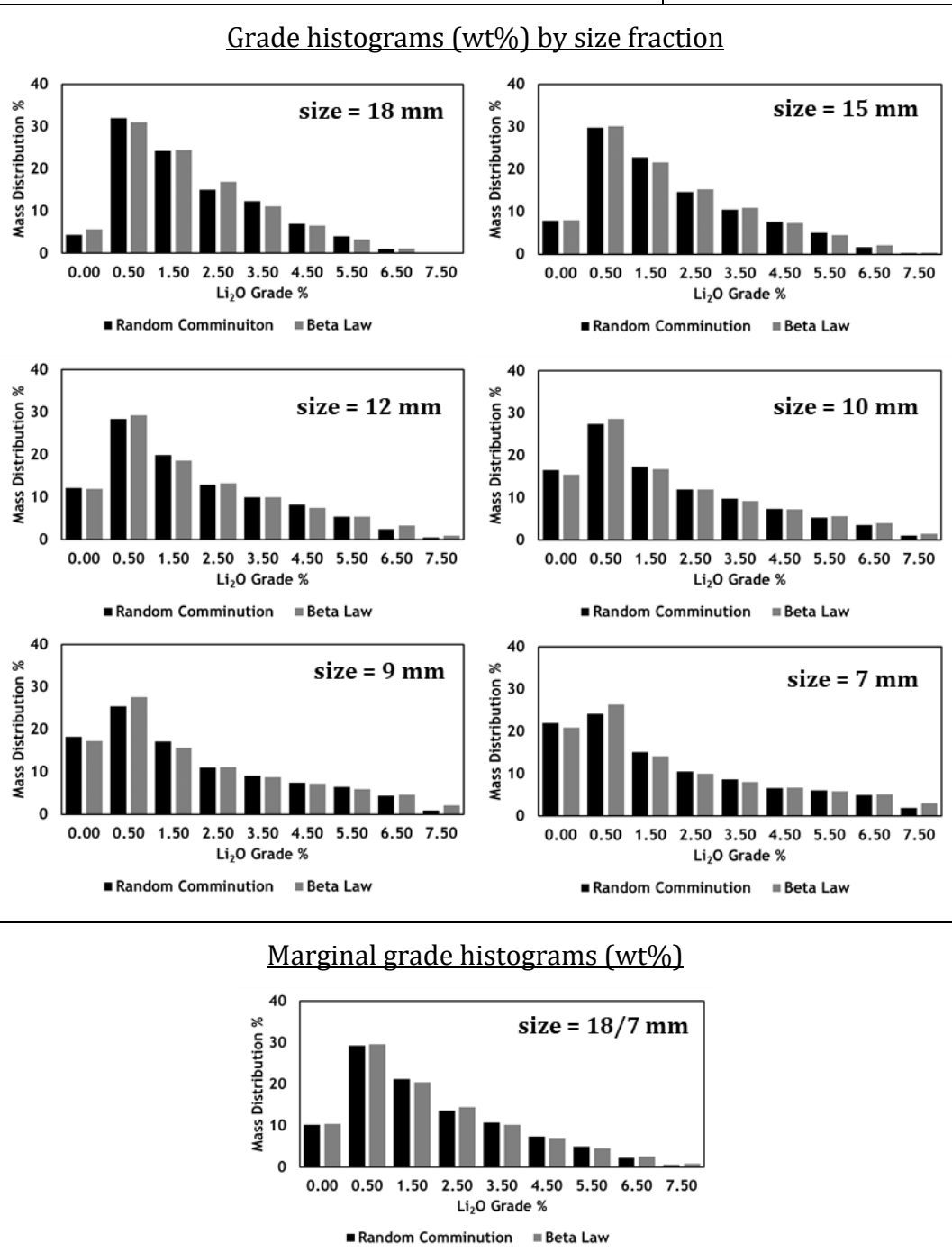

Fig. 89 - Fitting Beta Law Liberation Model to Grade Histograms (wt%) obtained by Random Comminution of digital textures – Alvarrões case.

The similarity between the grade histograms (wt%) predicted by the Beta law and those obtained using the random comminution model under the macro-texture was validated using the chi-squared test, as can be observed in Table 32.

Table 33 – Results of the Chi-squared test applied to the fitting of Alvarrões grade histograms (wt%) acquired by random comminution.

size (mm)	19.3/16	16/13.5	13.5/11	11/9.5	9.5/8	8/6.3
X^2	0.93	0.42	0.77	0.42	2.03	1.11

For a significance level of 5%, considering 8 degrees of freedom, the theoretical X^2 is 15.5. As all computed values are substantially below 15.5, so it is possible to confirm the feasibility of using the Beta law to fit the obtained grade histograms (wt%).

4.3.3.2 GRADE HISTOGRAMS OF BROKEN PARTICLES

The same process was applied to grade histograms (wt%) acquired using the broken particles. Fig. 90 show the acquired data for the case of São Pedro das Águias.

Fitting Beta to Broken Particles data	São Pedro das Águias

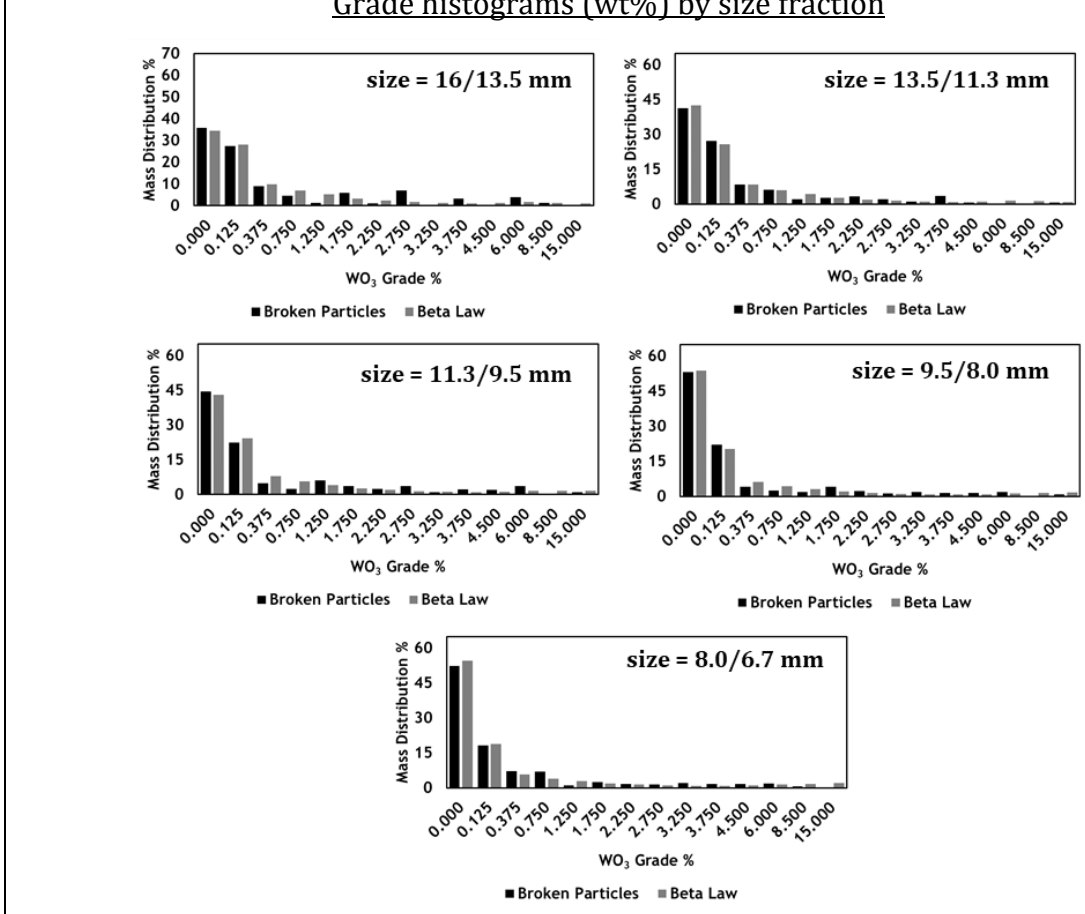

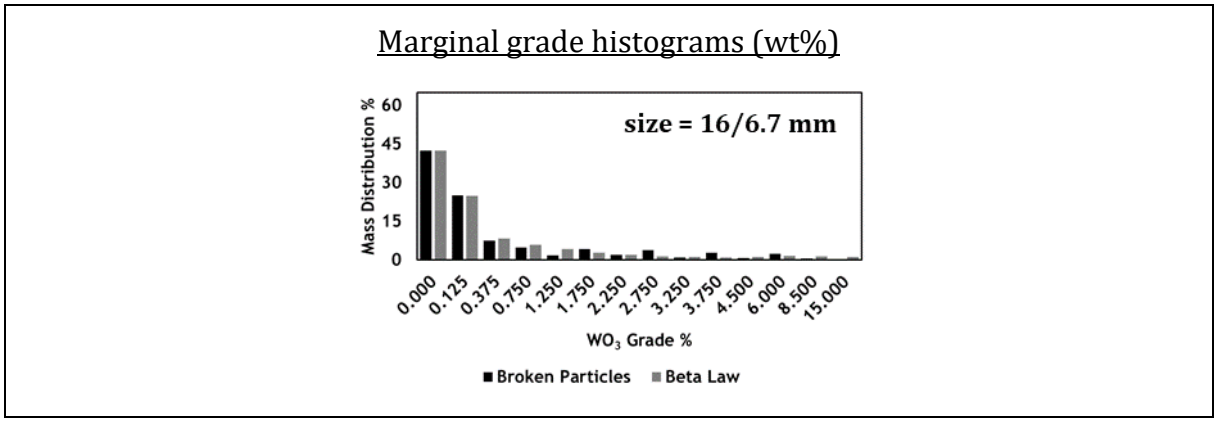

Fig. 90 - Fitting Beta Law Liberation Model to Grade Histograms of Broken Particles – São Pedro das Águias case.

As implemented in the previous cases, the chi-squared test was used to assess the goodness-of-fit, as can be observed in Table 34.

Table 34 – Results of Chi-squared test applied to the fitting of São Pedro das Águias grade histograms (wt%) acquired by random comminution.

size (mm)	16/13.5	13.5/11	11/9.5	9.5/8	8/6.3
X^2	21.44	3.40	9.27	5.22	6.24

For a significance level of 5% and considering 13 degrees of freedom, the theoretical X^2 is 22.36. According to this, all computed values are below 22.36, validating the feasibility of using the Beta law to fit the obtained grade histograms (wt%). However, the high values of X^2 obtained points to a higher discrepancy between observed and predicted values. The lack of representativeness of broken particles approach can be the main reason for these differences, due to the existence of some irregularities in the observed grade histograms (wt%), mainly for the high-grade classes.

Following the sequence, Beta liberation model was also applied to the case of Alvarrões, as can be observed in Fig. 91.

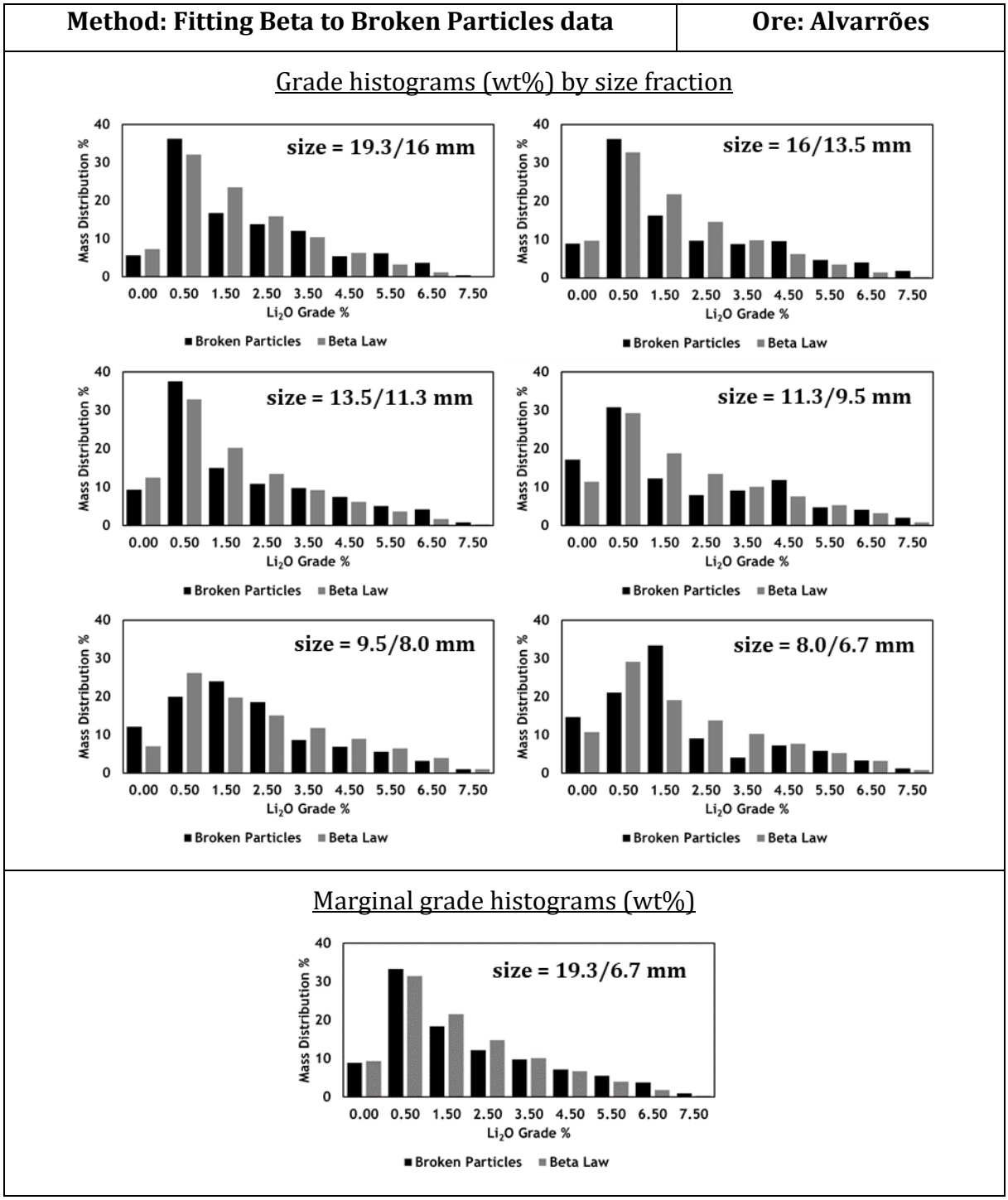

Fig. 91 - Fitting Beta Law Liberation Model to Grade Histograms of Broken Particles – Alvarrões.

Finally, the goodness-of-fit was assessed using the chi-squared test and the results are presented in Table 35.

Table 35 – Chi-squared tests applied to the fitting of Alvarrões grade histograms (wt%).

size (mm)	19.3/16	16/13.5	13.5/11	11/9.5	9.5/8	8/6.7
X^2	7.49	9.54	6.71	12.03	7.56	22.06

For a significance level of 5%, considering 8 degrees of freedom, the theoretical X^2 is 15.5. The use of Beta liberation model can be accepted for the size fraction 19.3/16, 16/13.5, 13.5/11, 11/9.5 and 9.5/8, and rejected for the size fraction 8/6.7mm. However, the deviation between observed and predicted values are higher than those obtained with the macro-texture data, indicating an improper adjustment of the Beta liberation model to the observed data. At first look, lack of representativity would be the main reason for the differences between observed and predicted data. As mentioned before, broken particles analysis was carried out over a limited number of particles, generating histograms with some irregularities.

4.3.3.3 DATA INTERPRETATION BASED ON BETA LIBERATION MODEL

The objective of using the Beta liberation model was not only to obtain accurate values that fit the grade histograms (wt%) acquired by image analysis of macro-textures and broken particles. It is known that the study of Beta function parameters (P and Q) by itself can conduct to a comprehensive interpretation of the ore liberation degree. Furthermore, it was expected that the comparison between the parameters obtained for the macro-texture and the broken particles' approaches could lead to important conclusions regarding ores comminution behaviour.

Table 36 and Table 37 show the parameters P and Q optimized for both case studies that conducted to the grade histograms (wt%) previously acquired by random comminution of the digital macro-texture and by broken particles analysis.

Table 36 – Optimized P and Q parameters - São Pedro das Águias case.

Size (mm)		16/13.5	13.5/11	11/9.5	9.5/8	8/6.7
Random Comminution	P	0.1329	0.1093	0.0893	0.0748	0.0598
	Q	16.0198	13.0891	10.4035	8.2662	6.2727
Broken Particles	P	0.1448	0.1148	0.1049	0.0769	0.0715
	Q	16.1933	14.6792	9.432	8.0042	5.5123

Table 37 – Optimized P and Q parameters – Alvarrões case.

Size (mm)		19.3/16	16/13.5	13.5/11	11/9.5	9.5/8	8/6.7
Random Comminution	P	0.9127	0.751	0.5861	0.494	0.4471	0.3788
	Q	2.8385	2.2003	1.6675	1.4146	1.2379	1.0536
Broken Particles	P	0.8262	0.7166	0.6224	0.6033	0.7392	0.6457
	Q	2.6910	2.4059	2.1684	1.7105	1.7422	1.8083

It is possible to state that P values are consistently lower than 1, while Q is higher than 1, being the differences much higher in the case of São Pedro das Águias than in the case of Alvarrões. Invoking the relation between the Beta function parameters, ore liberation degree, size and ore average grade (presented in Chapter III), is it possible to draw the following generic remarks:

- P and Q values indicate that all grade histograms have an L shape, meaning that both ores at crushing sizes exhibit a significant amount of liberated gangue and low-grade mixes, but low liberation of valuables, an effect that is much more pronounced in São Pedro das Águias case,
- Overlapping P and Q values of both ores in the iso-grade lines in the P and Q diagram, as shown in Fig. 92, it is possible to observe that the optimized values of P and Q are well aligned with the iso-grade lines for both ores, meaning that crushing was random: in the case of grade histograms obtained by the random comminution algorithm, this is not really a surprise. The slope of these iso-grade lines is consistent with the respective average ore grades:

0.99 %Scheelite (=0.80 %WO_3) for São Pedro das Águias; 25.6 %Lepidolite (=1.97 %Li_2O) for Alvarrões.

- Since the slope of the iso-grade line that represents the Scheelite ore is much higher than that of Lepidolite ore, the L shape of the Scheelite grade histogram is sharper, while the one of Lepidolite approximates an asymmetric bell shape.

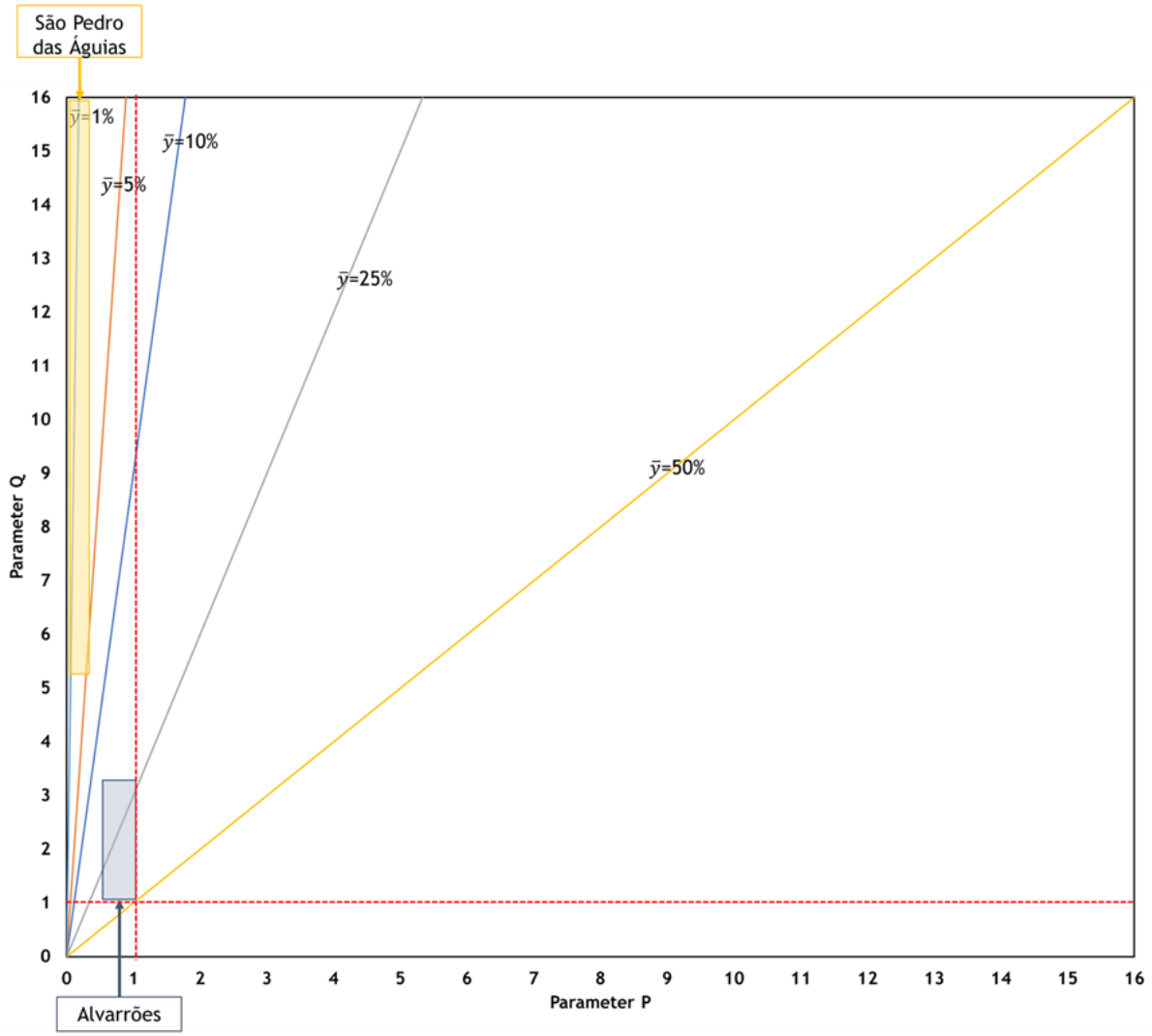

Fig. 92 - Setting the P and Q range for both ores in the theoretical iso-grade lines diagram.

According to the basics of Mineral Processing, the less abundant constituent will achieve liberation in a later stage of the size reduction process relative to the most abundant. Low grades tend to enhance this effect. This is exactly the cases of São Pedro das Águias (low grade) and Alvarrões (high grade). When P values tend to zero, gangue liberation is being achieved and when Q tends to zero, valuable liberation is being

achieved. In the case of São Pedro das Águias, P is lower, meaning higher gangue liberation, while in the case of Alvarrões Q is lower, meaning higher valuable mineral liberation.

P and Q values of both studied cases are going to be analyzed in more detail in relation to the iso-grade and iso-size lines of the Beta Law liberation model, complementing what was already said.

Concerning the iso-grade lines, shown in Fig. 93, the following remarks can be drawn:

- For each studied ore, P and Q values corresponding to the two types of grade histograms (particles generated by random comminution or broken particles) tend to be aligned with a unique iso-grade line, meaning that grade histograms (wt%) have a similar average grade, representing the same ore;
- Almost perfect alignment in the case of particles generated by the random comminution for each ore means exactly this condition – the constancy of grade in the different size fractions is a result of a random process;
- The tendency of the case of the broken particles to align with the iso-grade line validates that crushing developed at nearly random, more in the case of São Pedro das Águias than Alvarrões;

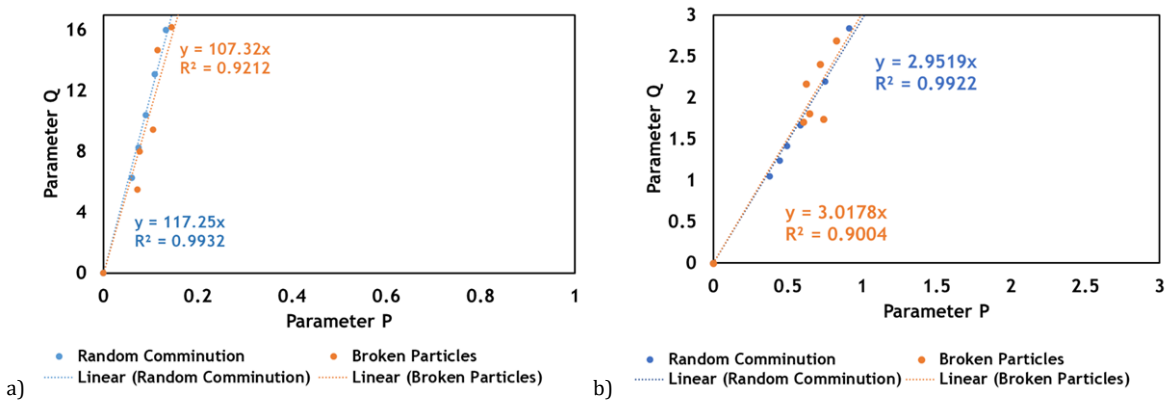

Fig. 93 –Iso-grade lines computation for both approaches: a) São Pedro das Águias case; b) Alvarrões case.

In what concerns the overlapping with iso-size lines of the Beta liberation model, results of the two types of grade histograms are compared for both studied ores and shown in Fig. 94.

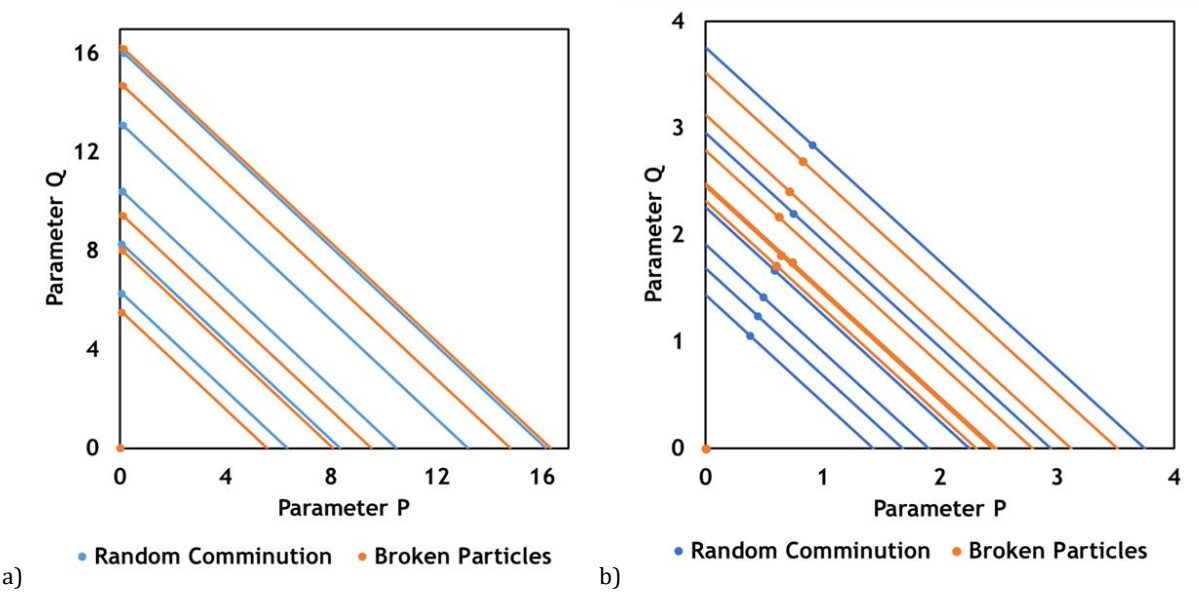

Fig. 94 - Iso-size line computed for both approaches: a) São Pedro das Águias; b) Alvarrões.

In the Beta Law liberation model, iso-size lines are always parallel and slope equal to -1, corresponding to each one an increasing size from the low left corner to high right corner. A proper overlapping of the iso-lines of the same size would be expected, corresponding to the grade histograms generated by the two developed approaches – random comminution vs broken particles.

In the case of São Pedro das Águias, the adjustment is acceptable, although showing some discrepancies in the size intervals [13.5/11.3]mm and [11.3/9.5] mm.

In the case of Alvarrões, there is a higher discrepancy, meaning that the grade histograms (wt%) of the same size fraction are describing different liberation degrees. Furthermore, the position of iso-size lines does not follow a pattern, meaning that the liberation degree of different size fractions is not progressing as expected. For example, in the case of the lower size fractions, iso-size lines corresponding to grade histograms of the broken particles are practically overlapped. These inconsistencies point out for the lack of representativeness of the data already mentioned.

Generally speaking, it can be said that Beta liberation model reinforces the consistency between grade histograms (wt%) generated by random comminution of macro-textures and by analysis of broken particles. However, this validation is weaker in the case of Alvarrões.

4.3.3.4 SIMULTANEOUS FITTING THE BETA LAW LIBERATION MODEL TO ALL AVAILABLE GRADE HISTOGRAMS

It can be said that the individual fitting of each grade histogram does not conduct to P and Q parameters corresponding to a single mineral texture. This situation can be avoided by making a simultaneous fitting of Beta Law covering the entire size range. Using the Beta Law Liberation Model, and the Topological Law ($\Phi(s)$) that correlates the size with the parameters P and Q using a topological constant (K), it is possible to simultaneous calibrate the iso-size lines [1, 2, 17]. Topological law can be used to improve the worse fits observed in the case of Alvarrões. Function $\Phi(s)$ can have different formulations, but when plotting the values of the topological law ($\Phi(s)$) against size, using the P and Q values obtained in the case of Alvarrões, as shown in Fig. 95, it is seen that, as expected, a linear approximation adheres well in the entire size range in the case of grade histograms of random comminution. In the case of grade histograms of broken particles, results are worse mainly in the lower size fractions, because a single texture is not able to justify the whole size range, or, as already mentioned, is the evidence of some data inconsistency (low representativeness).

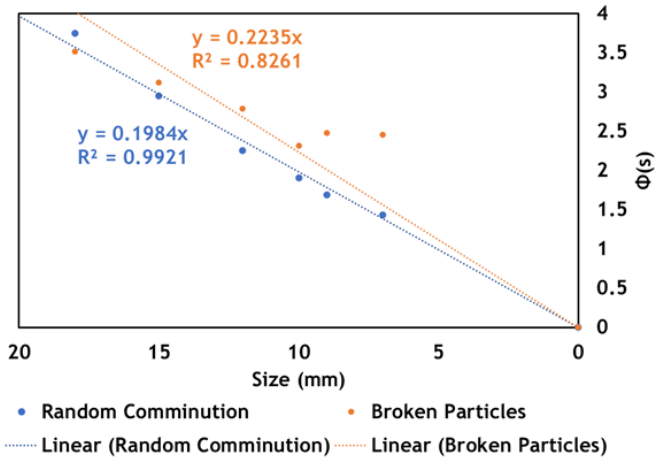

Fig. 95 – Fitting Topological Law ($\Phi(s)$) as a function of the obtained P and Q parameters. Note that size axis is represented from right to left, as adopted by some authors [2].

At this stage, a new challenge arose to adjust the topological constant (K) that simultaneously better fits the grade histograms (wt%) of broken particles in all size fractions – find the best topological constant (K) that optimizes the Topological Law Φ(s), minimizing the deviation between the predicted and observed grade histograms. Topological law is then used to determine all pairs of (P and Q) accordingly with the respective average ore grade.

Results of this simultaneous adjustment of the Beta Law Liberation Model to all grade histograms of broken particles (Alvarrões case), covering the entire size interval, led to the graphical representations of Fig. 96, which support the following considerations:

The linear approach for the Topological Law is much better and approximates the adjustment level achieved before for random comminution.

It is evident that the comparison between the iso-size lines of the P and Q diagram of the Beta Liberation Model, referring to the random comminution and broken particles, has significantly improved. However, there is a slight tendency of broken particles to predict higher liberation levels in the intermediate sizes than random comminution.

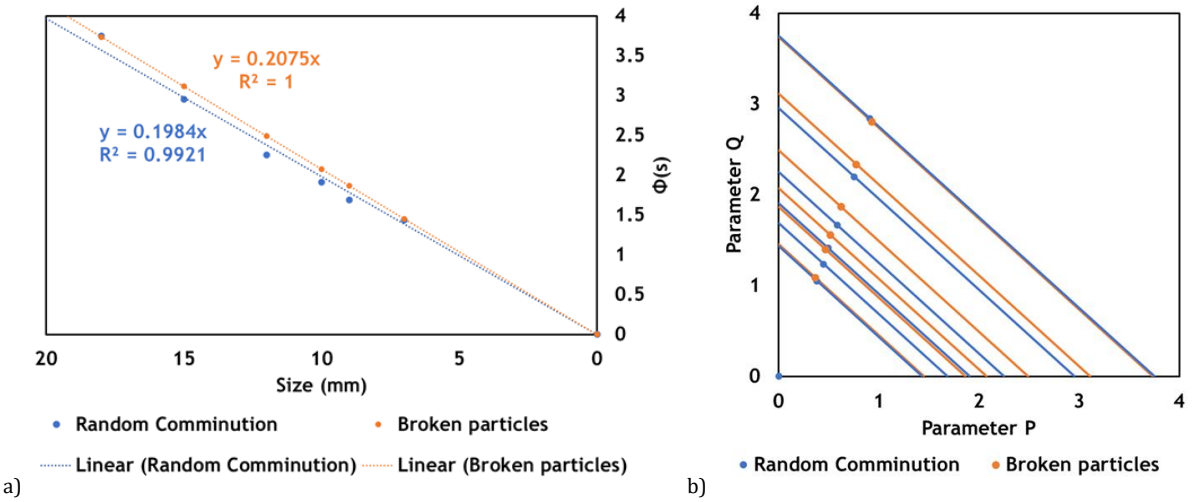

Fig. 96 – Comparison of Beta Law Liberation Model between random comminution individually fitted to each size fraction and broken particles simultaneously fitted to the entire size range: a) Topological law; b) Iso-size lines.

The negative aspect of this approach, but absolutely insuperable, is that the goodness-of-fit decreased considerably, as shown by the chi-squared test in Table 38,

where the deviations between the individual fitting of (P and Q) to each size fraction and the actual simultaneous fitting of (K) for the entire size interval are compared.

Table 38 – Chi-squared tests applied to the fitting of Alvarrões grade histograms (wt%).

size (mm)	19.3/16	16/13.5	13.5/11	11/9.5	9.5/8	8/6.3
Previous X^2	7.49	9.54	6.71	12.03	7.56	22.06
Actual X^2	8.80	10.39	4.64	7.53	11.52	22.63

However, it should be underlined that the main objective of this procedure was not the improvement of the fitting between predicted grade histograms (wt%) by the Beta Law Liberation Model and those obtained with broken particles, because the uncertainty of this data was already confirmed. The objective was to use the Beta liberation model to harmonize the grade histograms (wt%) of broken particles, obtaining a better similarity to those obtained by the random comminution of the digital macro-textures, which was accomplished (Fig. 97).

The application of the Beta liberation model approximated the data acquired under the broken particles to the data acquired under the macro-texture. Thus, taking into account the information enclosed in the broken particles grade histograms (wt%), the Beta liberation model was able to give some coherence to the data.

Random Comminution vs Broken Particles smoothed by the Beta Liberation Model	Alvarrões

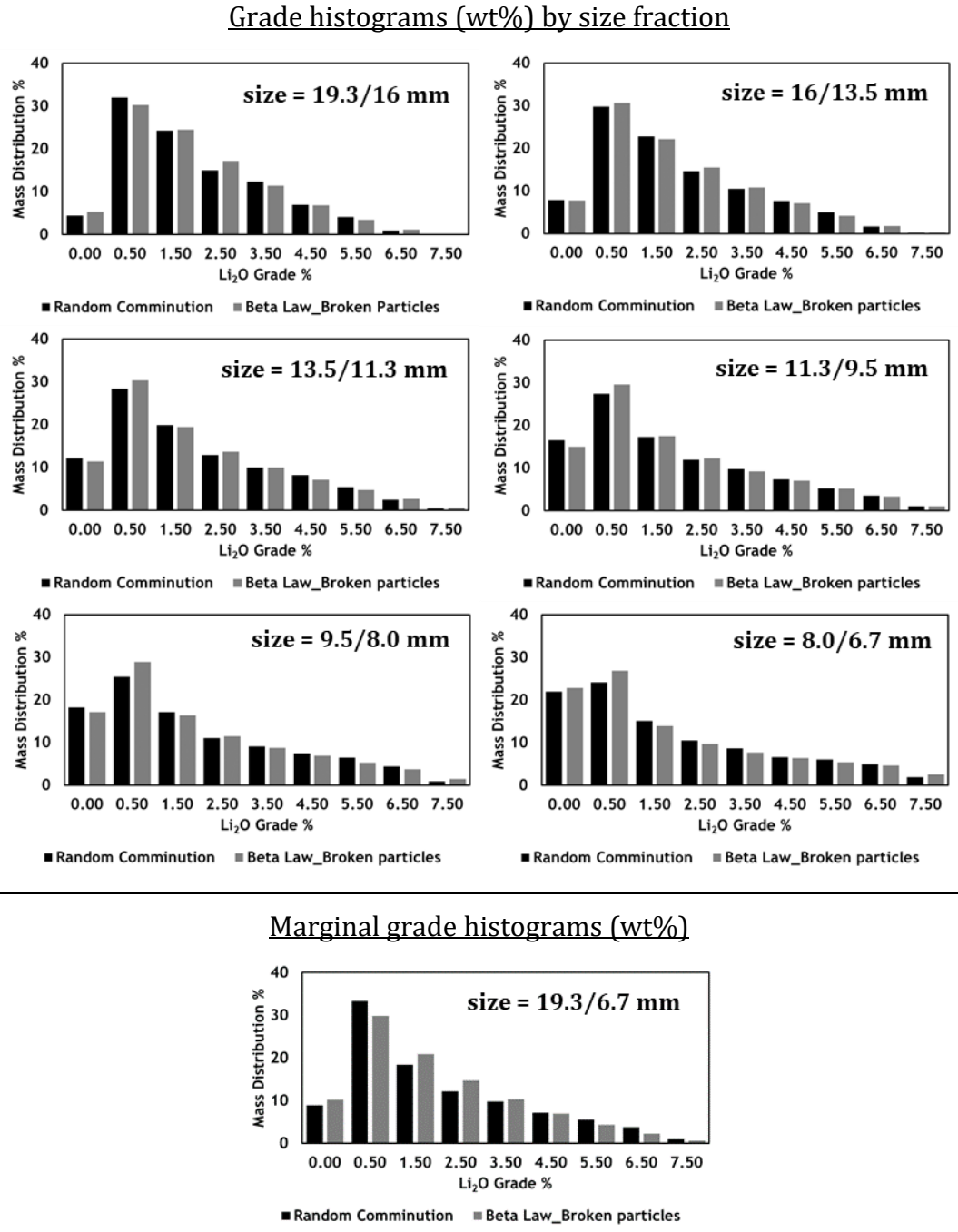

Fig. 97 - Comparison Between Grade Histograms generated by Random Comminution of a digital texture and by the application of the Beta liberation model to the Broken Particles data – Alvarrões case.

To verify the better fit of the new predicted data, Table 39 shows the deviation between the macro-texture grade histograms (wt%) and those obtained using the analysis of the broken particles (image analysis vs Beta liberation model).

Table 39 – Comparison of the deviation between the grade histograms (wt%) acquired using the broken particles analysis - image analysis vs Beta liberation model and the random commintuion grade histograms (wt%).

size (mm)	19.3/16	16/13.5	13.5/11	11/9.5	9.5/8	8/6.3
Broken Particles (image analysis)	13.24	24.58	6.62	7.05	11.60	28.31
Broken Particles (Beta liberation model)	0.78	0.35	0.48	0.40	1.20	0.97

A great improvement was observed when the broken particles grade histogram (wt%) was adjusted with the application of the Beta liberation model. According to this, it was possible to confirm the lack of representativeness of the image analysis carried out using broken particles, giving the confidence to accept the results obtained using a random comminution algorithm under the macro-texture.

4.4 FINAL REMARKS

In summary, the objective of this chapter was to describe the procedures used for data acquisition that will be used in the next chapter. The availability of mineral liberation data of the head material that feeds the separation processes, represented by means of the grade histogram (wt%), is indeed the fundamental key issue for the success of the forthcoming work, and due to that, special attention was given to this task.

Regarding the mineral liberation data at grinding sizes, a credible technique was applied based on QEMSCAN® mineralogical quantitative data, making unnecessary any kind of data validation. On the other hand, the acquisition of proper mineral liberation data at crushing sizes was one of the biggest challenges of this work. In line with this, two different approaches were developed and compared: i) digital images of hand samples representative of the ore macro-texture, acquired accordingly with a methodology developed for the purpose, were subjected to a random comminution simulator to generate grade histograms (wt%) for several size fractions; ii) the second approach

consisted in analyzing images of real broken particles using image analysis. The agreement between both approaches was fundamental to validate both methodologies.

In a second step, the Beta Law Liberation Model was applied to the obtained data, being fundamental to reduce the irregularities of the raw grade histograms (wt%). As Beta law parameters can be interpreted according to the theory of mineral liberation, the fitting of Beta function to the grade histograms (wt%) is fundamental to improve the coherency of data. Furthermore, in the case of Alvarrões, it was fundamental to confirm that some discrepancies between random comminution and broken particles analysis were due to a lack of representativeness.

Beta Liberation Model was a very useful tool to interpret the ore liberation, being able to acquire information from the real grade histograms and a straightforward way to add coherence to the data.

According to the objective of this thesis, the main output of this chapter was the preparation of the feed grade histograms (wt%) of both samples, representing the crushing and grinding stages, that will be used in next chapter for validation of the methodologies for assessment of separation efficiency. Thus, it would be preferable to use the grade histograms (wt%) smoothed by the Beta Law Liberation Model, instead of using the raw histograms generated by the image analysis, mainly to reduce the impact of samples representativeness – Beta Law follows a rational paradigm, so it seems to be a good interpolator.

The grade histograms (wt%) that will be used in the next chapter to characterize the feed material tested in the concentration testwork are presented in Fig. 98 – two samples of São Pedro das Águias ore and Fig. 135 – one sample of Alvarrões ore.

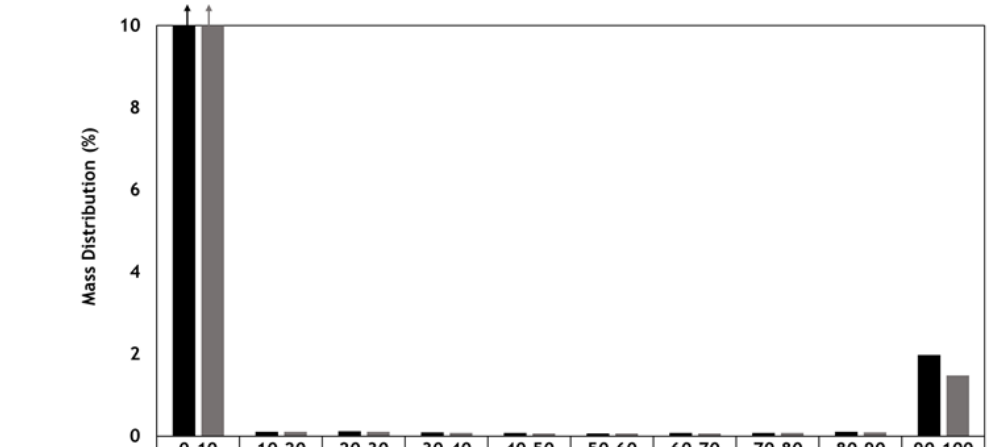

	0-10	10-20	20-30	30-40	40-50	50-60	60-70	70-80	80-90	90-100
SPA [cs=0.212]	97.30	0.11	0.12	0.09	0.08	0.07	0.07	0.08	0.11	1.97
SPA [cs=0.075]	97.84	0.10	0.11	0.08	0.07	0.07	0.07	0.08	0.10	1.47

Fig. 98 – Final grade histograms (wt%) after grinding stage – São Pedro das Águias.

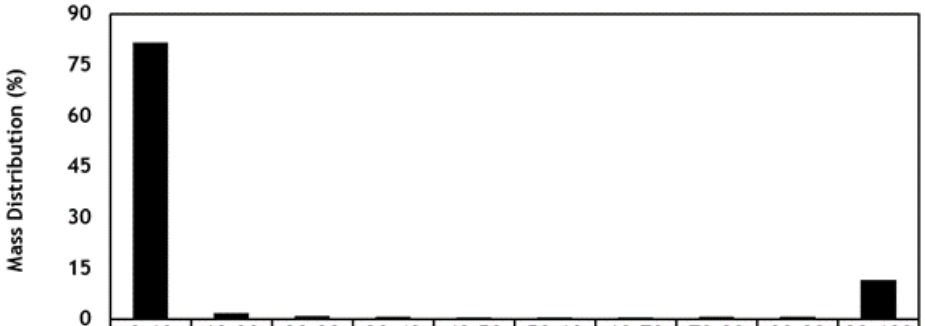

	0-10	10-20	20-30	30-40	40-50	50-60	60-70	70-80	80-90	90-100
Alvarrões	81.52	1.88	0.99	0.74	0.64	0.60	0.61	0.68	0.86	11.50

Fig. 99 – Final grade histogram (wt%) after grinding stage – Alvarrões.

In the case of São Pedro das Águias, the following conclusion can be drawn:

- The Histogram presents a U-shape for both size fractions, pointing to a high liberation degree;
- For both size fractions, approximately 97% of the mass is in the class 0-2 %scheelite, and almost 2% of material is pure scheelite (90-100% scheelite), confirming the high liberation degree of the ore;
- The coarser size fraction showed a higher content of almost pure scheelite particles, which can be due to the principle of equivalence. According to this, a smaller pure scheelite particle is density-equivalent to a larger middling particle. So, it is expected, a great number of 100% scheelite particles with a size below 0.212 mm in the coarser fraction;

- The high liberation degree observed in the fine crushed (to minus 3 mm) material of São Pedro das Águias points out to a very successful concentration stage.

In the case of Alvarrões, the obtained grade histogram (wt%) for the concentration stage supports the following conclusions:

- The U-shape of the grade histogram (wt%) points out for a high level of liberation;
- Approximately 82% of the mass is in the class 0-10 %lepidolite, and 11.50% of material is almost pure Lepidolite (90-100 %lepidolite), confirming the high liberation degree of the ore;
- As a final remark, it can be said that the concentration stage presents a high probability of success to produce high-grade concentrates if an adequate separation technique is applied.

All this information is very important to conduct mineral processing experimental testwork, being considered the first approach to the potential performance of mineral separation. However, the success of the separation process is not only due to mineral liberation but also to the applied separation method. This is exactly what will be discussed in the further chapters.

The grade histograms (wt%) that will be used in the next chapter as characterizing the material tested in the pre-concentration tests at crushing size are presented in Fig. 100.

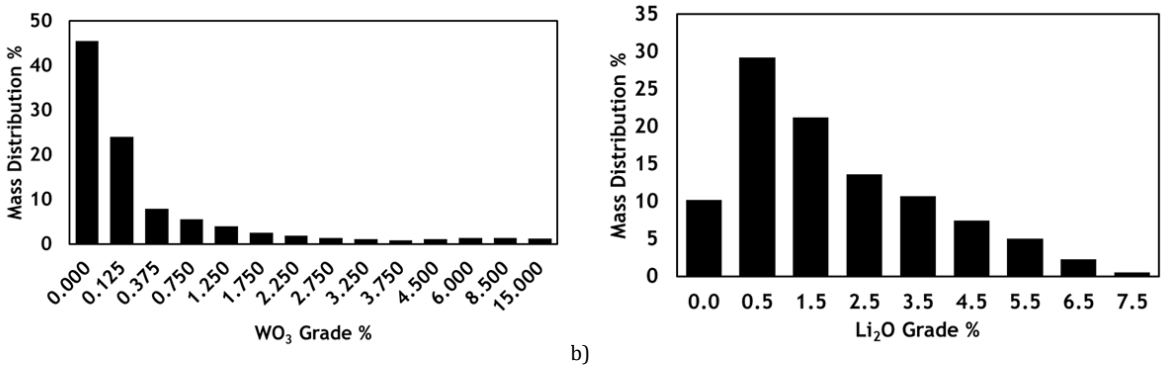

Fig. 100 – Final Marginal grade histograms of a broader size range: a) São Pedro das Águias ore [16/6.7mm]; b) Alvarrões ore [19.3/6.7mm].

In the case of São Pedro das Águias, the following conclusion can be drawn:

- The histogram presents an L-shape, meaning that at the respective crushing size there is a significant amount of almost pure gangue material already liberated, which was predictable due to the texture of the mineralized body and the low WO_3 content;
- Approximately 46 % of material present full gangue liberation (0 %WO_3) and 38 % material is low-grade middling with grade between]0/1.5] %WO_3;
- 46 % of mass can be rejected at a coarse particle size without any losses. However, it is necessary to apply a separator that can clearly distinguish these particles from particles with an average grade of 0.125 %WO_3.

In the case of Alvarrões, it can be said that:

- There is a slight amount of liberated gangue (around 10% of the mass in the 0% grade class);
- Approximately 58% of the material can be considered low-grade middling averaging between]0/2] %Li_2O grade;
- It is possible to observe 16.6% of mass with a grade above 4 %Li_2O, which point out for liberation at the crushing stage;

As a final remark, it can be said that pre-concentration presents a low probability of success to reject gangue material at coarse crushing sizes, due to the low level of liberated gangue. However, it is noticeable an interesting quantity of particles in the high-grade Li_2O fractions, pointing out to the possibility of producing marketable concentrates at a coarse crushing size. This aspect will be further discussed.

NOMENCLATURE AND GLOSSARY

α	Valuable mineral/metal grade of feed
β	Valuable mineral/metal grade of concentrate
ν	Valuable mineral/metal grade of tailings
γ	Yield
ε	Recovery
im2bw	Matlab command to convert RGB images into binary images
$C_{i,j}(x,y)$	Joint grade and size histogram
$B_{i,j}(x\|y)$	Conditional histogram of grade x given in the size y
$A_i(y)$	Marginal size histogram
$G_i(x)$	Marginal grade histogram
C_{pq}	Beta function constant
P,Q	Beta function parameters
$\phi(s)$	Topological law (function of size)
K	Topological constant
X^2	Chi-squared

REFERENCES

1. Madureira, C.M.N., M.R. Machado Leite, A. Cavalheiro and J. Silva, *Size, Grade and Liberation: a stochastic approach to the fundamental problem of mineral processing*, in *XVI International Mineral Processing Congress*, E.S. Publisher, Editor. 1988: Stockholm.
2. Machado Leite, M.R., *Liberation by size reduction. Consequences and improvements on flotation kinetics*, in *Innovations in Advanced Flotation Technology*, N.A. SERIES, Editor. 1992, Kluwer Academic Publishers. p. 149-170.
3. King, R.P., *A model for the quantitative estimation of mineral liberation by grinding.* International Journal of Mineral Processing, 1979. **6**(3): p. 207-220.
4. Kelly, E.G. and D.J. Spottiswood, *Introduction to mineral processing*. 1982: Wiley.
5. Reichert, M., C. Gerold, A. Fredriksson, G. Adolfsson and H. Lieberwirth, *Research of iron ore grinding in a vertical-roller-mill.* Minerals Engineering, 2014. **73**: p. 109-115.
6. Pascoe, R.D., M.R. Power and B. Simpson, *QEMSCAN analysis as a tool for improved understanding of a gravity separator performance.* Minerals Engineering, 2007. **20**: p. 487-495.
7. Baum, W., *Ore characterization, process mineralogy and lab automation a roadmap for future mining.* Minerals Engineering, 2014. **60**: p. 69-73.
8. Wang, L. and C. Zhao, *Hyperspectral Image Processing*. Springer-Verlag Berlin AND Heidelberg Gmbh & Colorado. KG, Springer-Verlag Berlin AND Heidelberg Gmbh & Colorado. K. 2016: Berlin.
9. Tusa, L., L. Andreani, M. Khodadadzadeh, C. Contreras, P. Ivascanu, R. Gloaguen and J. Gutzmer, *Mineral Mapping and Vein Detection in Hyperspectral Drill-Core Scans: Application to Porphyry-Type Mineralization.* Minerals, 2019. **9**(2).
10. Pérez-Barnuevo, L., S. Lévesque and C. Bazin, *Automated recognition of drill core textures: A geometallurgical tool for mineral processing prediction.* Minerals Engineering, 2018. **118**: p. 87-96.
11. Leigh, G.M., *Automatic ore texture analysis for process mineralogy.* Australasian Institute of Mining and Metallurgy Publication Series, 2008.

12. Hamilton, C., C. Martin, N. Mckay and S. Williams, *Correlating QemSCAN mineralogy with metallurgy in feasibility studies*, in *Applied Mineralogy*, e.a.E. Pecchio, Editor. 2004, Applied Mineralogy.
13. Rollinson, G., J.C. Andersen, R.J. Stickland, M. Boni and R. Fairhurst, *Characterisation of non-sulphide zinc deposits using QEMSCAN(R).* Minerals Engineering, 2011. **24**(8): p. 778-787.
14. Młynarczuk, M., A. Górszczyk and B. Ślipek, *The application of pattern recognition in the automatic classification of microscopic rock images.* Computers & Geosciences, 2013. **60**: p. 126-133.
15. Disckson, B. *Exploiting machine learning in cybersecurity*. TechCrunch 2017 [cited 2019 April]; Available from: https://techcrunch.com/2016/07/01/exploiting-machine-learning-in-cybersecurity/.
16. King, R.P., *Modeling and Simulation of Mineral Processing Systems*. Butterworth-Heinemann, ed. Elsevier. 2001, Oxford.
17. Cavalheiro, A., *Libertação de minério por cominuição - Modelo matemático*, 1984. *Departamento de Engenharia de Minas*,Universidade do Porto, PhD Thesis

5 Separation Efficiency

5.1 UPGRADING CURVES

5.1.1 OVERVIEW

Upgrading curves are widely used to represent experimental results of mineral separations processes. It is a straightforward way to compare the performance of different techniques or different settings of the same technique. As mentioned before, separation performance is commonly evaluated according to the positioning of its plots between the ideal and the non-upgrading lines, as discussed in Chapter III. For comparison purposes, when the experimental curve comes closer to the ideal upgrading curve, it means that the efficiency of the separation becomes better. Although it is an excellent tool to follow the experimental work, it gives no information about the origin of the separation inefficiencies.

As seen in the studied cases reported in Chapter III, the upgrading curve of a batch separation process is commonly obtained by linear interpolation of the data that represent the different obtained products. However, when experimental data points are scarce (less than 3), the accuracy of graphical representation made in this way is not good.

To improve these graphical representations it is common to use different types of mathematical approaches to fit experimental data to obtain a continuous representation.

In the following sections, results of real separations of São Pedro das Águias and Alvarrões ores are assessed plotting experimental data using the Mayer representation. Firstly using linear interpolation, as usual, and in the second step developing another approach based on the application of a proper model for the Efficiency Curve adapted from an approximation proposed by Lynch [1, 2].

5.1.2 USE OF UPGRADING CURVES TO ASSESS SEPARATION EFFICIENCY

5.1.2.1 CONCENTRATION AT GRINDING SIZES

Gravity concentration was indicated as a promising alternative to produce WO_3 concentrates from the São Pedro das Águias ore: two size fractions obtained by hydrosizing were upgraded using a Wilfley shaking table. In the case of Alvarrões ore, froth flotation was used for lepidolite upgrading. Results of experimental tests of both cases are plotted in a Mayer representation, as shown in Fig. 101.

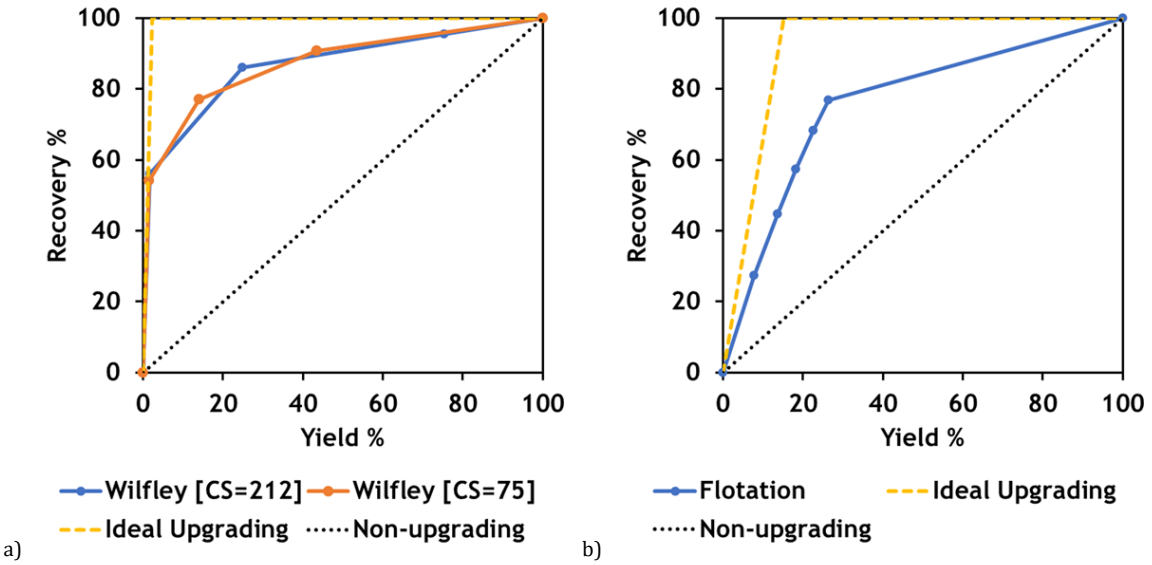

Fig. 101 - Mayer representation of concentration tests a) São Pedro das Águias ore; b) Alvarrões ore.

Concerning the gravity concentration results of São Pedro das Águias ore, the following conclusions can be drawn:

- The first data points of both size fractions correspond to a high concentrate grade, being practically superimposed to the Ideal Upgrading line, pointing out for the existence of liberated scheelite;
- The gap between experimental and Ideal Upgrading representations can be seen as the degree of global separation efficiency;
- In this sense, as scheelite liberation is good and similar for both size fractions, plots are almost superimposed;
- The gap to the Ideal Upgrading reveal the process inefficiency, which can be due to some scheelite not yet liberated or a few liberated scheelite that is not enough to fill the riffles in some areas of the shaking table and, on account of this, the product of the separation is a mixture of scheelite with light particles;
- In the case of the coarse fraction, the gap also can have the negative influence of the presence of fines due to problems occurred during elutriation of the feed;

Concerning the flotation results of Alvarrões ore, the following conclusions can be underlined:

- The most noticeable aspect of the batch kinetic test is the approximate constancy of the concentrate grade, while recovery is increasing along time,

which can be interpreted as zero-order kinetics: the abundance of liberated mica minerals consume all available bubbles (bubbles fully charged);

- It is also seen that since the beginning of flotation concentrate grade is clearly below the theoretical grade of lepidolite, which indicates that another mineral has floated along with lepidolite (other mica minerals) or even that fine inclusions of gangue minerals inside the Lepidolite grains can occur; this result is shown by the significant gap between the experimental and the Ideal Upgrading Curve.

5.1.2.2 PRE-CONCENTRATION AT CRUSHING SIZES

The same approach was used to build the experimental curves of pre-concentration tests of both ores, carried out at coarse crushing sizes.

As aforementioned, optical sorting was used for pre-concentration in both cases, taking advantage of scheelite fluorescence under UV-light and lepidolite purple color, contrasting with the color of gangue minerals (quartz, silicates, carbonates, fluorspar and others). In the case of Alvarrões, it was possible to send samples in the size range [20/6.3] mm to be tested in the laboratory of an equipment supplier in Germany; it was not the case for São Pedro das Águias, for which the laboratory pre-concentration testwork was carried out by handpicking and visual observation under UV light. Fig. 102 shows the Mayer upgrading curves of both case studies.

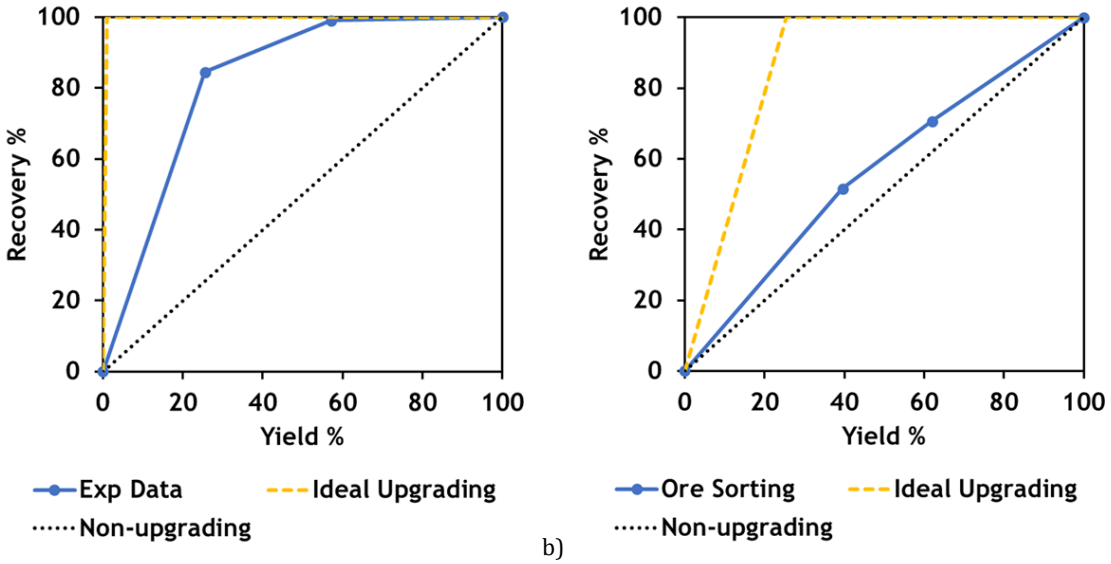

a) b)

Fig. 102 – Mayer representation of pre-concentration tests on a) São Pedro das Águias ore; b) Alvarrões ore.

Observing the upgrading curves in Fig. 102, it is possible to conclude that the shape of both Mayer experimental representations is far from the Ideal Upgrading curve, meaning that:

- Low level of the liberation of valuable minerals did not allow high grade concentrates in both cases:
- In the case of scheelite from S. Pedro das Águias, a recovery close to 90% was obtained under a yield of 25%, which is a nice figure for pre-concentration;
- In the case of lepidolite from Alvarrões, results show a very low global efficiency of optical sorting, which is expressed by the high proximity between the experimental graphical representation and the non-upgrading line;

5.1.3 PARTITION CURVE (TROMP CURVE) – A MATHEMATICAL OPERATOR OF THE SEPARATION PROCESS

As stated above, graphical upgrading curves are a clever way to collect information regarding the separation efficiency, namely when the shape of the representation is compared with the Ideal and the non-upgrading extreme cases. Sometimes, when the set of experimental data is limited, the connection of these points by linear interpolation could lead to less accurate comparisons. To avoid this, some mathematical functions, such as polynomial interpolation, are used to fit experimental data points, but in this case, polynomial coefficients are meaningless.

For this work, an alternative approach, supported by a higher level of interpretation, was developed, which is based on the following:

- Each set of data points is conceived as the result of a separation conducted by a Partition Curve (Efficiency Curve) that expresses the probability of every single fraction of particles in the feed to be collected in the concentrate. This Partition Curve can be conceived as a separation model – P_i - because its application to the feed grade histogram (wt%) – f_i - generates both Concentrate and Tailings Grade Histograms (wt%) – c_i and t_i respectively (i refers to each grade fraction), as can be seen in Eq. 27, Eq. 28 and Eq. 29.

$$Yield = \sum_i f_i \times P_i \qquad \text{Eq. 27}$$

$$c_i = \frac{f_i \times P_i}{Yield} \quad \text{Eq. 28}$$

$$t_i = \frac{f_i \times (1 - P_i)}{(1 - Yield)} \quad \text{Eq. 29}$$

- For the purpose of this work, a mathematical model proposed by Lynch [1, 2] will be adopted for the Partition Curve. This model is driven by two parameters, one controlling the shape and the other refering to the cut-point (corresponding to 50% efficiency). Lynch developed his model to typically describe the success of the classification/screening. However, these curves can be applied to any other separation process if the products can be separated into classes differing at least in one separation property [3, 4].
- Different separations are assumed to be driven by Partition Curves with similar shape factors but anchored at the respective cut-grade;
- Once the parameters are obtained by fitting the model to known experimental data points, it may be used to interpolate data between the experimental points, obtaining a more discretized representation.

The application of the Lynch approach to the Partition Curve of a grade-dependent separation uses the mathematical function shown in Eq. 1, which defines the particle weight percentage P_i (YY-axis) of a certain grade fraction x_i (XX grade-axis) in the feed that might report to the concentrate (i.e., the probability to incorporate the "concentrate").

$$P_i = \frac{e^{m \times \frac{x_i}{x_{50}}} - 1}{e^{m \times \frac{x_i}{x_{50}}} + e^m - 2} \quad \text{Eq. 30}$$

The parameter m controls the shape of the function and represents the sharpness of the separation - sharp separations are obtained with $m > 3$ [5]. The x_{50} (cut-grade value) indicates the particle grade (x_i) in the feed that has equal probability (50%) of to be reported either to the "concentrate" or to the "tails" [6]. It should be underlined that, mathematically, the efficiency P_i is a grade dependent function, having 2 parameters (m, x_{50}).

Sometimes separation efficiency is hindered by external conditions, such as turbulence, dragging, mixing and other non-discriminating effects, which lead to

efficiency curves that tend asymptotically to non-zero values for cut-grade close to zero. This effect, which may be conceived as being independent of the particles' grade, is not supported by the Lynch model, but can be included as a constant additive factor, corresponding to dragged material reported to the "concentrate". In Eq. 2 a new parameter AS_i was introduced to represent the fraction of feed material dragged to the "concentrate"; considering that this effect is not discriminated in grade, it can be considered constant, i.e., $AS_i = AS$ [1]:

$$P_i = AS + (100 - AS) \times \frac{e^{m \times \frac{x_i}{x_{50}}} - 1}{e^{m \times \frac{x_i}{x_{50}}} + e^m - 2} \qquad \text{Eq. 31}$$

Fig. 103 shows four different efficiency curves.

- Partition A represents a perfect separation (Heaviside step), in which all particles above x_{50} are reported to the "concentrate", and all particles below x_{50} (cut property value) are reported to the "tails"; Lynch mode fits the Heaviside function for sharpness factor $m > 20$;
- Partition B represents a real, non-perfect separation, in which the inefficiency decreases with the distance to x_{50} and tends to zero on left and to 100% on the right;
- Partition C corresponds to a real separation with dragged effect only in the "concentrate" (AS);

[1] An asymptote to values less than 100% for high cut-grades can be theoretically accepted as referring to the fraction of particles dragged to "tails" (AI). Experience has shown that the dragging effect on the "tails" is difficult to identify. Therefore, for the purpose of this work, only AS will be considered in the computation of partition curves.

$$P_i = AS + (100 - AS - AI) \times \frac{e^{m \times \frac{x_i}{x_{50}}} - 1}{e^{m \times \frac{x_i}{x_{50}}} + e^m - 2}$$

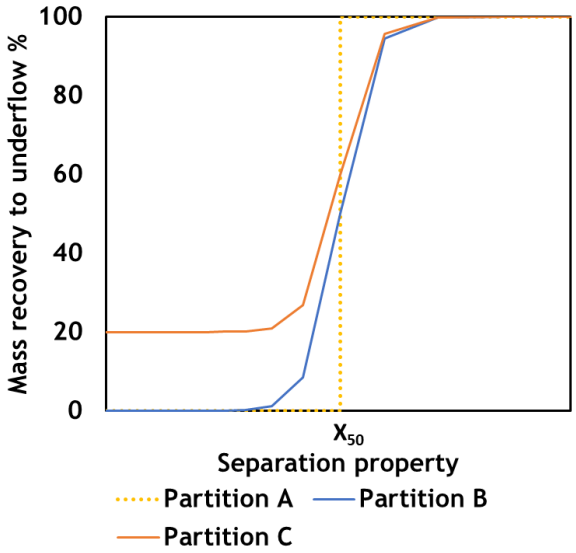

Fig. 103 – Different partition curves obtained with the same cut-size.

Thus, the computation and adjustment of the Partition Curve that defines the performance of a given separation are developed according to the following steps:

1. Model definition according to Eq. 2;
2. Calibration of the model by determining the parameters m, x_{50} and AS of the Partition Curve that, when applied to the experimental grade histogram (wt%) of the ore that feeds the separation, better fit the experimental results (yield, recovery and concentrate grade);
3. The determination of the best fit is usually done by back-calculation and least square criterion algorithm;
4. Application of the adjusted model for interpolation of the values for a desired discretization of the cut-grade axis to obtain an approximation to a continuous upgrading curve.

The generation of a concentrate is then obtained by positioning the Partition Curve, led by such a set of parameters m, x_{50} and AS, upon the respective grade histogram (wt%) that represents the feed to the separator; in the following step the respective concentrate grade, yield and mineral recovery are calculated accordingly with the following equations:

$$Yield = \sum_i f_i \times P_i \qquad \text{Eq. 32}$$

$$Concentrate\ average\ grade\ (c) = \frac{\sum_i f_i \times P_i \times x_i}{Yield} \quad \text{Eq. 33}$$

$$Recovery = \frac{\sum_i f_i \times P_i \times x_i}{\sum_i f_i \times P_i} = \frac{Yield \times c}{Feed\ average\ grade\ (f)} \quad \text{Eq.34}$$

Where P_i is the Partition Curve, f_i is the grade histogram (wt%) of the material that feeds the separator and x_i is the average grade of each histogram class i. This procedure is repeated successively to define the set of m, x_{50} and AS that minimizes the least square of the differences between the experimental and the simulated values, which would be the better fit.

Thus, as shown in Fig. 104, the application of a partition curve (P_i) to the grade histogram (f_i) of the separator feed will generate the concentrate grade histogram (c_i). P_i is determined using Eq. 32, Eq. 33 and Eq.34. as the partition curve that best fits the experimental data – yield and concentrate grade; recovery is then calculated.

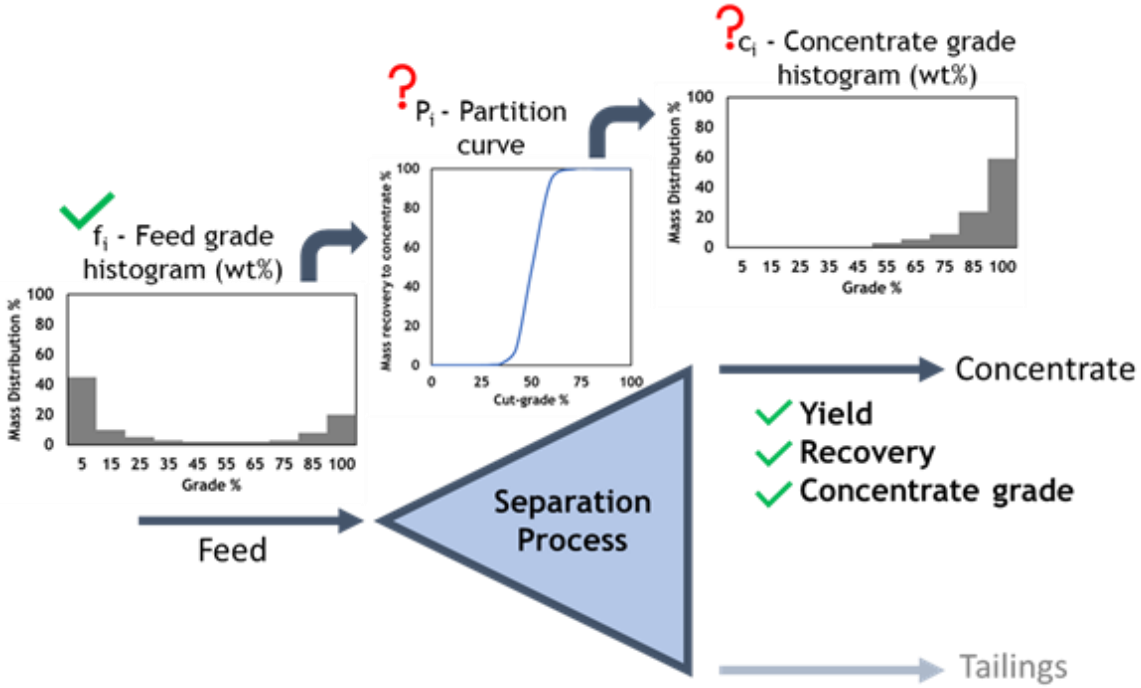

Fig. 104 - Methodology for computing the Partition Curve of a specific separation process.

This methodology was applied to the separation processes studied during this work. According to this, Mayer upgrading curves of all experimental separations previously reported, were generated by interpolation between data points, based on the application of the described efficiency model, following the next steps:

1. For each experimental data point, parameters *m*, x_{50} and *AS* are fitted by back-calculation (using a numerical optimization algorithm) to obtain the Partition Curve that, when applied to the feed grade histogram (wt%), will generate the concentrate grade histogram (wt%), which should match the experimental yield, recovery and concentrate average grade:
   a. When working with an ore and a given separator, it is expected that similar *m* values for the sharpness of the partition curve would be obtained for each cut-point (x_{50}); if so, it is possible to assume that a single partition curve shape can simulate all experimental data points through the variation of the cut grade point.
   b. Thus, based on the parameters generated at 1., the best values for *AS* are determined and the dependency of *AS* with x_{50} would be established;
2. Sliding the model for different cut-points (x_{50}) an extended interpolation of the experimental upgrading curve is calculated.

It should be noticed that the experimental determination of the feed grade histogram (wt%), as presented and discussed in Chapter IV, is the fundamental input of the proposed efficiency model of the Partition Curve.

5.1.3.1 FITTING PARTITION CURVE TO EXPERIMENTAL DATA OF CONCENTRATION TESTS AND DETERMINATION OF THE MAYER UPGRADING CURVE

The methodology above described was applied to the results of the concentration processes of both studied ores: scheelite from São Pedro das Águias using a shaking table and lepidolite from Alvarrões ore using a batch flotation cell.

First, the parameters *m*, x_{50} and *AS* of the Partition Curve that applied to the feed grade histogram (wt%) better fit the experimental results were individually calculated - each set of parameters corresponds to a certain cut-point. The results of this fitting exercise are presented in Table 40 for the case of São Pedro das Águias and in Table 41 for the case of Alvarrões.

Table 40 – Results of fitting the Lynch model parameters to the experimental data of São Pedro das Águias (1st cut grade - rich concentrate; 2nd cut grade – rich concentrate + rich middlings; 3rd cut grade - rich concentrate + rich middlings + poor middlings).

Cut-point	SPA [CS=212]			SPA[CS=75]		
	m	AS	x_{50}	m	AS	x_{50}
1st cut-grade	10.5	11.83	74.8	10.2	0.29	75.3
2nd cut-grade	11.8	23.4	64.7	9.9	12.6	67.4
3rd cut-grade	9.2	74.8	62.0	10.5	42.4	61.6

Table 41 – Results of fitting the Lynch model parameters to the experimental data of Alvarrões concentration tests.

Cut-point	m	AS	x_{50}
1st cut-grade	16.1	4.1	7.7
2nd cut-grade	16.0	7.8	7.2
3rd cut-grade	16.0	10.9	7.0
4th cut-grade	15.9	13.8	6.6
5th cut-grade	16.0	16.8	6.2

As expected, *m* values are very similar, x_{50} decreases according to cut grade and *AS* varies from low values (low non-discriminating dragging) at high cut grades to very high values at low cut-grades. Fig. 105 shows the correlations between *AS* and x_{50} for both size fractions of São Pedro das Águias ore and for Alvarrões ore.

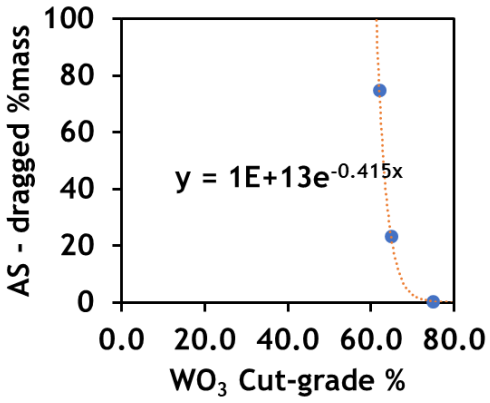

a)

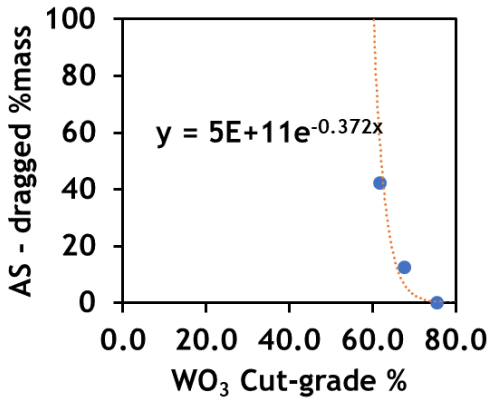

b)

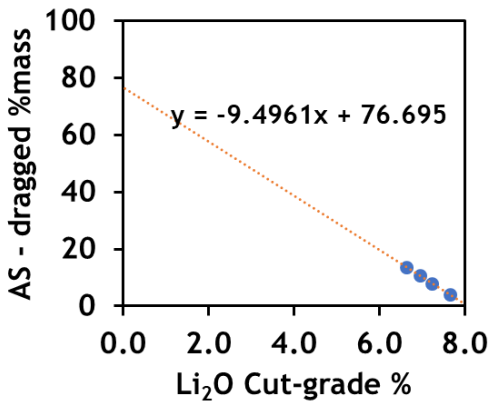

c)

Fig. 105 - Definition of the relation between *AS* and X_{50}: a) São Pedro das Águias [cs=212 µm]; b) São Pedro das Águias [cs=75µm]; c) Alvarrões;

In the case of São Pedro das Águias, it is clear that parameter *AS* increases exponentially with the decrease of x_{50}, which means that, in zones of the shaking table, where liberated scheelite is not enough to fulfill the riffles, the product collects a mixture of scheelite with light particles that were "dragged" to the concentrate, not on account of their density, but because there was room for them. In the case of Alvarrões, a linear relationship was found between *AS* and x_{50}, which is compatible with the selectivity of the used collector for mica minerals, not exclusive to Li-mica, making for muscovite to be also attached to bubbles ("dragged" to the concentrate, in the concept in discussion).

Once defined the correlation between *AS* and x_{50}, new adjustments of x_{50} and a single *m* parameter that fits all cut-grades were carried out for each size fraction. The final values of the parameters that control the model can be observed in Table 42 and Table 43.

Table 42 – Final Lynch model parameters to fit results of São Pedro das Águias concentration tests.

Sample	m	AS^1	x_{50}^1	AS^2	x_{50}^2	AS^3	x_{50}^3
CS=212µm	10.5	0.4	74.6 %WO_3	23.7	64.5 %WO_3	74.7	61.7 %WO_3
CS=75µm	10.1	0.3	75.7 %WO_3	11.84	65.9 %WO_3	42.7	62.4 %WO_3

Table 43 – Final Lynch model parameters to fit results of Alvarrões concentration tests.

m	AS^1	x_{50}^1	AS^2	x_{50}^2	AS^3	x_{50}^3	AS^4	x_{50}^4	AS^5	x_{50}^5
15.4	4.1	7.7 %Li_2O	7.9	7.2 %Li_2O	10.7	6.9 %Li_2O	13.5	6.6 %Li_2O	17.0	6.2 %Li_2O

Those parameters were further used to calculate the respective Partition Curves, presented in Table 44 and Table 45. Then, applying the Eq. 32, Eq. 33 and Eq.34 it was possible to calculate the yield, concentrate grade and recovery of each separation cut-grade point. The results were compared to experimental results to validate the obtained Partition Curves.

Table 44 – Calculation of Partition Curves for the concentration of both size fractions of São Pedro das Águias.

SPA [CS=212µm]				
Feed grade hist.		**Partition curves**		
xi, %	fi,%	p_i^1, %	p_i^2, %	p_i^3, %
0.00	0.36	0.36	23.69	74.69
2.42	0.36	0.36	23.69	74.69
4.03	0.36	0.36	23.69	74.69
5.64	0.37	0.37	23.69	74.70
7.25	0.37	0.37	23.70	74.70
12.08	0.37	0.37	23.70	74.70
20.13	0.41	0.41	23.74	74.71
28.18	0.50	0.50	23.89	74.78
36.23	0.80	0.80	24.44	75.02
44.29	1.73	1.73	26.41	75.93
52.34	4.51	4.51	32.92	78.94
60.39	12.23	12.23	49.51	85.90
68.44	29.88	29.88	73.70	93.88
73.27	45.61	45.61	85.27	96.89
74.88	51.26	51.26	88.14	97.56
76.49	56.87	56.87	90.54	98.11
78.10	62.32	62.32	92.51	98.53
79.71	67.48	67.48	94.11	98.87
f, %	1.86	**Calculated data**		
Yield, %		1.70	25.15	75.20
c, %		62.36	6.30	2.38
Rec, %		56.82	85.14	96.03
		Experimental data		
Yield, %		1.69	24.88	75.29
c, %		61.88	6.47	2.37
Rec, %		56.06	86.10	95.51

SPA [CS=75µm]				
Feed grade hist.		**Partition curves**		
xi, %	fi,%	p_i^1, %	p_i^2, %	p_i^3, %
0.03	97.00	0.31	11.84	42.73
2.42	0.20	0.31	11.85	42.73
4.03	0.08	0.31	11.85	42.73
5.64	0.04	0.31	11.85	42.73
7.25	0.05	0.32	11.85	42.74
12.08	0.10	0.32	11.86	42.74
20.13	0.11	0.36	11.92	42.79
28.18	0.08	0.48	12.11	42.95
36.23	0.07	0.81	12.76	43.54
44.29	0.06	1.78	14.92	45.60
52.34	0.06	4.51	21.63	52.06
60.39	0.08	11.72	38.35	66.66
68.44	0.10	27.73	64.47	84.30
73.27	0.08	42.17	78.56	91.57
74.88	0.06	47.47	82.31	93.28
76.49	0.08	52.83	85.55	94.68
78.10	0.11	58.13	88.30	95.81
79.71	1.63	63.25	90.59	96.72
f, %	1.85	**Calculated data**		
Yield, %		1.54	13.45	43.85
c, %		63.37	10.99	3.80
Rec, %		52.85	79.86	90.00
		Experimental data		
Yield, %		1.59	14.08	43.54
c, %		64.45	10.34	3.93
Rec, %		54.15	77.13	90.72

Table 45 – Calculation of Partition Curves for the concentration of Alvarrões.

Feed grade hist.		Partition curves				
xi, %	fi,%	p_i^1, %	p_i^2, %	p_i^3, %	p_i^4, %	p_i^5, %
0.12	81.52	4.09	7.91	10.67	13.58	17.02
1.16	1.88	4.09	7.91	10.67	13.58	17.02
1.93	0.99	4.09	7.91	10.67	13.59	17.02
2.70	0.74	4.09	7.91	10.68	13.59	17.03
3.47	0.64	4.11	7.94	10.71	13.64	17.11
4.24	0.60	4.19	8.06	10.90	13.93	17.64
5.01	0.61	4.55	8.70	11.90	15.64	21.01
5.78	0.68	6.19	11.84	17.09	24.63	38.05
6.55	0.86	13.19	25.06	37.43	54.08	74.73
7.32	11.50	35.67	57.65	73.43	86.29	94.93
f, %	**1.17**	**Calculated data**				
Yield, %		7.82	13.81	18.17	22.38	26.64
c, %		4.09	3.78	3.69	3.57	3.36
Rec, %		27.33	44.66	57.35	68.26	76.66
		Experimental data				
Yield, %		7.81	13.73	18.30	22.54	26.45
c, %		4.10	3.82	3.67	3.55	3.40
Rec, %		27.33	44.69	57.30	68.19	76.78

The respective Partition curves are illustrated in Fig. 106, Fig. 107 and Fig. 108. In each representation, it is also shown the efficiency curve without the dragging effect (AS), commonly referred to as reduced efficiency curves.

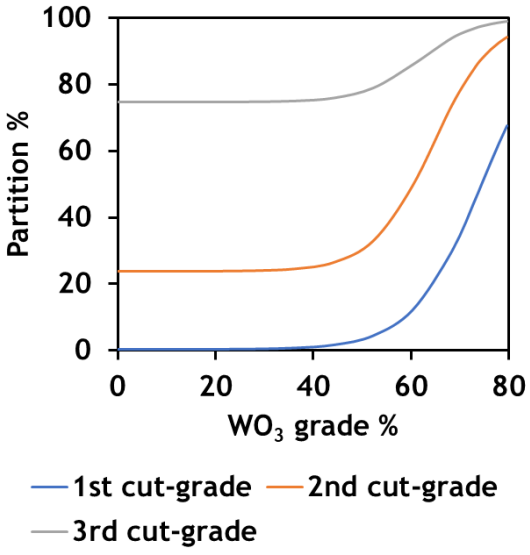

a)

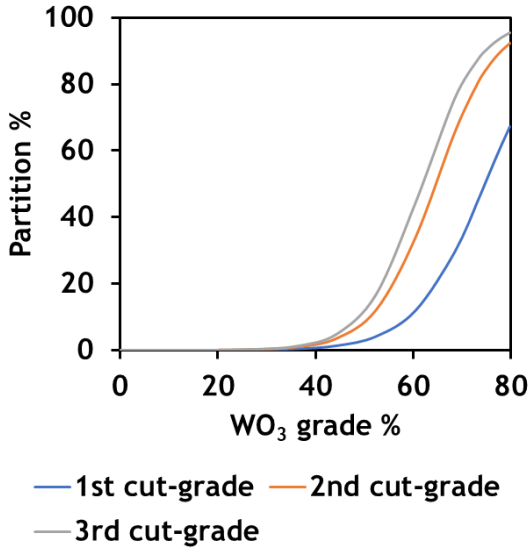

b)

Fig. 106 – Partition curves obtained by fitting the Lynch model to experimental data of São Pedro das Águias [cs=212 µm]: a) Partition curve; b) Reduced Partition curve; (XX-axis is limited to the stoichiometric composition of scheelite).

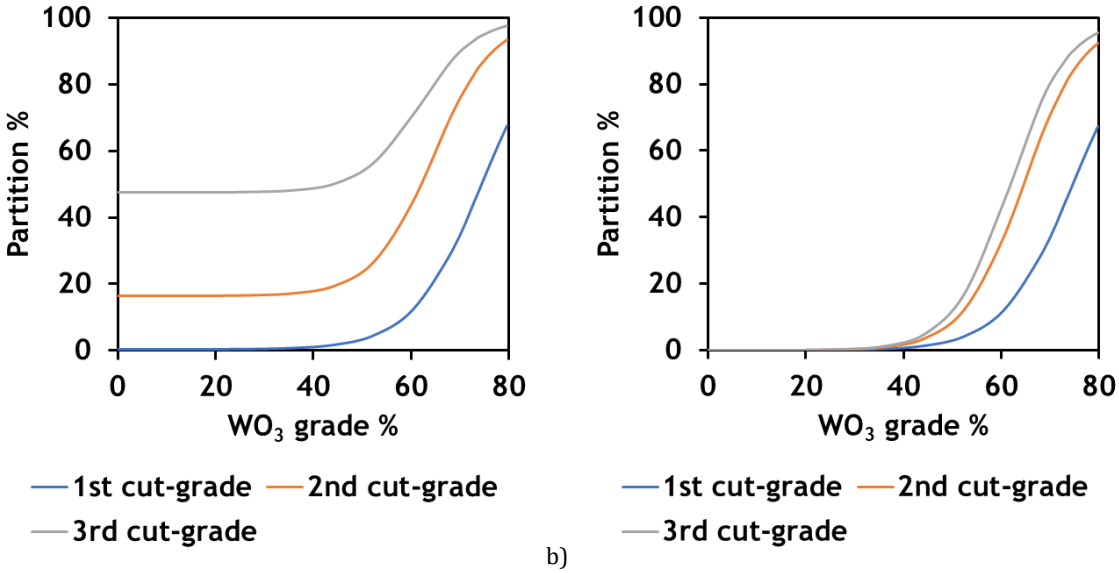

Fig. 107 –Partition curves obtained by fitting the Lynch model to experimental data of São Pedro das Águias [cs=75 µm]: a) Partition curve; b) Reduced Partition curve; (XX-axis is limited to the stoichiometric composition of scheelite).

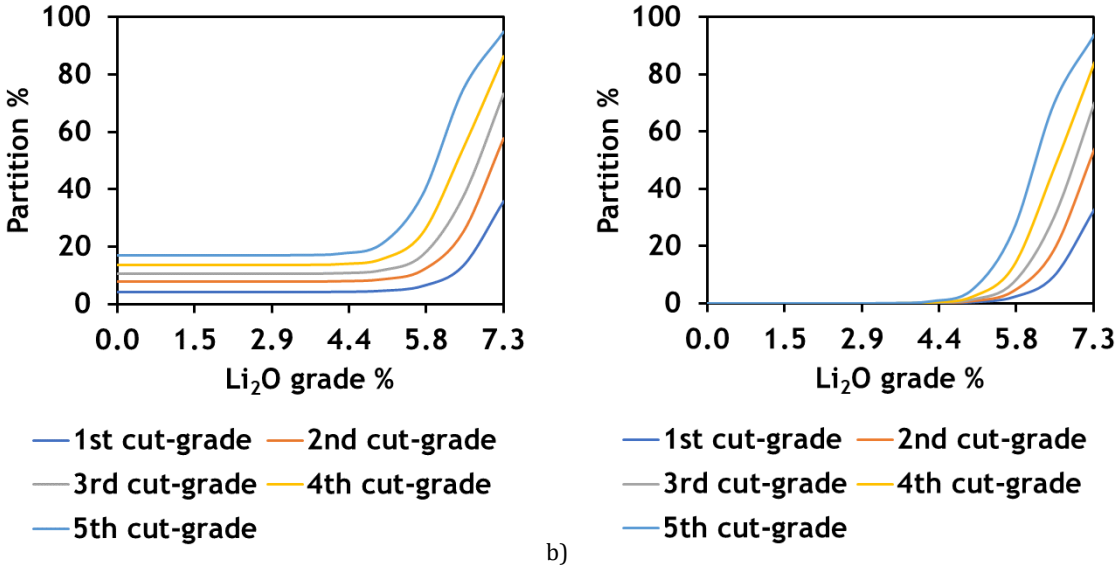

Fig. 108 –Partition curves obtained by fitting the Lynch model to experimental data of Alvarrões concentration tests: a) Partition curve; b) Reduced Partition curve. (XX-axis is limited to the stoichiometric composition of lepidolite).

Based on the computed partition curves of São Pedro das Águias concentration tests, the following considerations can be drawn:

- The product collection zones in the shaking table tests were defined using a visual criterion, illuminating the table with UV light. First collection zone, corresponding to the 1st cut-grade, was defined to produce a rich concentrate, and the last collection zone, corresponding to the 3rd cut-grade was designed to reach a high recovery product;
- Similar *m* values were computed for both size fractions. However, higher values of *AS* dragging effect were observed for the coarser size fraction (cs=212μm), which can be due to the inefficiency of the previous elutriation step, in which low density and fine particles were reported to the underflow, being misplaced in the concentration of the coarser size fraction.

In the case of Alvarrões flotation, the observation of partition curves conducted to the following remarks:

- Low dragging effect (*AS*) points to low entrainment level during the flotation process;
- High cut-grade values (x_{50}) indicate a high degree of liberation;
- The partition value in the higher grades increases with the increasing of flotation time (cut-grade decrease), pointing out for the necessity of long residence times to maximize lepidolite recovery (low flotation kinetics);

Attention should be given to a phenomenon that occurs in both separations: partition values do not reach 100% when the cut-grade is close to the maximum, meaning that at this cut-point some full-liberated particles are not being collected in the concentrate. To overcome this effect, the collection zone of the shaking table must be enlarged and flotation time must be prolonged, accepting a higher dragging effect by reporting non-valuable particles to the concentrate.

Finally, sliding the obtained partition curve along the XX cut-grade axis – using the same *m* shape factor, while changing x_{50} and *AS* calculated accordingly with x_{50} - all possible separation scenarios are simulated and the corresponding yield, recovery and grade are calculated. Fig. 109 shows Mayer upgrading curves obtained in this way, in which it is observed a very good adjustment to the experimental points.

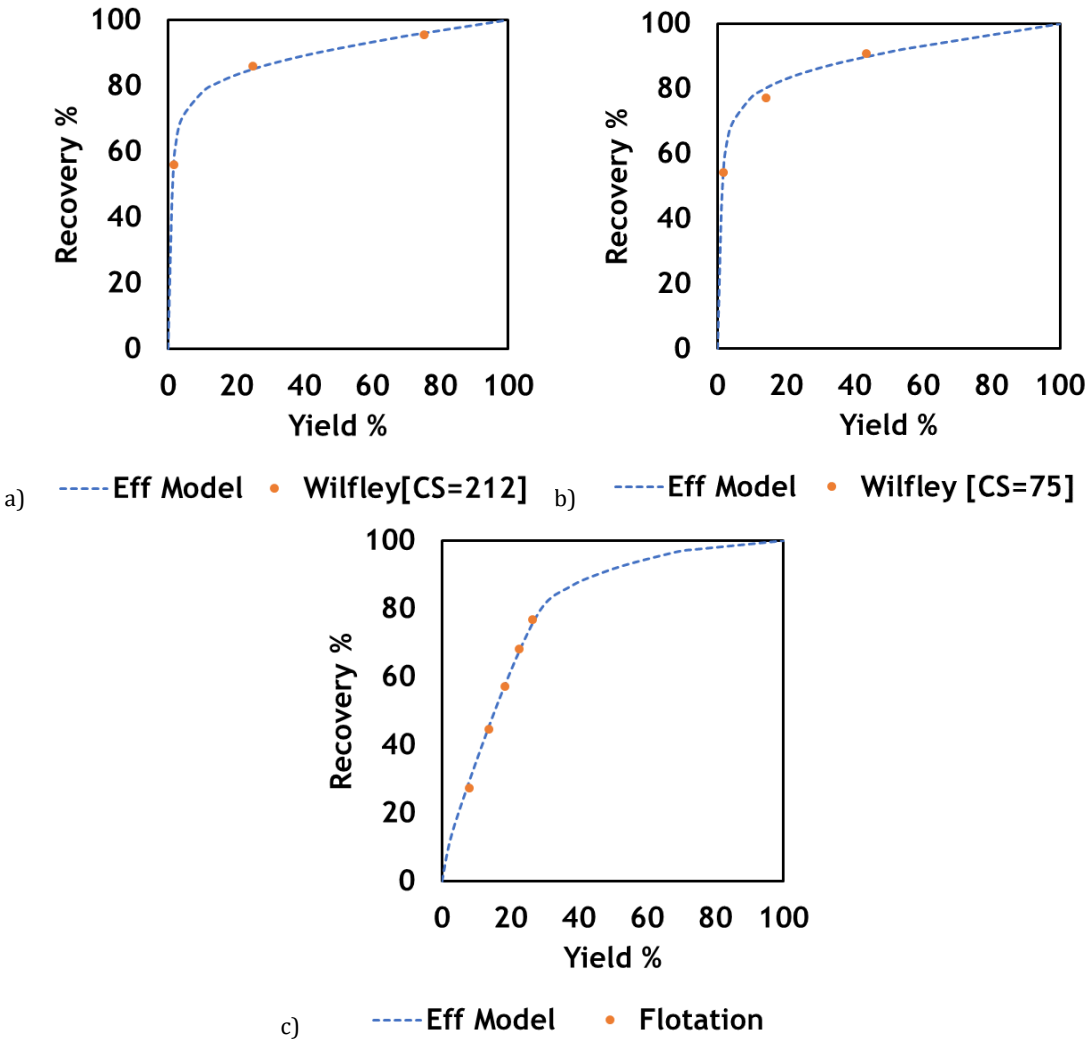

Fig. 109 – Comparison between Mayer upgrading curve based on the efficiency model (Eff model) prediction and experimental data: a) São Pedro das Águias [cs=212 µm]; b) São Pedro das Águias [cs=75µm]; c) Alvarrões flotation test.

5.1.3.2 FITTING PARTITION CURVE TO EXPERIMENTAL DATA OF PRE-CONCENTRATION TESTS AND DETERMINATION OF THE MAYER UPGRADING CURVE

The procedure developed in the previous section was also applied to data acquired in pre-concentration testwork at crushing sizes. In both studied cases, pre-concentration was done by optical sorting at sizes in the range of [20/6] mm: scheelite from São Pedro das Águias was handpicked and lepidolite from Alvarrões was electronically optical sorted (Chapter III).

As stated, the first step was to define the correlation between x_{50} and *AS*, fitting the Partition Curve to each data-point corresponding to the respective cut-grade. As two different cut-grades were applied for both ores, the respectively fitted *m*, *AS* and x_{50} (Table 46) generated the respective Partition Curves.

Table 46 – Results of fitting the Lynch model parameters to the experimental data.

	São Pedro das Águias			Alvarrões		
	m	**AS**	**x_{50}**	**m**	**AS**	**x_{50}**
1st cut-grade	0.05	0.99	0.59	3.20	29.9	5.2
2nd cut-grade	5.1	6.1	0.06	2.9	55.1	5.0

In the case of hand-sorting separation carried out with São Pedro das Águias ore, the fitting procedure resulted in the acquisition of very distinct *m* values. The comprehension of these results is connected with the experimental procedure:

- It should be remembered that handpicking was carried out, doing a particle-by-particle identification under UV light to identify particles with visible scheelite content;
- In the first cut-grade grade, particles with a large visible area of scheelite were reported to the concentrate, trying to produce a high-grade product. This separation criterion is subjective and weak because did not take into consideration the quantification of the particle surface.
- In the second cut-grade, the separation criterion was clearer: particles with non-visible scheelite were reported to the tailings product.
- This discrepancy related to the robustness of the separation criterion would be the reason for the distinct separation efficiency of both cut-grades.

In line with the above-mentioned remarks, there is no reason to analyze the relation between *AS* and x_{50} for the pre-concentration of São Pedro das Águias, nor to fit the Partition Curves of both cut-grade with a single *m* value. Therefore, both cut-grades were considered as separations carried out by different separators. Partition curves obtained with different *m* values are presented in Table 48.

In the case of Alvarrões ore, Fig. 110 shows the linear relationships between *AS* and x_{50} for both cases that will be used in the efficiency model.

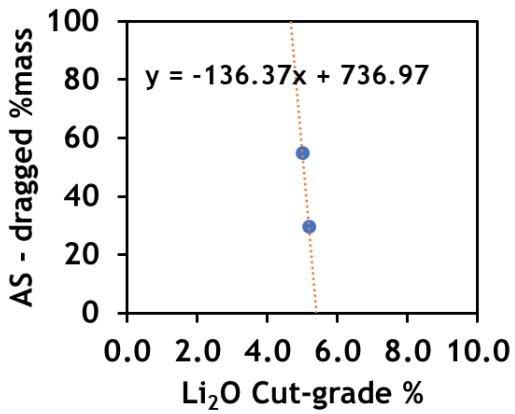

Fig. 110 - Definition of the relation between AS and X_{50} in the case of Alvarrões pre-concentration;

The final best parameters adjusted to experimental data of Alvarrões pre-concentration test are presented in Table 47, which conducted to the computation of the respective Partition Curves shown in Table 48.

Table 47 – Final Lynch model parameters to fit the results of Alvarrões Pre-concentration tests.

m	AS^1	X_{50}^1	AS^2	X_{50}^2
2.5	25.8	4.9 %Li_2O	52.4	4.6 %Li_2O

Table 48 – Calculation of Partition Curves for the pre-concentration of both studied ore.

São Pedro das Águias			
Feed grade hist.		**Partition curves**	
xi, %	fi,%	p_i^1, %	p_i^2, %
0.00	45.54	0.99	6.10
0.13	24.07	17.85	99.63
0.38	7.85	38.96	100.00
0.75	5.50	56.27	100.00
1.25	4.00	68.58	100.00
1.75	2.55	75.72	100.00
2.25	1.82	80.37	100.00
2.75	1.38	83.63	100.00
3.25	1.08	86.05	100.00
3.75	0.87	87.92	100.00
4.50	1.03	90.02	100.00
6.00	1.41	92.79	100.00
8.50	1.30	95.34	100.00
15.00	1.18	98.02	100.00
25.00	0.34	99.29	100.00
42.50	0.06	99.85	100.00
62.50	0.00	99.97	100.00
f, %	**0.87**	**Calculated data**	
Yield, %		24.9	57.2
c, %		85.1	99.9
Rec, %		3.0	1.5
		Experimental data	
Yield, %		25.6	57.2
c, %		84.5	99.1
Rec, %		2.9	1.5

Alvarrões			
Feed grade hist.		**Partition curves**	
xi, %	fi,%	p_i^1, %	p_i^2, %
0.00	10.40	29.84	55.45
0.50	29.57	30.92	56.16
1.50	20.49	34.16	58.34
2.50	14.40	39.41	61.91
3.50	10.20	47.17	67.22
4.50	7.01	57.28	74.05
5.50	4.51	68.42	81.38
6.50	2.58	78.68	87.85
7.30	0.84	85.28	91.85
f, %	**1.96**	**Calculated data**	
Yield, %		39.6	62.0
c, %		2.5	2.2
Rec, %		50.7	69.4
		Experimental data	
Yield, %		39.6	62.0
c, %		2.8	2.5
Rec, %		50.7	69.4

Fig. 111 and Fig. 112 show the respective Partition and reduced Partition Curves that define the pre-concentration at crushing sizes for each studied ore[2].

[2] In the case of scheelite pre-concentration from São Pedro das Águias the grade-axis Fig. 111 was restricted up to 10 %WO_3 for better readability of the graphical representation.

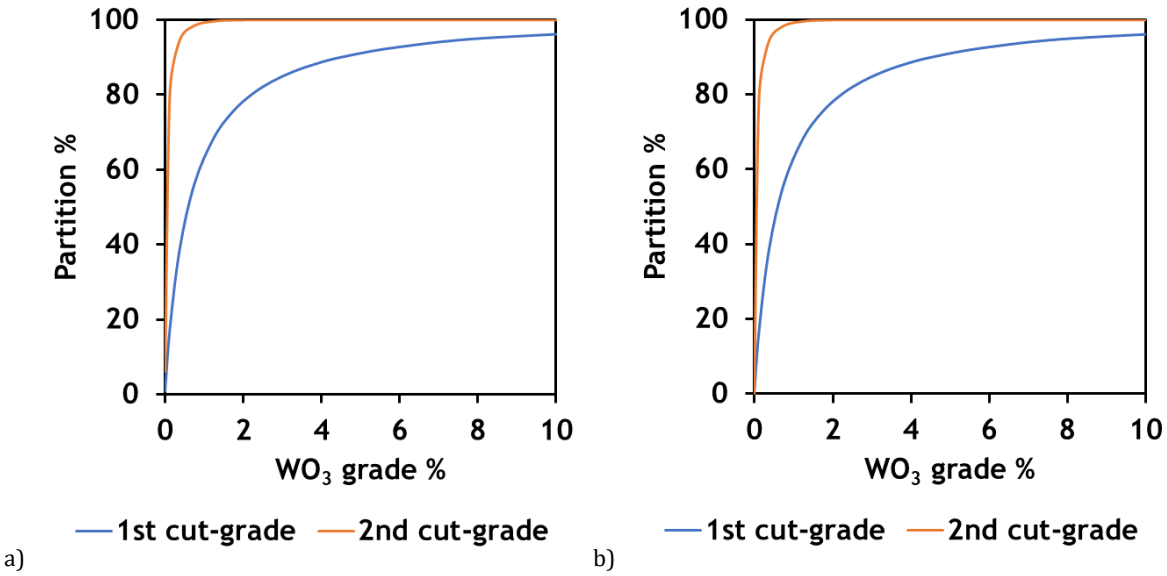

Fig. 111 – Partition curves obtained by fitting the Lynch model to experimental data of São Pedro das Águias: a) Partition curve; b) Reduced Partition curve.

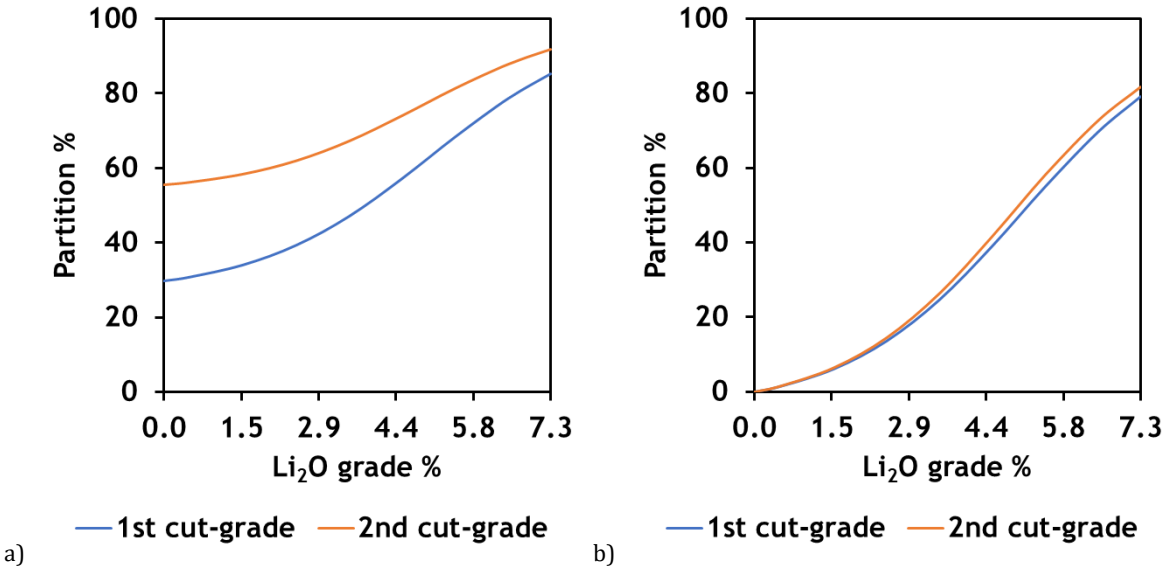

Fig. 112 – Partition curves obtained by fitting the Lynch model to experimental data of Alvarrões: a) Partition curve; b) Reduced Partition curve.

At this point, some reflections about the separation performance of the processes applied in the pre-concentration tests can be drawn:

- In the case of São Pedro das Águias, the adjusted low x_{50} values points to a typical pre-concentration stage, in which the main objective is to reject mainly gangue material. The adjusted sharp Partition Curve indicates a good efficiency of the second cut-grade that is close to the Heaviside step. Conversely, in the first cut-

grade, the lower verticality of the Partition Curve near the x_{50} points out for lower separation efficiency, which was already justified by the weak separation criterion.

- In the case of Alvarrões, the tendency of Partition Curves to be horizontal points out to the poor performance of the pre-concentration: high x_{50} adjusted values indicate that separator settings were not conveniently optimized for a pre-concentration stage; also high values of AS indicates high quantities of gangue material dragged into the "concentrate";

Finally, sliding the Partition Curve along the XX grade-axis, using the set of fitted parameters – *m*, x_{50} and *AS* - allows to compute the respective yield, grade and recovery values for all separation scenarios. As in the previous cases, having access to this data, it is possible to draw the respective interpolated upgrading curve. As in the case of São Pedro das Águias it was not possible to fit a single m value, this sliding procedure is not applicable. Fig. 113 shows the computation of Mayer upgrading curves for Alvarrões pre-concentration, where it is possible to observe a great goodness-of-fit between the prediction of the efficiency model and experimental data.

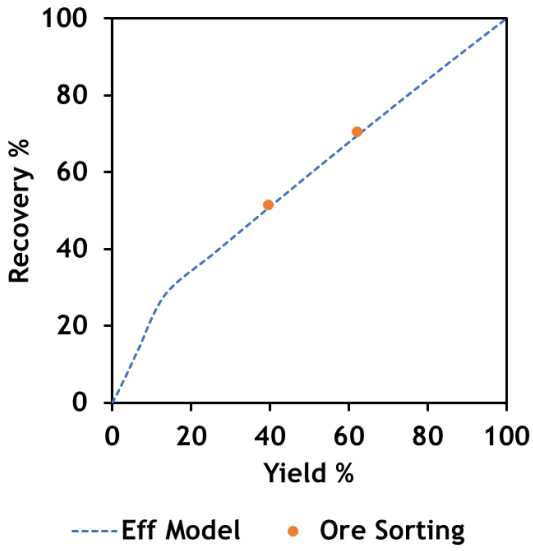

Fig. 113 – Comparison between the Mayer upgrading curve based on Lynch model prediction and experimental data of Alvarrões optical sorting.

5.1.3.3 PREDICTING CONCENTRATE GRADE HISTROGRAMS (WT%)

The possibility of determining the Partition Curves, through the adjustment of the developed mathematical model to experimental data of concentration tests, opens a new window to make predictive simulations of the processes. In fact, the availability of the developed methodology to calculate the yield and recovery of the separation was based on the ability of the mathematical model to split each feed grade fraction in the part that is collected in the concentrate and the other that goes to the tailings.

This can be done by the application of the fitted Partition Curves to the respective feed Grade Histogram (wt%), which according to Eq. 35 would allow for the calculation of the concentrate grade histogram (wt%) - c_i.

$$c_i = \frac{f_i \times p_i}{Yield} \qquad \text{Eq. 35}$$

Fig. 114 shows the Partition Curves superimposed on the feed Grade Histograms (wt%) for the case of São Pedro das Águias concentration. The application of Eq. 35 would result in the concentrate grade histograms (wt%) represented in Fig. 115.

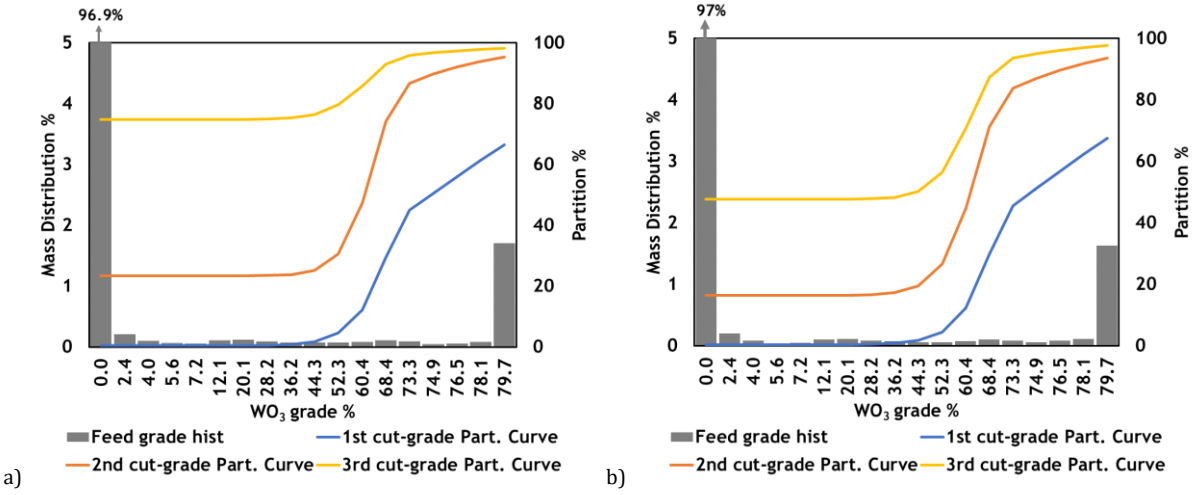

Fig. 114 – Application of the obtained partition curve to the feed grade histogram (wt%) - São Pedro das Águias concentration tests: a) [CS=212µm]; b) [CS=75µm].

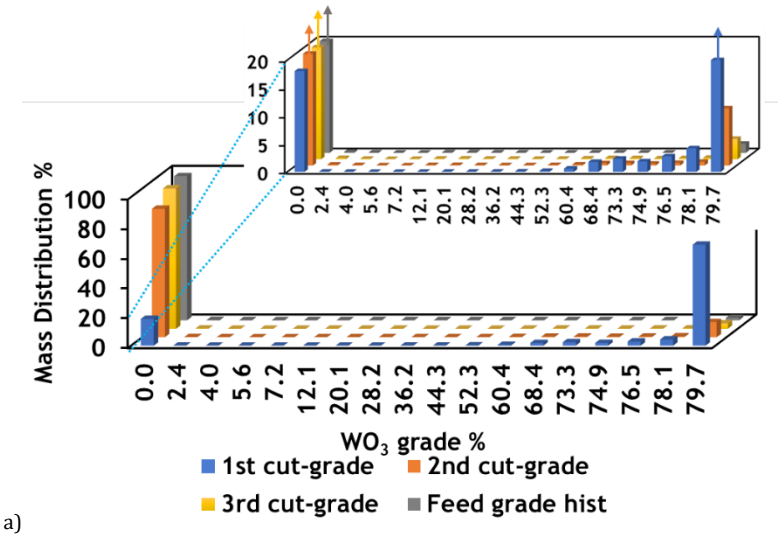

a)

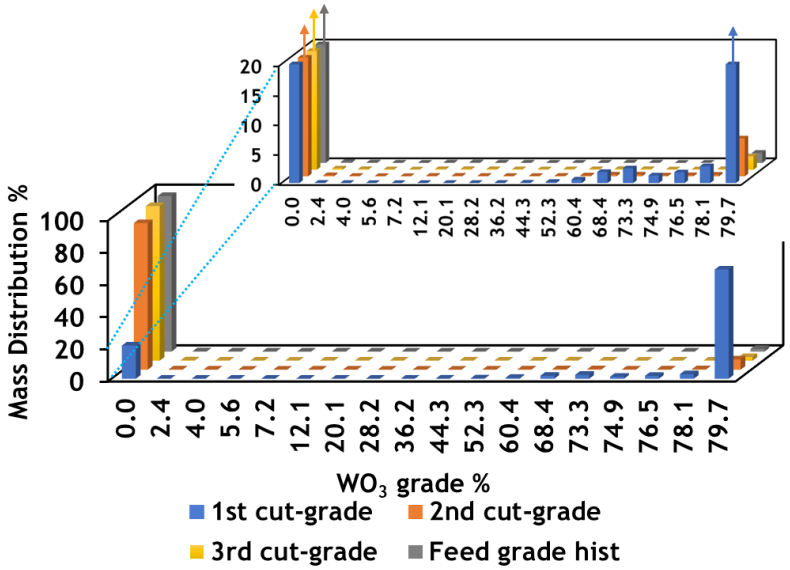

b)

Fig. 115 – São Pedro das Águias concentration tests - Grade histograms (wt%) of separation products and partial representation for better observation of the mid-grade classes: a) [CS=212µm]; b) [CS=75µm].

Both grade histograms (wt%) presented in Fig. 115 show similar behavior. As expected, when the cut-grade increases the % of material in the lower grade classes decreases and increases in the higher grade classes. As discussed before, liberated scheelite particles are not enough to fulfill the riffles in the lower levels of the shaking table, which is also indicated bt the calculated *AS* parameter: in the 2nd and 3rd cut-grade products, the quantity of low-grade material is high, meaning the presence of dragged gangue particles in the concentrate products. Only the 1st cut-grade (the greater one) was able to produce a high-concentrate grade, although showing some low-grade particles "dragged" into the concentrate (imperfection of the elutriation?).

The same approach was applied to the concentration tests of Alvarrões ore. Fig. 116 shows the feed grade histogram(wt%) and the obtained partition curves and Fig. 117 shows the grade histograms (wt%) obtained by applying the partition curves to the feed grade histogram (wt%).

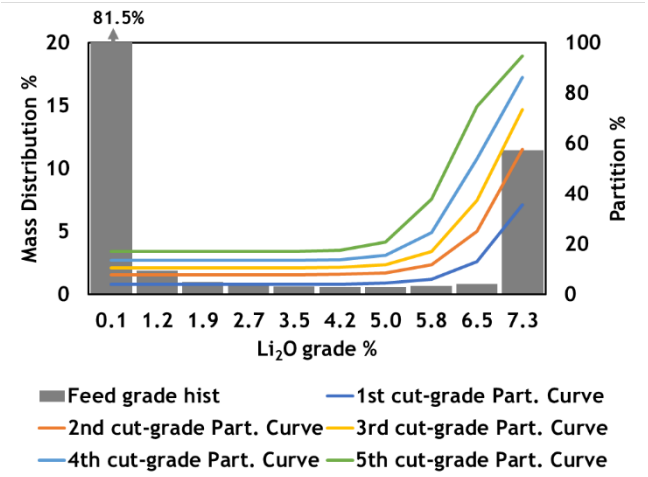

Fig. 116 – Application of the obtained partition curve to the feed grade histogram (wt%) - Alvarrões concentration test (kinetic test).

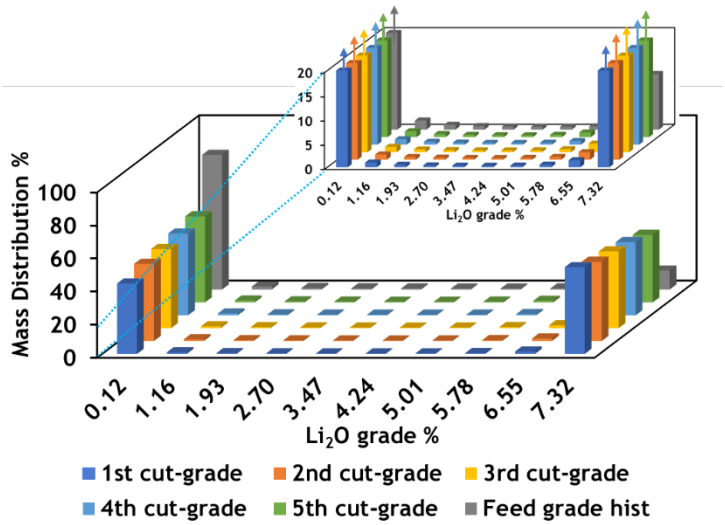

Fig. 117 – Alvarrões concentration test (kinetic test) - Grade histograms (wt%) of separation products and partial representation for better observation of the mid-grade classes.

Also, in this case, an increase of the % of higher grade material is observed when cut grade increases, while conversely the % of lower grade material is reduced. These differences are very slight and are compatible with a global low kinetic flotation rate and almost constant along time. At the same time, the presence of low-grade fractions in the

concentrates shows that the collector is specific for mica minerals and less selective for Li-mica.

The same procedure was applied to the case of pre-concentration stages. Fig. 118 shows the case of pre-concentration tests by hand-picking of scheelite ore from São Pedro das Águias and pre-concentration of lepidolite ore from Alvarrões by electronic optical sorting.

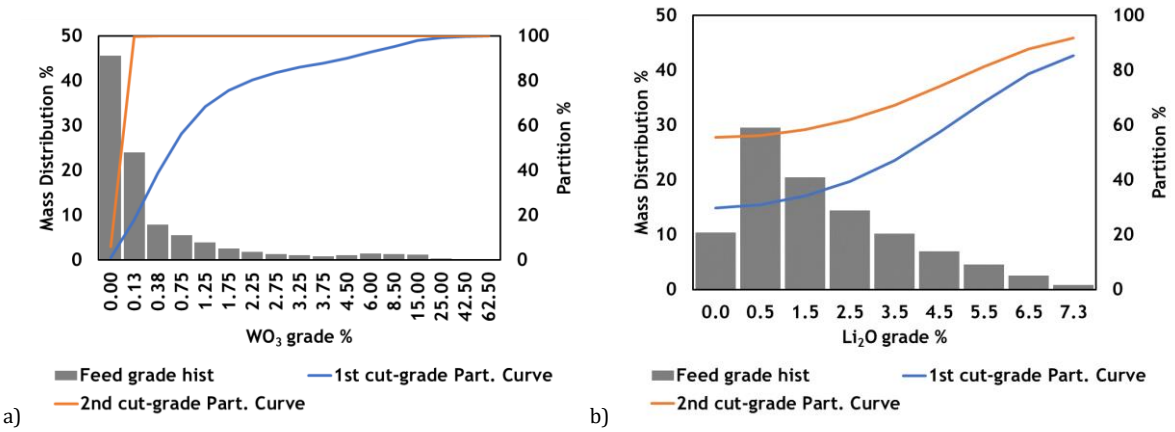

Fig. 118 – Application of the obtained partition curve to the feed grade histogram (wt%) a) São Pedro das Águias pre-concentration test (handpicking); b) Alvarrões pre-concentration test (Optical sorting).

These data were then applied to compute the concentrate grade histograms (wt%). Fig. 119 shows the predicted Grade Histograms (wt%) of the products collected during the ore sorting tests applied to São Pedro das Águias and Alvarrões ores.

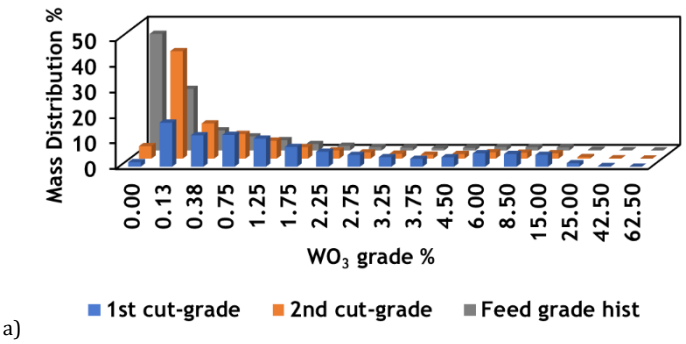

b)

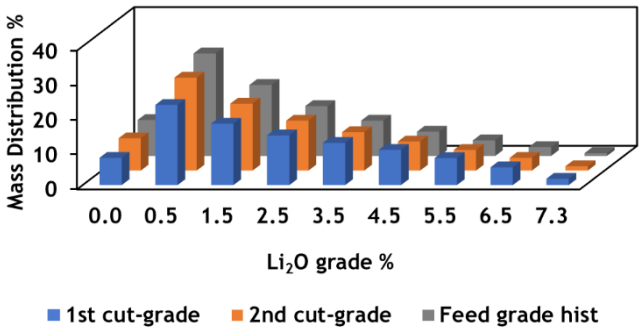

Fig. 119 – Grade histograms (wt%) of separation products – a) São Pedro das Águias concentration test (hand-picking); b) Alvarrões pre-concentration test (Optical sorting).

In the case of pre-concentration of São Pedro das Águias, it is possible to observe that the quantity of material in the 0.0% grade class is reduced, which is in accordance with the *AS* values determined and to the experimental procedure – particles with no visible scheelite were rejected. The greater difference between the concentrates of 1st and 2nd cut-grade is the percentage of material in the second-lowest grade class. These results point out that an electronic optical sorting under UV light (so far simulated only by a hand-picking laboratory procedure) would be feasible to reject gangue material at the tested crushing size, a conclusion that is supported by the obtained shape for the Partition Curve for the 2nd cut-grade.

In the case of pre-concentration tests of Alvarrões ore by optical sorting, the similarity between feed and concentrates histograms' shape point out for a great inefficiency of the optical sorting, which was already concluded from the horizontality of the adjusted Partition Curves.

In conclusion, it can be said that the Efficiency Model would be an interesting tool for the assessment of the separation efficiency in mineral processing. There are two fundamental characteristics of the efficiency model that must be considered:

1- Higher separation efficiency is achieved when the shape of the Partition Curve is closer to the Heaviside step function;
2- High values of the dragging parameter (*AS*) indicate lower efficiencies since it implies that the material from the low-grade fractions can be reported to the concentrate, and this can usually happen in scavenging separations (low cut-grades).

5.2 THE CONCEPT OF ULTIMATE UPGRADING – A NEW WINDOW ON SEPARATION EFFICIENCY

As previously discussed, upgrading curves are interesting tools to describe the separation process itself, by collecting important information about the efficiency. During many years, upgrading curves were used to compare different separations tests, aiming to select the best set of separation settings. Usually, this is accomplished by comparing the shape and attitude of the upgrading curves with the respective ideal and non-upgrading lines. As demonstrated in Chapter II, although upgrading curves can provide useful information about the performance of the separation, such representations sometimes can be biased from reality, namely when only a few experimental data are available and linear interpolations between data points are used. As discussed in the previous paragraphs, the developed Efficiency Model provides a realistic contribution to obtaining more discretized upgrading curves, better than simple linear interpolations or other mathematical models based on parameters of no physical meaning.

Those upgrading curves can be used to assess separation efficiency considering the distance between the experimental and the ideal upgrading curves, bearing in mind that ideal separation occurs when minerals are fully liberated, and the separation is technically perfect. However, at this level, it is not possible to justify the gap between both curves, i.e., to identify the reasons for the observed inefficiency.

It is commonly mentioned that global inefficiency can be caused by technical inefficiency (related to the separation technique) and by lack of liberation. For example, in the case of pre-concentration, only non-valuables are partially liberated, meaning a global low degree of liberation and, a high gap between experimental and ideal upgrading curves would be observed, as in the case of Alvarrões pre-concentration. Nevertheless, it is not possible to distinguish which part of the inefficiency is due to the lack of liberation and the other that derives from the low performance of the optical sorter.

One contribution of this thesis is the proposal of a methodology aiming at quantifying the share of both inefficiencies in the global performance of the separation. For this purpose, the conceived concept of the Ultimate Upgrading curve (UUC) will be developed and presented in the next section.

5.2.1 ULTIMATE UPGRADING CURVE – THE APPROACH

Separation Efficiency (SE) is highly dependent on the mineral liberation degree and on the technical performance of the used separator, being both factors expressed (but not discriminated) by the gap between the experimental and the ideal upgrading curves, as shown in Fig. 120. That gap should be reduced by improving both dependencies.

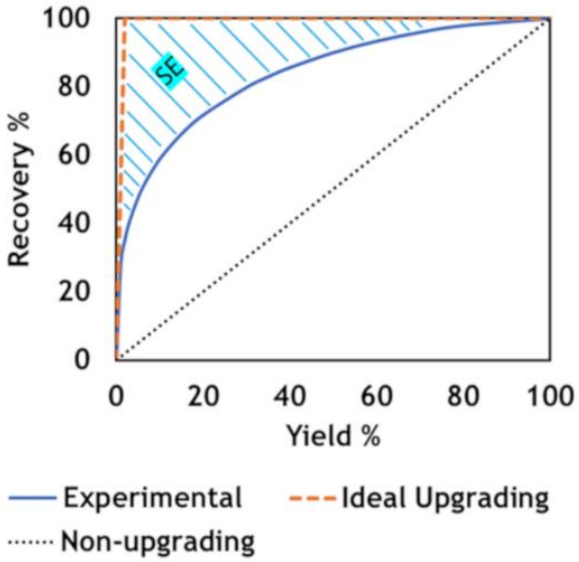

Fig. 120 – Identification of the distance between the experimental curve and ideal upgrading line using the Mayer diagram.

The challenge is now to distinguish between both influences on the separation process, trying to quantify to what extent each dependency can or should be improved. This is exactly what is intended with the introduction of the Ultimate Upgrading concept, which represents the separation of a given ore, at a given degree of liberation, but conducted under a perfect separation, i.e., a separation 100% technically efficient.

For this purpose, the UUC can be determined by the application of Partition Curves mathematically represented by the Heaviside step function to the feed Grade Histogram (wt%), centred at successive cut-grades.

For this purpose, the required feed Grade Histograms (wt%) can be experimentally determined, for instance, using quantitative mineral liberation analyzers as QEMSCAN® or other methodologies for particle analysis (as the one proposed in Chapter IV) and shown in Fig. 121, in which particles (mass) are grouped together accordingly with the respective grade class.

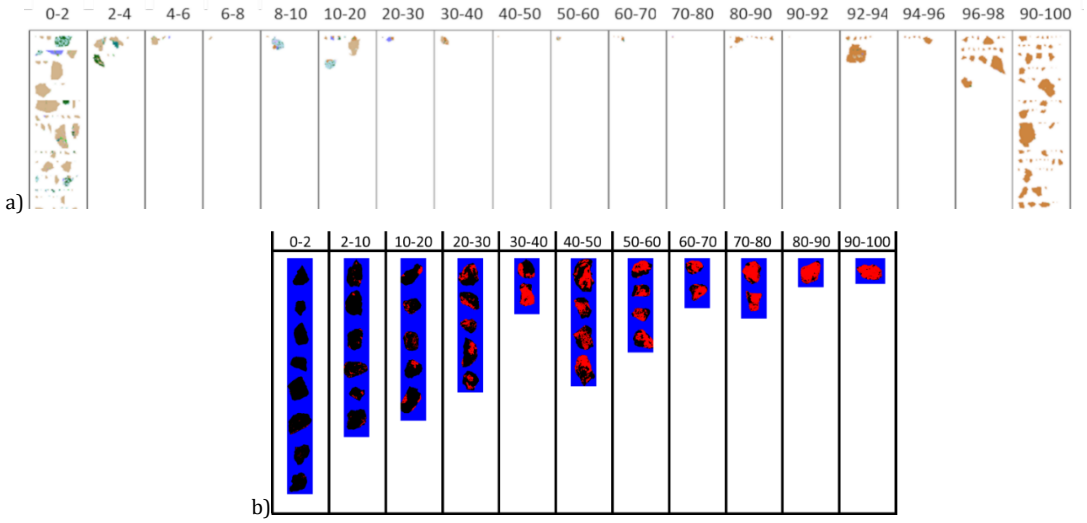

Fig. 121 - Liberation analysis by a) QEMSCAN® and b) methodology developed in this work.

As before, sliding a perfect Partition Curve, in the form of a Heaviside step function, centred in successive cut-grades, conducts to the construction of the Ultimate Upgrading Curve, as seen in Fig. 122 using a Mayer representation.

It should be noticed that mineral liberation analyzers use direct measurements of mineralogical data of the ore texture. In this context, the UUC can be seen as the limit of the technical efficiency for a certain degree of liberation, represented by the Grade Histogram (wt%). In other terms, the region above UUC would be unachievable unless liberation is improved by more powerful comminution. At this point, it is possible to compare the experimental Mayer curve with the Mayer UUC and with the Mayer Ideal upgrading line, as can be observed in Fig. 122.

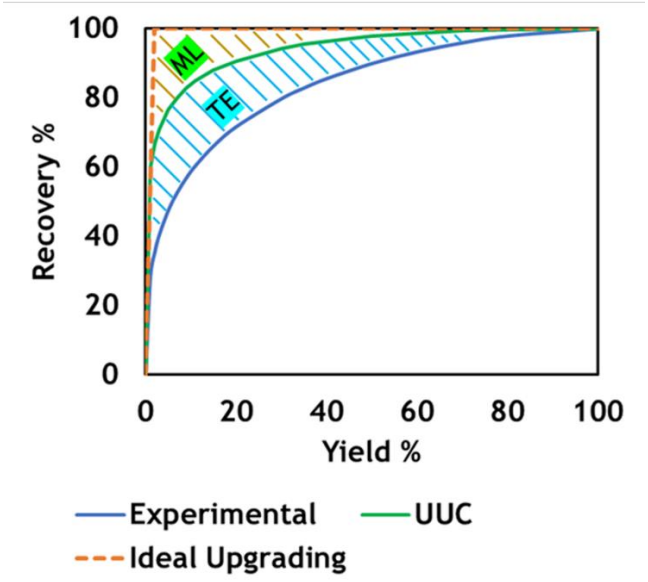

Fig. 122 – Comparison UUC, ideal upgrading and experimental curve using the Mayer diagram.

In the graphical Mayer representation (Fig. 122), TE (distance between the UUC and the Experimental curve) refers to the technical inefficiency of the process, whilst ML (the distance between UUC and the Ideal Upgrading) indicates the lack of liberation. In this way, it is possible to quantify the share of the lack of liberation and the technical inefficiencies of the separator in the global process inefficiency.

It should be highlighted, that UUC can be applied to any other type of upgrading graphical representation, for instance to the common Grade vs Recovery curves as can be observed in

Fig. 123. Mineral liberation analysis is used to compute the theoretical grade-recovery curves, defining the zone of unachievable grade-recovery unless liberation would be improved. Thus, any experimental separation performance can be assessed taking into account its distances to the theoretical curves [7, 8], UUC and Ideal.

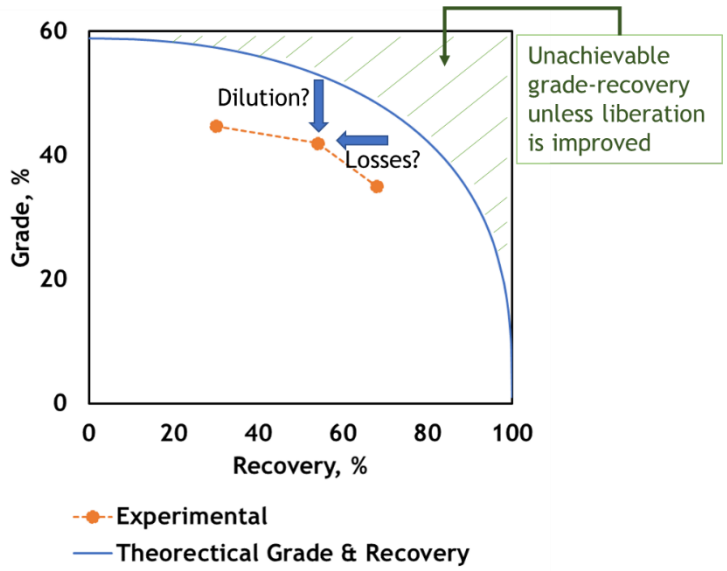

Fig. 123 - Representation of a theoretical Grade Recovery curve and the comparison with an experimental separation [7].

5.2.2 ACQUISITION OF MAYER ULTIMATE UPGRADING CURVES AND ASSESSMENT OF SEPARATION EFFICIENCY

5.2.2.1 COMPUTATION OF MAYER ULTIMATE UPGRADING CURVES

As aforementioned, acquired quantitative mineralogical data, expressed by the grade histograms (wt%) are fundamental for the computation of the ultimate upgrading curve [9].

Mayer representations were selected to demonstrate the use of the UUC to assess the separation efficiency of concentration and pre-concentration tests of São Pedro das Águias and Alvarrões ores.

As before, UUC can be computed by sliding a Heaviside step function $H[xi\text{-}x5_0]$ (centred in the defined cut-grade) along the grade histogram (wt%). The result of this sliding procedure is that all particles with a grade below the cut-grade will be rejected and particles with a grade above the cut-grade will be reported to the concentrate. Knowing the mass and grade of particles reported to concentrate (given by the grade histogram (wt%)) it is possible to compute the respective yield, recovery and concentrate and tailings grade, using similar equations as before:

$$Yield = \sum_i f_i \times H[x_i - x_{50}] \quad \text{Eq. 36}$$

$$Concentrate\ average\ grade\ (c) = \frac{\sum_i f_i \times H[x_i - x_{50}] \times x_i}{Yield} \quad \text{Eq. 37}$$

$$Tailings\ average\ grade\ (e) = \frac{\sum_i f_i \times H[x_{50} - x_i] \times x_i}{1 - Yield} \quad \text{Eq. 38}$$

$$Recovery = \frac{Yield \times c}{feed\ average\ grade\ (f)} \quad \text{Eq.39}$$

The Heaviside step function, $H(x_i\text{-}x_{50})=1$ when $x_i>x_{50}$ and $H(x_i\text{-}x_{50})=0$ when $x_i<x_{50}$. Keeping the same nomenclature, f_i is the feed grade histogram wt(%) and x_i is the grade class.

These equations were first applied to the data obtained during the study of the concentration processes of both studied ores. Table 49 and Table 50 shows the cumulative recovery, yield and grade computed for both size fractions of São Pedro das Águias ore.

Table 49 - Mathematical manipulation of grade histogram (wt%) data – São Pedro das Águias ore [cs=0.212].

Scheelite grade fraction, %	**WO_3 average grade, %**	**Grade Histogram, %**	**Yield, %**	**Concentrate average grade, %**	**Recovery, %**
Scheelite = 80.52% WO_3	x_i	f_i	$\sum_i f_i \times H[x_i - x_{50}]$	$\frac{\sum_i f_i \times H[x_i - x_{50}] \times x_i}{Yield}$	$\frac{Yield \times c}{f}$
			100.00	1.85	100.00
0-2	0.0	96.87	3.13	59.48	100.00
2-4	2.4	0.21	2.92	63.61	99.73
4-6	4.0	0.10	2.82	65.72	99.51
6-8	5.6	0.07	2.75	67.20	99.31
8-10	7.2	0.05	2.70	68.34	99.11
10-20	12.1	0.11	2.59	70.69	98.40
20-30	20.1	0.12	2.47	73.12	97.12
30-40	28.2	0.09	2.38	74.78	95.78
40-50	36.2	0.08	2.31	76.06	94.30
50-60	44.3	0.07	2.24	77.08	92.59
60-70	52.3	0.07	2.16	77.92	90.51
70-80	60.4	0.08	2.08	78.62	87.84
80-90	68.4	0.11	1.97	79.16	83.96
90-92	73.3	0.09	1.88	79.45	80.33
92-94	74.9	0.04	1.84	79.55	78.64
94-96	76.5	0.05	1.79	79.65	76.43
96-98	78.1	0.08	1.71	79.71	73.19
98-100	79.7	1.71	0.00	0.00	0.00
Feed avg grade (f)		**1.86**			

Table 50 - Mathematical manipulation of grade histogram (wt%) data – São Pedro das Águias ore [cs=0.075].

Scheelite grade fraction, %	**WO_3 average grade, %**	**Grade Histogram, %**	**Yield, %**	**Concentrate average grade, %**	**Recovery, %**
Scheelite = 80.52% WO_3	x_i	f_i	$\sum_i f_i \times H[x_i - x_{50}]$	$\frac{\sum_i f_i \times H[x_i - x_{50}] \times x_i}{Yield}$	$\frac{Yield \times c}{f}$
			100.00	1.85	100.00
0-2	0.03	97.00	3.00	60.77	98.52
2-4	2.4	0.20	2.80	64.94	98.26
4-6	4.0	0.08	2.72	66.73	98.09
6-8	5.6	0.04	2.68	67.64	97.97
8-10	7.2	0.05	2.63	68.77	97.77
10-20	12.1	0.10	2.53	71.09	97.10
20-30	20.1	0.11	2.41	73.46	95.87
30-40	28.2	0.08	2.33	75.09	94.60
40-50	36.2	0.07	2.26	76.33	93.19
50-60	44.3	0.06	2.20	77.20	91.75
60-70	52.3	0.06	2.14	77.90	90.05
70-80	60.4	0.08	2.06	78.55	87.55
80-90	68.4	0.10	1.96	79.06	83.94
90-92	73.3	0.08	1.88	79.32	80.60
92-94	74.9	0.06	1.82	79.46	78.17
94-96	76.5	0.08	1.74	79.60	74.86
96-98	78.1	0.11	1.63	79.70	70.22
98-100	79.7	1.63	0.00	0.00	0.00
Feed avg grade (f)		**1.85**			

In the case of Alvarrões ore, the mineral liberation analysis of the flotation feed also allowed for the construction of the Mayer UUC, based on the computation of the cumulative recovery, yield and grade, as can be observed in Table 51.

Table 51 - Mathematical manipulation of grade histogram (wt%) data – Alvarrões ore.

Lepidolite grade fraction, %	**Li_2O average grade, %**	**Grade Histogram, %**	**Yield, %**	**Concentrate average grade, %**	**Recovery, %**
Lepidolite = 7.70% Li_2O	x_i	f_i	$\sum_i f_i \times H[x_i - x_{50}]$	$\frac{\sum_i f_i \times H[x_i - x_{50}] \times x_i}{Yield}$	$\frac{Yield \times c}{f}$
			100.00	1.17	100.00
0-10	0.12	81.52	18.48	5.82	91.95
10-20	1.2	1.88	16.61	6.34	90.09
20-30	1.9	0.99	15.62	6.62	88.47
30-40	2.7	0.74	14.88	6.82	86.77
40-50	3.5	0.64	14.25	6.97	84.88
50-60	4.2	0.60	13.65	7.09	82.71
60-70	5.0	0.61	13.03	7.18	80.09
70-80	5.8	0.68	12.36	7.26	76.74
80-90	6.5	0.86	11.50	7.31	71.92
90-100	7.3	11.50	0.00	0.00	0.00
Feed avg grade (*f*)		**1.17**			

These data can now be easily converted to a graphical representation. Fig. 124 shows, respectively, the Mayer UUC of São Pedro das Águias (two size fractions; the finer size fraction shows a liberation level slightly higher) and Alvarrões ores used in the concentration tests.

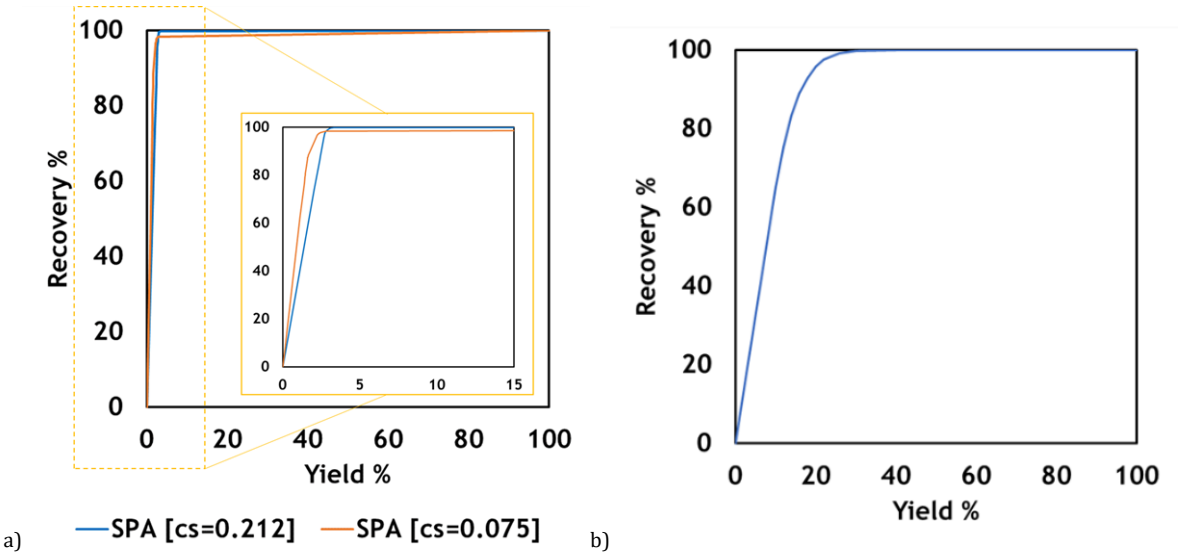

Fig. 124 – Mayer UUC for a) both size fractions of São Pedro das Águias ore and b) flotation feed of Alvarrões ore.

The same approach can be applied for the computation of Mayer UUC for the study of the pre-concentration process after the crushing stage of both studied ores. Table 52 and Table 53 present the data required to construct Mayer UUC of São Pedro das Águias and Alvarrões ores, respectively.

Table 52 – Mathematical manipulation of grade histogram (wt%) data – São Pedro das Águias ore.

Scheelite grade fraction, %	**WO_3 average grade, %**	**Grade Histogram, %**	**Yield, %**	**Concentrate average grade, %**	**Recovery, %**
Scheelite = 80.52% WO_3	x_i	f_i	$\sum_i f_i \times H[x_i - x_{50}]$	$\frac{\sum_i f_i \times H[x_i - x_{50}] \times x_i}{Yield}$	$\frac{Yield \times c}{f}$
			100.00	0.87	100.00
0	0	45.54	54.46	1.61	100.00
0-0.3	0.125	24.07	30.39	2.78	96.56
0.3-0.8	0.375	7.85	22.54	3.61	93.19
0.8-1.4	0.75	5.50	17.04	4.54	88.47
1.4-2.2	1.25	4.00	13.04	5.55	82.75
2.2-2.8	1.75	2.55	10.49	6.47	77.64
2.8-3.4	2.25	1.82	8.67	7.36	72.95
3.4-4	2.75	1.38	7.29	8.23	68.61
4-4.7	3.25	1.08	6.20	9.10	64.58
4.7-5.3	3.75	0.87	5.33	9.98	60.82
5.3-6.5	4.5	1.03	4.30	11.30	55.52
6.5-9.3	6	1.41	2.89	13.88	45.86
9.3-13.7	8.5	1.30	1.59	18.29	33.20
13.7-26.7	15	1.18	0.40	27.99	12.87
26.7-43.5	25	0.34	0.06	45.44	3.05
43.5-74.5	42.5	0.06	0.00	0.00	0.00
74.5-100	62.5	0.00	0.00	0.00	0.00
Feed avg grade (*f*)		**0.87**			

Table 53 – Mathematical manipulation of grade histogram (wt%) data – Alvarrões ore.

Lepidolite grade fraction, %	Li_2O average grade, %	Grade Histogram, %	Yield, %	Concentrate average grade, %	Recovery, %
Lepidolite = 7.70% Li_2O	x_i	f_i	$\sum_i f_i \times H[x_i - x_{50}]$	$\frac{\sum_i f_i \times H[x_i - x_{50}] \times x_i}{Yield}$	$\frac{Yield \times c}{f}$
			100.00	1.96	100.00
0	0.00	10.40	89.60	2.19	100.00
0-13	0.5	29.57	60.03	3.03	92.47
13-26	1.5	20.49	39.54	3.82	76.83
26-39	2.5	14.40	25.14	4.57	58.51
39-52	3.5	10.20	14.94	5.30	40.34
52-64	4.5	7.01	7.93	6.02	24.28
64-78	5.5	4.51	3.42	6.70	11.66
78-91	6.5	2.58	0.84	7.30	3.12
91-100	7.3	0.84	0.00	0.00	0.00
Feed avg grade (*f*)		**1.96**			

Fig. 125 show the Mayer UUC for both studied ores after the crushing stage, which can be defined as the technical limitations of pre-concentration at this liberation degree.

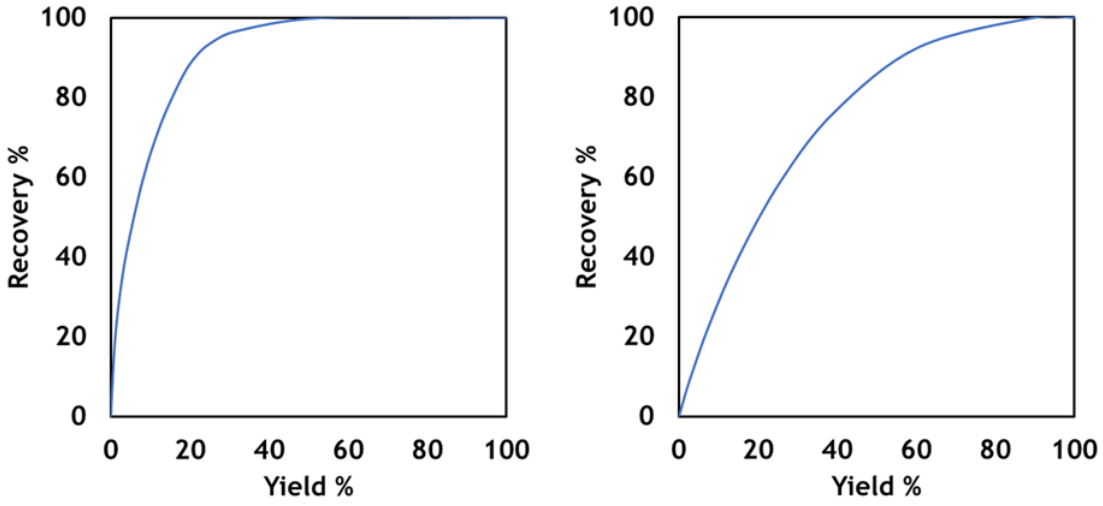

Fig. 125 – UUC represented by means of Mayer diagram – São Pedro das Águias (left) and Alvarrões (right).

At this point, all components required to apply the proposed approach were assembled. The next sections are dedicated to assessing the separation comparing the experimental upgrading curve with both the ideal and the ultimate upgrading curves and, using the Mayer representation.

5.2.2.2 ASSESSMENT OF CONCENTRATION EFFICIENCY

Remembering, in the case of São Pedro das Águias two different size fractions were tested using a Wilfley shaking table. Fig. 126 show the comparison between Mayer UUC computed as above described, the experimental data, interpolated using the developed Efficiency model and the ideal upgrading curve.

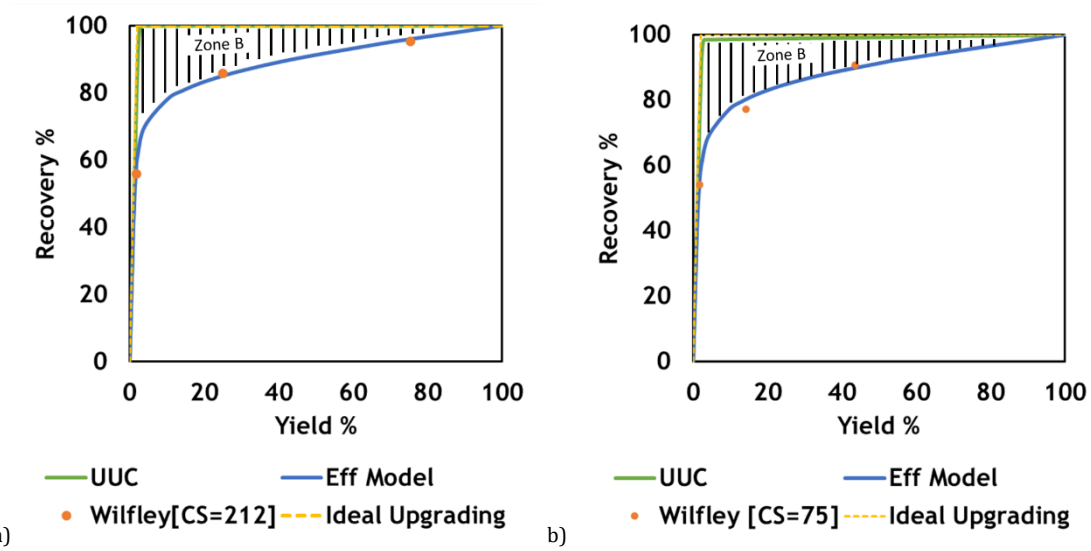

Fig. 126 - Assessment of concentration efficiency of São Pedro das Águias ore: a) [cs=212] and b) [cs=75].

The distance between ideal upgrading curve and UUC is practically non-existent meaning that São Pedro das Águias ore is well liberated in both size fractions. Conversely, the experimental upgrading curve is detached from the UUC (labelled as zone B in Fig. 126), which means that the technical performance plays a major role in the total process inefficiency. In this case, as total inefficiency is due to technical issues, there is room for shaking table operational conditions to be optimized to improve the separation performance (middlings recirculation, for instance).

Now, it is possible to assess different separation scenarios. Fig. 127 show that, for both size fractions, technical inefficiency is higher for a high cut-grade than for a low cut-grade, which means that, in the tested operational conditions, shaking table was more efficient in the rejection of a low-grade product than in the production of a high-grade and recovery product. In this case, a high-grade product can be collected but only with a recovery of about 60% for the coarser size fraction and 50% for the finer size fraction.

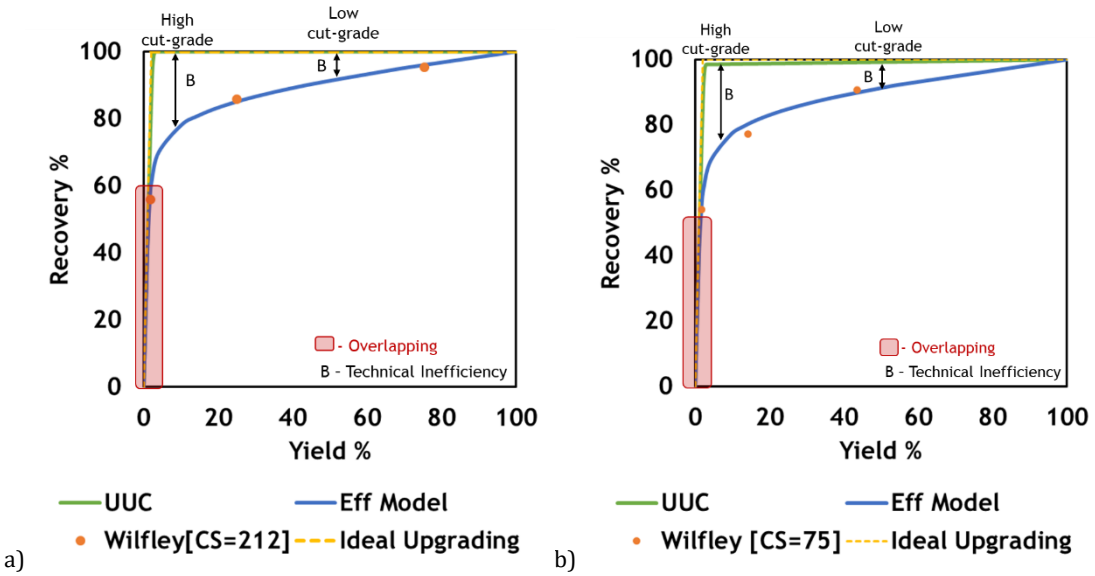

a) b)

Fig. 127 – Assessment of different separation scenarios in the concentration stage of São Pedro das Águias ore: a) [cs=212] and b) [cs=75].

This approach can be complemented considering that: i) overlapping between UUC and Ideal upgrading points to a high degree of liberation; ii) when the experimental curve and UUC are overlapped, it means maximum technical efficiency; iii) if the three curves are overlapped, the experimental separation was carried out under maximum technical efficiency with full mineral liberation.

In real scenarios, these overlappings can be expected only in the extremes sides of the Mayer representations. In the case of São Pedro das Águias, the shaking table can be used to produce pure scheelite concentrates with a recovery of about 60% for the coarser size fraction and 50% for the finer size fraction (overlapping zone). For higher recoveries the shaking table starts losing efficiency in distinguish high-grade from middlings particles, and, as pointed by the Efficiency model, dragged gangue particles are also being reported to the concentrate, reducing its grade. Conversely, there is no overlapping between UUC and experimental upgrading curve in the zone of 100% recovery, which means that it is not possible to reject a pure gangue material using the shaking table. However, due to the overlap between ideal upgrading and UUC, it can be said that with the improvement of the shaking table technical efficiency, pure gangue material can be rejected.

The same procedure was applied to assess the efficiency of the Alvarrões concentration stage. In the case of the flotation test, it is possible to observe gaps between UUC and experimental upgrading curve (zone B) and between UUC and ideal upgrading

curve (zone A), as shown in Fig. 128 a). According to this, technical inefficiency and lack of liberation are both contributing to the global inefficiency of the flotation process. Thus, in this case, the optimization of flotation conditions would bring the upgrading curve closer to UUC, unless liberation is improved.

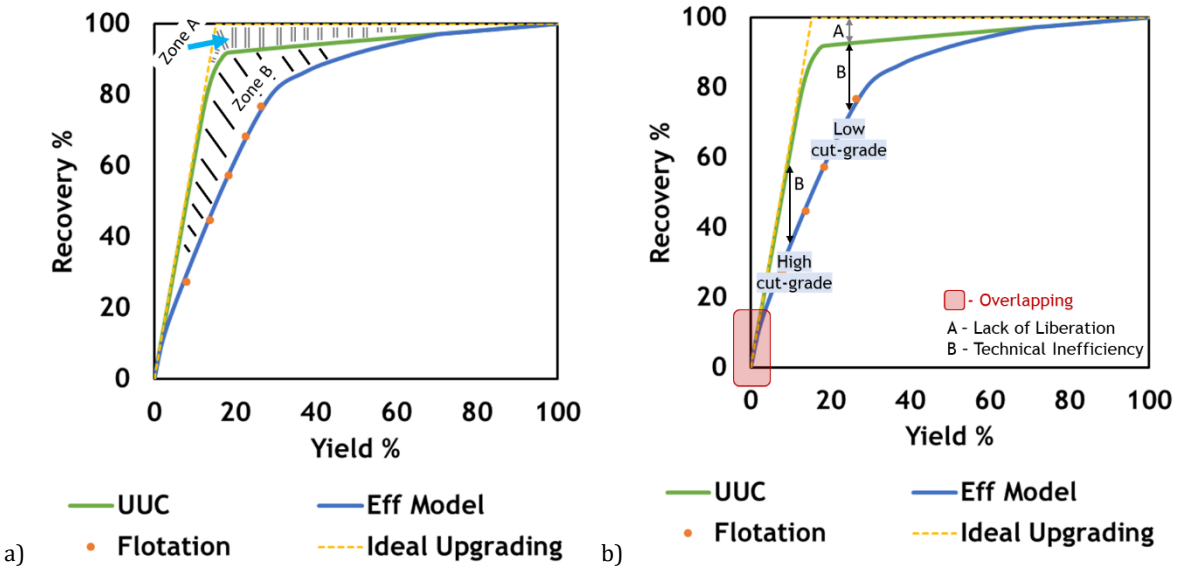

Fig. 128 – Analysis of Alvarrões concentration efficiency: a) Assessment of batch flotation efficiency; b) Assessment of different separation scenarios.

Fig. 128 b) shows the analysis of different separation scenarios, in which it is possible to observe a great probability for the production of high-grade concentrates with an adequate optimization of the technical process since some lepidolite is well liberated (overlap between UUC and ideal upgrading). Concerning technical inefficiency, it is possible to observe a similar impact for a wide range of cut-grades, pointing out for the constant performance of flotation, as already indicated by the analysis of the grade histograms (wt%) produced during the application of the Efficiency model.

As in the case of São Pedro das Águias, the overlapping between UUC and experimental curve occurs in the zone of lower recovery and yield, meaning that flotation, in the tested conditions, allowed for the production of about 15% of pure Lepidolite. If the flotation conditions can be improved, mainly using a collector able to distinguish Li-mica from muscovite, the overlapping between UUC and ideal upgrading points out for the possibility of producing better concentrate products. Conversely, the production of an almost pure gangue material is not possible.

5.2.2.3 ASSESSMENT OF PRE-CONCENTRATION EFFICIENCY

Similarly, the same approach was applied to assess the efficiency of Pre-concentration tests. In the case of São Pedro das Águias, the efficiency of hand-sorting separation is shown in Fig. 129, by the comparison between Mayer UUC, experimental data and ideal upgrading curve.

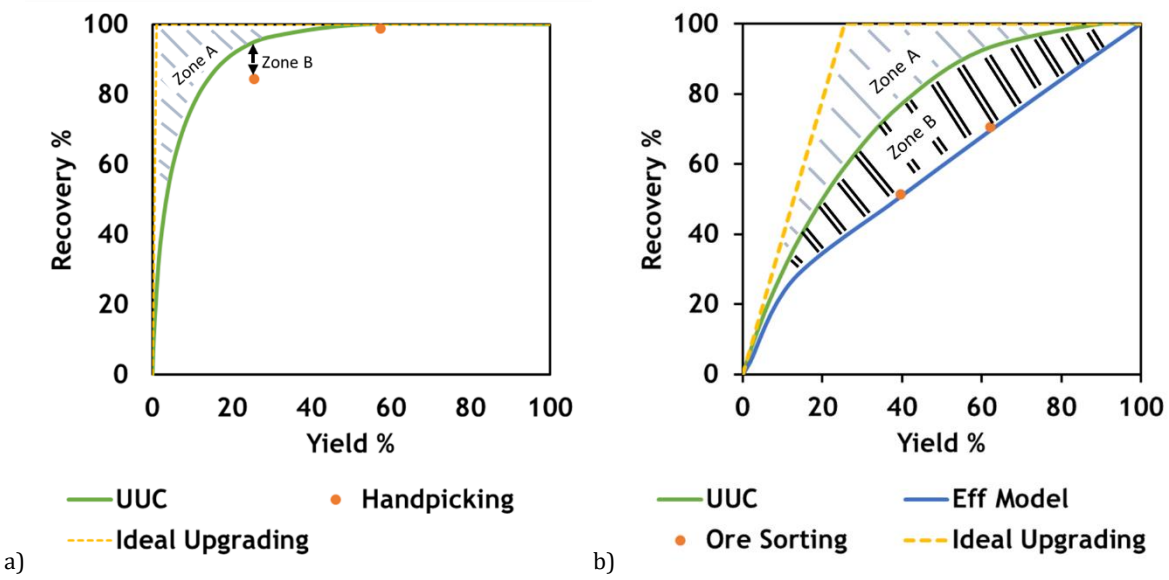

Fig. 129 – Assessment of Pre-concentration efficiency: a) hand-sorting applied to São Pedro das Águias ore; b) optical sorting applied to Alvarrões ore.

According to what has been said, the following conclusions can be drawn:

- In the case of São Pedro das Águias, hand-sorting was carried out under a high efficiency level: a good gangue liberation is observed, pointing out for the possibility of mass rejection under good levels of recovery;
- In the case of Alvarrões, the non-negligible distance between UUC and Ideal Upgrading indicates the low liberation degree of the ore, which is likely due to the superimposition of pegmatitic and aplitic textures. The experimental curve is also far from the UUC, meaning low efficiency of the optical sorting separation.

A deep analysis of the pre-concentration assessment of both ores can be carried out supported by Fig. 130.

In the case of São Pedro das Águias, the application of the efficiency model does not allow for the computation of a continuous Mayer upgrading curve. Thus, considering the 1st cut-grade a high cut-grade, it is possible to observe that the impact of technical inefficiency is higher than the impact of liberation, proving that, as predicted before, the

1st cut-grade was applied under a weak separation criterium. For the low cut-grade, an almost perfect separation is observed, producing an almost pure gangue material. It is easy to consider an overlap between UUC, ideal upgrading and experimental curve in the zone marked by the red box (Fig. 130 a), pointing out for the existence of at around 40% of gangue liberated particles that can be successfully rejected by ore sorting using a UV light sensor.

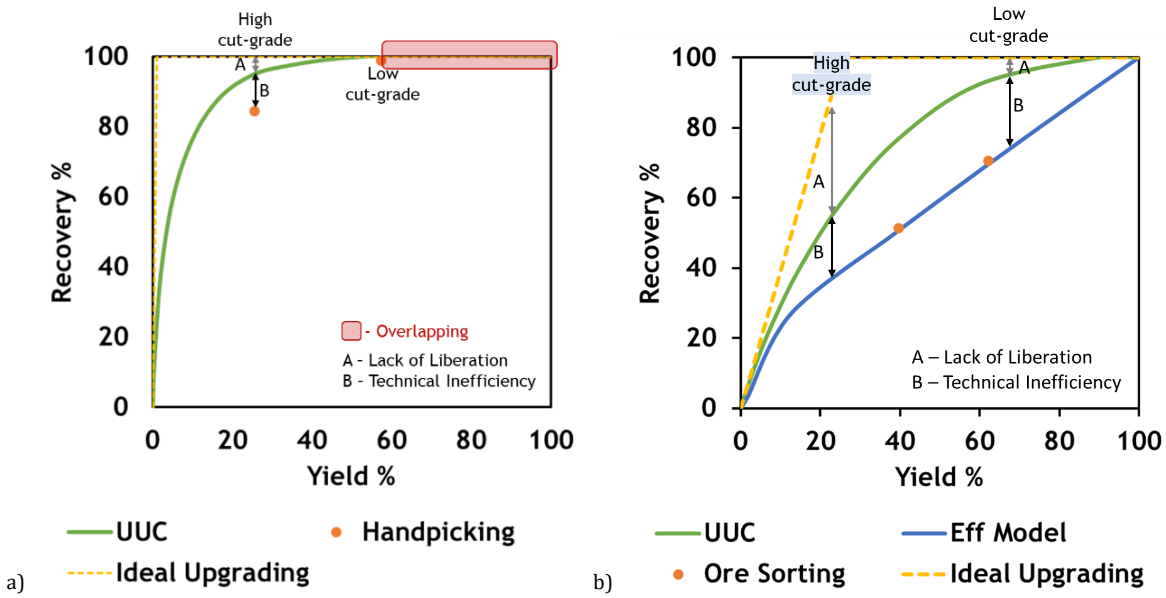

Fig. 130 - Identification of the influence of lack of liberation and technical efficiency in the global efficiency of the separation – São Pedro das Águias ore.

In the case of Alvarrões ore, the influence of technical inefficiency (B) is lower when a high cut-grade is applied, meaning that the optical sorting separator exhibit a better performance to recognize high-grade particles. On the other hand, for a low cut-grade, the influence of technical inefficiency (B) increases, meaning that the optical separator reveals lower resolution when colour contrast decreases. Conversely, the influence of the lack of liberation (A) is lower for a low cut-grade, meaning that some gangue is liberated, while lepidolite is practically non-liberated. There is no overlapping between UUC, ideal upgrading and experimental curves, meaning that ore sorting would not be able to generate a pure gangue or a pure lepidolite product.

5.2.3 ACQUISITION OF HENRY ULTIMATE UPGRADING CURVES AND ASSESSMENT OF PRE-CONCENTRATION FEASIBILITY

5.2.3.1 COMPUTATION OF HENRY ULTIMATE UPGRADING CURVES

So far in this work, Mayer curve has been applied to plot upgrading curves, however other traditional Mineral Processing representations can be used, such that known as Henry Curve, or also Washability Curve when applied to coal processing.

This Henry function relates yield with cut-grade and allows for the calculation and plot of the auxiliary Concentrate and Tailings average grade curves, in the same representation, as functions of the cut-grade, which is an important parameter to tune any concentration process. The respective recovery is then calculated using simple maths.

Thus, the Henry Curve can be applied for the optimization of the pre-concentration process, because it allows for the prediction of the mass rejection at a certain cut-grade, compatible with the desired recovery. As will be demonstrated in the next paragraphs, Henry Curve seems to be also a suitable tool to assess separation feasibility.

According to the procedures developed in previous paragraphs, starting with the feed grade histograms (wt%) of both studied ore for pre-concentration at crushing stages (scheelite from São Pedro das Águias and lepidolite from Alvarrões), it would be possible to calculate the Henry Ultimate Upgrading Curve (UUC), which figures can be observed in Table 54 and Table 55.

Table 54 – Mathematical manipulation of grade histogram (wt%) data – São Pedro das Águias.

Feed grade histogram, %		Yield, %	Concentrate average grade, %	Recovery, %	Tailings average grade, %
x_i	f_i	$\sum_i f_i \times H[x_i - x_{50}]$	$\frac{\sum_i f_i \times H[x_i - x_{50}] \times x_i}{Yield}$	$\frac{Yield \times c}{f}$	$\frac{\sum_i f_i \times (1 - H[x_i - x_{50})] \times x_i}{1 - Yield}$
		100.00	0.87	100	
0.00	45.54	54.46	1.61	100.00	0.00
0.13	24.07	30.39	2.78	96.56	0.04
0.38	7.85	22.54	3.61	93.19	0.08
0.75	5.50	17.04	4.54	88.47	0.12
1.25	4.00	13.04	5.55	82.75	0.17
1.75	2.55	10.49	6.47	77.64	0.22
2.25	1.82	8.67	7.36	72.95	0.26
2.75	1.38	7.29	8.23	68.61	0.30
3.25	1.08	6.20	9.10	64.58	0.33
3.75	0.87	5.33	9.98	60.82	0.36
4.50	1.03	4.30	11.30	55.52	0.41
6.00	1.41	2.89	13.88	45.86	0.49
8.50	1.30	1.59	18.29	33.20	0.59
15.00	1.18	0.40	27.99	12.87	0.76
25.00	0.34	0.06	45.44	3.05	0.85
42.50	0.06	0.00	0.00	0.00	0.87
62.50	0.00	0.00	0.00	0.00	0.87
f = 0.87 WO_3%					

Table 55 – Mathematical manipulation of grade histogram (wt%) data – Alvarrões.

Feed grade histogram, %		Yield, %	Concentrate average grade, %	Recovery, %	Tailings average grade, %
x_i	f_i	$\sum_i f_i \times H[x_i - x_{50}]$	$\frac{\sum_i f_i \times H[x_i - x_{50}] \times x_i}{Yield}$	$\frac{Yield \times c}{f}$	$\frac{\sum_i f_i \times (1 - H[x_i - x_{50})] \times x_i}{1 - Yield}$
		100.00	1.96	100	
0.00	10.40	89.60	2.19	100.00	0.00
0.50	29.57	60.03	3.03	92.47	0.37
1.50	20.49	39.54	3.82	76.83	0.75
2.50	14.40	25.14	4.57	58.51	1.09
3.50	10.20	14.94	5.30	40.34	1.38
4.50	7.01	7.93	6.02	24.28	1.62
5.50	4.51	3.42	6.70	11.66	1.80
6.50	2.58	0.84	7.30	3.12	1.92
7.30	0.84	0.00			1.96
f = 1.96 %Li_2O					

Based on these data, the Henry Ultimate Upgrading Curves of both studied ores can be computed, as shown in Fig. 131 and Fig. 132.

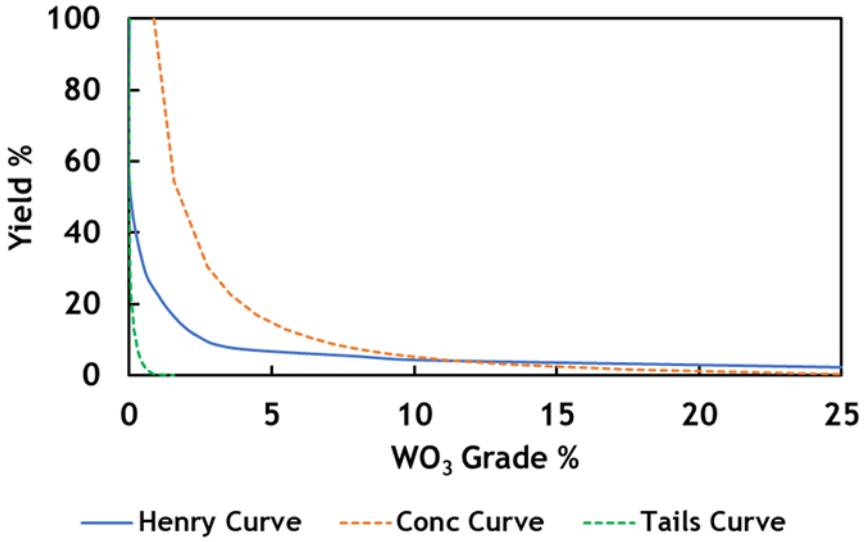

Fig. 131 – Henry Upgrading Curve for São Pedro das Águias.

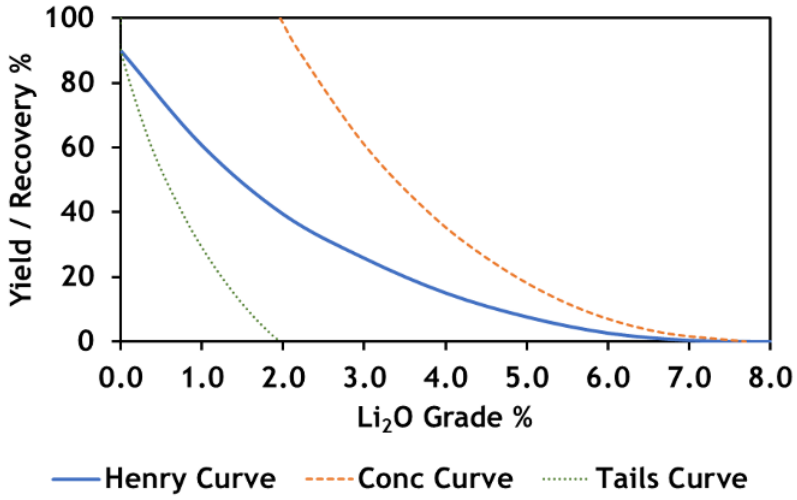

Fig. 132 – Henry Upgrading Curve for Alvarrões ore.

In the following section, the acquired Henry UUC is used to assess the pre-concentration feasibility of both studied ores.

5.2.3.2 PRE-CONCENTRATION FEASIBILITY

The main objective of pre-concentration is the rejection of gangue material in an early stage of the comminution process – crushing stage, which will increase the feed

grade of the final concentration process. However, residual metal losses must be guaranteed for the feasibility of pre-concentration. Having this in mind, it makes sense to use the Ultimate upgrading to predict the theoretical limit of the separation performance, as it is the result of a perfect separation of the ore in a given liberation level, itself described by the respective feed grade histogram (wt%) [10].

Fig. 133 shows the procedure to read the most important separation indicators described by the Henry Curve, considering different cut-grades of the separation as input, in the case of São Pedro das Águas pre-concentration of scheelite; four examples are given: cut-grade at 0% WO_3, meaning that the separator rejects only particles 0% WO_3; cut-grade 0.25% WO_3 accepts all material above that grade; so on using cut-grades of 1% and 2% WO_3:

1. Define the desired cut-grade;
2. The intersection with Henry curve gives the %yield of the separation (YY-axis);
3. The intersection of the %yield and Concentrate curve is used to read the Concentrate average grade in the XX-axis:
4. Similarly, the intersection of the %yield and Tails curve could be used to read the Tails average grade in the XX-axis (not marked in the plot);

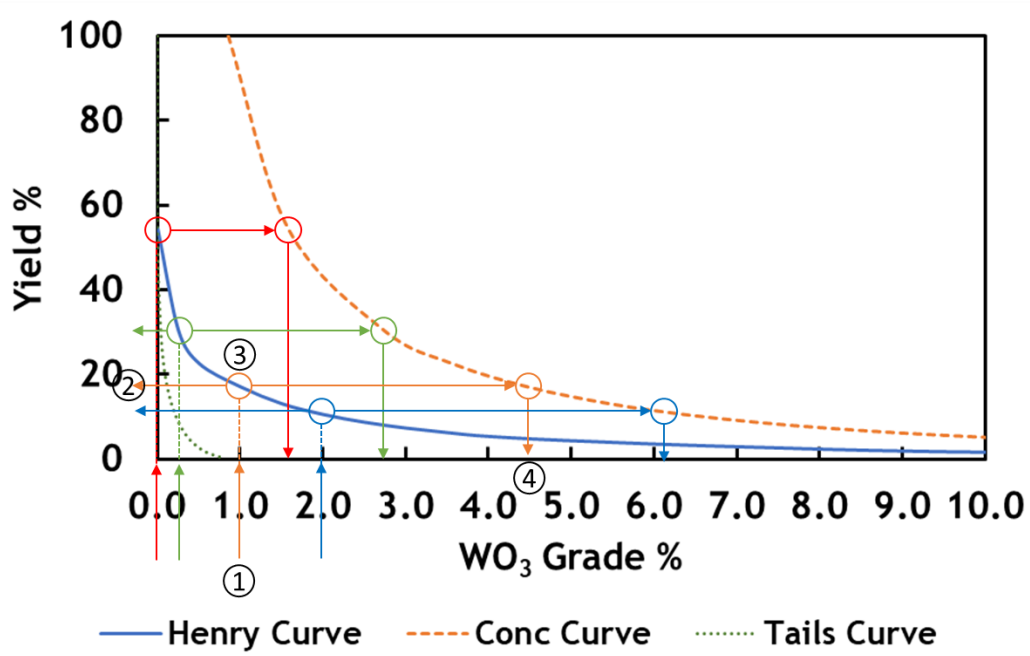

Fig. 133 - Assessment of pre-concentration using the Henry UUC – São Pedro das Águias.

Table 56 shows the resume of figures collected in the graph of Henry UUC and that can be used to assess pre-concentration performance. Recovery values are not traditionally represented in the Henry Curve plot but are computed based on the yield and concentrate and feed grades.

Table 56 - Assessment of pre-concentration feasibility - São Pedro das Àguias.

cut-grade	Yield,%	Concentrate grade, %	Recovery,%
0.00	54.46	1.59	100.00
0.25	30.40	2.74	96.52
1.00	17.04	4.48	88.33
2.00	10.50	6.37	77.39

Based on this analysis, the following conclusions, concerning pre-concentration feasibility, can be drawn:

- A separator that can distinguish particles of 0 %WO_3 will allow for the rejection of 45.54% of the material, without any metal losses;
- If a cut-grade of 0.25 %WO_3 was applied to the separator it would lead to the rejection of 69.60% material, producing a concentrate with 2.74 %WO_3 with 3.52% of metal losses;
- Higher cut-grades will lead to metal losses of 11.67% and 22.61%, respectively for cut-grades of 1.0 and 2.0 %WO_3, which can represent losses greater than what is adequate for a pre-concentration step;

The same approach was applied in the case of Alvarrões pre-concentration. Fig. 134 shows the representation of the respective Henry UUC, in which it is possible to observe the plot of some cut-grades to predict the ultimate separation performance.

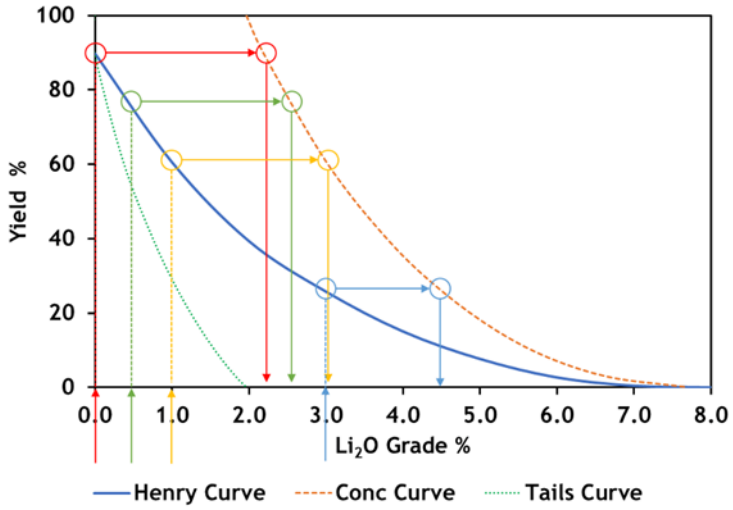

Fig. 134 – Assessment of pre-concentration using the Henry UUC – Alvarrões.

Table 57 presents some simulations of pre-concentration for different cut-grades based on Henry UUC.

Table 57 – Assessment of Pre-concentration feasibility – Alvarrões.

cut-grade	Yield,%	Concentrate grade, %	Recovery,%
0.0	90.00	2.19	100.00
0.5	75.00	2.60	99.10
1.0	61.00	3.00	92.60
3.0	28.00	4.50	64.10

Ultimate prediction of pre-concentration of Alvarrões ore at crushing size conducted to the following conclusion:

- Rejection of pure gangue would not be greater than 10%;
- Accepting Li losses in the order of 1%, mass rejection would reach only 25%;
- Operating with a cut-grade of 1% Li_2O it would be possible to reject almost 40% mass accepting 7.4% Li losses, which would be the most desirable scenario.
- Using a cut-grade of 3 %Li_2O a high-grade concentrate of about 4.5 %Li_2O could be produced, which could be appropriate for metallurgical Li extraction, however under losses above 35 % Li.

These examples were used to demonstrated the value of Henry UUC to have a quick assessment of the pre-concentration feasibility, defining the possible scenarios for the pre-concentration stage at crushing sizes.

Nevertheless, it is fundamental to emphasize that these results were obtained simulating a perfect separator, and for this reason, the presented Henry curve is called Ultimate Upgrading. Thus, it should be expected that the performance of any real separation would be lower than that predicted by the UUC unless very precise technology is applied.

In the case of São Pedro das Águias, Dense Media Separation (DMS) or ore sorting by X-Ray Transmission may be efficient options. In the case of Alvarrões, Optical ore sorting can be the most promising technique for pre-concentration. However, to achieve the predicted scenarios, ore sorting techniques must be equipped with high-resolution detectors, which can increase the equipment cost. In the case of DMS, a high-density contrast between scheelite and another gangue mineral must be observed.

5.2.4 FINAL REMARKS ON SEPARATION EFFICIENCY

One of the main challenges of mineral processing is the choice and adoption of adequate indicators or descriptors to assess separation efficiency. These indicators are fundamental to define the most suitable separation conditions to conduct process optimization.

The present thesis proposes a modest contribution to the interpretation of the separation performance, supported by two novel approaches:

- Development of a complex Efficiency model to calculate the Partition Curves that can be used to interpolate a few sets of experimental data to build the Upgrading Curves as appropriate descriptors of the performance of the separation;
- Development of the concept of Ultimate Upgrading as an effective way to distinguish between mineral and equipment limitations and, on account of this, be a selective descriptor of the separation efficiency.

Furthermore, the comparison between the experimental upgrading curve, the UUC and the ideal upgrading curve can be considered an indicator of the ore liberation degree.

The advantage of this approach seems to be unwavering. Moreover, all the journey crossed to accomplish the objective of the work allowed for the acquisition of other important concepts not foreseen since the beginning of the conception of the thesis:

- The conception of a consistent Efficiency model, evolved from the Lynch model, makes it applicable to build more realistic representations of the experimental Upgrading Curves, predicting process performance in a wide range of cut-grades;
- The sliding of the Efficiency Model along the feed Grade Histogram makes for the development of the concept of Ultimate Upgrading, which, by itself, allows the distinction between inefficiencies related to the lack of liberation and those resulting from limitations or misadjustments of the separator;
- The introduction of the "dragging" parameter AS in the formulation of the Efficiency model, initially claimed for the need to include non-discriminating separation effect on particle grade, recognizes the existence of a specific phenomenon already known from the practical experience: the presence of low-grade particles in the concentrates of shaking tables due to the absence of enough liberated material to fill the riffles (or a stratum in an intermediate region of a jigging bed), or of collector selectivity for such type of minerals (inability to efficiently distinguish between minerals of the same group, such as mica and Li-mica, for instance).

Another important issue that should be taken into account is the present growing availability of gathering representative mineralogical data from particulate systems, allowed by the modern devices of MLA (mineral liberation analyzers) or equivalent, which are able to experimentally determine the necessary Grade Histograms that are in the basis of developed calculation around the concept of ultimate upgrading.

NOMENCLATURE AND GLOSSARY

P_i	Partition function	
f_i	Mass distribution by grade classe i in the feed	
c_i	Mass distribution by grade classe i in the concentrate	
t_i	Mass distribution by grade classe i in the tailings	
x_i	Grade fraction	
x_{50}	Cut-grade	
m	Partition function parameter	
As	Partition function parameter	
c	Concentrate average grade	
f	Feed average grade	
e	Tailings average grade	
H	Heaviside function	-

REFERENCES

1. Lynch, A.J. and T.C. Rao. *Modelling and scale-up of hydrocyclone classifiers*. in *Proceedings of the 11th International Mineral Processing Conference*. 1975.
2. Nageswararao, K., *Reduced efficiency curves of industrial hydrocyclones - An analysis for plant practice.* Minerals Engineering, 1999. **12**(5): p. 517-544.
3. Leißner, T., K. Bachmann, J. Gutzmer and U.A. Peuker, *MLA-based partition curves for magnetic separation.* Minerals Engineering, 2016. **94**: p. 94-103.
4. Schach, E., M. Buchamann, R. Tolosana-Delgado, T. Leibner, M. Kern, K. Gerald van den Boogart, M. Rudolph and U.A. Peuker, *Multidimensional characterization of separation process - Part 1: Introduction kernel methods and entropy in the context of mineral processing using SEM-based image analysis.* Minerals Engineering, 2019. **137**: p. 78-86.
5. Plitt, L.R., *A mathematical model of the hydrociclone classifier.* CIM Bulletin - Mineral Processing, 1976. **69**: p. 114-123.
6. Bradley, D., *The hydrocyclone - Bradley.* London: Pergamon Press ltd, 1965.
7. Goodall, W., A. Crop and D. Bradshaw, *The influence of textural variation and gangue mineralogy on recovery of copper by flotation from porphyry ore: a review.* 2013.
8. Bradshaw, D., *The role of process mineralogy in improving the performance of complex sulphide ores.* IMPC 2014 - 27th International Mineral Processing Congress, 2014.
9. Sousa, R., B. Simons, K. Bru, A.B. de Sousa, G. Rollinson, J. Andersen, M. Martin and M. Machado Leite, *Use of mineral liberation quantitative data to assess separation efficiency in mineral processing – Some case studies.* Minerals Engineering, 2018. **127**: p. 134-142.
10. Sousa, R., A. Futuro, A. Fiúza and M.M. Leite, *Pre-concentration at crushing sizes for low-grade ores processing – Ore macro texture characterization and liberation assessment.* Minerals Engineering, 2020. **147**: p. 106156.

6 CONCLUSIONS AND FUTURE WORK

6.1 FINAL REMARKS

The aims proposed for this work were by means of the application of some new procedures and some existing models that were crucial for the success of this thesis. The most relevant findings of this work are resumed in this section.

The first challenge faced was to acquire reliable mineralogical quantitative data at concentration and pre-concentration size ranges. For concentration size ranges, a well-established technology was applied, while for the case of pre-concentration, a new methodology had to be developed. Table 58 shows the main findings/outcomes of this task.

Table 58 – Resume of the main findings of the acquisition of quantitative mineralogical data.

Acquisition of quantitative mineralogical data		
Size range	**Method**	**Findings**
Concentration	QEMSCAN®	✓ Established methodology to ensure the acquisition of reliable data.
Pre-concentration	Developed by the author	✓ The visual contrast between valuable minerals and gangues allows for easy identification of the correspondent surfaces; ✓ Machine learning techniques are fundamental for proper calibration of the image analysis procedure; ✓ A prompt characterization of the ore macro-texture may be useful in feasibility studies;

After acquiring the required quantitative mineralogical data, it was necessary to compute the grade histograms (wt%) for the studied cases – scheelite from São Pedro das Águias deposit and lepidolite from Alvarrões deposit at both size ranges (concentration and pre-concentration). Then, the second main challenge of this thesis was the fitting of these grade histograms (wt%) using the Beta statistical function and its validation based on the Beta liberation model. Table 59 shows the main findings found during this task.

Table 59 – Resume of the main findings of applying beta liberation model.

Size range	Findings
Concentration	✓ Goodness-of-fit points out for the great quality of grade histograms (wt%) obtained using QEMSCAN® mineralogical quantitative data.
Pre-concentration	✓ Grade histograms (wt%) produced by applying a comminution algorithm to the macro-texture were effectively fitted to Beta function for both studied ores. In contrary to what has happened to broken particles (only for the case of Alvarrões ore), pointing out for lack of representativity of data; ✓ Discrepancies between macro-texture and broken particles analysis were assessed using the Beta liberation model, by defining the topological constant that characterizes the texture of the lepidolite ore from Alvarrões, which pointed out for discrepancies on the broken particles histograms; ✓ Broken particles histograms were then adjusted based on the Beta liberation model, and compared with those acquired under the macro-texture, showing a better approximation between both approaches;

After the validation of the obtained grade histograms (wt%) that were used to compute Ultimate Upgrading Curves in a further stage of the work, a new challenge arose: The application of a partition curve to fit experimental results and produce a more discretized experimental upgrading curve. Furthermore, partition curve parameters provide useful information regarding the separation efficiency of the applied process and can be used to simulate the concentrate grade histograms. Table 60 shows the main findings reached during this task.

Table 60 – Resume of the main findings of the fitting experimental data using an efficiency model.

Size range	Findings	
Concentration	Shaking table of São Pedro das Águias ore	✓ Adjusted m parameter was around 10, pointing out for a good separation efficiency; ✓ *AS* increases exponentially with the decrease of x_{50}, which is related to the occupation of the zone behind the riffles, meaning that when liberated scheelite is not enough to fulfil the riffles, the product collects a mixture of scheelite with light particles that were "dragged" to the concentrate, not on account of their density, but because there was room for them;
	Froth Flotation of Alvarrões ore	✓ The m parameter was around 15 which is consistent to a good separation efficiency; ✓ A linear relationship was found between *AS* and x_{50}, as a result of the collector selectivity for mica minerals, not exclusive to Li-mica, making for muscovite flotation that is "dragged" to the concentrate;
Pre-concentration	Hand-sorting of São Pedro das Águias ore	✓ Due to the experimental procedure, it was not possible to adjust a similar m value for the different separation cut-grades, which avoid the production of a discretized experimental upgrading curve; ✓ Low AS values indicate that the separation was carried under a great level of separation efficiency;
	Optical sorting of Alvarrões ore	✓ The obtained values for the m parameter was at around 3, pointing out for a lower separation efficiency; ✓ High values of AS were observed, indicating a high amount of material "dragged" to the concentrate. This can be related to the equipment calibration that does not allow for a proper distinction between lepidolite and gangues colour;

Finally, having access to grade histograms (wt%) and more discretized experimental upgrading curves, the final challenge of this thesis was the application of the

ultimate upgrading concept to assess separation efficiency and feasibility. Table 61 shows the main findings of the application of the methodology proposed in this work to the studied cases.

Table 61 – Resume of the main findings of the assessment of separation efficiency/feasibility using the Ultimate Upgrading concept.

Size range	Findings	
Concentration	The efficiency of Shaking table	✓ A very high degree of liberation was found due to the overlapping between UUC and Ideal Upgrading Curve; ✓ Some technical inefficiency was observed; ✓ Overall separation efficiency only can be improved by acting under the technical process; ✓ Pure concentrates can be obtained with recoveries varying between 50 and 60% according to the size fraction;
	The efficiency of Froth Flotation of Alvarrões ore	✓ It was observed a good liberation degree of lepidolite, but with room for improvement; ✓ Technical efficiency is good, but can also be enhanced; ✓ Overall separation efficiency can be improved by acting under mineral liberation degree and technical aspects of the separation; ✓ 15% of lepidolite can be recovered as a pure concentrate product;
Pre-concentration	The efficiency of Hand-sorting of São Pedro das Águias ore	✓ As expected at this size range, a low liberation degree was observed; ✓ Technical efficiency of hand-sorting was very high, as can be observed by the overlapping of UUC and experimental points; ✓ It is possible to reject 40% of gangue, without associated losses;
	Feasibility of Pre-concentration	✓ A separator that can distinguish particles of 0 %WO3 will allow for the rejection of 45.54% of the material, without any metal losses;

	of São Pedro das Águias ore	✓ If a cut-grade of 0.25 %WO3 is applied to the separator it will lead to the rejection of 69.60% material, producing a concentrate with 2.74 %WO3 with 3.52% of metal losses; ✓ Higher cut-grades will lead to metal losses of 11.67% and 22.61%, respectively for cut-grades of 1.0 and 2.0 %WO3, which can represent losses greater than what is adequate for a pre-concentration step;
	The efficiency of Optical sorting of Alvarrões ore	✓ A low liberation degree was found; ✓ Technical efficiency was disappointing, which can be observed by the great gap between UUC and experimental upgrading curve; ✓ Pure gangue rejection is not possible at this liberation degree and using this optical sorter;
	Feasibility of Pre-concentration of Alvarrões ore	✓ Rejection of pure gangue would not be greater than 10%; ✓ Accepting Li losses between 1 - 8%, would conduct a mass rejection between 25 - 40%; ✓ High-grade concentrate of about 4.5 %Li_2O could be produced in a pre-concentration stage;

6.2 GLOBAL APPRECIATION

This thesis was conducted having as main objective the development of a methodology to assess mineral separation efficiency, based on the acquisition of proper mineralogical quantitative data. As previously mentioned, the results of experimental testwork were only used as case studies/demonstrators, showing the applicability of the methodology and its contribution to a better understanding of the experimental results. Some of the applied approaches – Beta Liberation Model, Partition Curves and application of mineral liberation data to define the technical limit of the separation, were already discussed by other authors. However, this work pretended to combine, in a novel and integrated way, all these concepts. Based on this concept, it is possible to highlight the following main contributions:

- Development of a straightforward methodology that, based on photos of macro-texture/coarse particles, allowed for the acquirement of quantitative mineralogical data: the advance on image analysis was fundamental for the obtention of proper quantitative mineralogical data. Mineral liberation analysis of fine particles (concentration size range) using systems as QEMSCAN® is widely and effectively applied. On the other hand, coarse particles/surfaces (pre-concentration size range) are much more difficult to obtain.

The first objective of the work was accomplished, the acquisition of quantitative mineralogical data in size ranges of the two separation processes, Pre-concentration and Concentration.

- Conversion of quantitative mineralogy data into grade histograms (wt%): Quantitative mineralogical data can be powerful information but must be well exploited to become a powerful tool for any mineral processing engineer. In line with this, the acquired data was converted into the grade histograms (wt%). In the case of QEMSCAN® data, a simple mathematical manipulation allowed for the acquisition of grade histograms (wt%). In the case of the developed methodology, a random comminution algorithm was applied under the macro-texture data to simulate particles and compute the respective grade histogram (wt%). Regarding the broken particles, grade histograms (wt%) were easily computed, once the access to each particle grade was directly calculated by the image analysis procedure.

The second main objective was the computation of the grade histograms(wt%) of both studied samples for the pre-concentration and concentration size ranges.

- Fitting Beta liberation model to the acquired grade histograms (wt%): Beta function parameters allowed for an adequate interpretation of the degree of liberation. In the case of pre-concentration, in which two different methods were compared - image analysis of macro-texture followed by the application of an algorithm of random comminution vs image analysis of crushed/broken particles,

the Beta liberation model was fundamental to smooth the obtained data to amend the lack of data representativity, namely in the case of broken particles. It also allowed for the detection of discrepancies in the acquired data.

The third main objective was the validation of the computed grade histograms (wt%) and the validation of the methodology developed to assess quantitative mineralogical data at coarse particle size (macro-texture vs broken particles).

- Development of an Efficiency Model to fit experimental data: The methodology proposed to assess mineral separation efficiency requires the availability of experimental data on real separations to compute the experimental upgrading curves, which triggered a bottleneck - experimental data typically consists only in a few data points, forcing the interpolation between them or the application of non-interpretable polynomial models. To overcome this issue, it is proposed a novel procedure that, using the grade histogram (wt%) of the material that feeds the separator, and an efficiency model based on the Partition Curve (using a shape parameter - m and % dragging material - AS), it was possible to compute a more discretized experimental curve. During the development of this model, it was found a relationship between the value of the AS parameter and the efficiency of the applied procedure.

The fourth main objective was the production of more discretized Experimental Upgrading Curves, by applying an efficiency model, in which its parameters can be interpreted and associated with the technical efficiency of the applied separation method.

- Representation of Ultimate Upgrading Curves and assessment of separation efficiency/feasibility: Finally, having access to grade histograms(wt%), the Ultimate Upgrading Curves can be computed, representing the limit of the technical efficiency at a certain liberation degree. Then, comparing Ultimate, Ideal and Experimental Upgrading Curves a new window over the assessment of separation efficiency, based on the Mayer representation, was explored, allowing for the distinction between the effect of lack of liberation and lack of technical

efficiency in the global separation efficiency. Furthermore, it was found that Ultimate Upgrading Curve (represented employing Henry Curve) by itself can be a suitable tool to assess the feasibility of separation, especially in the case of pre-concentration, in which a prompt insight regarding its feasibility could be crucial for the viability of a mining project.

The final main objective was to collect deeper information on the separation efficiency and feasibility, using the developed Ultimate Upgrading concept, based on the integration and interpretation of quantitative mineralogical data.

6.3 FUTURE WORK

During the development of this thesis, many ideas emerge to enhance the data quality or the purposed model, and there is always room for improvement. This thesis has to have a final dot, but the developed work must have two more final dots. In line with this, some proposals for future work are described in the following paragraphs.

The first one is evident, the acquisition of quantitative mineralogical data under macro-textures/coarse particles can be improved, taking advantage of the recent developments in the field of image analysis, with the application of innovative technologies as hyperspectral.

Then, the algorithm of random comminution applied to macro-texture images to produce the respective grade histograms (wt%) can be improved by allowing the simulation of particles with diversified shapes and considering stereological corrections.

Beta liberation model, deeply exploited in the framework of this thesis, revealed to be an important tool for mineral liberation interpretation. Further work must be carried out to test its application in different ore textures. This would be important because Beta liberation model allows for the characterization of the ore texture using the topological constant, and then it is possible to simulate the grade histograms (wt%) at any desired size range, which means that it is possible to assess different liberation degrees without repeat the quantitative mineralogical analysis.

Finally, the efficiency model that was exploited to produce more discretized experimental upgrading curves can be improved. The partition curve formula can be

adjusted to achieve better goodness-of-fit. Having access to data from other separation processes, it would be possible to define the relationship between the AS parameter, as done for the cases of shaking table and froth flotation. The reliability of this fitting exercise can be proved by acquiring the grade histograms (wt%) of the concentrate products, using the methodologies as QEMSCAN® in the case of fine sizes. Then, these grade histograms (wt%) can be compared with the grade histograms (wt%) simulated by applying the adjusted partition curve to the feed grade histogram (wt%).

APPENDIX

A.1.1 SEPARATION EFFICIENCY OF PILOT PLANT TEST

As described in Chapter 3, the procedure to assess the separation efficiency presented in Chapter 5 can also be applied to the case of Alvarrões pilot plant tests. The objective is to offer a more straightforward review of the process.

I. Acquisition of feed grade histograms (wt%)

The grade histogram (wt%) of the material that fed the pilot plant trials were computed using mineral liberation analysis data, as can be observed in Fig. 135.

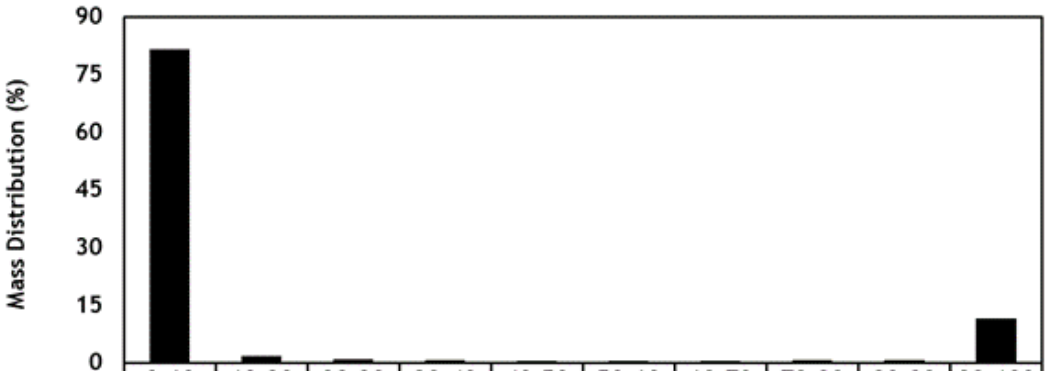

	0-10	10-20	20-30	30-40	40-50	50-60	60-70	70-80	80-90	90-100
Alvarrões	81.52	1.88	0.99	0.74	0.64	0.60	0.61	0.68	0.86	11.50

Fig. 135 – Final grade histogram (wt%) after grinding stage – Alvarrões.

II. Experimental data representation using the Mayer diagram

Pilot plant trials were carried using the same feed material but under different strategies. Pilot#1 aimed to accomplish a high-grade concentrate, and Pilot#2 was designed to enhance the recovery. The observation of Fig. 136 indicates that Pilot#1 was more efficient than Pilot#2 due to the proximity to the ideal upgrading line.

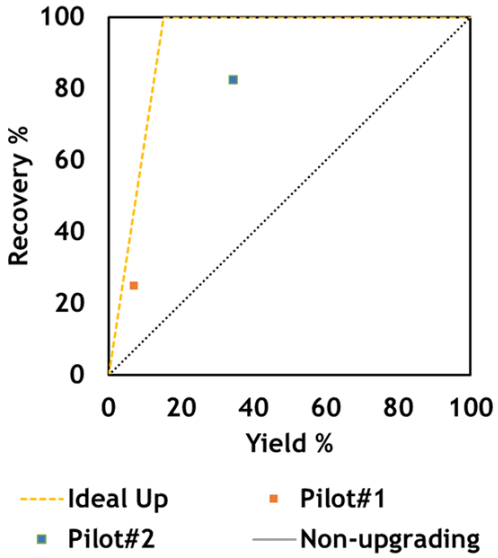

Fig. 136 – Mayer representation of Alvarrões pilot plant test.

III. Fitting Partition Curve

Parameters m, x50 and AS (Table 62) are fitted by back-calculation to obtain the Partition Curve that applied to the feed grade histogram (wt%) will generate the concentrate grade histogram (wt%), matching the experimental yield, recovery and concentrate average grade.

Table 62 – Final Lynch model parameters to fit the results of pilot plant tests.

	m	AS[1]	X_{50}
Pilot#1	17.71	3.73	7.68 % Li_2O
Pilot#2	9.97	25.03	5.50 %Li_2O

The respective partition and reduced partition curves are represented in Fig. 137.

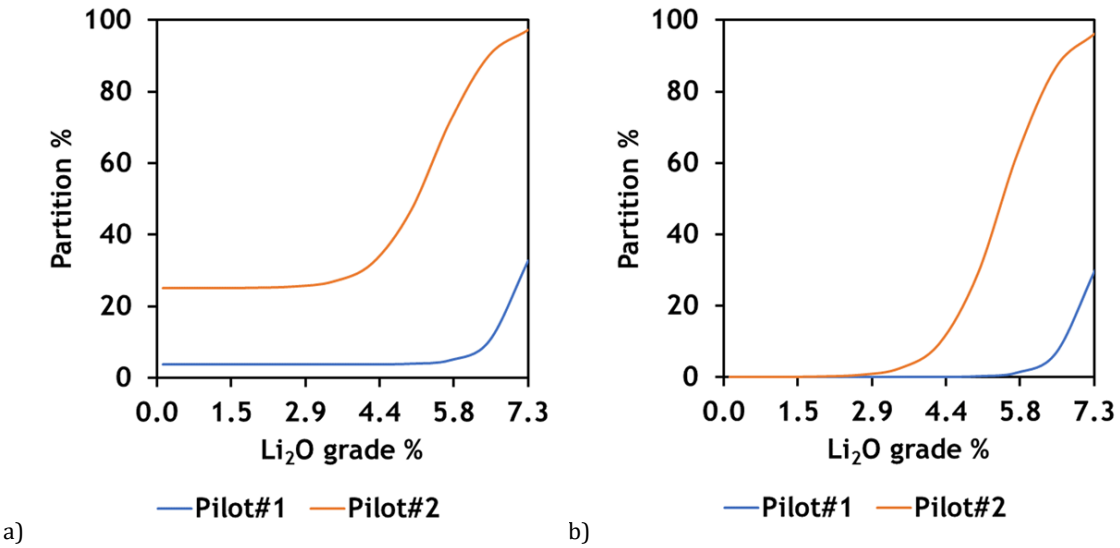

Fig. 137 - Partition curves obtained by fitting the Lynch model to experimental data of Alvarrões concentration tests at the pilot plant: a) Partition curve; b) Reduced Partition curve.

It is possible to observe a higher quantity of gangue material dragged to the concentrate of the test Pilot#2 than in the Pilot#1. Thus, when the pilot plant was adjusted to enhance the recovery of lepidolite by decreasing the cut-grade, the dragging of gangue material to the concentrate increased, parallel to the incorporation of low-grade middlings.

IV. Predicting concentrate grade histograms (wt%)

Based on the obtained Partition Curves, it is possible to predict the concentrate grade histograms (wt%). Fig. 138 shows the feed grade histogram (wt%) and the partition curves applied in each pilot test, that conducted to the concentrate grade histograms, illustrated in Fig. 139.

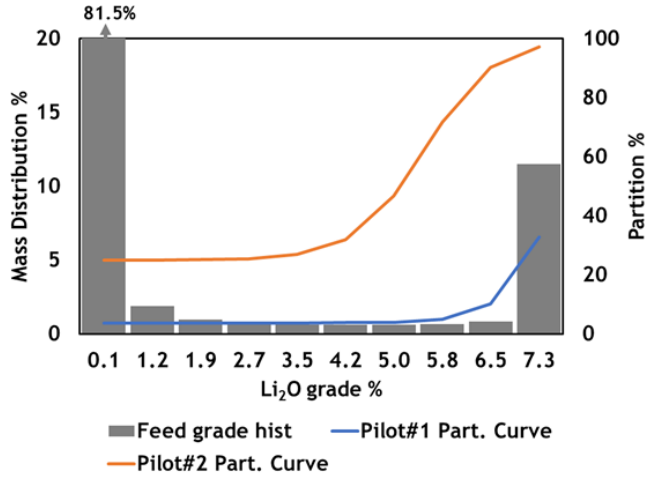

Fig. 138 – Application of the obtained partition curve to the feed grade histogram (wt%) - Alvarrões concentration test (pilot tests).

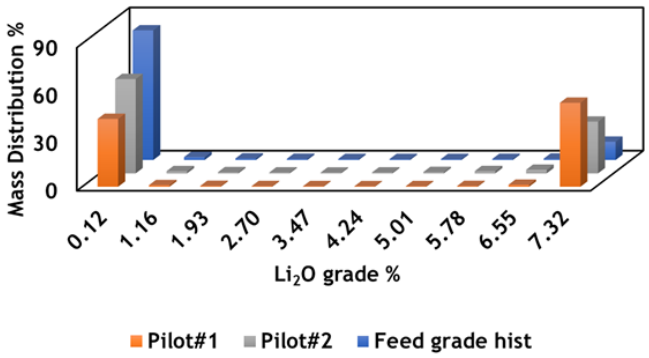

Fig. 139 – Grade histograms (wt%) of separation products – Alvarrões concentration test (pilot tests).

As indicated by the partition curve parameters, Pilot#1 test generated a concentrated product with a higher % of material in the high-grade class than Pilot#2. However, the recovery of lepidolite was too low. Changing the flotation strategy from Pilot#1 to Pilot#2 test, it was possible to increase the recovery, by collecting particles with lepidolite low-grade. This was already pointed out by the analysis of the AS parameter.

V. Assessment of separation efficiency

Finally, using the feed grade histogram (wt%), experimental data and Mayer Diagram, it is possible to assess the separation efficiency of both pilot plant trials. It must be highlighted that, as in the case of São Pedro das Águias handpicking, each separation conducted to the obtention of two products, refusing the possibility of obtaining a continuous experimental curve, using the Separation Efficiency model. Thus, the efficiency only can be assessed in the individual data points, as can be observed in Fig. 140.

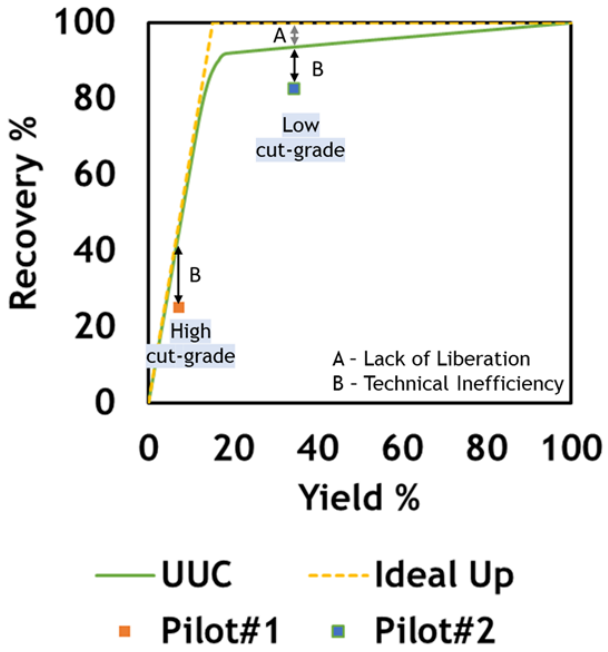

Fig. 140 - Assessment of pilot plant tests the efficiency of Alvarrões ore.

In the Pilot#1 test, the applied flotation strategy conducted to the application of a high-cut grade, producing a high-concentrate product under low recovery. Due to the overlapping of UUC and Ideal Upgrading, it is possible to assume that with the application of a high cut-grade, a pure lepidolite concentrate can be achieved. However, due to technical inefficiency (B), non-pure particles were floated along with lepidolite, avoiding the obtention of a pure concentrate product. The flotation strategy applied in the Pilot#2 test conducted to an increase of the mineral recovery. The technical efficiency seems to be improved from Pilot#1 to Pilot#2. However, in the second case, global efficiency is also affected by the lack of liberation.

A.1.2 SUPPLEMENTARY IMAGES OF MACRO-TEXTURES AND BROKEN PARTICLES

In this section, some figures used in the mineral liberation analysis at crushing sizes are presented. Fig. 141 shows photos of sawn lump particles collected in the Alvarrões deposit used in the macrotexture analysis. Photos were cropped and converted into a digital image following the procedure presented in chapter 4.

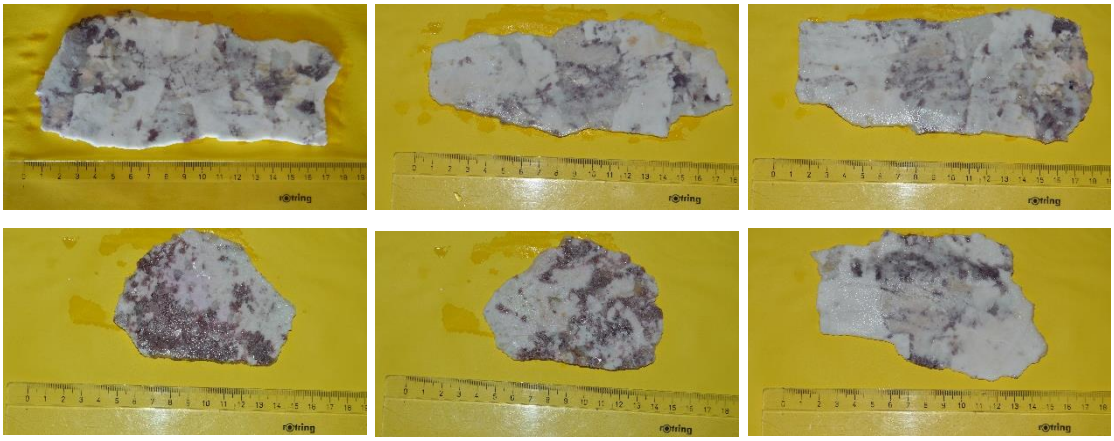

Fig. 141 – Photo of sawn lump particles collected in Alvarrões deposit.

In the case of São Pedro das Águias, some pieces of drill cores were photographed at visible and under UV light. Visible photos were used to identify the borders of the drill cores. Based on this information, photos under UV light were processed to determine the scheelite (fluorescence) pixels. Fig. 142 shows some examples of photographed drill cores.

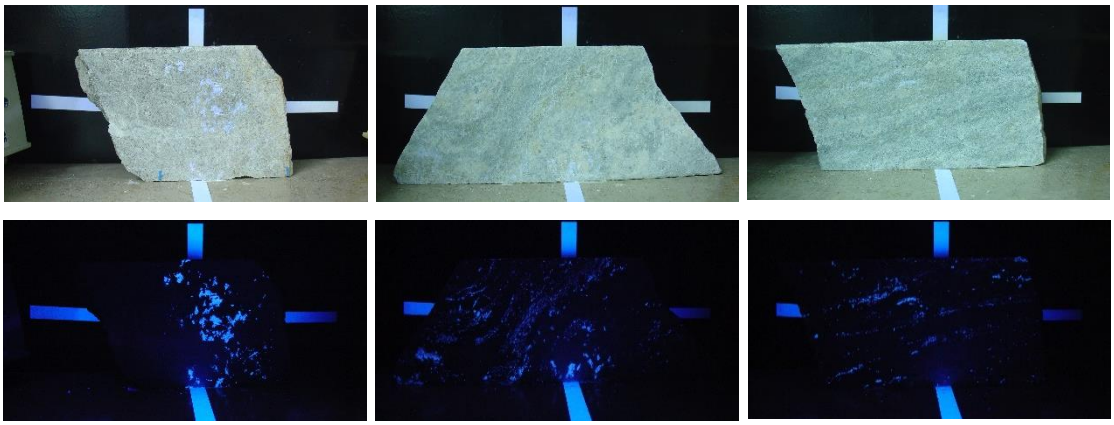

Fig. 142 – Photos of drill cores collected in São Pedro das Águias deposit.

For the analysis of the broken particle, several sets of particles were photographed and converted into digital binary images, allowing for the computation of the mineral grade of each particle. Fig. 143 and Fig. 144 show some examples of photos obtained from both studied ores.

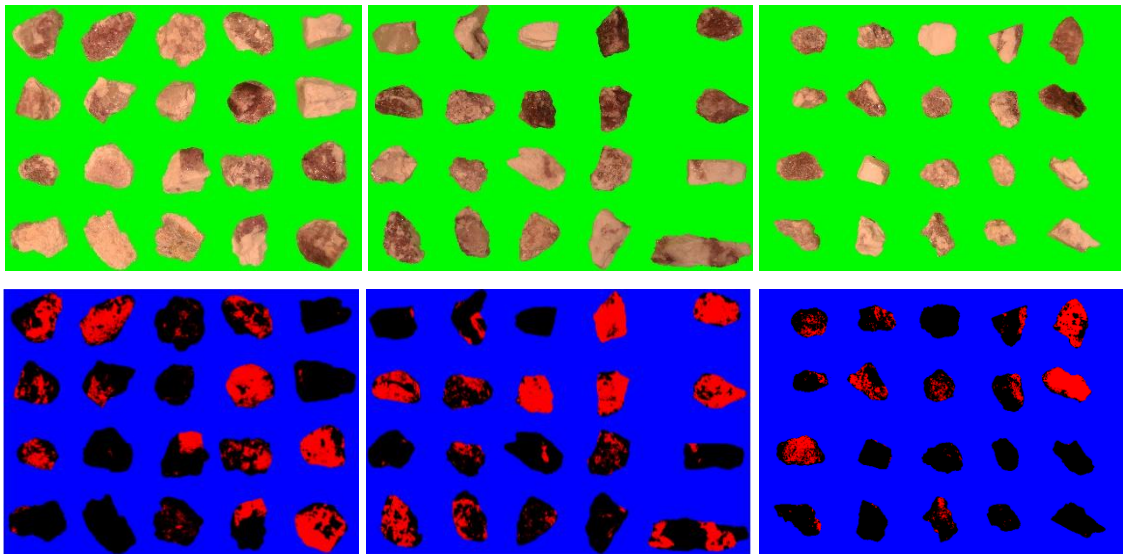

Fig. 143 – Photos of broken particles from Alvarrões ore. The upper images were collected under visible light and lower images were converted into binary images.

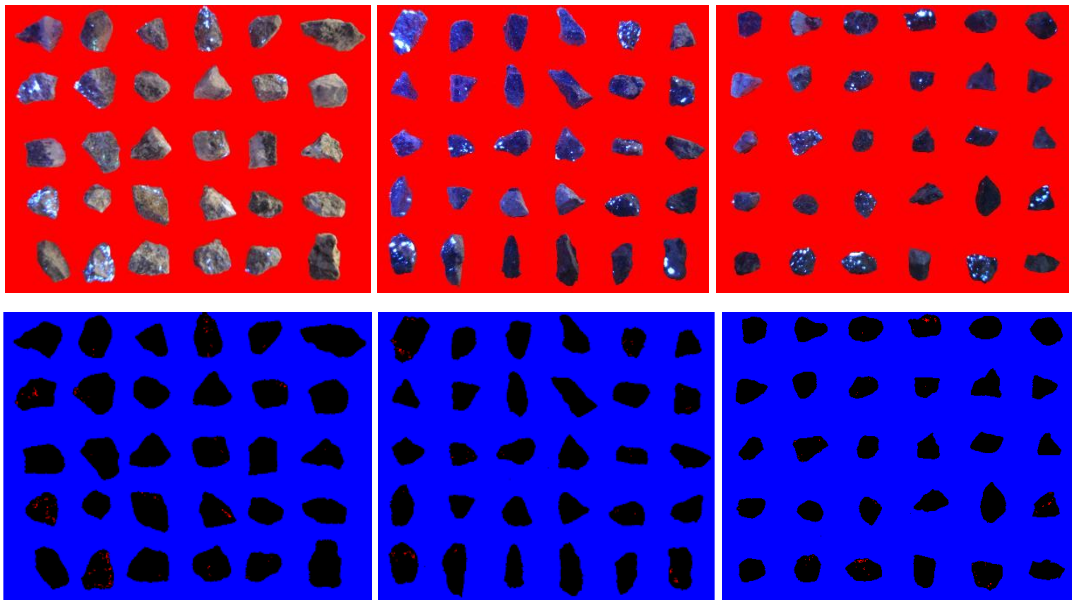

Fig. 144 – Photos of broken particles from São Pedro das Águias ore. The upper images were collected under UV light and lower images were converted into binary images.